ERROR ESTIMATES OF NUMERICAL METHODS FOR THE LONG-TIME DYNAMICS OF THE NONLINEAR KLEIN-GORDON EQUATION

FENG YUE

NATIONAL UNIVERSITY OF SINGAPORE

2020

ERROR ESTIMATES OF NUMERICAL METHODS FOR THE LONG-TIME DYNAMICS OF THE NONLINEAR KLEIN-GORDON EQUATION

by

FENG YUE

(M.Sc., Zhejiang University)

A THESIS SUBMITTED

FOR THE DEGREE OF DOCTOR OF PHILOSOPHY

DEPARTMENT OF MATHEMATICS

NATIONAL UNIVERSITY OF SINGAPORE

2020

Supervisor:
Professor Bao Weizhu

Examiners:
Dr Cai Zhenning
Dr Tong Xin
Professor Christophe Besse, Université Toulouse 3 Paul Sabatier

Declaration

I hereby declare that this thesis is my original work and it has been written by me in its entirety. I have duly acknowledged all the sources of information which have been used in the thesis.

This thesis has also not been submitted for any degree in any university previously.

冯悦

FENG YUE

10 June 2020

Acknowledgements

It is my great honor here to thank those who made this thesis possible.

First and foremost, I would express my most heartfelt gratitude to my supervisor Prof. Weizhu Bao, who introduced me to this interesting research field and helped me overcome all the problems throughout my Ph.D candidature, for his constructive suggestions, patient guidance and encouragement, as well as generous support. His broad knowledge in various areas and profound insight always impressed me. I learnt a lot from him not only in research, but also in life. His guidance will be a great fortune in my future path.

I would like to express my sincere appreciation to my collaborators, Dr. Chunmei Su and Prof. Wenfan Yi, for their fruitful discussions and contribution to the work. This project can not be done without their invaluable help and advice.

Besides, many thanks also go to all the former colleagues and fellow graduates in our group, especially Prof. Yan Wang, Prof. Yongyong Cai, Prof. Qinglin Tang, Prof. Xiaofei Zhao, Dr. Weijie Huang, Dr. Jia Yin, Dr. Xinran Ruan, Dr. Quan Zhao, Mr. Teng Zhang, Mr. Bo Lin and Mr. Yichen Guo for their help and suggestions. My time at NUS was enjoyable due to all the group members and friends that became a good memory in my life.

I am grateful to NUS for awarding me the Research Scholarship during my Ph.D candidature, and the financial support for the conference leaves. I would also like to thank all my lecturers for teaching me. They improved my knowledge and skills in various research topics.

Last but not least, thank my dearest family for their unconditional love, support, encouragement and consideration. Without them, I would never have arrived at this stage of my life and follow my dreams.

Feng Yue

June 2020

Contents

Summary

The Klein-Gordon equation is a relativistic wave equation describing the motion of spinless particles like the pion. It plays a fundamental role in quantum electrodynamics, particle and/or plasma physics within the framework of quantum mechanics and Einstein's special relativity. The nonlinear Klein-Gordon equation (NKGE) can be seen as the relativistic and nonlinear version of the Schrödinger equation. The long-time behavior of the NKGE is an interesting topic in both analytical and numerical aspects and has gained a surge of attentions in recent years.

The aim of this thesis is to establish error estimates of different numerical methods for the NKGE with weak nonlinearity, while the nonlinearity strength is charaterized by ε^2 with $\varepsilon \in (0, 1]$ a dimensionless parameter, for the long-time dynamics up to the time at $O(\varepsilon^{-2})$. Rigorous proofs for different numerical methods are presented and particular attentions are paid to study the error bounds of the numerical methods in the long-time regime and how the error bounds depend explicitly on the mesh size, time step as well as the small parameter ε, which indicates how to choose the mesh size and time step in the long-time numerical simulations. Numerical results are reported to verify the error estimates and compare the performance of these numerical methods. This thesis is mainly composed of the following three parts.

In the first part, the NKGE with weak nonlinearity is discretized by the finite difference method in time including the Crank-Nicolson, two semi-implicit and leap-frog finite difference schemes. Combined with the central finite difference discretization in space, four widely used finite difference time domain (FDTD) methods are applied to numerically solve the NKGE in the long-time regime. The error bounds of the FDTD methods up to the time at $O(\varepsilon^{-\beta})$ with $0 \leq \beta \leq 2$ are rigorously established, which depend on the mesh size h, time step size τ as well as the small parameter ε. Based on the error bounds, to obtain "correct" numerical solution of the NKGE with weak nonlinearity in the long-time regime, the ε-scalability (or meshing strategy requirement) of the FDTD methods should be taken as: $h = O(\varepsilon^{\beta/2})$ and $\tau = O(\varepsilon^{\beta/2})$. In order to improve the spatial resolution capacity of the FDTD methods, the fourth-order compact finite difference (4cFD) method and finite difference Fourier pseudospectral (FDFP)

method are used to solve this problem. The error bounds indicate that the 4cFD method offers advantages over those FDTD methods regarding the meshing strategy requirement in space for resolving the NKGE in the long-time regime. The spatial error bound of the FDFP method is uniform, which preforms much better than the FDTD and 4cFD methods. The spatial/temporal resolution of these finite difference methods are exhibited through various numerical examples.

The second part is devoted to studying the uniform error bounds of the numerical schemes for the long-time dynamics of the NKGE with weak nonlinearity. The error bound of the exponential wave integrator Fourier pseudospectral (EWI-FP) method is carried out, which is uniform spectral accuracy in space and second order in time up to the time at $O(\varepsilon^{-2})$. Numerical results confirm the error estimates and show that they are sharp. Then the NKGE is rewritten as a relativistic nonlinear Schrödinger equation (NLSE). The time-splitting Fourier pseudospectral (TSFP) method is adapted to solve it and uniform error bound of the TSFP method is rigorously established. For comparisons, the exponential wave integrator and time-splitting method are also combined with central finite difference and fourth-order compact finite difference discretizations in space. Numerical studies and comparisons show that when $0 < \varepsilon \ll 1$, the TSFP method offers the best approximation among these numerical methods for solving the NKGE in the long-time regime. With the TSFP method, the problem can be solved effectively in 2D and 3D cases.

The last part is to rescale the NKGE with $O(\varepsilon^2)$ nonlinearity and $O(1)$ initial data (or $O(1)$ nonlinearity and $O(\varepsilon)$ initial data) to an oscillatory NKGE. The solution of the oscillatory NKGE propagates waves with amplitude at $O(1)$, wavelength $O(1)$ and $O(\varepsilon^\beta)$ in space and time, respectively, and wave velocity at $O(\varepsilon^{-\beta})$, which is quite different from the oscillatory nature of the NKGE in the nonrelativistic limit regime. The FDTD methods, EWI-FP method and TSFP method are applied to solve the oscillatory NKGE and corresponding error estimates are obtained straightforwardly. Extensive numerical tests are reported to support our error estimates and to demonstrate that they are sharp. Comparisons of different numerical methods are summarized for convenience.

List of Tables

List of Figures

List of Symbols and Abbreviations

t	time
$\mathbf{x}$	spatial variable
$\hbar$	Planck constant
c	speed of light
$\mathbb{R}^d$	d-dimensional Euclidean space
$\mathbb{C}^d$	d-dimensional complex space
$\mathbb{T}^d$	d-dimensional torus
i	imaginary unit
h	space mesh size
τ	time step size
ε	a dimensionless parameter in (0,1]
∇	gradient
$\Delta = \nabla \cdot \nabla$	Laplacian
$A \lesssim B$	$A \leq C \cdot B$ for some generic constant $C > 0$
$\bar{f}$	conjugate of a complex function f
1D	one dimension
2D	two dimension
3D	three dimension
NKGE	nonlinear Klein-Gordon equation
CNFD	Crank-Nicolson finite difference
SIFD	semi-implicit finite difference
LFFD	leap-frog finite difference
4cFD	fourth-order compact finite difference

FDFP	finite difference Fourier pseudospectral
EWI	exponential wave integrator
EWI-FP	exponential wave integrator Fourier pseudospectral
EWI-FD	exponential wave integrator finite difference
EWI-4cFD	exponential wave integrator fourth-order compact finite difference
TSFP	time-splitting Fourier pseudospectral
TS-FD	time-splitting finite difference
TS-4cFD	time-splitting fourth-order compact finite difference
Fig.	figure
Tab.	table

Chapter 1

Introduction

This chapter serves as an introduction of the thesis. A brief overview of the nonlinear Klein-Gordon equation (NKGE) and comparisons of different scalings are presented, and the existing results of the NKGE are reviewed, as well as the problems to study and the scope of the thesis are shown.

1.1 The nonlinear Klein-Gordon equation

The Schrödinger equation is a linear partial differential equation describing the wave function of a quantum system such as atomic, molecular and subatomic systems [24, 127, 142]. In quantum mechanics, the Schrödinger equation plays the important role as the Newton's second law in classical mechanics. However, it could not be used when the particles travel at high velocity so that special relativity should be applied with quantum mechanics together. In 1926, the Klein-Gordon equation was proposed by the physicists Oskar Klein and Walter Gordon to describe the motion of spinless particles like the pion [25, 39, 124, 128, 161]. Denoting by $m > 0$ the mass of particle, c the speed of light and $\hbar$ the Planck constant, the Klein-Gordon equation is

$$\frac{\hbar^2}{mc^2}\partial_{tt}u(\mathbf{x},t) - \frac{\hbar^2}{m}\Delta u(\mathbf{x},t) + mc^2 u(\mathbf{x},t) = 0, \quad \mathbf{x} \in \mathbb{R}^d, \quad t > 0, \tag{1.1.1}$$

where t is time, $\mathbf{x}$ is the spatial coordinate, $u = u(\mathbf{x},t)$ is a complex-valued scalar field. The wave function needs to be a complex scalar when it describes charged particles, while it is enough to be a real scalar for neutral particles [117]. The Klein-Gordon equation can be expressed as the form of a Schrödinger equation which includes two coupled differential equations and each of them is first order in time. The Klein-Gordon equation is Lorentz covariant while the Schrödinger equation is not [135].

In the relativistic regime, i.e. the speed of light $c = 1$, taking the units $\hbar = m = 1$, we have the following dimensionless Klein-Gordon equation

$$\partial_{tt}u(\mathbf{x}, t) - \Delta u(\mathbf{x}, t) + u(\mathbf{x}, t) = 0, \quad \mathbf{x} \in \mathbb{R}^d, \quad t > 0. \tag{1.1.2}$$

The Klein-Gordon equation (1.1.2) admits the plane wave solution $u(\mathbf{x}, t) = Ae^{i(\boldsymbol{\xi}\cdot\mathbf{x}-\omega t)}$ with the amplitude A, spatial wave number $\boldsymbol{\xi} = (\xi_1, \cdots, \xi_d)^T \in \mathbb{R}^d$ and time frequency $\omega = \omega(\boldsymbol{\xi})$ satisfying the following dispersion relation [22, 90, 107, 157, 163]:

$$\omega = \omega(\boldsymbol{\xi}) = \pm\sqrt{1 + |\boldsymbol{\xi}|^2}, \quad \boldsymbol{\xi} \in \mathbb{R}^d. \tag{1.1.3}$$

The nonlinear Klein-Gordon equation (NKGE) is the relativistic and nonlinear version of the Schrödinger equation and widely used to model many types of phenomena including nonlinear optics, charge density waves, the behavior of elementary particles and the propagation of dislocations in crystals [23, 68, 70, 126, 153, 158, 164]. The NKGE in d dimensions ($d = 1, 2, 3$) reads [105, 106, 108, 148]

$$\frac{\hbar^2}{mc^2}\partial_{tt}u(\mathbf{x}, t) - \frac{\hbar^2}{m}\Delta u(\mathbf{x}, t) + mc^2u(\mathbf{x}, t) + f(u(\mathbf{x}, t)) = 0, \quad \mathbf{x} \in \mathbb{R}^d, \quad t > 0, \tag{1.1.4}$$

where $f(u) : \mathbb{C} \to \mathbb{C}$ is a given gauge invariant function independent of c and m, describing the nonlinear interaction and satisfies [8, 56, 124, 140]

$$f(e^{is}u) = e^{is}f(u), \quad \forall s \in \mathbb{R}. \tag{1.1.5}$$

In most applications and theoretical studies in the literature [56, 62, 104, 114, 126, 129, 150], $f(u)$ is taken as the pure power nonlinearity, i.e.

$$f(u) = g(|u|^2)u, \text{ with } g(\rho) = \lambda\rho^p \text{ for some } \lambda \in \mathbb{R}, \ p \in \mathbb{N}_0 := \mathbb{N} \cup \{0\}. \tag{1.1.6}$$

In particular, when $f(u) = \lambda u^3$, the equation is called ϕ^4-nonlinear Klein-Gordon equation (ϕ^4-model) arising in quantum field theory with the dimensionless coupling constant λ and has various applications in condensed matter physics. In a quantum field theory, if λ is much smaller than 1, the theory is said to be weakly coupled. The

ϕ^4-model can be used to describe the structural phase transitions in ferroelectric or ferromagnetic materials and interpret the displacive and order-disorder systems [125]. The kink solutions are related to the motion of the topological excitations in linear polymeric chains such as polyacetylene [29, 49].

In order to study the dynamics of the NKGE (1.1.4), the initial data is usually taken as

$$u(\mathbf{x}, 0) = \phi(\mathbf{x}), \quad \partial_t u(\mathbf{x}, 0) = \gamma(\mathbf{x}), \quad \mathbf{x} \in \mathbb{R}^d. \tag{1.1.7}$$

Similar to the linear case, in the relativistic regime, we have the following dimensionless NKGE [85, 121, 138]:

$$\begin{cases} \partial_{tt} u(\mathbf{x}, t) - \Delta u(\mathbf{x}, t) + u(\mathbf{x}, t) + f(u(\mathbf{x}, t)) = 0, \quad \mathbf{x} \in \mathbb{R}^d, \quad t > 0, \\ u(\mathbf{x}, 0) = \phi(\mathbf{x}), \quad \partial_t u(\mathbf{x}, 0) = \gamma(\mathbf{x}), \quad \mathbf{x} \in \mathbb{R}^d. \end{cases} \tag{1.1.8}$$

We remark here that when the initial data $\phi(\mathbf{x}), \gamma(\mathbf{x}) : \mathbb{R}^d \to \mathbb{R}$ and $f(u) : \mathbb{R} \to \mathbb{R}$, the solution $u(\mathbf{x}, t)$ is real-valued. In this case, the gauge invariant condition (1.1.5) is not necessary [8, 56, 108]. Thus, the classical NKGE with the real-valued solution is a special case of the NKGE (1.1.8) [8, 47, 52, 56, 113, 129, 134]. The NKGE (1.1.8) is time symmetric or time reversible, i.e., with $t \to -t$, $u(\mathbf{x}, -t)$ is still the solution of the NKGE (1.1.8). In addition, if $u(\cdot, t) \in H^1(\mathbb{R}^d)$ and $\partial_t u(\cdot, t) \in L^2(\mathbb{R}^d)$, for $f(u) = g(|u|^2)u$ with $g(\cdot)$ a real-valued function, it also conserves the energy [85, 151, 153]:

$$\begin{aligned} E(t) &:= \int_{\mathbb{R}^d} \left[|\partial_t u(\mathbf{x}, t)|^2 + |\nabla u(\mathbf{x}, t)|^2 + |u(\mathbf{x}, t)|^2 + F(|u(\mathbf{x}, t)|^2) \right] d\mathbf{x} \\ &\equiv \int_{\mathbb{R}^d} \left[|\gamma(\mathbf{x})|^2 + |\nabla \phi(\mathbf{x})|^2 + |\phi(\mathbf{x})|^2 + F(|\phi(\mathbf{x})|^2) \right] d\mathbf{x} \\ &= E(0), \quad t \geq 0, \end{aligned} \tag{1.1.9}$$

with $F(\rho) := \int_0^\rho g(s) ds$.

1.2 Comparisons of different scalings

In this section, we compare different scalings of the complex NKGE with the nonlinearity $f(u) = |u|^2 u$.

In the weakly nonlinear regime, we have the following dimensionless NKGE [37, 43, 44, 71]

$$\begin{cases}\partial_{tt}u(\mathbf{x},t)-\Delta u(\mathbf{x},t)+u(\mathbf{x},t)+\varepsilon^2|u(\mathbf{x},t)|^2u(\mathbf{x},t)=0, \quad \mathbf{x}\in\mathbb{R}^d, \quad t>0,\\ u(\mathbf{x},0)=\phi(\mathbf{x}), \quad \partial_t u(\mathbf{x},0)=\gamma(\mathbf{x}), \quad \mathbf{x}\in\mathbb{R}^d.\end{cases} \tag{1.2.1}$$

Here, the strength of the nonlinearity is characterized by ε^2 with $\varepsilon\in(0,1]$ a dimensionless parameter. Formally, the amplitude of the solution $u(\mathbf{x},t)$ is at $O(1)$. In addition, under proper regularity of the solution, the complex NKGE (1.2.1) is time symmetric or time reversible and conserves the energy [9, 13, 47] as

$$\begin{aligned}E_1(t):=E_1(u(\cdot,t))&=\int_{\mathbb{R}^d}\left[|\partial_t u(\mathbf{x},t)|^2+|\nabla u(\mathbf{x},t)|^2+|u(\mathbf{x},t)|^2+\frac{\varepsilon^2}{2}|u(\mathbf{x},t)|^4\right]d\mathbf{x}\\ &\equiv\int_{\mathbb{R}^d}\left[|\gamma(\mathbf{x})|^2+|\nabla\phi(\mathbf{x})|^2+|\phi(\mathbf{x})|^2+\frac{\varepsilon^2}{2}|\phi(\mathbf{x})|^4)\right]d\mathbf{x}\\ &=E_1(0)=O(1), \quad t\ge 0.\end{aligned}$$

Plugging the plane wave solution $u(\mathbf{x},t)=Ae^{i(\boldsymbol{\xi}\cdot\mathbf{x}-\omega_1 t)}$ (with A the amplitude, $\boldsymbol{\xi}$ the spatial wave number and $\omega_1:=\omega_1(\boldsymbol{\xi})$ the time frequency) into the complex NKGE (1.2.1), we get the dispersion relation:

$$\omega_1=\omega_1(\boldsymbol{\xi})=\pm\sqrt{1+|\boldsymbol{\xi}|^2+\varepsilon^2A^2}=O(1), \qquad \boldsymbol{\xi}\in\mathbb{R}^d, \tag{1.2.2}$$

which immediately implies the group velocity [74, 123, 151]

$$\mathbf{v}_1:=\mathbf{v}_1(\boldsymbol{\xi})=\nabla\omega_1(\boldsymbol{\xi})=\pm\frac{\boldsymbol{\xi}}{\sqrt{1+|\boldsymbol{\xi}|^2+\varepsilon^2A^2}}=O(1). \tag{1.2.3}$$

Thus, the solution of the complex NKGE (1.2.1) propagates waves with amplitude at $O(1)$, wavelength in space and time at $O(1)$ and wave velocity at $O(1)$. To illustrate this, Figure 1.1 depicts the solutions of the NKGE (1.2.1) with different ε in 1D.

In fact, by introducing $w(\mathbf{x},t)=\varepsilon u(\mathbf{x},t)$, we can reformulate the NKGE (1.2.1) with weak nonlinearity (and initial data with amplitude at $O(1)$) into the following complex NKGE with small initial data (and $O(1)$ nonlinearity strength):

$$\begin{cases}\partial_{tt}w(\mathbf{x},t)-\Delta w(\mathbf{x},t)+w(\mathbf{x},t)+|w(\mathbf{x},t)|^2w(\mathbf{x},t)=0, \quad \mathbf{x}\in\mathbb{R}^d, \quad t>0,\\ w(\mathbf{x},0)=\varepsilon\phi(\mathbf{x}), \quad \partial_t w(\mathbf{x},0)=\varepsilon\gamma(\mathbf{x}), \quad \mathbf{x}\in\mathbb{R}^d.\end{cases} \tag{1.2.4}$$

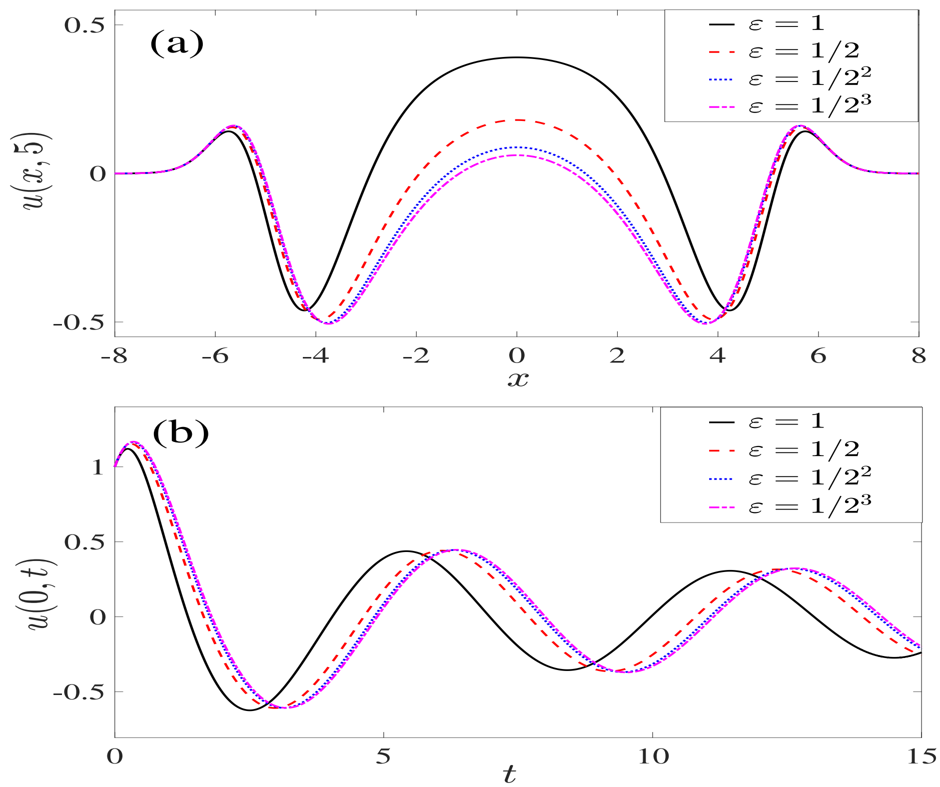

Figure 1.1: The solutions of the NKGE (1.2.1) with $d = 1$ and initial data $\phi(x) = e^{-x^2}$ and $\gamma(x) = \text{sech}(x^2)$ for different ε: (a) $u(x, 5)$, (b) $u(0, t)$.

Noticing that the amplitude of the initial data in (1.2.4) is at $O(\varepsilon)$, formally we can get the amplitude of the solution $w(\mathbf{x}, t)$ of NKGE (1.2.4) is at $O(\varepsilon)$, too. Similarly, the complex NKGE (1.2.4) is time symmetric or time reversible and conserves the energy as

$$\begin{aligned}
E_2(t) &:= E_2(\omega(\cdot, t)) = \int_{\mathbb{R}^d} \left[|\partial_t w(\mathbf{x}, t)|^2 + |\nabla w(\mathbf{x}, t)|^2 + |w(\mathbf{x}, t)|^2 + \frac{1}{2}|w(\mathbf{x}, t)|^4 \right] d\mathbf{x} \\
&\equiv \int_{\mathbb{R}^d} \left[|\varepsilon\gamma(\mathbf{x})|^2 + |\varepsilon\nabla\phi(\mathbf{x})|^2 + |\varepsilon\phi(\mathbf{x})|^2 + \frac{1}{2}|\varepsilon u_0(\mathbf{x})|^4 \right] d\mathbf{x} \\
&= \varepsilon^2 \int_{\mathbb{R}^d} \left[|\gamma(\mathbf{x})|^2 + |\nabla\phi(\mathbf{x})|^2 + |\phi(\mathbf{x})|^2 + \frac{\varepsilon^2}{2}|\phi(\mathbf{x})|^4 \right] d\mathbf{x} \\
&= E_2(0) = \varepsilon^2 E_1(0) = O(\varepsilon^2), \quad t \geq 0.
\end{aligned}$$

In addition, plugging the plane wave solution $\omega(\mathbf{x}, t) = \varepsilon A e^{i(\boldsymbol{\xi}\cdot\mathbf{x} - \omega_1 t)}$ into the complex NKGE (1.2.4), we get the same dispersion relation (1.2.2) and the same group velocity (1.2.3) of the complex NKGE (1.2.1), i.e., the complex NKGEs (1.2.4) and (1.2.1) share the same dispersion relation (1.2.2) and the same group velocity (1.2.3). Again, the solution of the complex NKGE (1.2.4) propagates waves with amplitude at $O(\varepsilon)$, wavelength in space and time at $O(1)$ and wave velocity at $O(1)$. Figure 1.2 shows the solutions of the NKGE (1.2.4) with different ε in 1D.

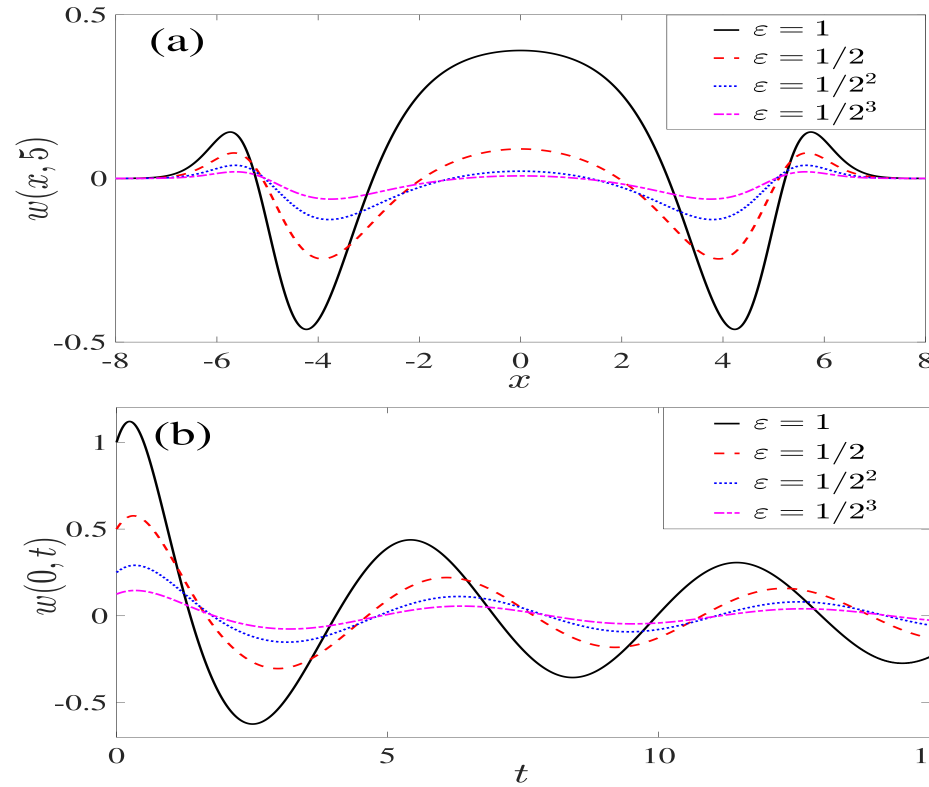

Figure 1.2: The solutions of the NKGE (1.2.4) with $d = 1$ and initial data $\phi(x) = e^{-x^2}$ and $\gamma(x) = \mathrm{sech}(x^2)$ for different ε: (a) $w(x, 5)$, (b) $w(0, t)$.

Introducing a re-scale in time

$$t = \frac{s}{\varepsilon^{\beta}} \Leftrightarrow s = \varepsilon^{\beta} t, \quad v(\mathbf{x}, s) = u(\mathbf{x}, t), \tag{1.2.5}$$

with $0 < \beta \leq 2$ fixed, we can reformulate the NKGE (1.2.1) into the following oscillatory complex NKGE [13, 22, 57, 58]:

$$\begin{cases} \partial_{ss} v(\mathbf{x}, s) + \dfrac{1}{\varepsilon^{2\beta}} \left(-\Delta + 1\right) v(\mathbf{x}, s) + \dfrac{|v(\mathbf{x}, s)|^2}{\varepsilon^{2\beta-2}} v(\mathbf{x}, s) = 0, \ \mathbf{x} \in \mathbb{R}^d, \ s > 0, \\ v(\mathbf{x}, 0) = \phi(\mathbf{x}), \quad \partial_s v(\mathbf{x}, 0) = \dfrac{1}{\varepsilon^{\beta}} \gamma(\mathbf{x}), \quad \mathbf{x} \in \mathbb{R}^d. \end{cases} \tag{1.2.6}$$

Formally, the amplitude of the solution $v(\mathbf{x}, t)$ of the oscillatory complex NKGE (1.2.6) is at $O(1)$. The oscillatory complex NKGE (1.2.6) is also time symmetric or time reversible and conserves the energy as

$$
\begin{aligned}
E_3(s) &:= E_3(v(\cdot,s)) = \int_{\mathbb{R}^d}\left[|\partial_s v|^2 + \frac{1}{\varepsilon^{2\beta}}(|\nabla v|^2 + |v(\mathbf{x},t)|^2) + \frac{1}{2\varepsilon^{2\beta-2}}|v|^4\right]d\mathbf{x}\\
&\equiv \frac{1}{\varepsilon^{2\beta}}\int_{\mathbb{R}^d}\left[|\gamma(\mathbf{x})|^2 + |\nabla\phi(\mathbf{x})|^2 + |\phi(\mathbf{x})|^2 + \frac{\varepsilon^2}{2}|\phi(\mathbf{x})|^4)\right]d\mathbf{x}\\
&= E_3(0) = \frac{1}{\varepsilon^{2\beta}}E_1(0) = O(\varepsilon^{-2\beta}), \quad s \geq 0.
\end{aligned}
$$

Again, plugging the plane wave solution $v(\mathbf{x},s) = Ae^{i(\boldsymbol{\xi}\cdot\mathbf{x}-\omega_2 s)}$ into the oscillatory complex NKGE (1.2.6), we get the dispersion relation:

$$
\omega_2 = \omega_2(\boldsymbol{\xi}) = \pm\frac{1}{\varepsilon^{\beta}}\sqrt{1+|\boldsymbol{\xi}|^2+\varepsilon^2A^2} = O(\varepsilon^{-\beta}), \quad \boldsymbol{\xi}\in\mathbb{R}^d, \tag{1.2.7}
$$

which immediately implies the group velocity

$$
\mathbf{v}_2 := \mathbf{v}_2(\boldsymbol{\xi}) = \nabla\omega_2(\boldsymbol{\xi}) = \pm\frac{\boldsymbol{\xi}}{\varepsilon^{\beta}\sqrt{1+|\boldsymbol{\xi}|^2+\varepsilon^2A^2}} = O(\varepsilon^{-\beta}). \tag{1.2.8}
$$

Thus, the solution of the complex NKGE (1.2.6) propagates waves with amplitude at $O(1)$, wavelength in space and time at $O(1)$ and $O(\varepsilon^{\beta})$, respectively, and wave velocity at $O(\varepsilon^{-\beta})$. Figure 1.3 depicts the solutions of the NKGE (1.2.6) with different ε in 1D to give an intuitive understanding of the oscillatory nature and the outgoing waves.

Similarly, introducing another re-scale in time and space

$$
t = \frac{s}{\varepsilon^{\beta}} \Leftrightarrow s = \varepsilon^{\beta}t, \qquad \mathbf{x} = \frac{\mathbf{y}}{\varepsilon^{\beta}} \Leftrightarrow \mathbf{y} = \varepsilon^{\beta}\mathbf{x}, \qquad w(\mathbf{y},s) = u(\mathbf{x},t), \tag{1.2.9}
$$

with $0 < \beta \leq 2$ fixed, we can reformulate the NKGE (1.2.1) into the following oscillatory complex NKGE

$$
\begin{cases}
\partial_{ss}w(\mathbf{y},s) + \left(-\Delta + \frac{1}{\varepsilon^{2\beta}}\right)w(\mathbf{y},s) + \frac{|w(\mathbf{y},s)|^2}{\varepsilon^{2\beta-2}}w(\mathbf{y},s) = 0, \ \mathbf{y}\in\mathbb{R}^d, \ s>0,\\
w(\mathbf{y},0) = \phi(\frac{\mathbf{y}}{\varepsilon^{\beta}}), \quad \partial_s w(\mathbf{y},0) = \frac{1}{\varepsilon^{\beta}}\gamma(\frac{\mathbf{y}}{\varepsilon^{\beta}}), \quad \mathbf{y}\in\mathbb{R}^d.
\end{cases} \tag{1.2.10}
$$

Formally, the amplitude of the solution $w(\mathbf{y},s)$ of the oscillatory complex NKGE (1.2.10) is at $O(1)$. Also, the oscillatory complex NKGE (1.2.10) is time symmetric or time reversible and conserves the energy as

$$
\begin{aligned}
E_4(s) &:= E_4(w(\cdot,s)) = \int_{\mathbb{R}^d}\left[|\partial_s w|^2 + |\nabla w|^2 + \frac{1}{\varepsilon^{2\beta}}|w(\mathbf{x},t)|^2 + \frac{1}{2\varepsilon^{2\beta-2}}|w|^4\right]d\mathbf{x}\\
&\equiv \varepsilon^{(d-2)\beta}\int_{\mathbb{R}^d}\left[|\gamma(\mathbf{x})|^2 + |\nabla\phi(\mathbf{x})|^2 + |\phi(\mathbf{x})|^2 + \frac{\varepsilon^2}{2}|\phi(\mathbf{x})|^4)\right]d\mathbf{x}\\
&= E_4(0) = \varepsilon^{(d-2)\beta}E_1(0) = O(\varepsilon^{(d-2)\beta}), \quad s\geq 0.
\end{aligned}
$$

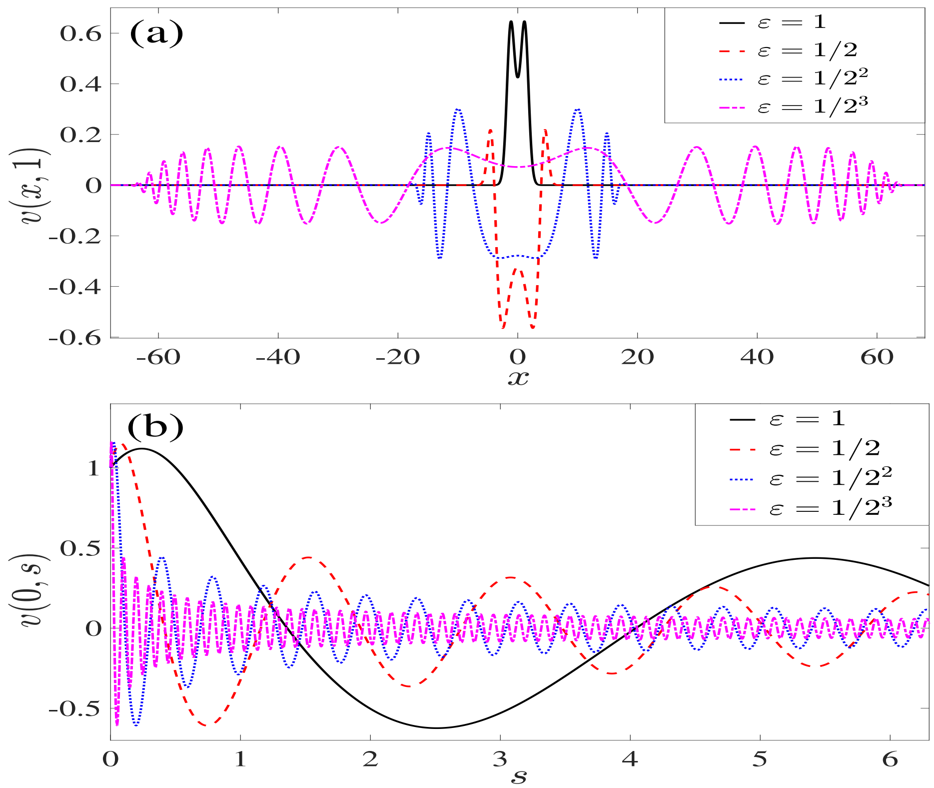

Figure 1.3: The solutions of the NKGE (1.2.6) with $d = 1$ and initial data $\phi(x) = e^{-x^2}$ and $\gamma(x) = \mathrm{sech}(x^2)$ for different ε: (a) $v(x, 1)$, (b) $v(0, s)$.

Again, plugging the plane wave solution $w(\mathbf{y}, s) = Ae^{i(\boldsymbol{\xi}\cdot\mathbf{y}/\varepsilon^\beta - \omega_3 s)}$ into the oscillatory complex NKGE (1.2.10), we get the same dispersion relation:

$$\omega_3 = \omega_3(\boldsymbol{\xi}) = \pm\frac{1}{\varepsilon^\beta}\sqrt{1 + |\boldsymbol{\xi}|^2 + \varepsilon^2 A^2} = O(\varepsilon^{-\beta}), \quad \boldsymbol{\xi} \in \mathbb{R}^d, \tag{1.2.11}$$

which immediately implies the group velocity

$$\mathbf{v}_3 := \mathbf{v}_3(\boldsymbol{\xi}) = \nabla\omega_3(\boldsymbol{\xi}) = \pm\frac{\boldsymbol{\xi}}{\varepsilon^\beta\sqrt{1 + |\boldsymbol{\xi}|^2 + \varepsilon^2 A^2}} = O(\varepsilon^{-\beta}). \tag{1.2.12}$$

Thus, the solution of the complex NKGE (1.2.10) propagates waves with amplitude at $O(1)$, wavelength in space and time at $O(\varepsilon^\beta)$ and wave velocity at $O(\varepsilon^{-\beta})$. Of course, in this scaling, one has to consider the initial data with spatial wavelength at $O(\varepsilon^\beta)$. Figure 1.4 depicts the solutions of the NKGE (1.2.10) with different ε in 1D.

We also compare the above scalings of the NKGE with the complex NKGE in the nonrelativistic limit regime, i.e. $c \gg 1$, which has been widely used and studied in the

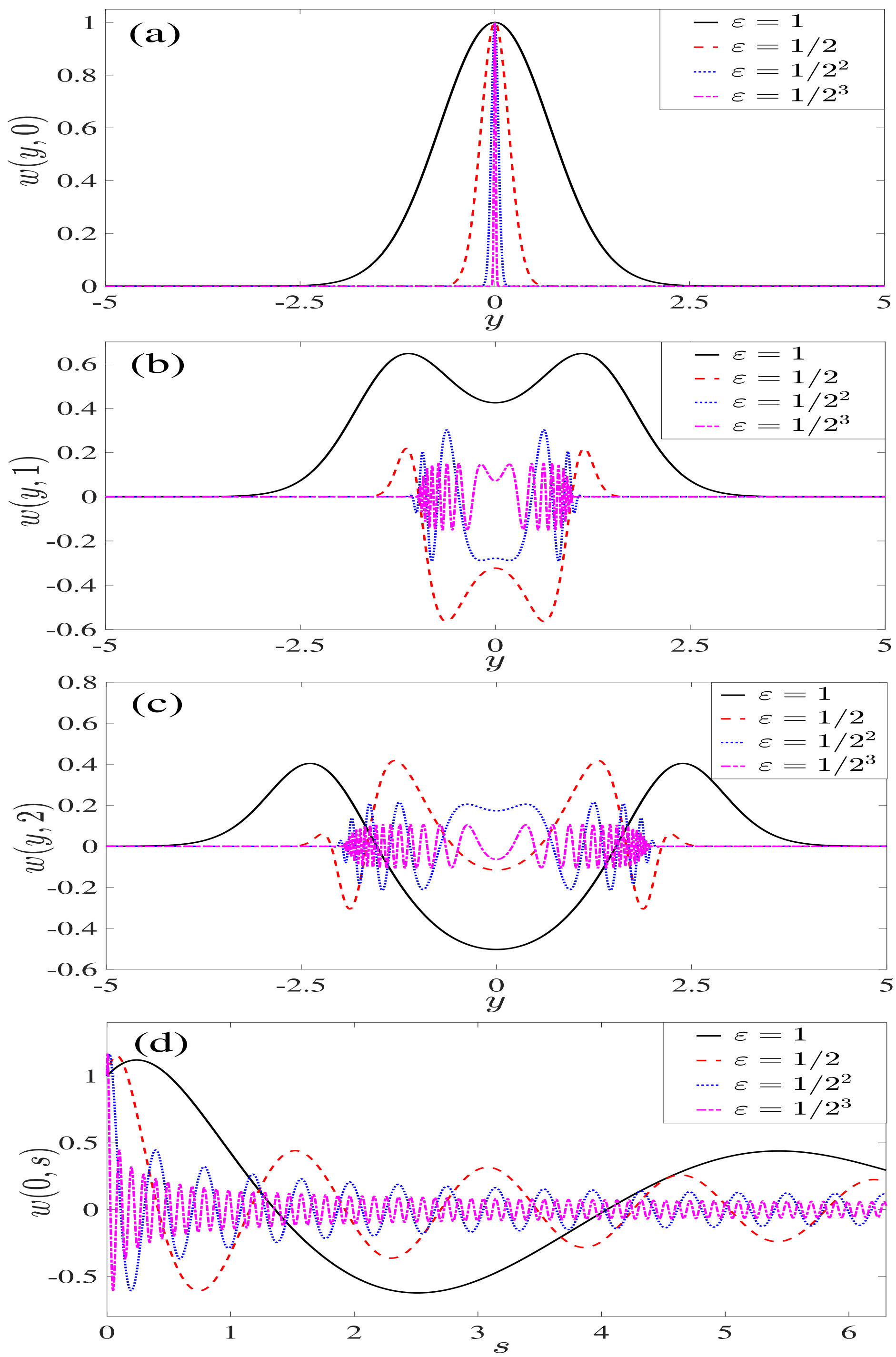

Figure 1.4: The solutions of the NKGE (1.2.10) with $d = 1$ and initial data $\phi(x) = e^{-x^2}$ and $\gamma(x) = \text{sech}(x^2)$ for different ε: (a) $w(y, 0)$, (b) $w(y, 1)$, (c) $w(y, 2)$, (d) $w(0, s)$.

literature [22, 33, 56, 104, 105, 106]. Introducing the dimensionless variables in (1.1.4): $t \to \frac{\hbar}{m\varepsilon^2 c^2} t$ and $\mathbf{x} \to \frac{\hbar}{m\varepsilon c}\mathbf{x}$, we can obtain the following dimensionless NKGE

$$\begin{cases} \partial_{tt} u(\mathbf{x},t) - \dfrac{1}{\varepsilon^2}\Delta u(\mathbf{x},t) + \dfrac{1}{\varepsilon^4} u(\mathbf{x},t) + \dfrac{|u(\mathbf{x},t)|^2}{\varepsilon^2} u(\mathbf{x},t) = 0, \ \mathbf{x} \in \mathbb{R}^d, \ t > 0, \\ u(\mathbf{x},0) = \phi(\mathbf{x}), \quad \partial_t u(\mathbf{x},0) = \dfrac{1}{\varepsilon^2}\gamma(\mathbf{x}), \quad \mathbf{x} \in \mathbb{R}^d, \end{cases} \tag{1.2.13}$$

where the dimensionless parameter $0 < \varepsilon \le 1$ is inversely proportional to the speed of light c. The complex NKGE also conserves the energy as

$$\begin{aligned} E_5(t) := E_5(u(\cdot,t)) &= \int_{\mathbb{R}^d} \left[|\partial_t u(\mathbf{x},t)|^2 + \frac{1}{\varepsilon^2}|\nabla u(\mathbf{x},t)|^2 + \frac{1}{\varepsilon^4}|u(\mathbf{x},t)|^2 + \frac{1}{2\varepsilon^2}|u(\mathbf{x},t)|^4 \right] d\mathbf{x} \\ &\equiv \frac{1}{\varepsilon^4}\int_{\mathbb{R}^d} \left[|\gamma(\mathbf{x})|^2 + \varepsilon^2 |\nabla \phi(\mathbf{x})|^2 + |\phi(\mathbf{x})|^2 + \frac{\varepsilon^2}{2}|\phi(\mathbf{x})|^4) \right] d\mathbf{x} \\ &= E_5(0) = O(\varepsilon^{-4}), \quad t \ge 0. \end{aligned}$$

Plugging the plane wave solution $u(\mathbf{x},t) = Ae^{i(\boldsymbol{\xi}\cdot\mathbf{x} - \omega_4 t)}$ into the oscillatory complex NKGE (1.2.13), we get the dispersion relation:

$$\omega_4 = \omega_4(\boldsymbol{\xi}) = \pm\frac{1}{\varepsilon^2}\sqrt{1 + \varepsilon^2|\boldsymbol{\xi}|^2 + \varepsilon^2 A^2} = O(\varepsilon^{-2}), \quad \boldsymbol{\xi} \in \mathbb{R}^d, \tag{1.2.14}$$

which immediately implies the group velocity

$$\mathbf{v}_4 := \mathbf{v}_4(\boldsymbol{\xi}) = \nabla\omega_4(\boldsymbol{\xi}) = \pm\frac{\boldsymbol{\xi}}{\sqrt{1 + \varepsilon^2|\boldsymbol{\xi}|^2 + \varepsilon^2 A^2}} = O(1). \tag{1.2.15}$$

Thus, the solution of the complex NKGE (1.2.13) propagates waves with amplitude at $O(1)$, wavelength in space and time at $O(1)$ and $O(\varepsilon^2)$, respectively, and wave velocity at $O(1)$. Figure 1.5 shows the solutions of the NKGE (1.2.13) with different ε in 1D.

For convenience, we show the properties of the solution of the complex NKGE under different scalings in Table 1.1.

1.3 Review of existing results

The nonlinear Klein-Gordon equation (NKGE) in different scalings has gained a surge of attentions in both analytical and numerical aspects. In this section, we are going to review the existing results.

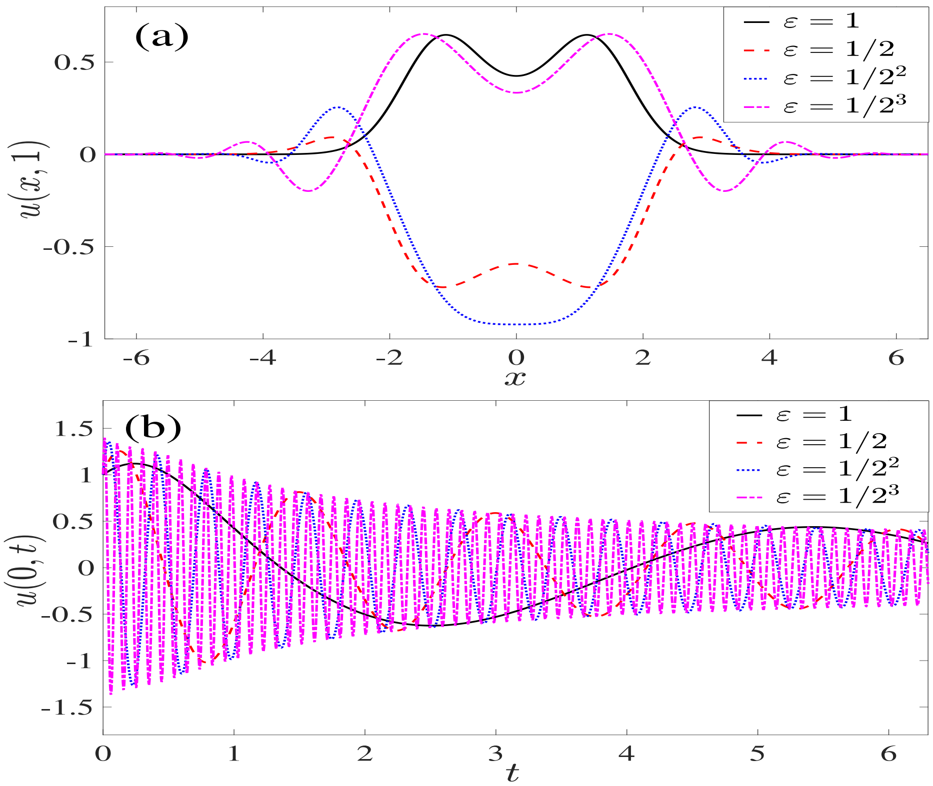

Figure 1.5: The solutions $u(x,1)$ and $u(0,t)$ of the NKGE (1.2.13) with $d = 1$ and initial data $\phi(x) = e^{-x^2}$ and $\gamma(x) = \mathrm{sech}(x^2)$ for different ε: (a) $u(x,1)$, (b) $u(0,t)$.

	(1.2.1)	(1.2.4)	(1.2.6) with $\beta = 2$	(1.2.10) with $\beta = 2$	(1.2.13)
amplitude	$O(1)$	$O(\varepsilon)$	$O(1)$	$O(1)$	$O(1)$
spatial wavelength	$O(1)$	$O(1)$	$O(1)$	$O(\varepsilon^2)$	$O(1)$
temporal wavelength	$O(1)$	$O(1)$	$O(\varepsilon^2)$	$O(\varepsilon^2)$	$O(\varepsilon^2)$
wave velocity	$O(1)$	$O(1)$	$O(\varepsilon^{-2})$	$O(\varepsilon^{-2})$	$O(1)$
energy	$O(1)$	$O(\varepsilon^2)$	$O(\varepsilon^{-4})$	$O(\varepsilon^{2d-4})$	$O(\varepsilon^{-4})$
life-span	$O(\varepsilon^{-2})$	$O(\varepsilon^{-2})$	$O(1)$	$O(1)$	$O(1)$

Table 1.1: Comparisons of the complex NKGE under different scalings.

For the relativistic regime ($O(1)$ - speed of light), the Cauchy problem was studied in the literature [1, 27, 62, 63, 89, 120, 132, 134]. The global existence of the solution and asymptotic behavior of the NKGE with various kinds of nonlinearity were investigated [82, 101, 114, 139]. The solution globally exists for the defocusing case ($F(u) \geq 0$) while it blows up in possible finite time for the focusing case ($F(u) \leq 0$) [1, 27, 87, 116]. For more scattering results, one can refer to [28, 112, 113, 115, 122, 137] and references therein. For the numerical aspect, different numerical schemes were proposed and analyzed [85, 121], including the finite difference time domain (FDTD) methods [9, 48, 95, 138], finite element method [149], radial basis function methods [40, 41] and spectral method [30, 69, 160].

In the nonrelativistic limit regime, i.e. $0 < \varepsilon \ll 1$, the analysis of the NKGE (1.2.13) is complicated due to the unbounded energy $E_5(t)$ when $\varepsilon \to 0$. The nonrelativistic limit of the Cauchy problem was studied in different spaces. The analytical results show that the solution converges to the corresponding solution of the nonlinear Schrödinger equation and propagates waves with wavelength $O(1)$ and $O(\varepsilon^2)$ in space and time, respectively [104, 106, 108, 150]. Along the numerical front, the highly oscillatory nature in time makes the numerical approximations in the nonrelativistic regime extremely challenging [9, 56]. The classical numerical schemes require severe time step restrictions depending on the small parameter ε, including the FDTD methods, exponential wave integrator Fourier pseudospectral (EWI-FP) method, time-splitting Fourier pseudospectral (TSFP) method and asymptotic preserving (AP) method [9, 47, 56, 64, 156]. Based on the analysis of the above numerical methods, in order to obtain the "correct" solution of the NKGE (1.2.13), there are some requirements on the mesh size and time step. Recently, different uniformly accurate numerical methods have been proposed and analyzed for the NKGE in the nonrelativistic limit regime, including the multiscale time integrator (MTI) method [8, 19, 20], the two-scale formulation (TSF) method [21, 32] and two uniformly and optimally accurate (UOA) methods [22, 119].

In the weakly nonlinear regime, there are extensive analytical results in the literature for the NKGE (1.2.1) (or (1.2.4)). For the existence of global classical solutions and almost periodic solutions as well as asymptotic behavior of solutions, we refer to [3, 26, 35, 50, 80, 100, 154, 152] and references therein. For the Cauchy problem with small initial data (or weak nonlinearity), the global existence and asymptotic behavior of solutions were studied in different space dimensions and with different nonlinear terms [76, 88, 89, 97, 118, 148, 168]. By the techniques of Birkhoff normal forms and modulated Fourier expansions in time, the long-time behaviors have been investigated including the conservation of energy, momentum and the harmonic actions [2, 37, 52, 53, 54, 60]. Recently, more attentions have been devoted to analyzing the life-span of the solutions to the NKGE (1.2.4) [42, 88, 97, 99]. The analytical results indicate that the life-span of a smooth solution to the NKGE (1.2.4) (or (1.2.1)) is at least up to time at $O(\varepsilon^{-2})$ [43, 44, 96, 167]. For more details related to this topic, we refer to [45, 51, 75, 83, 96, 164, 166] and references therein.

1.4 Problems to study

There are two different dynamical problems related to the time evolution of the NKGE (1.2.1) (or (1.2.4)): (i) when $\varepsilon = \varepsilon_0$ (e.g. $\varepsilon = 1$) fixed, i.e. in the standard nonlinearity strength regime, to study the finite time dynamics of (1.2.1) (or (1.2.4)) for $t \in [0, T]$ with $T = O(1)$; and (ii) when $0 < \varepsilon \ll 1$, i.e. in the weak nonlinearity strength regime, to study the long-time dynamics of (1.2.1) (or (1.2.4)) for $t \in [0, T_\varepsilon]$ with $T_\varepsilon = O(\varepsilon^{-2})$. Extensive analytical and numerical studies have been done in the literature for the finite time dynamics of (1.2.1) with $\varepsilon = 1$, i.e. in the standard nonlinearity strength regime. As is pointed out in the previous section, in the weak nonlinearity strength regime, the analytical results show that the life-span of a smooth solution to the NKGE (1.2.1) is at least up to the time at $O(\varepsilon^{-2})$. However, to the best of our knowledge, there are very few numerical analysis results on the error bounds of different numerical methods for the the long-time dynamics of the NKGE (1.2.1) in the literature, especially the error bounds up to the time at $T_\varepsilon = O(\varepsilon^{-2})$ and how the error bounds depend explicitly on the mesh size h and time step τ as well as the small parameter $\varepsilon \in (0, 1]$. This motivates us to establish the long-time error estimates of different numerical methods for solving the NKGE (1.2.1).

We consider the following NKGE with a cubic nonlinearity on the unit torus $\mathbb{T}^d$ $(d = 1, 2, 3)$ as

$$\begin{cases} \partial_{tt} u(\mathbf{x}, t) - \Delta u(\mathbf{x}, t) + u(\mathbf{x}, t) + \varepsilon^2 u^3(\mathbf{x}, t) = 0, \quad \mathbf{x} \in \mathbb{T}^d, \quad t > 0, \\ u(\mathbf{x}, 0) = \phi(\mathbf{x}), \quad \partial_t u(\mathbf{x}, 0) = \gamma(\mathbf{x}), \quad \mathbf{x} \in \mathbb{T}^d, \end{cases} \tag{1.4.1}$$

where $u := u(\mathbf{x}, t)$ is a real-valued scalar field, $\varepsilon \in (0, 1]$ is a dimensionless parameter used to characterize the nonlinearity strength, and the initial data $\phi(\mathbf{x})$ and $\gamma(\mathbf{x})$ are two given real-valued functions which are independent of the parameter ε. In addition, if $u(\cdot, t) \in H^1(\mathbb{T}^d)$ and $\partial_t u(\cdot, t) \in L^2(\mathbb{T}^d)$, the NKGE (1.4.1) is time symmetric or time reversible and conserves the energy [37, 72, 110] as

$$\begin{aligned} E(t) &:= \int_{\mathbb{T}^d} \left[|\partial_t u(\mathbf{x}, t)|^2 + |\nabla u(\mathbf{x}, t)|^2 + |u(\mathbf{x}, t)|^2 + \frac{\varepsilon^2}{2} |u(\mathbf{x}, t)|^4 \right] d\mathbf{x} \\ &\equiv \int_{\mathbb{T}^d} \left[|\gamma(\mathbf{x})|^2 + |\nabla \phi(\mathbf{x})|^2 + |\phi(\mathbf{x})|^2 + \frac{\varepsilon^2}{2} |\phi(\mathbf{x})|^4 \right] d\mathbf{x} \\ &= E(0) = O(1), \quad t \geq 0. \end{aligned}$$

Specifically, the purpose of the study is to carry out the error bounds of different numerical methods for the NKGE (1.4.1) up to the time at $O(\varepsilon^{-2})$ and investigate how the error bounds depend explicitly on the mesh size h and time step τ as well as the small parameter $\varepsilon \in (0, 1]$. We aim to prove the error estimates rigorously and validate them through numerical examples.

1.5 Scope of the thesis

The thesis is organized as follows.

Chapter 2 focuses on the finite difference temporal discretization to study the long-time dynamics of the NKGE (1.4.1). The explicit/semi-implicit/implicit finite difference discretizations in time combined with different spatial discretizations are applied to solve the NKGE (1.4.1) in the long-time regime. For the finite difference time domain (FDTD) methods, fourth-order compact finite difference (4cFD) method and finite difference Fourier pseudospectral (FDFP) method, we analyze their properties of the stability, energy conservation and solvability. The error bounds of these finite difference methods are rigorously proved up to the time at $O(\varepsilon^{-\beta})$ with $0 \leq \beta \leq 2$ and spatial/temporal resolutions for the NKGE (1.4.1) are inferred in the long-time regime. Numerical results are carried out to support the error estimates and comparisons of different spatial discretizations are presented.

In Chapter 3, the exponential wave integrator (EWI) with the Gautschi-type quadrature is adapted to discretize the NKGE (1.4.1) in time. Rigorous error estimates for the EWI method with Fourier pseudospectral (EWI-FP) spatial discretization are carried out up to the time at $O(\varepsilon^{-\beta})$ with $0 \leq \beta \leq 2$. The error bounds indicate that the EWI-FP method is uniformly spectral accurate in space and second-order accurate in time for all $\varepsilon \in (0, 1]$. The EWI-FP method and the long-time error estimates are extended to the EWI method combined with other spatial discretizations including the exponential wave integrator finite difference (EWI-FD) method and the exponential wave integrator fourth-order compact finite difference (EWI-4cFD) method. Numerical tests are reported to confirm the error bounds of these EWI methods.

Chapter 4 deals with the uniform error bounds for the time-splitting Fourier pseudospectral (TSFP) method to solve the NKGE (1.4.1). First, the NKGE is reformulated into a relativistic nonlinear Schrödinger equation (NLSE). By the time-splitting technique, the NLSE is decomposed into the linear part which can be solved exactly in phase space and the nonlinear part which can be integrated exactly in physical space. Error estimates with detailed proof are carried out and numerical results show that the TSFP method performs much better than other numerical methods, especially when $0 < \varepsilon \ll 1$. Then, comparisons of above time integrators to solve the NKGE (1.4.1) in the long-time regime are presented. Some applications for wave interactions in 2D and 3D are also studied.

Chapter 5 is devoted to extending the numerical methods and error estimates to an oscillatory NKGE which propagates waves with wavelength in space and time at $O(1)$ and $O(\varepsilon^{\beta})$, respectively, and wave velocity at $O(\varepsilon^{-\beta})$. The highly oscillatory nature in time of the solution makes the numerical simulations extremely challenging when $\varepsilon \to 0^+$. The FDTD, EWI-FP and TSFP methods are used to solve the oscillatory NKGE. Rigorous error estimates and spatial/temporal resolutions are established for each numerical scheme. In addition, extensive numerical results and comparisons of different numerical methods to solve the oscillatory NKGE are presented to give an intuitive understanding.

Finally, conclusions are drawn in Chapter 6 and some possible future work is discussed.

Research in this thesis mainly focuses on the long-time error analysis of different numerical methods for the nonlinear Klein-Gordon equation. It compares various numerical schemes and extends the classical error estimates in the fixed time to the long-time regime. These results are very useful for practical computations on how to select mesh size and time step such that the numerical results are trustable.

This thesis mainly deals with the nonlinear Klein-Gordon equation in 1D. Extensions to 2D and 3D are straightforward with minor modifications and we omit the details for brevity. Furthermore, throughout this thesis, we adopt the notation $A \lesssim B$ to represent that there exists a generic constant $C > 0$, which is independent of the mesh size h and time step τ as well as ε such that $|A| \leq CB$.

Chapter 2

Error Estimates of Finite Difference Methods

In this chapter, we discretize the NKGE (1.4.1) by the finite difference method in time combined with different spatial discretizations including the central finite difference method, fourth-order compact finite difference method and spectral method. For all methods considered here, rigorous error estimates are carried out with particular attention on how the error bounds depend explicitly on the mesh size h and time step τ as well as the small parameter $\varepsilon \in (0, 1]$.

2.1 The NKGE in 1D

For simplicity of notations, we only show the numerical schemes in one dimension (1D) and all the notations and results can be easily generalized to higher dimensions with minor modifications. In 1D, the NKGE (1.4.1) collapses to

$$\begin{cases} \partial_{tt}u(x,t) - \partial_{xx}u(x,t) + u(x,t) + \varepsilon^2 u^3(x,t) = 0, \quad x \in \Omega = (a,b), \quad t > 0, \\ u(x,0) = \phi(x), \qquad \partial_t u(x,0) = \gamma(x), \qquad x \in \overline{\Omega} = [a,b], \end{cases} \tag{2.1.1}$$

with periodic boundary conditions. For the intuitive understanding of the solution to the NKGE (2.1.1), Figure 2.1 shows the solutions $u(x,2)$ and $u(\pi,t)$ of the NKGE (2.1.1) for different ε.

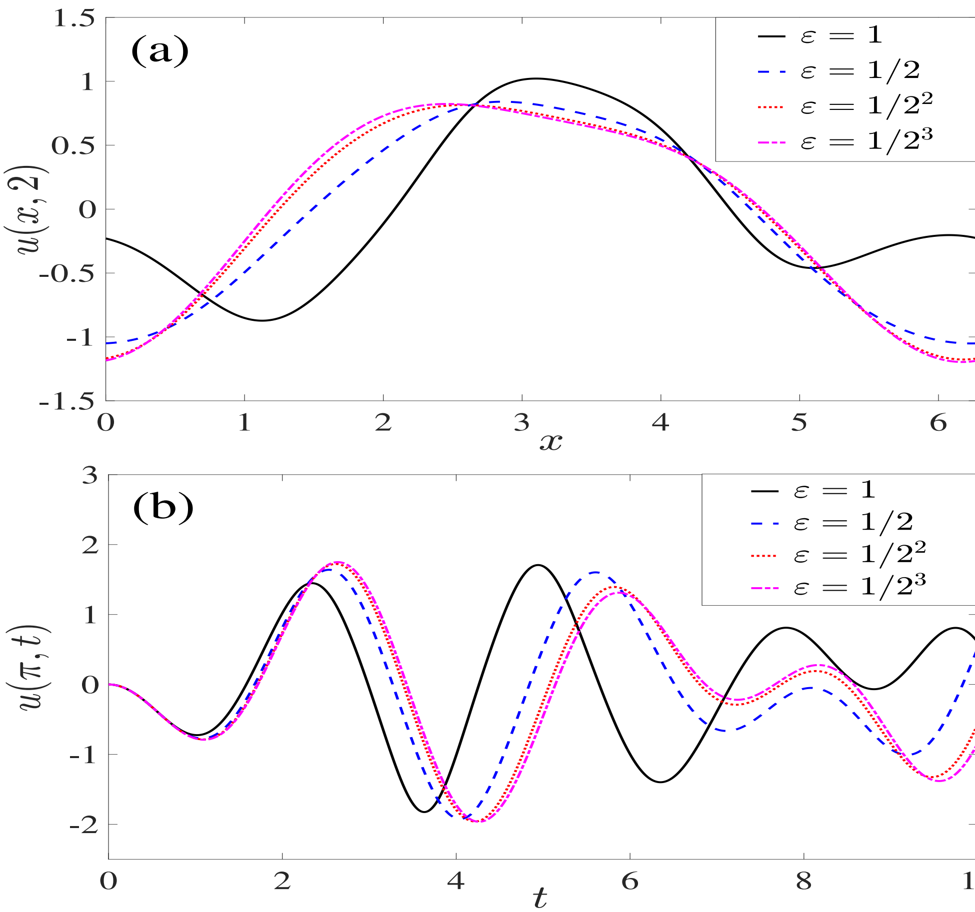

Figure 2.1: The solutions of the NKGE (2.1.1) with initial data $\phi(x) = \cos(x) + \cos(2x)$ and $\gamma(x) = \sin(x)$ for different ε: (a) $u(x, 2)$, (b) $u(\pi, t)$.

2.2 Semi-discretizaiton in time by finite difference methods

Let $\tau := \Delta t > 0$ be the time step size, and denote time steps by $t_n := n\tau$ for $n = 0, 1, 2, \cdots$. For a sequence $\{u^n\}$, define the standard finite difference operators as

$$\delta_t^+ u^n := \frac{u^{n+1} - u^n}{\tau}, \quad \delta_t^- u^n := \frac{u^n - u^{n-1}}{\tau}, \quad \delta_t^2 u^n := \frac{u^{n+1} - 2u^n + u^{n-1}}{\tau^2}.$$

Then the finite difference (FD) integrator for solving the NKGE (2.1.1) reads [9, 11, 48, 93]:

I. The Crank-Nicolson finite difference integrator

$$\delta_t^2 u^n - \frac{1}{2}\frac{d}{dx^2}\left(u^{n+1} + u^{n-1}\right) + \frac{1}{2}\left(u^{n+1} + u^{n-1}\right) + \varepsilon^2 G\left(u^{n+1}, u^{n-1}\right) = 0, \ n \geq 1; \quad (2.2.1)$$

II. A semi-implicit energy conservative finite difference integrator

$$\delta_t^2 u^n - \frac{d}{dx^2} u^n + \frac{1}{2}\left(u^{n+1} + u^{n-1}\right) + \varepsilon^2 G\left(u^{n+1}, u^{n-1}\right) = 0, \ n \geq 1; \tag{2.2.2}$$

III. Another semi-implicit finite difference integrator

$$\delta_t^2 u^n - \frac{1}{2}\frac{d}{dx^2}\left(u^{n+1} + u^{n-1}\right) + \frac{1}{2}\left(u^{n+1} + u^{n-1}\right) + \varepsilon^2 \left(u^n\right)^3 = 0, \ n \geq 1; \tag{2.2.3}$$

IV. The leap-frog finite difference integrator

$$\delta_t^2 u^n - \frac{d}{dx^2} u^n + u^n + \varepsilon^2 \left(u^n\right)^3 = 0, \ n \geq 1. \tag{2.2.4}$$

Here,

$$G(v, w) = \frac{F(v) - F(w)}{v - w}, \quad \forall\, v, w \in \mathbb{R}, \quad F(v) = \int_0^v s^3 ds = \frac{v^4}{4}, \quad v \in \mathbb{R}. \tag{2.2.5}$$

The initial and boundary conditions in (2.1.1) are discretized as

$$u^{n+1}(a) = u^{n+1}(b), \quad \frac{d}{dx} u^{n+1}(a) = \frac{d}{dx} u^{n+1}(b), \quad n \geq 0; \quad u^0 = \phi(x), \tag{2.2.6}$$

where the initial velocity $\gamma(x)$ is employed to update the first step u^1 by the Taylor expansion and the NKGE (2.1.1) as

$$u^1 = \phi(x) + \tau\gamma(x) + \frac{\tau^2}{2}\left[\frac{d}{dx^2}\phi(x) - \phi(x) - \varepsilon^2\phi^3(x)\right]. \tag{2.2.7}$$

2.3 FDTD methods

In this section, four different finite difference time domain (FDTD) methods are adapted to discretize the NKGE (2.1.1) and rigorous error bounds are established in the long-time regime.

2.3.1 The methods

Choose the spatial mesh size $h := \Delta x > 0$, and denote $M = (b-a)/h$ being a positive integer and the grid points as:

$$x_j := a + jh, \quad j = 0, 1, \ldots, M. \tag{2.3.1}$$

Denote $X_M = \{u = (u_0, u_1, \ldots, u_M)^T | u_j \in \mathbb{R}, j = 0, 1, \ldots, M, u_0 = u_M\}$ and we always use $u_{-1} = u_{M-1}$ and $u_{M+1} = u_1$ if they are involved. The standard discrete l^2, semi-H^1 and l^∞ norms and inner product in X_M are defined as

$$\|u\|_{l^2}^2 = h\sum_{j=0}^{M-1} |u_j|^2, \quad \|\delta_x^+ u\|_{l^2}^2 = h\sum_{j=0}^{M-1} |\delta_x^+ u_j|^2,$$
$$\|u\|_{l^\infty} = \max_{0\le j\le M-1} |u_j|, \quad (u, v) = h\sum_{j=0}^{M-1} u_j v_j,$$

with $\delta_x^+ u \in X_M$ defined as $\delta_x^+ u_j = (u_{j+1} - u_j)/h$ for $j = 0, 1, \ldots, M-1$.

Let u_j^n be the numerical approximation of $u(x_j, t_n)$ for $j = 0, 1, \ldots, M$, $n \ge 0$ and denote the numerical solution at time $t = t_n$ as $u^n = (u_0^n, u_1^n, \ldots, u_M^n)^T \in X_M$. We introduce the spatial finite difference operators as

$$\delta_x^+ u_j^n = \frac{u_{j+1}^n - u_j^n}{h}, \quad \delta_x^- u_j^n = \frac{u_j^n - u_{j-1}^n}{h}, \quad \delta_x^2 u_j^n = \frac{u_{j+1}^n - 2u_j^n + u_{j-1}^n}{h^2},$$

then four frequently used FDTD methods to discretize the NKGE (2.1.1) reads:

I. The Crank-Nicolson finite difference (CNFD) method

$$\delta_t^2 u_j^n - \frac{1}{2}\delta_x^2\left(u_j^{n+1} + u_j^{n-1}\right) + \frac{1}{2}\left(u_j^{n+1} + u_j^{n-1}\right) + \varepsilon^2 G\left(u_j^{n+1}, u_j^{n-1}\right) = 0, \ n \ge 1; \tag{2.3.2}$$

II. A semi-implicit energy conservative finite difference (SIFD1) method

$$\delta_t^2 u_j^n - \delta_x^2 u_j^n + \frac{1}{2}\left(u_j^{n+1} + u_j^{n-1}\right) + \varepsilon^2 G\left(u_j^{n+1}, u_j^{n-1}\right) = 0, \ n \ge 1; \tag{2.3.3}$$

III. Another semi-implicit finite difference (SIFD2) method

$$\delta_t^2 u_j^n - \frac{1}{2}\delta_x^2\left(u_j^{n+1} + u_j^{n-1}\right) + \frac{1}{2}\left(u_j^{n+1} + u_j^{n-1}\right) + \varepsilon^2\left(u_j^n\right)^3 = 0, \ n \ge 1; \tag{2.3.4}$$

IV. The leap-frog finite difference (LFFD) method

$$\delta_t^2 u_j^n - \delta_x^2 u_j^n + u_j^n + \varepsilon^2\left(u_j^n\right)^3 = 0, \qquad j = 0, 1, \ldots, M-1, \ n \ge 1. \tag{2.3.5}$$

The initial and boundary conditions in (2.1.1) are discretized as

$$u_0^{n+1} = u_M^{n+1}, \quad u_{-1}^{n+1} = u_{M-1}^{n+1}, \quad n \ge 0; \quad u_j^0 = \phi(x_j), \quad j = 0, 1, \ldots, M, \tag{2.3.6}$$

and the first step u^1 is computed by

$$u_j^1 = \phi(x_j) + \tau\gamma(x_j) + \frac{\tau^2}{2}\left[\delta_x^2\phi(x_j) - \phi(x_j) - \varepsilon^2\left(\phi(x_j)\right)^3\right], \quad j = 0, 1, \ldots, M. \quad (2.3.7)$$

It is easy to check that the above FDTD methods are all time symmetric or time reversible, i.e., they are unchanged if interchanging $n+1 \leftrightarrow n-1$ and $\tau \leftrightarrow -\tau$. In addition, the LFFD (2.3.5) is explicit and might be the simplest and most efficient discretization for the NKGE (2.1.1) with the computational cost per time step at $O(M)$. The others are implicit schemes. Nevertheless, the CNFD (2.3.2) and SIFD1 (2.3.3) can be solved via either a direct solver or an iterative solver with the computational cost per time step depending on the solver, which is usually larger than $O(M)$, especially in two dimensions (2D) and three dimensions (3D). Meanwhile, the solution of the SIFD2 (2.3.4) can be explicitly updated in the Fourier space with $O(M \ln M)$ computational cost per time step, and such approach is valid in higher dimensions.

2.3.2 Stability

The stability of numerical schemes is very important since it is impossible to avoid errors in any numerical simulations. Simply, stability means that the numerical scheme does not amplify errors, i.e., the small errors made in each time step do not grow too fast in later time steps [94]. In numerical analysis, von Neumann stability analysis is widely used to check the stability of numerical schemes applied to solve partial differential equations.

Let $T_0 > 0$ be a fixed constant and $0 \leq \beta \leq 2$, and denote

$$\sigma_{\max} := \max_{0 \leq n \leq T_0\varepsilon^{-\beta}/\tau} \|u^n\|_{l^\infty}^2. \quad (2.3.8)$$

Following the von Neumann stability analysis of the classical FDTD methods for the NKGE in the nonrelativistic limit regime [9, 94], we can conclude the stability of the above FDTD methods for the NKGE (2.1.1) up to the time $t = T_0/\varepsilon^\beta$ in the following lemma.

Lemma 2.3.1. *For the above FDTD methods applied to the NKGE* (2.1.1) *up to the time $t = T_0/\varepsilon^\beta$, we have:*

(i) The CNFD (2.3.2) *is unconditionally stable for any* $h > 0, \tau > 0$ *and* $0 < \varepsilon \leq 1$.

(ii) When $h \geq 2$*, the SIFD1* (2.3.3) *is unconditionally stable for any* $h > 0$ *and* $\tau > 0$*; and when* $0 < h < 2$*, this scheme is conditionally stable under the stability condition*

$$0 < \tau < \frac{2h}{\sqrt{4 - h^2}}, \quad h > 0, \quad 0 < \varepsilon \leq 1. \tag{2.3.9}$$

(iii) When $\sigma_{\max} \leq \varepsilon^{-2}$*, the SIFD2* (2.3.4) *is unconditionally stable for any* $h > 0$ *and* $\tau > 0$*; and when* $\sigma_{\max} > \varepsilon^{-2}$*, this scheme is conditionally stable under the stability condition*

$$0 < \tau < \frac{2}{\sqrt{\sigma_{\max} - 1}}, \quad h > 0, \quad 0 < \varepsilon \leq 1. \tag{2.3.10}$$

(iv) The LFFD (2.3.5) *is conditionally stable under the stability condition*

$$0 < \tau < \frac{2h}{\sqrt{4 + h^2(1 + \sigma_{\max})}}, \quad h > 0, \quad 0 < \varepsilon \leq 1. \tag{2.3.11}$$

Proof. Replacing the nonlinear term by $f(u) = \varepsilon^2 \sigma_{\max} u$, plugging

$$u_j^{n-1} = \sum_l \hat{U}_l e^{2ijl\pi/M}, \quad u_j^n = \sum_l \xi_l \hat{U}_l e^{2ijl\pi/M}, \quad u_j^{n+1} = \sum_l \xi_l^2 \hat{U}_l e^{2ijl\pi/M},$$

into (2.3.2) - (2.3.5), with ξ_l the amplification factor of the lth mode in phase space, we have the characteristic equation with the following structure

$$\xi_l^2 - 2\theta_l \xi_l + 1 = 0, \quad l = -\frac{M}{2}, \cdots, \frac{M}{2} - 1, \tag{2.3.12}$$

where $\theta_l \in \mathbb{R}$ is determined by the corresponding numerical methods. S Solving the characteristic equation (2.6.6), we have $\xi_l = \theta_l \pm \sqrt{\theta_l^2 - 1}$. The stability of the numerical schemes amounts to

$$|\xi_l| \leq 1 \iff |\theta_l| \leq 1, \quad l = -\frac{M}{2}, \cdots, \frac{M}{2} - 1. \tag{2.3.13}$$

(i) For the CNFD (2.3.2), we have

$$0 \leq \theta_l = \frac{2}{2 + \tau^2(1 + \lambda_l^2 + \varepsilon^2 \sigma_{\max})} \leq 1, \quad l = -\frac{M}{2}, \cdots, \frac{M}{2} - 1, \tag{2.3.14}$$

with

$$\lambda_l = \frac{2}{h}\sin\left(\frac{\pi l}{M}\right), \quad \mu_l = \frac{2\pi l}{b-a}, \quad l = -\frac{M}{2}, \cdots, \frac{M}{2}-1. \tag{2.3.15}$$

This implies that the CNFD (2.3.2) is unconditionally stable for any $h > 0$, $\tau > 0$ and $0 < \varepsilon \leq 1$.

(ii) For the SIFD1 (2.3.3), we have

$$\theta_l = \frac{2-\tau^2\lambda_l^2}{2+\tau^2(1+\varepsilon^2\sigma_{\max})}, \quad l = -\frac{M}{2}, \cdots, \frac{M}{2}-1. \tag{2.3.16}$$

Noticing $0 \leq \lambda_l^2 \leq \frac{4}{h^2}$, when $h \geq 2$, or $0 < h < 2$ with the condition (2.3.9), we can get

$$\tau^2(\lambda_l^2 - \varepsilon^2\sigma_{\max} - 1) \leq \tau^2(\lambda_l^2 - 1) \leq 4 \implies |\theta_l| \leq 1, \quad l = -\frac{M}{2}, \cdots, \frac{M}{2}-1.$$

(iii) For the SIFD2 (2.3.4), we have

$$\theta_l = \frac{2-\tau^2\varepsilon^2\sigma_{\max}}{2+\tau^2(1+\lambda_l^2)}, \quad l = -\frac{M}{2}, \cdots, \frac{M}{2}-1. \tag{2.3.17}$$

When $\sigma_{\max} \leq \varepsilon^{-2}$, or $\sigma_{\max} > \varepsilon^{-2}$ with the condition (2.3.10), we get

$$\tau^2(\varepsilon^2\sigma_{\max} - 1 - \lambda_l^2) \leq \tau^2(\varepsilon^2\sigma_{\max} - 1) \leq 4 \implies |\theta_l| \leq 1, \quad l = -\frac{M}{2}, \cdots, \frac{M}{2}-1.$$

(iv) For the LFFD (2.3.5), we have

$$\theta_l = \frac{2-\tau^2(\lambda_l^2+1+\varepsilon^2\sigma_{\max})}{2}, \quad l = -\frac{M}{2}, \cdots, \frac{M}{2}-1. \tag{2.3.18}$$

Combining the condition (2.3.11), we can get

$$\tau^2(\lambda_l^2+1+\varepsilon^2\sigma_{\max}) \leq \tau^2(\frac{4}{h^2}+1+\varepsilon^2\sigma_{\max}) \leq 4 \implies |\theta_l| \leq 1, \quad l = -\frac{M}{2}, \cdots, \frac{M}{2}-1.$$

The proof is completed. □

Remark 2.3.1. *The stability of schemes* (2.3.4)-(2.3.5) *is related to* $\sigma_{\max}$*, dependent on the boundedness of the* l^∞ *norm of the numerical solution* u^n *at the previous time step. The convergence estimates up to the previous time step could ensure such a bound in the* l^∞ *norm, by making use of the discrete Sobolev inequality, and such an error estimate could be recovered at the next time step, as given by the theorems presented in Section 2.4.*

2.3.3 Energy conservation and solvability for CNFD

For the CNFD (2.3.2), we can show that it conserves the energy in the discretized level with the proof proceeding in the analogous lines as those in [9, 95, 138] and we omit the details here for brevity.

Lemma 2.3.2. *(energy conservation) For $n \geq 0$, the CNFD* (2.3.2) *conserves the discrete energy as*

$$\begin{aligned} E^n &:= \|\delta_t^+ u^n\|_{l^2}^2 + \frac{1}{2}\sum_{k=n}^{n+1} \|\delta_x^+ u^k\|_{l^2}^2 + \frac{1}{2}\sum_{k=n}^{n+1} \|u^k\|_{l^2}^2 + \frac{\varepsilon^2 h}{4}\sum_{j=0}^{M-1}\left[(u_j^n)^4 + (u_j^{n+1})^4\right] \\ &\equiv E^0. \end{aligned} \tag{2.3.19}$$

Based on Lemma 2.3.2, we can show the unique solvability of the CNFD (2.3.2) at each time step as follows.

Lemma 2.3.3. *(solvability) For any given u^n, u^{n-1} ($n \geq 1$), the solution u^{n+1} of the CNFD* (2.3.2) *is unique at each time step.*

Proof. Firstly, we prove the existence of the solution for the CNFD (2.3.2). To simplify the notations, we denote the grid function $[\![u]\!]^n \in X_M$ with

$$[\![u]\!]_j^n = \frac{u_j^{n+1} + u_j^{n-1}}{2}, \quad j = 0, 1, \ldots, M, \quad n \geq 1. \tag{2.3.20}$$

For any $u^{n-1}, u^n, u^{n+1} \in X_M$, we rewrite the CNFD (2.3.2) as

$$[\![u]\!]^n = u^n + \frac{\tau^2}{2} F^n([\![u]\!]^n), \quad n \geq 1, \tag{2.3.21}$$

where $F^n : X_M \to X_M$ with

$$F_j^n(v) = \delta_x^2 v_j - \left[1 + \frac{\varepsilon^2}{2}(|u_j^{n-1}|^2 + |2v_j - u_j^{n-1}|^2)\right] v_j, \quad j = 0, 1, \ldots, M, \quad n \geq 1.$$

Define a map $K^n : X_M \to X_M$ as

$$K^n(v) = v - u^n - \frac{\tau^2}{2} F^n(v), \quad v \in X_M, \quad n \geq 1. \tag{2.3.22}$$

It is obvious that K^n $(n \geq 1)$ is continuous from X_M to X_M. Moreover, the fact

$$(K^n(v), v) = \|v\|_{l^2}^2 - (u^n, v) + \frac{\tau^2}{2}\left[\|\delta_x^+ v\|_{l^2}^2 + \|v\|_{l^2}^2 + \frac{\varepsilon^2}{2}\left(|u^{n-1}|^2 + |2v - u^{n-1}|^2, v^2\right)\right]$$
$$\geq \left(\|v\|_{l^2} - \|u^n\|_{l^2}\right)\|v\|_{l^2}, \quad n \geq 1,$$

implies

$$\lim_{\|v\|_{l^2} \to \infty} \frac{(K^n(v), v)}{\|v\|_{l^2}} = \infty, \quad n \geq 1. \tag{2.3.23}$$

Then, we can conclude that there exists a solution v^* such that $K^n(v^*) = 0$ by applying the Brouwer fixed point theorem [5, 16, 92]. In other words, the CNFD (2.3.2) is solvable.

Now, we proceed to verify the uniqueness. From (2.3.19), we can get

$$\|u^n\|_{l^2}^2 + \|\delta_x^+ u^n\|_{l^2}^2 \leq 2E^n = 2E^0, \quad n \geq 0. \tag{2.3.24}$$

Hence, by employing the discrete Sobolev inequality [5, 147], we can obtain

$$\|u^n\|_{l^\infty} \lesssim \|u^n\|_{l^2} + \|\delta_x^+ u^n\|_{l^2} \lesssim \sqrt{E^0}, \quad n \geq 0. \tag{2.3.25}$$

For any $v \in X_M$, we define a functional $S(v) : X_M \to \mathbb{R}$ as

$$S(v) := \sum_{j=0}^{M-1}\left[\frac{-2u_j^n + u_j^{n-1}}{\tau^2} - \frac{1}{2}\delta_x^2 u_j^{n-1} + \frac{1}{2}u_j^{n-1} + \frac{\varepsilon^2}{4}\left(u_j^{n-1}\right)^3\right]v_j + \frac{1}{4}\sum_{j=0}^{M-1}\left(\delta_x^+ v_j\right)^2$$
$$+ \sum_{j=0}^{M-1}\left\{\left[\frac{1}{2\tau^2} + \frac{1}{4} + \frac{\varepsilon^2}{8}\left(u_j^{n-1}\right)^2\right]v_j^2 + \frac{\varepsilon^2}{12}u_j^{n-1}v_j^3 + \frac{\varepsilon^2}{16}v_j^4\right\}.$$

It is easy to check that $S(v)$ is strictly convex with the gradient of it denoted as $\nabla S(v) := [\partial_{v_0} S(v), \ldots, \partial_{v_M} S_M(v)]^T$ turning out to be

$$\partial_{v_j} S(v) = \frac{v_j - 2u_j^n + u_j^{n-1}}{\tau^2} - \frac{1}{2}\delta_x^2\left(v_j + u_j^{n-1}\right) + \frac{1}{2}\left(v_j + u_j^{n-1}\right) + \varepsilon^2 G\left(v_j, u_j^{n-1}\right).$$

By the strict convexity of $S(v)$, we can get the uniqueness of $\nabla S(v) = 0$, which yields the uniqueness of $u^{n+1} \in X_M$ immediately. Thus, the proof is completed. □

Remark 2.3.2. *The energy conservation and solvability for the SIFD1* (2.3.3) *can be obtained similarly to the CNFD* (2.3.2) *in Lemma 2.3.2 and Lemma 2.3.3. There exists a unique solution of the SIFD2* (2.3.4) *due to the fact that it solves a linear system with a strictly diagonally dominant matrix. The solvability and uniqueness for the LFFD* (2.3.5) *are straightforward since it is explicit.*

2.4 Error estimates of FDTD methods

In this section, we will establish the error bounds of the FDTD methods [13].

2.4.1 Main results

Motivated by the analytical results in [43, 44, 88, 89, 97, 118, 148] and references therein, we make the following assumptions on the exact solution u of the NKGE (2.1.1) up to the time $t = T_0/\varepsilon^2$:

$$(A) \qquad \begin{aligned} u \in\ & C([0, T_0/\varepsilon^2]; W_p^{4,\infty}) \cap C^2([0, T_0/\varepsilon^2]; W^{2,\infty}) \\ & \cap C^3([0, T_0/\varepsilon^2]; W^{1,\infty}) \cap C^4([0, T_0/\varepsilon^2]; L^\infty), \\ & \left\| \frac{\partial^{r+q}}{\partial t^r \partial x^q} u(x,t) \right\|_{L^\infty} \lesssim 1, \quad 0 \le r \le 4, \quad 0 \le r+q \le 4, \end{aligned}$$

where $L^\infty = L^\infty([0, T_0/\varepsilon^2]; L^\infty)$ and $W_p^{m,\infty} = \{u \in W^{m,\infty} | \frac{\partial^l}{\partial x^l} u(a) = \frac{\partial^l}{\partial x^l} u(b),\ 0 \le l < m\}$ for $m \ge 1$.

Denote $M_0 = \sup_{\varepsilon \in (0,1]} \|u(x,t)\|_{L^\infty}$ and the grid 'error' function $e^n \in X_M (n \ge 0)$ as

$$e_j^n = u(x_j, t_n) - u_j^n, \quad j = 0, 1, \ldots, M, \quad n = 0, 1, 2, \ldots, \tag{2.4.1}$$

where $u^n \in X_M$ is the numerical approximation of the NKGE (2.1.1).

For the CNFD (2.3.2), we can establish the following error estimates up to the time $t = T_0/\varepsilon^\beta$ with $0 \le \beta \le 2$ (see its detailed proof in Section 2.4.2):

Theorem 2.4.1. *Under the assumption (A), there exist constants $h_0 > 0$ and $\tau_0 > 0$ sufficiently small and independent of ε, such that, for any $0 < \varepsilon \le 1$, when $0 < h \le h_0 \varepsilon^{\beta/2}$ and $0 < \tau \le \tau_0 \varepsilon^{\beta/2}$, we have the following error estimates for the CNFD (2.3.2) with (2.3.6) and (2.3.7)*

$$\|e^n\|_{l^2} + \|\delta_x^+ e^n\|_{l^2} \lesssim \frac{h^2}{\varepsilon^\beta} + \frac{\tau^2}{\varepsilon^\beta}, \quad \|u^n\|_{l^\infty} \le 1 + M_0, \quad 0 \le n \le \frac{T_0/\varepsilon^\beta}{\tau}. \tag{2.4.2}$$

For the LFFD (2.3.5), the error estimates can be established as follows (see its detailed proof in Section 2.4.3):

Theorem 2.4.2. *Assume $\tau \le \frac{1}{2}\min\{1,h\}$ and under the assumption (A), there exist constants $h_0>0$ and $\tau_0>0$ sufficiently small and independent of ε, such that for any $0<\varepsilon\le 1$, when $0<h\le h_0\varepsilon^{\beta/2}$ and $0<\tau\le \tau_0\varepsilon^{\beta/2}$ and under the stability condition (2.3.11), we have the error estimates for the LFFD (2.3.5) with (2.3.6) and (2.3.7) as*

$$\|e^n\|_{l^2}+\|\delta_x^+ e^n\|_{l^2} \lesssim \frac{h^2}{\varepsilon^\beta}+\frac{\tau^2}{\varepsilon^\beta}, \quad \|u^n\|_{l^\infty}\le 1+M_0, \quad 0\le n\le \frac{T_0/\varepsilon^\beta}{\tau}. \tag{2.4.3}$$

Similarly, for the SIFD1 (2.3.3) and SIFD2 (2.3.4), we have the following error estimates (their proofs are quite similar and thus they are omitted for brevity):

Theorem 2.4.3. *Assume $\tau \lesssim h$ and under the assumption (A), there exist constants $h_0>0$ and $\tau_0>0$ sufficiently small and independent of ε, such that for any $0<\varepsilon\le 1$, when $0<h\le h_0\varepsilon^{\beta/2}$, $0<\tau\le \tau_0\varepsilon^{\beta/2}$ and under the stability condition (2.3.9), we have the following error estimates for the SIFD1 (2.3.3) with (2.3.6) and (2.3.7)*

$$\|e^n\|_{l^2}+\|\delta_x^+ e^n\|_{l^2} \lesssim \frac{h^2}{\varepsilon^\beta}+\frac{\tau^2}{\varepsilon^\beta}, \quad \|u^n\|_{l^\infty}\le 1+M_0, \quad 0\le n\le \frac{T_0/\varepsilon^\beta}{\tau}. \tag{2.4.4}$$

Theorem 2.4.4. *Under the assumption (A), there exist constants $h_0>0$ and $\tau_0>0$ sufficiently small and independent of ε, such that for any $0<\varepsilon\le 1$, when $0<h\le h_0\varepsilon^{\beta/2}$, $0<\tau\le \tau_0\varepsilon^{\beta/2}$ and under the stability condition (2.3.10), we have the following error estimates for the SIFD2 (2.3.4) with (2.3.6) and (2.3.7)*

$$\|e^n\|_{l^2}+\|\delta_x^+ e^n\|_{l^2} \lesssim \frac{h^2}{\varepsilon^\beta}+\frac{\tau^2}{\varepsilon^\beta}, \quad \|u^n\|_{l^\infty}\le 1+M_0, \quad 0\le n\le \frac{T_0/\varepsilon^\beta}{\tau}. \tag{2.4.5}$$

Remark 2.4.1. *In 2D with $d=2$ and 3D with $d=3$ cases, the above theorems are still valid under the technical conditions $0<h\lesssim \varepsilon^{\beta/2}\sqrt{C_d(h)}$ and $0<\tau\lesssim\varepsilon^{\beta/2}\sqrt{C_d(h)}$ where $C_d(h)=1/|\ln h|$ when $d=2$, and $C_d(h)=h^{1/2}$ when $d=3$. The reason is due to the discrete Sobolev inequality [5, 18, 147]:*

$$\|u^n\|_{l^\infty}\lesssim \frac{1}{C_d(h)}\left(\|\delta_x^+ u^n\|_{l^2}+\|u^n\|_{l^2}\right). \tag{2.4.6}$$

Hence, the four FDTD methods studied here share the same spatial/temporal resolution capacity for the NKGE (2.1.1) up to the time at $O(\varepsilon^{-\beta})$ with $0 \leq \beta \leq 2$. In fact, given an accuracy bound $\delta_0 > 0$, the ε-scalability (or meshing strategy requirement) of the FDTD methods should be taken as

$$h = O(\varepsilon^{\beta/2}\sqrt{\delta_0}) = O(\varepsilon^{\beta/2}), \quad \tau = O(\varepsilon^{\beta/2}\sqrt{\delta_0}) = O(\varepsilon^{\beta/2}), \quad 0 < \varepsilon \leq 1. \tag{2.4.7}$$

This implies that, in order to get "correct" numerical solution up to the time at $O(\varepsilon^{-1})$, one has to take the meshing strategy: $h = O(\varepsilon^{1/2})$ and $\tau = O(\varepsilon^{1/2})$; and resp., in order to get "correct" numerical solution up to the time at $O(\varepsilon^{-2})$, one has to take the meshing strategy: $h = O(\varepsilon)$ and $\tau = O(\varepsilon)$. These results are very useful for practical computations to how to select mesh size and time step such that the numerical results are trustable.

2.4.2 Proof for CNFD

For the CNFD (2.3.2), we establish the error estimates in Theorem 2.4.1. The key of the proof is to deal with the nonlinearity and overcome the main difficulty in uniformly bounding the numerical solution u^n, i.e., $\|u^n\|_{l^\infty} \lesssim 1$. Here, we adapt the cut-off technique which has been widely used in the literature [4, 5, 147], i.e., the nonlinearity is truncated to a global Lipschitz function with compact support.

Denote $B = (1 + M_0)^2$, choose a smooth function $\rho(\theta) \in C_0^\infty(\mathbb{R}^+)$ and define

$$F_B(\theta) = \rho\left(\theta/B\right)\theta, \quad \theta \in \mathbb{R}^+, \quad \rho(\theta) = \begin{cases} 1, & 0 \leq \theta \leq 1, \\ \in [0,1], & 1 \leq \theta \leq 2, \\ 0, & \theta \geq 2, \end{cases} \tag{2.4.8}$$

then $F_B(\theta)$ has compact support and is smooth and global Lipschitz, i.e., there exists C_B independent of h, τ and ε, such that

$$|F_B(\theta_1) - F_B(\theta_2)| \leq C_B|\sqrt{\theta_1} - \sqrt{\theta_2}|, \quad \forall \theta_1,\ \theta_2 \in \mathbb{R}^+. \tag{2.4.9}$$

Set $\hat{u}^0 = u^0$, $\hat{u}^1 = u^1$ and determine $\hat{u}^{n+1} \in X_M$ for $n \geq 1$ as follows

$$\delta_t^2 \hat{u}_j^n - \delta_x^2 [\![\hat{u}]\!]_j^n + [\![\hat{u}]\!]_j^n + \frac{\varepsilon^2}{2}\left(F_B((\hat{u}_j^{n+1})^2) + F_B((\hat{u}_j^{n-1})^2)\right)[\![\hat{u}]\!]_j^n = 0,\ j = 0, 1, \ldots, M-1. \tag{2.4.10}$$

In fact, $\hat{u}_j^n$ can be viewed as another approximation of $u(x_j,t_n)$ for $j=0,1,\ldots,M$ and $n\geq 0$. It is easy to verify that the scheme (2.4.10) is uniquely solvable for sufficiently small τ by using the properties of ρ and standard techniques in Section 2. Define the corresponding 'error' function $\hat{e}^n\in X_M$ as

$$\hat{e}_j^n=u(x_j,t_n)-\hat{u}_j^n,\quad j=0,1,\ldots,M,\quad n\geq 0, \tag{2.4.11}$$

and we can establish the following estimates:

Theorem 2.4.5. *Under the assumption (A), there exist constants $h_0>0$ and $\tau_0>0$ sufficiently small and independent of ε, such that for any $0<\varepsilon\leq 1$, when $0<h\leq h_0\varepsilon^{\beta/2}$ and $0<\tau\leq\tau_0\varepsilon^{\beta/2}$, we have the following error estimates*

$$\|\hat{e}^n\|_{l^2}+\|\delta_x^+\hat{e}^n\|_{l^2}\lesssim h^2\varepsilon^{-\beta}+\tau^2\varepsilon^{-\beta},\quad \|\hat{u}^n\|_{l^\infty}\leq 1+M_0,\quad 0\leq n\leq T_0\varepsilon^{-\beta}/\tau. \tag{2.4.12}$$

We begin with the local truncation error $\hat{\xi}^n\in X_M$ of the scheme (2.4.10) given as

$$\begin{aligned}
\hat{\xi}_j^0 &:= \delta_t^+u(x_j,0)-\gamma(x_j)-\frac{\tau}{2}\left[\delta_x^2\phi(x_j)-\phi(x_j)-\varepsilon^2(\phi(x_j))^3\right],\quad j=0,1,\ldots,M-1,\\
\hat{\xi}_j^n &:= \delta_t^2u(x_j,t_n)-\frac{1}{2}\left[\delta_x^2u(x_j,t_{n+1})+\delta_x^2u(x_j,t_{n-1})\right]+\frac{1}{2}\left[u(x_j,t_{n+1})+u(x_j,t_{n-1})\right]\\
&\quad+\frac{\varepsilon^2}{4}\left(F_B(u(x_j,t_{n+1})^2)+F_B(u(x_j,t_{n-1})^2)\right)\left(u(x_j,t_{n+1})+u(x_j,t_{n-1})\right),\quad n\geq 1.
\end{aligned} \tag{2.4.13}$$

The following estimates hold for $\hat{\xi}^n$.

Lemma 2.4.1. *Under the assumption (A), we have*

$$\|\hat{\xi}^0\|_{l^2}+\|\delta_x^+\hat{\xi}^0\|_{l^2}\lesssim h^2+\tau^2,\quad \|\hat{\xi}^n\|_{l^2}\lesssim h^2+\tau^2,\quad 1\leq n\leq T_0\varepsilon^{-\beta}/\tau-1. \tag{2.4.14}$$

Proof. Under the assumption (A), by applying the Taylor expansion to (2.4.13), it leads to

$$\begin{aligned}
|\hat{\xi}_j^0| &\lesssim \tau^2\|\partial_{ttt}u\|_{L^\infty}+h\tau\|\phi'''\|_{L^\infty}\lesssim h^2+\tau^2,\quad j=0,1,\ldots,M-1,\\
|\hat{\xi}_j^n| &\lesssim \tau^2\left[\|\partial_{tttt}u\|_{L^\infty}+\|\partial_{ttxx}u\|_{L^\infty}+(1+\varepsilon^2\|u\|_{L^\infty}^2)\|\partial_{tt}u\|_{L^\infty}+\varepsilon^2\|u\|_{L^\infty}\|\partial_tu\|_{L^\infty}^2\right]\\
&\quad+h^2\|\partial_{xxxx}u\|_{L^\infty}\lesssim\ h^2+\tau^2,\quad n\geq 1.
\end{aligned}$$

Similarly, we have $|\delta_x^+\hat{\xi}_j^0| \lesssim h^2 + \tau^2$ for $0 \le j \le M-1$. These immediately imply (2.4.14). $\square$

Next, we control the nonlinear term as follows.

Lemma 2.4.2. *For $j = 0, 1, \ldots, M$ and $1 \le n \le T_0\varepsilon^{-\beta}/\tau - 1$, denote the error of the nonlinear term*

$$\begin{aligned}\hat{\eta}_j^n =& \frac{\varepsilon^2}{4}\left(F_B(u(x_j,t_{n+1})^2) + F_B(u(x_j,t_{n-1})^2)\right)(u(x_j,t_{n+1}) + u(x_j,t_{n-1})) \\ &- \frac{\varepsilon^2}{4}\left(F_B((\hat{u}_j^{n+1})^2) + F_B((\hat{u}_j^{n-1})^2)\right)\left(\hat{u}_j^{n+1} + \hat{u}_j^{n-1}\right),\end{aligned} \tag{2.4.15}$$

under the assumption (A), we have

$$\|\hat{\eta}^n\|_{l^2} \lesssim \varepsilon^2\left(\|\hat{e}^{n-1}\|_{l^2} + \|\hat{e}^{n+1}\|_{l^2}\right). \tag{2.4.16}$$

Proof. Noticing (2.4.9) and (2.4.15), direct calculation for $j = 0, 1, \ldots, M$ and $1 \le n \le T_0\varepsilon^{-\beta}/\tau - 1$ leads to

$$|\hat{\eta}_j^n| \le \; C\varepsilon^2\left[M_0 + |F_B((\hat{u}_j^{n+1})^2)| + |F_B((\hat{u}_j^{n-1})^2)|\right]\left(|\hat{e}_j^{n+1}| + |\hat{e}_j^{n-1}|\right), \tag{2.4.17}$$

where the constant C is independent of h, τ and ε. Under the assumption (A) and the properties of F_B, we have

$$\|\hat{\eta}^n\|_{l^2} \lesssim \varepsilon^2\left[\|\hat{e}^{n+1}\|_{l^2} + \|\hat{e}^{n-1}\|_{l^2}\right], \quad 1 \le n \le T_0\varepsilon^{-\beta}/\tau - 1, \tag{2.4.18}$$

which completes the proof. $\square$

Now, we proceed to study the growth of the errors and verify Theorem 2.4.5. Subtracting (2.4.10) from (2.4.13), the error $\hat{e}^n \in X_M$ satisfies

$$\begin{aligned}&\delta_t^2\hat{e}_j^n - \frac{1}{2}\left(\delta_x^2\hat{e}_j^{n+1} + \delta_x^2\hat{e}_j^{n-1}\right) + \frac{1}{2}\left(\hat{e}_j^{n+1} + \hat{e}_j^{n-1}\right) = \hat{\xi}_j^n - \hat{\eta}_j^n,\ 1 \le n \le T_0\varepsilon^{-\beta}/\tau - 1,\\ &\hat{e}_j^0 = 0, \quad \hat{e}_j^1 = \tau\hat{\xi}_j^0, \quad j = 0, 1, \ldots, M-1.\end{aligned} \tag{2.4.19}$$

Define the "energy" for the error vector $\hat{e}^n$ as

$$\hat{S}^n = \|\delta_t^+\hat{e}^n\|_{l^2}^2 + \frac{1}{2}\left(\|\delta_x^+\hat{e}^n\|_{l^2}^2 + \|\delta_x^+\hat{e}^{n+1}\|_{l^2}^2\right) + \frac{1}{2}\left(\|\hat{e}^n\|_{l^2}^2 + \|\hat{e}^{n+1}\|_{l^2}^2\right), \quad n \ge 0. \tag{2.4.20}$$

It is easy to see that

$$\hat{S}^0 = \|\hat{\xi}^0\|_{l^2}^2 + \frac{\tau^2}{2}\|\delta_x^+\hat{\xi}^0\|_{l^2}^2 + \frac{\tau^2}{2}\|\hat{\xi}^0\|_{l^2}^2 \lesssim \left(h^2+\tau^2\right)^2. \tag{2.4.21}$$

Proof. (**Proof of Theorem 2.4.5**) When $n = 0$, the estimates in (2.4.12) are obvious and the $n = 1$ case is already verified in Lemma 3.1 for sufficiently small $0 < \tau < \tau_1$ and $0 < h < h_1$. Thus, we only need to prove (2.4.12) for $2 \le n \le T_0\varepsilon^{-\beta}/\tau$.

Multiplying both sides of (2.4.19) by $h\left(\hat{e}_j^{n+1} - \hat{e}_j^{n-1}\right)$, summing up for j, noticing the fact $0 \le \beta \le 2$ and making use of the Young's inequality and Lemmas 2.4.1&2.4.2, we derive

$$\begin{aligned}\hat{S}^n - \hat{S}^{n-1} &= h\sum_{j=0}^{M-1}\left(\hat{\xi}_j^n - \hat{\eta}_j^n\right)\left(\hat{e}_j^{n+1} - \hat{e}_j^{n-1}\right)\\ &\le \tau\varepsilon^{-\beta}\left(\|\hat{\xi}^n\|_{l^2}^2 + \|\hat{\eta}^n\|_{l^2}^2\right) + \tau\varepsilon^{\beta}\left(\|\delta_t^+\hat{e}^n\|_{l^2}^2 + \|\delta_t^+\hat{e}^{n-1}\|_{l^2}^2\right)\\ &\lesssim \varepsilon^{\beta}\tau\left(\hat{S}^n + \hat{S}^{n-1}\right) + \tau\varepsilon^{-\beta}\left(h^2+\tau^2\right)^2, \quad 1 \le n \le T_0\varepsilon^{-\beta}/\tau - 1.\end{aligned} \tag{2.4.22}$$

Summing the above inequalities for time steps from 1 to n, there exists a constant $C > 0$ such that

$$\hat{S}^n \le \hat{S}^0 + C\varepsilon^{\beta}\tau\sum_{m=0}^{n}\hat{S}^m + CT_0\varepsilon^{-2\beta}\left(h^2+\tau^2\right)^2, \quad 1 \le n \le T_0\varepsilon^{-\beta}/\tau - 1. \tag{2.4.23}$$

Hence, the discrete Gronwall's inequality suggests that there exists a constant $\tau_2 > 0$ sufficiently small, such that when $0 < \tau \le \tau_2$, the following holds

$$\begin{aligned}\hat{S}^n &\le 1\left(\hat{S}^0 + CT_0\varepsilon^{-2\beta}\left(h^2+\tau^2\right)^2\right)e^{2C(n+1)\varepsilon^{\beta}\tau}\\ &\lesssim \varepsilon^{-2\beta}\left(h^2+\tau^2\right)^2, \quad 1 \le n \le T_0\varepsilon^{-\beta}/\tau - 1.\end{aligned} \tag{2.4.24}$$

Recalling $\|\hat{e}^{n+1}\|_{l^2}^2 + \|\delta_x^+\hat{e}^{n+1}\|_{l^2}^2 \le 2\hat{S}^n$ when $0 < \varepsilon \le 1$, we can obtain the error estimate

$$\|\hat{e}^{n+1}\|_{l^2} + \|\delta_x^+\hat{e}^{n+1}\|_{l^2} \lesssim h^2\varepsilon^{-\beta} + \tau^2\varepsilon^{-\beta}, \quad 1 \le n \le T_0\varepsilon^{-\beta}/\tau - 1. \tag{2.4.25}$$

Finally, we estimate $\|\hat{u}^{n+1}\|_{l^\infty}$ for $1 \le n \le T_0\varepsilon^{-\beta}/\tau - 1$. The discrete Sobolev inequality implies

$$\|\hat{e}^n\|_{l^\infty} \lesssim \|\hat{e}^n\|_{l^2} + \|\delta_x^+\hat{e}^n\|_{l^2} \lesssim h^2\varepsilon^{-\beta} + \tau^2\varepsilon^{-\beta}. \tag{2.4.26}$$

Thus, there exist $h_2 > 0$ and $\tau_3 > 0$ sufficiently small, when $0 < h \le h_2\varepsilon^{\beta/2}$ and $0 < \tau \le \tau_3\varepsilon^{\beta/2}$, we obtain

$$\|\hat{u}^n\|_{l^\infty} \le \|u(x,t_n)\|_{L^\infty} + \|\hat{e}^n\|_{l^\infty} \le M_0 + 1. \tag{2.4.27}$$

The proof is completed by choosing $h_0 = \min\{h_1, h_2\}$ and $\tau_0 = \min\{\tau_1, \tau_2, \tau_3\}$. □

Proof. (**Proof of Theorem 2.4.1**) In view of the definition of ρ, Theorem 2.4.5 implies that (2.4.10) collapses to (2.3.2). By the unique solvability of the CNFD, $\hat{u}^n$ is identical to u^n. Thus, Theorem 2.4.1 is a direct consequence of Theorem 2.4.5. □

2.4.3 Proof for LFFD

For the LFFD (2.3.5), we establish the error estimates in Theorem 2.4.2. Throughout this section, the stability condition (2.3.11) is assumed. Here, we sketch the proof and omit those parts similar to the proof of Theorem 2.4.1 in Section 2.4.2.

Proof. Denote the local truncation error as $\tilde{\xi}^n \in X_M$

$$\begin{aligned}
\tilde{\xi}_j^0 &:= \delta_t^+ u(x_j,0) - \gamma(x_j) - \frac{\tau}{2}\left[\delta_x^2\phi(x_j) - \phi(x_j) - \varepsilon^2\phi^3(x_j)\right], \ j = 0,1,\ldots,M-1, \\
\tilde{\xi}_j^n &:= \delta_t^2 u(x_j,t_n) - \delta_x^2 u(x_j,t_n) + u(x_j,t_n) + \varepsilon^2 u^3(x_j,t_n), \ 1 \le n \le T_0\varepsilon^{-\beta}/\tau - 1,
\end{aligned} \tag{2.4.28}$$

and the error of the nonlinear term as $\tilde{\eta}^n \in X_M$

$$\tilde{\eta}_j^n := \varepsilon^2\left(u^3(x_j,t_n) - (u_j^n)^3\right), \quad j = 0,1,\ldots,M-1, \quad 1 \le n \le T_0\varepsilon^{-\beta}/\tau - 1. \tag{2.4.29}$$

Similar to Lemma 2.4.1, under the assumption (A), we have

$$\|\tilde{\xi}^0\|_{l^2} + \|\delta_x^+\tilde{\xi}^0\|_{l^2} \lesssim h^2 + \tau^2, \quad \|\tilde{\xi}^n\|_{l^2} \lesssim h^2 + \tau^2, \quad 1 \le n \le T_0\varepsilon^{-\beta}/\tau - 1. \tag{2.4.30}$$

The error equation for the LFFD (2.3.5) can be derived as

$$\begin{aligned}
&\delta_t^2 e_j^n - \delta_x^2 e_j^n + e_j^n = \tilde{\xi}_j^n - \tilde{\eta}_j^n, \quad 1 \le n \le T_0\varepsilon^{-\beta}/\tau - 1, \\
&e_j^0 = 0, \quad e_j^1 = \tau\tilde{\xi}_j^0, \quad j = 0,1,\ldots,M-1.
\end{aligned} \tag{2.4.31}$$

We adapt the mathematical induction to prove Theorem 2.4.2, i.e., we want to demonstrate that there exist $h_0 > 0$ and $\tau_0 > 0$, such that, when $0 < h < h_0$ and $0 < \tau < \tau_0$, under the stability condition (2.3.11), the error bounds hold

$$\|e^n\|_{l^2} + \|\delta_x^+ e^n\|_{l^2} \le C_1 \left(h^2\varepsilon^{-\beta} + \tau^2\varepsilon^{-\beta}\right), \quad \|u^n\|_{l^\infty} \le 1 + M_0, \tag{2.4.32}$$

for all $0 \le n \le T_0\varepsilon^{-\beta}/\tau$ and $0 \le \beta \le 2$, where C_1, τ_0 and h_0 will be classified later. For $n = 0$, (2.4.32) is trivial. For $n = 1$, the error equation (2.4.31) and the estimate (2.4.30) imply

$$\|e^1\|_{l^2} = \tau\|\tilde{\xi}^0\|_{l^2} \le C_2\tau(h^2 + \tau^2), \quad \|\delta_x^+ e^1\|_{l^2} = \tau\|\delta_x^+\tilde{\xi}^0\|_{l^2} \le C_2\tau(h^2 + \tau^2). \tag{2.4.33}$$

In view of the triangle inequality, discrete Sobolev inequality and the assumption (A), there exist $h_1 > 0$ and $\tau_1 > 0$ sufficiently small, when $0 < h \le h_1$ and $0 < \tau \le \tau_1$, we have

$$\|u^1\|_{l^\infty} \le \|u(x, t_1)\|_{L^\infty} + \|e^1\|_{l^\infty} \le \|u(x, t_1)\|_{L^\infty} + \|e^1\|_{l^2} + \|\delta_x^+ e^1\|_{l^2} \le M_0 + 1. \tag{2.4.34}$$

In other words, the error bounds in (2.4.32) also hold for $n = 1$.

Now we assume that (2.4.32) is valid for all $0 \le n \le m - 1 \le T_0\varepsilon^{-\beta}/\tau - 1$, then we need to show that it is still valid when $n = m$. From (2.4.29), the error of the nonlinear term can be controlled as

$$\|\tilde{\eta}^n\|_{l^2} \le C_3\varepsilon^2\|e^n\|_{l^2}, \quad 1 \le n \le m - 1. \tag{2.4.35}$$

Define the "energy" for the error vector $e^n (n = 0, 1, \dots)$ as

$$S^n := \left(1 - \frac{\tau^2}{2} - \frac{\tau^2}{h^2}\right)\|\delta_t^+ e^n\|_{l^2}^2 + \frac{1}{2}\sum_{k=n}^{n+1}\|e^k\|_{l^2}^2 + \frac{1}{2h}\sum_{j=0}^{M-1}\left[\left(e_{j+1}^{n+1} - e_j^n\right)^2 + \left(e_{j+1}^n - e_j^{n+1}\right)^2\right],$$

where

$$S^0 = \left(1 - \frac{\tau^2}{2} - \frac{\tau^2}{h^2}\right)\|\delta_t^+ e^0\|_{l^2}^2 + \left(\frac{1}{2} + \frac{1}{h^2}\right)\|e^1\|_{l^2}^2 = \|\tilde{\xi}^0\|_{l^2}^2 \le C_4(\tau^2 + h^2)^2.$$

Under the assumption $\tau \le \frac{1}{2}\min\{1, h\}$, we have $1 - \tau^2/2 - \tau^2/h^2 \ge \frac{1}{4} > 0$. Since

$$\|\delta_x^+ e^{n+1}\|_{l^2}^2 = \frac{1}{h}\sum_{j=0}^{M-1}(e_{j+1}^{n+1} - e_j^n - \tau\delta_t^+ e_j^n)^2 \le \frac{2}{h}\sum_{j=0}^{M-1}(e_{j+1}^{n+1} - e_j^n)^2 + \frac{2\tau^2}{h^2}\|\delta_t^+ e^n\|_{l^2}^2,$$

we can conclude that

$$S^n \geq \frac{1}{4}\|\delta_x^+ e^{n+1}\|_{l^2}^2 + \frac{1}{2}\left(\|e^n\|_{l^2}^2 + \|e^{n+1}\|_{l^2}^2\right), \quad 1 \leq n \leq m-1. \tag{2.4.36}$$

Similar to the proof in Section 2.4.2, there exists $\tau_2 > 0$ sufficiently small, when $0 < \tau \leq \tau_2$,

$$S^n \leq C_5\left(h^2\varepsilon^{-\beta} + \tau^2\varepsilon^{-\beta}\right)^2, \quad 1 \leq n \leq m-1, \tag{2.4.37}$$

where C_5 depends on T_0 and the exact solution $u(x,t)$. Letting $n = m$, we have

$$\|e^m\|_{l^2} + \|\delta_x^+ e^m\|_{l^2} \leq C_6(h^2\varepsilon^{-\beta} + \tau^2\varepsilon^{-\beta}), \quad 1 \leq m \leq T_0\varepsilon^{-\beta}/\tau \tag{2.4.38}$$

where C_6 depends on T_0 and the exact solution $u(x,t)$.

It remains to estimate $\|u^n\|_{l^\infty}$ for $n = m$. In fact, the discrete Sobolev inequality implies

$$\|e^m\|_{l^\infty} \lesssim \|e^m\|_{l^2} + \|\delta_x^+ e^m\|_{l^2} \lesssim h^2\varepsilon^{-\beta} + \tau^2\varepsilon^{-\beta}. \tag{2.4.39}$$

Thus, there exist $h_2 > 0$ and $\tau_3 > 0$ sufficiently small, when $0 < h \leq h_2\varepsilon^{\beta/2}$ and $0 < \tau \leq \tau_3\varepsilon^{\beta/2}$, we obtain

$$\|u^m\|_{l^\infty} \leq \|u(x,t_m)\|_{L^\infty} + \|e^m\|_{l^\infty} \leq M_0 + 1, \quad 1 \leq m \leq T_0\varepsilon^{-\beta}/\tau. \tag{2.4.40}$$

Under the stability condition (2.3.11) and the choices of $h_0 = \min\{h_1, h_2\}$, $\tau_0 = \min\{\tau_1, \tau_2, \tau_3\}$ and $C_1 = \max\{C_2, C_6\}$, the error bounds in (2.4.32) are still valid when $n = m$. Hence, the mathematical induction process is done and the proof of Theorem 2.4.2 is completed. $\square$

2.5 Numerical results of FDTD methods and comparisons

In this section, we present the numerical results of FDTD methods for the NKGE (2.1.1) up to the time at $O(\varepsilon^{-\beta})$ with $0 \leq \beta \leq 2$ to verify our error bounds.

Denote $u_{h,\tau}^n$ as the numerical solution at time $t = t_n$ obtained by a numerical method with mesh size h and time step τ. In order to quantify the numerical results, we define the error function as follows:

$$e_{h,\tau}(t_n) = \sqrt{\|u(\cdot,t_n) - u_{h,\tau}^n\|_{l^2}^2 + \|\delta_x^+(u(\cdot,t_n) - u_{h,\tau}^n)\|_{l^2}^2}.$$

We show the numerical results for the CNFD (2.3.2) and SIFD2 (2.3.4) and results for other FDTD methods are quite similar which are omitted for brevity. In the numerical experiments, we take $a = 0$, $b = 2\pi$ and choose the initial data as

$$\phi(x) = \cos(x) + \cos(2x), \qquad \gamma(x) = \sin(x), \qquad 0 \leq x \leq 2\pi. \tag{2.5.1}$$

The 'exact' solution is obtained numerically by the exponential wave integrator Fourier pseudospectral method [9, 47] with a very fine mesh size and a very small time step, e.g. $h_e = \pi/2^{15}$ and $\tau_e = 10^{-5}$. Here we study the following three cases with respect to different $0 \leq \beta \leq 2$:

Case I. Fixed time dynamics up to the time at $O(1)$, i.e., $\beta = 0$;

Case II. Intermediate long-time dynamics up to the time at $O(\varepsilon^{-1})$, i.e., $\beta = 1$;

Case III. Long-time dynamics up to the time at $O(\varepsilon^{-2})$, i.e., $\beta = 2$.

We first test the spatial discretization errors at $t_\varepsilon = 1/\varepsilon^\beta$ for different $0 < \varepsilon \leq 1$. In order to do this, we fix the time step as $\tau_e = 10^{-5}$ such that the temporal error can be ignored, and solve the NKGE (2.1.1) under different mesh size h. Tables 2.1, 2.3 and 2.5 depict the spatial errors for the CNFD method with $\beta = 0$, $\beta = 1$ and $\beta = 2$, respectively. Then we check the temporal errors at $t_\varepsilon = 1/\varepsilon^\beta$ for different $0 < \varepsilon \leq 1$ with different time step τ and a fine mesh size $h_e = \pi/2^{15}$ such that the spatial errors can be neglected. Tables 2.2, 2.4 and 2.6 show the temporal errors for the CNFD method and Tables 2.7-2.9 list the temporal errors for the SIFD2 method with $\beta = 0$, $\beta = 1$ and $\beta = 2$, respectively.

From Tables 2.1-2.6 for the CNFD method, Tables 2.7-2.9 for the SIFD2 method, and additional similar numerical results for other FDTD methods not shown here for brevity, we can draw the following observations:

(i) For any fixed $\varepsilon = \varepsilon_0 > 0$ or $\beta = 0$, the FDTD methods are uniformly second-order accurate in both spatial and temporal discretizations (cf. Tables 2.1, 2.2, 2.7 and the first rows in Tables 2.3-2.6&2.8-2.9), which agree with those results in the literature.

(ii) In the intermediate long-time regime, i.e. $\beta = 1$, the second order convergence in space and time of the FDTD methods can be observed only when $0 < h \lesssim \varepsilon^{1/2}$ and $0 < \tau \lesssim \varepsilon^{1/2}$ (cf. upper triangles above the diagonals (corresponding to $h \sim \varepsilon^{1/2}$ and

$e_{h,\tau_e}(t=1/\varepsilon^\beta)$	$h_0=\pi/16$	$h_0/2$	$h_0/2^2$	$h_0/2^3$	$h_0/2^4$	$h_0/2^5$
$\varepsilon_0=1$	3.77E-2	9.65E-3	2.43E-3	6.09E-4	1.52E-4	3.84E-5
order	-	1.97	1.99	2.00	2.00	1.98
$\varepsilon_0/2$	3.33E-2	8.35E-3	2.09E-3	5.22E-4	1.31E-4	3.34E-5
order	-	2.00	2.00	2.00	1.99	1.97
$\varepsilon_0/2^2$	3.48E-2	8.74E-3	2.19E-3	5.47E-4	1.37E-4	3.50E-5
order	-	1.99	2.00	2.00	2.00	1.97
$\varepsilon_0/2^3$	3.55E-2	8.92E-3	2.23E-3	5.58E-4	1.40E-4	3.57E-5
order	-	1.99	2.00	2.00	1.99	1.97
$\varepsilon_0/2^4$	3.57E-2	8.97E-3	2.24E-3	5.61E-4	1.40E-4	3.59E-5
order	-	1.99	2.00	2.00	2.00	1.96

Table 2.1: Spatial errors of the CNFD (2.3.2) for the NKGE (2.1.1) with $\beta=0$ and initial data (2.5.1).

$e_{h_e,\tau}(t=1/\varepsilon^\beta)$	$\tau_0=0.05$	$\tau_0/2$	$\tau_0/2^2$	$\tau_0/2^3$	$\tau_0/2^4$	$\tau_0/2^5$
$\varepsilon_0=1$	3.27E-2	8.57E-3	2.19E-3	5.53E-4	1.39E-4	3.48E-5
order	-	1.93	1.97	1.99	1.99	2.00
$\varepsilon_0/2$	2.10E-2	5.45E-3	1.39E-3	3.49E-4	8.76E-5	2.20E-5
order	-	1.96	1.97	1.99	1.99	1.99
$\varepsilon_0/2^2$	1.84E-2	4.75E-3	1.21E-3	3.04E-4	7.63E-5	1.91E-5
order	-	1.95	1.97	1.99	1.99	2.00
$\varepsilon_0/2^3$	1.78E-2	4.59E-3	1.17E-3	2.94E-4	7.37E-5	1.85E-5
order	-	1.96	1.97	1.99	2.00	1.99
$\varepsilon_0/2^4$	1.77E-2	4.56E-3	1.16E-3	2.91E-4	7.31E-5	1.83E-5
order	-	1.96	1.97	2.00	1.99	2.00

Table 2.2: Temporal errors of the CNFD (2.3.2) for the NKGE (2.1.1) with $\beta=0$ and initial data (2.5.1).

$e_{h,\tau_e}(t=1/\varepsilon^\beta)$	$h_0=\pi/16$	$h_0/2$	$h_0/2^2$	$h_0/2^3$	$h_0/2^4$	$h_0/2^5$
$\varepsilon_0=1$	**3.77E-2**	9.65E-3	2.43E-3	6.09E-4	1.52E-4	3.84E-5
order	**-**	1.97	1.99	2.00	2.00	1.98
$\varepsilon_0/4$	7.31E-2	**1.77E-2**	4.38E-3	1.09E-3	2.74E-4	7.02E-5
order	-	**2.05**	2.01	2.01	1.99	1.96
$\varepsilon_0/4^2$	6.60E-1	1.71E-1	**4.31E-2**	1.08E-2	2.70E-3	6.91E-4
order	-	1.95	**1.99**	2.00	2.00	1.97
$\varepsilon_0/4^3$	2.78	7.25E-1	1.80E-1	**4.50E-2**	1.13E-2	2.88E-3
order	-	1.94	2.01	**2.00**	1.99	1.97
$\varepsilon_0/4^4$	5.67	8.48E-1	3.96E-1	1.10E-1	**2.81E-2**	7.22E-3
order	-	2.74	1.10	1.85	**1.97**	1.96

Table 2.3: Spatial errors of the CNFD (2.3.2) for the NKGE (2.1.1) with $\beta=1$ and initial data (2.5.1).

$e_{h_e,\tau}(t=1/\varepsilon^\beta)$	$\tau_0=0.05$	$\tau_0/2$	$\tau_0/2^2$	$\tau_0/2^3$	$\tau_0/2^4$	$\tau_0/2^5$
$\varepsilon_0=1$	**3.27E-2**	8.57E-3	2.19E-3	5.53E-4	1.39E-4	3.48E-5
order	**-**	1.93	1.97	1.99	1.99	2.00
$\varepsilon_0/4$	4.01E-2	**9.95E-3**	2.49E-3	6.22E-4	1.56E-4	3.89E-5
order	-	**2.01**	2.00	2.00	2.00	2.00
$\varepsilon_0/4^2$	3.45E-1	8.79E-2	**2.21E-2**	5.53E-3	1.38E-3	3.46E-4
order	-	1.97	**1.99**	2.00	2.00	2.00
$\varepsilon_0/4^3$	1.47	3.69E-1	9.19E-2	**2.29E-2**	5.74E-3	1.43E-3
order	-	1.99	2.01	**2.00**	2.00	2.01
$\varepsilon_0/4^4$	8.58E-1	7.05E-1	2.20E-1	5.75E-2	**1.45E-2**	3.64E-3
order	-	0.28	1.68	1.94	**1.99**	1.99

Table 2.4: Temporal errors of the CNFD (2.3.2) for the NKGE (2.1.1) with $\beta=1$ and initial data (2.5.1).

$e_{h,\tau_e}(t=1/\varepsilon^\beta)$	$h_0=\pi/16$	$h_0/2$	$h_0/2^2$	$h_0/2^3$	$h_0/2^4$	$h_0/2^5$
$\varepsilon_0=1$	**3.77E-2**	9.65E-3	2.43E-3	6.09E-4	1.52E-4	3.84E-5
order	**-**	1.97	1.99	2.00	2.00	1.98
$\varepsilon_0/2$	3.98E-2	**9.56E-3**	2.39E-3	5.97E-4	1.49E-4	3.81E-5
order	-	**2.06**	2.00	2.00	2.00	1.97
$\varepsilon_0/2^2$	7.17E-1	1.82E-1	**4.55E-2**	1.14E-2	2.85E-3	7.27E-4
order	-	1.98	**2.00**	2.00	2.00	1.97
$\varepsilon_0/2^3$	2.78	6.54E-1	1.58E-1	**3.92E-2**	9.78E-3	2.50E-3
order	-	2.09	2.05	**2.01**	2.00	1.97
$\varepsilon_0/2^4$	3.31	1.78	5.92E-1	1.55E-1	**3.93E-2**	1.01E-2
order	-	0.89	1.59	1.93	**1.98**	1.96

Table 2.5: Spatial errors of the CNFD (2.3.2) for the NKGE (2.1.1) with $\beta=2$ and initial data (2.5.1).

$e_{h_e,\tau}(t=1/\varepsilon^\beta)$	$\tau_0=0.05$	$\tau_0/2$	$\tau_0/2^2$	$\tau_0/2^3$	$\tau_0/2^4$	$\tau_0/2^5$
$\varepsilon_0=1$	**3.27E-2**	8.57E-3	2.19E-3	5.53E-4	1.39E-4	3.48E-5
order	**-**	1.93	1.97	1.99	1.99	2.00
$\varepsilon_0/2$	2.56E-2	**6.32E-3**	1.58E-3	3.94E-4	9.86E-5	2.47E-5
order	-	**2.02**	2.00	2.00	2.00	2.00
$\varepsilon_0/2^2$	3.91E-1	9.83E-2	**2.46E-2**	6.16E-3	1.54E-3	3.85E-4
order	-	1.99	**2.00**	2.00	2.00	2.00
$\varepsilon_0/2^3$	1.40	3.32E-1	8.14E-2	**2.03E-2**	5.06E-3	1.26E-3
order	-	2.08	2.03	**2.00**	2.00	2.01
$\varepsilon_0/2^4$	1.81	1.13	3.16E-1	8.07E-2	**2.03E-2**	5.07E-3
order	-	0.68	1.84	1.97	**1.99**	2.00

Table 2.6: Temporal errors of the CNFD (2.3.2) for the NKGE (2.1.1) with $\beta=2$ and initial data (2.5.1).

$e_{h_e,\tau}(t=1/\varepsilon^\beta)$	$\tau_0=0.05$	$\tau_0/2$	$\tau_0/2^2$	$\tau_0/2^3$	$\tau_0/2^4$	$\tau_0/2^5$
$\varepsilon_0=1$	1.85E-2	4.80E-3	1.22E-3	3.07E-4	7.71E-5	1.93E-5
order	-	1.95	1.98	1.99	1.99	2.00
$\varepsilon_0/2$	1.73E-2	4.46E-3	1.13E-3	2.85E-4	7.16E-5	1.79E-5
order	-	1.96	1.98	1.99	1.99	2.00
$\varepsilon_0/2^2$	1.75E-2	4.51E-3	1.14E-3	2.88E-4	7.23E-5	1.81E-5
order	-	1.96	1.98	1.98	1.99	2.00
$\varepsilon_0/2^3$	1.76E-2	4.54E-3	1.15E-3	2.90E-4	7.28E-5	1.82E-5
order	-	1.95	1.98	1.99	1.99	2.00
$\varepsilon_0/2^4$	1.76E-2	4.54E-3	1.15E-3	2.91E-4	7.29E-5	1.83E-5
order	-	1.95	1.98	1.98	2.00	1.99

Table 2.7: Temporal errors of the SIFD2 (2.3.4) for the NKGE (2.1.1) with $\beta=0$ and initial data (2.5.1).

$e_{h_e,\tau}(t=1/\varepsilon^\beta)$	$\tau_0=0.05$	$\tau_0/2$	$\tau_0/2^2$	$\tau_0/2^3$	$\tau_0/2^4$	$\tau_0/2^5$
$\varepsilon_0=1$	**1.85E-2**	4.80E-3	1.22E-3	3.07E-4	7.71E-5	1.93E-5
order	**-**	1.95	1.98	1.99	1.99	2.00
$\varepsilon_0/4$	3.79E-2	**9.40E-3**	2.35E-3	5.88E-4	1.47E-4	3.68E-5
order	-	**2.01**	2.00	2.00	2.00	2.00
$\varepsilon_0/4^2$	3.44E-1	8.76E-2	**2.20E-2**	5.51E-3	1.38E-3	3.45E-4
order	-	1.97	**1.99**	2.00	2.00	2.00
$\varepsilon_0/4^3$	1.47	3.69E-1	9.19E-2	**2.29E-2**	5.74E-3	1.43E-3
order	-	1.99	2.01	**2.00**	2.00	2.01
$\varepsilon_0/4^4$	8.59E-1	7.05E-1	2.20E-1	5.75E-2	**1.45E-2**	3.64E-3
order	-	0.29	1.68	1.94	**1.99**	1.99

Table 2.8: Temporal errors of the SIFD2 (2.3.4) for the NKGE (2.1.1) with $\beta=1$ and initial data (2.5.1).

$e_{h_e,\tau}(t=1/\varepsilon^\beta)$	$\tau_0=0.05$	$\tau_0/2$	$\tau_0/2^2$	$\tau_0/2^3$	$\tau_0/2^4$	$\tau_0/2^5$
$\varepsilon_0=1$	**1.85E-2**	4.80E-3	1.22E-3	3.07E-4	7.71E-5	1.93E-5
order	**-**	1.95	1.98	1.99	1.99	2.00
$\varepsilon_0/2$	2.00E-2	**4.94E-3**	1.23E-3	3.09E-4	7.72E-5	1.93E-5
order	-	**2.02**	2.01	1.99	2.00	2.00
$\varepsilon_0/2^2$	3.73E-1	9.38E-2	**2.35E-2**	5.88E-3	1.47E-3	3.67E-4
order	-	1.99	**2.00**	2.00	2.00	2.00
$\varepsilon_0/2^3$	1.38	3.28E-1	8.05E-2	**2.00E-2**	5.00E-3	1.25E-3
order	-	2.07	2.03	**2.01**	2.00	2.00
$\varepsilon_0/2^4$	1.81	1.13	3.15E-1	8.04E-2	**2.02E-2**	5.06E-3
order	-	0.68	1.84	1.97	**1.99**	2.00

Table 2.9: Temporal errors of the SIFD2 (2.3.4) for the NKGE (2.1.1) with $\beta=2$ and initial data (2.5.1).

$\tau \sim \varepsilon^{1/2}$, and being labelled in bold letters) in Tables 2.3-2.4&2.8), which confirm our error bounds.

(iii) In the long-time regime, i.e. $\beta=2$, the second order convergence in space and time of the FDTD methods can be observed only when $0<h\lesssim\varepsilon$ and $0<\tau\lesssim\varepsilon$ (cf. upper triangles above the diagonals (corresponding to $h\sim\varepsilon$ and $\tau\sim\varepsilon$, and being labelled in bold letters) in Tables 2.5-2.6&2.9), which again confirm our error bounds.

In summary, our numerical results confirm our rigorous error bounds and show that they are sharp.

For the above FDTD methods, all schemes are time symmetric. The CNFD method is fully implicit and depends on a direct solver or an iterative solver which is quite time-consuming. Thus, the CNFD method is usually not adopted in practical computation especially in high dimensions. However, the other FDTD methods naturally suffer from stability problems. The four FDTD methods share the same spatial/temporal resolution capacity for the NKGE (2.1.1) up to the time at $O(\varepsilon^{-\beta})$ with $0\le\beta\le 2$. It is necessary to choose the time step satisfying the stability conditions for the numerical simulations of the SIFD1, SIFD2 and LFFD methods.

2.6 A semi-implicit fourth-order compact method

In order to improve the spatial resolution capacity of the FDTD methods, we consider the full-discretization with the fourth-order compact finite difference (4cFD) method [57].

2.6.1 The method and its stability

We introduce the following finite difference operator

$$\mathcal{A}u_j^n = \left(1 + \frac{h^2}{12}\delta_x^2\right) u_j^n = \frac{1}{12}(u_{j-1}^n + 10u_j^n + u_{j+1}^n).$$

To simplify notations, for a function $u(x,t)$ and a grid function $u^n \in X_M (n \geq 0)$, we denote for $n \geq 1$,

$$u(x, t_{[n]}) = \frac{u(x,t_{n+1}) + u(x,t_{n-1})}{2}, \ x \in \bar{\Omega}; \quad u_j^{[n]} = \frac{u_j^{n+1} + u_j^{n-1}}{2}, \ j = 0, 1, \cdots, M.$$

A fourth-order approximation is implemented by replacing the central difference operator δ_x^2 with $(1 - \frac{h^2}{12}\delta_x^2)\delta_x^2$, which requires a five-point stencil. In order to obtain a compact three-point stencil, $(1 - \frac{h^2}{12}\delta_x^2)\delta_x^2$ is approximated by $(1 + \frac{h^2}{12}\delta_x^2)^{-1}\delta_x^2$ [92, 98, 103, 111, 155].

We consider the following semi-implicit fourth-order compact finite difference (4cFD) method:

$$\delta_t^2 u_j^n - \mathcal{A}^{-1}\delta_x^2 u_j^{[n]} + u_j^{[n]} + \varepsilon^2 (u_j^n)^3 = 0, \quad j = 0, 1, \cdots, M-1, \quad n \geq 1. \tag{2.6.1}$$

The initial and boundary conditions in (2.1.1) are discretized as

$$u_0^{n+1} = u_M^{n+1}, \quad u_{-1}^{n+1} = u_{M-1}^{n+1}, \quad n \geq 0; \quad u_j^0 = \phi(x_j), \quad j = 0, 1, \cdots, M, \tag{2.6.2}$$

where the first step u^1 is updated by the initial data and Taylor expansion as

$$u_j^1 = \phi(x_j) + \tau\gamma(x_j) + \frac{\tau^2}{2}\left[\phi''(x_j) - \phi(x_j) - \varepsilon^p \left(\phi(x_j)\right)^{p+1}\right], \ j = 0, 1, \cdots, M. \tag{2.6.3}$$

Remark 2.6.1. *For the first step u^1, we can also replace $\phi''(x_j)$ by $\mathcal{A}^{-1}\delta_x^2\phi(x_j)$ when it is not easy to calculate $\phi''(x)$.*

Remark 2.6.2. *The other three finite difference discretizations in time mentioned in Section 2.2 combined with the fourth-order compact finite difference discretization in space are similar with the semi-implicit 4cFD method and we omit the details here for brevity.*

Clearly, the semi-implicit 4cFD method is time symmetric or time reversible, i.e., it is unchanged if interchanging $n+1 \leftrightarrow n-1$ and $\tau \leftrightarrow -\tau$. The semi-implicit 4cFD (2.6.1) can be explicitly updated in the Fourier space with $O(M \ln M)$ computational cost per time step [5, 13].

Let $T_0 > 0$ be a fixed constant and $0 \le \beta \le 2$, and denote

$$\sigma_{\max} := \max_{0 \le n \le T_0\varepsilon^{-\beta}/\tau} \|u^n\|_{l^\infty}^2. \tag{2.6.4}$$

By using the standard von Neumann analysis [9, 13], we have the following lemma for the stability of the semi-implicit 4cFD method for the NKGE (2.1.1).

Lemma 2.6.1. *(stability) For the semi-implicit 4cFD method applied to the NKGE* (2.1.1) *up to the time $t = T_0/\varepsilon^\beta$, when $\sigma_{\max} \le \varepsilon^{-2}$, the scheme is unconditionally stable for any $h > 0$ and $\tau > 0$; and when $\sigma_{\max} > \varepsilon^{-2}$, it is conditionally stable under the stability condition*

$$0 < \tau < \frac{2}{\sqrt{\sigma_{\max} - 1}}, \quad h > 0, \quad 0 < \varepsilon \le 1. \tag{2.6.5}$$

Proof. Replacing the nonlinear term by $f(u) = \varepsilon^2\sigma_{\max}u$, plugging

$$u_j^{n-1} = \sum_l \hat{U}_l e^{2ijl\pi/M}, \quad u_j^n = \sum_l \xi_l \hat{U}_l e^{2ijl\pi/M}, \quad u_j^{n+1} = \sum_l \xi_l^2 \hat{U}_l e^{2ijl\pi/M},$$

into (2.6.1), with ξ_l the amplification factor of the lth mode in phase space, we have the following characteristic equation

$$\xi_l^2 - 2\frac{2 - \tau^2\varepsilon^2\sigma_{\max}}{2 + \tau^2(1 + c\lambda_l^2)}\xi_l + 1 = 0, \quad l = -\frac{M}{2}, \cdots, \frac{M}{2} - 1, \tag{2.6.6}$$

with

$$c = \frac{3}{3 - \sin^2\left(\frac{\pi l}{M}\right)}, \quad \lambda_l = \frac{2}{h}\sin\left(\frac{\pi l}{M}\right), \quad \mu_l = \frac{2\pi l}{b-a}. \tag{2.6.7}$$

Solving the characteristic equation (2.6.6), we have $\xi_l = \theta_l \pm \sqrt{\theta_l^2 - 1}$. The stability of the numerical scheme amounts to

$$|\xi_l| \leq 1 \iff |\theta_l| \leq 1, \quad l = -\frac{M}{2}, \cdots, \frac{M}{2} - 1. \tag{2.6.8}$$

Noticing $c \geq 1$ and $0 \leq \lambda_l^2 \leq \frac{4}{h^2}$, when $\sigma_{\max} \leq \varepsilon^{-2}$, or $\sigma_{\max} > \varepsilon^{-2}$ with the condition (2.6.5), we can get

$$\tau^2(\varepsilon^2\sigma_{\max} - 1 - c\lambda_l^2) \leq \tau^2(\varepsilon^2\sigma_{\max} - 1) \leq 4 \implies |\theta_l| \leq 1, \quad l = -\frac{M}{2}, \cdots, \frac{M}{2} - 1.$$

The proof is completed. $\square$

Remark 2.6.3. *The stability of the semi-implicit 4cFD* (2.6.1) *is related to* $\sigma_{\max}$*, dependent on the boundedness of the* l^∞ *norm of the numerical solution* u^n*. The error estimates up to the previous time step could ensure the boundedness, by the inverse inequality, and such an error estimate could be recovered at the next time step, as given by the Theorem presented in Section 2.6.2.*

2.6.2 Error estimates

According to the known results in [43, 44, 89] and references therein, we can make the assumptions on the exact solution u of the NKGE (2.1.1) up to the time $t = T_0/\varepsilon^2$:

$$(B) \quad \begin{aligned} &u \in C([0, T_0/\varepsilon^p]; W_p^{6,\infty}) \cap C^2([0, T_0/\varepsilon^p]; W^{4,\infty}) \cap C^4([0, T_0/\varepsilon^p]; W^{2,\infty}), \\ &\left\| \frac{\partial^{r+q}}{\partial t^r \partial x^q} u(x,t) \right\|_{L^\infty} \lesssim 1, \quad 0 \leq r \leq 4, \quad 0 \leq r+q \leq 6, \end{aligned}$$

here $W_p^{m,\infty} = \{u \in W^{m,\infty} | \frac{\partial^l}{\partial x^l}u(a) = \frac{\partial^l}{\partial x^l}u(b), \quad 0 \leq l < m\}$ for $m \geq 1$.

We have the following error estimates for the semi-implict 4cFD (2.6.1) with (2.6.2) and (2.6.3) up to the time $t = T_0/\varepsilon^\beta$ with $0 \leq \beta \leq 2$:

Theorem 2.6.1. *Under the assumption (B), there exist constants* $h_0 > 0$ *and* $\tau_0 > 0$ *sufficiently small and independent of* ε*, such that for any* $0 < \varepsilon \leq 1$*, when* $0 < h \leq$

$h_0\varepsilon^{\beta/4}$, $0 < \tau \le \tau_0\varepsilon^{\beta/2}$ and under the stability condition (2.6.5)*, the following two error estimates of the scheme* (2.6.1) *with* (2.6.2) *and* (2.6.3) *hold*

$$\|e^n\|_{l^2} + \|\delta_x^+ e^n\|_{l^2} \lesssim \frac{h^4}{\varepsilon^\beta} + \frac{\tau^2}{\varepsilon^\beta}, \quad \|u^n\|_{l^\infty} \le 1 + M_0, \quad 0 \le n \le \frac{T_0/\varepsilon^\beta}{\tau}. \tag{2.6.9}$$

Remark 2.6.4. *The above error bounds in Theorem 2.6.1 are still valid in higher dimensions, i.e., $d = 2, 3$, provided the technical conditions $0 < h \lesssim \varepsilon^{\beta/4}\sqrt{C_d(h)}$ and $0 < \tau \lesssim \varepsilon^{\beta/2}\sqrt{C_d(h)}$.*

Based on the above theorem, the 4cFD method has the following spatial/temporal resolution capacity for the NKGE (2.1.1) in the long-time regime. In fact, given an accuracy bound $\delta_0 > 0$, the ε-scalability of the 4cFD method is:

$$h = O(\varepsilon^{\beta/4}\sqrt{\delta_0}) = O(\varepsilon^{\beta/4}), \quad \tau = O(\varepsilon^{\beta/2}\sqrt{\delta_0}) = O(\varepsilon^{\beta/2}), \quad 0 < \varepsilon \le 1. \tag{2.6.10}$$

Compared with the FDTD methods, the results can attain higher order accuracy in space for a given mesh size or improve the spatial resolution capacity, i.e., it needs less grid points while maintaining the same accuracy.

In order to prove Theorem 2.6.1, we first present some useful lemmas. The operator $\mathcal{A}$ can be written as a matrix

$$A = \frac{1}{12}\begin{pmatrix} 10 & 1 & & 1 \\ 1 & 10 & 1 & \\ & \ddots & \ddots & \\ 1 & & 1 & 10 \end{pmatrix}. \tag{2.6.11}$$

It is easy to check that A is an $(M+1)\times(M+1)$ positive definite matrix, then we can introduce a new discrete norm $\|u\|_* = \sqrt{(A^{-1}u, u)}$ for $u \in X_M$. The proofs of the following lemmas proceed in the analogous lines as in [103, 155] and we just show the proof of Lemma 2.6.4 in detail here for brevity.

Lemma 2.6.2. *For any two grid functions $u, v \in X_M$, it holds*

$$(\delta_x^+\delta_x^- u, v) = -(\delta_x^+ u, \delta_x^+ v). \tag{2.6.12}$$

Lemma 2.6.3. *The operators $\mathcal{A}$ and $\mathcal{A}^{-1}$ are commutative with δ_x^+ and δ_x^-, i.e., for any grid function $u \in X_M$,*

$$\begin{aligned}
&\delta_x^+ \mathcal{A} u = \mathcal{A} \delta_x^+ u, \quad \delta_x^- \mathcal{A} u = \mathcal{A} \delta_x^- u, \\
&\delta_x^+ \mathcal{A}^{-1} u = \mathcal{A}^{-1} \delta_x^+ u, \quad \delta_x^- \mathcal{A}^{-1} u = \mathcal{A}^{-1} \delta_x^- u.
\end{aligned} \tag{2.6.13}$$

Lemma 2.6.4. *The discrete norms $\|\cdot\|_*$ and $\|\cdot\|_{l^2}$ are equivalent. In fact, for any grid function $u \in X_M$, it holds*

$$\|u\|_{l^2} \le \|u\|_* \le \frac{\sqrt{6}}{2}\|u\|_{l^2}. \tag{2.6.14}$$

Proof. For $\forall x \in \mathbb{R}^{M+1}$, $x = (x_0, x_2, \cdots, x_M)^T$, we have

$$\begin{aligned}
12x^T A x &= 10\sum_{j=0}^{M} x_j^2 + 2\sum_{j=1}^{M} x_{j-1}x_j + 2x_0 x_M \\
&= 10\sum_{j=0}^{M} x_j^2 + \sum_{j=1}^{M}(x_{j-1}+x_j)^2 - \sum_{j=1}^{M}(x_{j-1}^2 + x_j^2) + (x_0+x_M)^2 - (x_0^2 + x_M^2) \\
&= 8\sum_{j=0}^{M} x_j^2 + \sum_{j=1}^{M}(x_{j-1}+x_j)^2 + (x_0+x_M)^2 \\
&\ge 8x^T x
\end{aligned} \tag{2.6.15}$$

and

$$\begin{aligned}
12x^T A x &= 10\sum_{j=0}^{M} x_j^2 + 2\sum_{j=1}^{M} x_{j-1}x_j + 2x_0 x_M \\
&\le 10\sum_{j=0}^{M} x_j^2 + \sum_{j=1}^{M}(x_{j-1}^2 + x_j^2) + (x_0^2 + x_M^2) \\
&= 12\sum_{j=0}^{M} x_j^2 \\
&= 12x^T x.
\end{aligned} \tag{2.6.16}$$

As we know,

$$\lambda_{\min} x^T x \le x^T A x \le \lambda_{\max} x^T x, \tag{2.6.17}$$

where $\lambda_{\min}$ and $\lambda_{\max}$ are the minimal and maximal eigenvalues of the matrix A, respectively. We take the left (right) equal if and only if x is the eigenvector of $\lambda_{\min}(\lambda_{\max})$. From (2.6.15) and (2.6.16), we could obtain

$$\frac{2}{3} \leq \lambda_{\min} \leq \lambda_{\max} \leq 1.$$

Applying (2.6.17) to the matrix A^{-1}, we have

$$\|u\|_{l^2}^2 \leq \min_{\lambda_j \in \sigma(A^{-1})} \lambda_j \|u\|_{l^2}^2 \leq \|u\|_*^2 \leq \max_{\lambda_j \in \sigma(A^{-1})} \lambda_j \|u\|_{l^2}^2 \leq \frac{3}{2}\|u\|_{l^2}^2,$$

which implies

$$\|u\|_{l^2} \leq \|u\|_* \leq \frac{\sqrt{6}}{2}\|u\|_{l^2}.$$

□

Based on the above lemmas, we will establish the error bounds in Theorem 2.6.1 by the method of mathematical induction [5, 7]. Throughout the proof, the stability condition (2.6.5) is assumed.

Denote the local truncation error as $\xi^n \in X_M$ for $0 \leq n \leq \frac{T_0/\varepsilon^\beta}{\tau} - 1$

$$\begin{aligned} \xi_j^0 &:= \delta_t^+ u(x_j, 0) - \gamma(x_j) - \frac{\tau}{2}\left[\phi''(x_j) - \phi(x_j) - \varepsilon^2(\phi(x_j))^3\right], \; j = 0, 1, \cdots, M-1, \\ \xi_j^n &:= \delta_t^2 u(x_j, t_n) - \mathcal{A}^{-1}\delta_x^2 u(x_j, t_{[n]}) + u(x_j, t_{[n]}) + \varepsilon^2 u^3(x_j, t_n), \; n \geq 1, \end{aligned} \tag{2.6.18}$$

and the error of the nonlinear term as $\eta^n \in X_M$

$$\eta_j^n := \varepsilon^2\left(u^3(x_j, t_n) - (u_j^n)^3\right), \quad j = 0, 1, \cdots, M, \quad 1 \leq n \leq \frac{T_0/\varepsilon^\beta}{\tau} - 1. \tag{2.6.19}$$

We begin with the error estimates of local truncation error $\xi^n \in X_M$.

Lemma 2.6.5. *Under the assumption (B), we have*

$$\|\xi^0\|_{l^2} + \|\delta_x^+ \xi^0\|_{l^2} \lesssim \tau^2, \quad \|\xi^n\|_{l^2} \lesssim h^4 + \tau^2, \quad 1 \leq n \leq \frac{T_0/\varepsilon^\beta}{\tau} - 1. \tag{2.6.20}$$

Proof. Under the assumption (B), by applying the Taylor expansion, Young's inequality and Lemma 2.6.3, we have

$$
\begin{aligned}
|\xi_j^0| &\lesssim \tau^2 \|\partial_{ttt} u\|_{L^\infty} \lesssim \tau^2, \quad j = 0, 1, \cdots, M-1, \\
|\mathcal{A}\xi_j^n| &\lesssim \tau^2 \left[\|\partial_{tt} u\|_{L^\infty} + \|\partial_{tttt} u\|_{L^\infty} + \|\partial_{ttxx} u\|_{L^\infty} + \|\partial_{ttttxx} u\|_{L^\infty}\right] \\
&\quad + h^4 \left[\|\partial_{xxxx} u\|_{L^\infty} + \|\partial_{ttxxxx} u\|_{L^\infty} + \|\partial_{xxxxxx} u\|_{L^\infty}\right] \lesssim\ h^4 + \tau^2,\ n \geq 1,
\end{aligned}
$$

which leads to $|\xi_j^n| \lesssim\ h^4 + \tau^2$ for $j = 0, 1, \cdots, M-1,\ n \geq 1$. Similarly, we have $|\delta_x^+ \xi_j^0| \lesssim \tau^2$ for $j = 0, 1, \cdots, M-1$. These immediately imply the estimates in (2.6.20). □

Next, the error equation for the semi-implicit 4cFD (2.6.1) is

$$
\begin{aligned}
&\delta_t^2 e_j^n - \mathcal{A}^{-1}\delta_x^2 e_j^{[n]} + e_j^{[n]} = \xi_j^n - \eta_j^n, \quad 1 \leq n \leq \frac{T_0/\varepsilon^\beta}{\tau}, \\
&e_j^0 = 0, \quad e_j^1 = \tau\xi_j^0, \quad j = 0, 1, \cdots, M-1.
\end{aligned}
\tag{2.6.21}
$$

Then, we are going to prove Theorem 2.6.1 by the method of mathematical induction. For $n = 0$, (2.6.9) is trivial. For $n = 1$, the error function (2.6.21) and the error estimates of the local truncation error (2.6.20) imply

$$
\|e^1\|_{l^2} = \tau\|\xi^0\|_{l^2} \leq C_1\tau^3, \quad \|\delta_x^+ e^1\|_{l^2} = \tau\|\delta_x^+\xi^0\|_{l^2} \leq C_1\tau^3.
$$

By the triangle inequality, discrete Sobolev inequality and the assumption (B), there exists a constant $\tau_1 > 0$ sufficiently small, when $0 < \tau < \tau_1$, we have

$$
\|u^1\|_{l^\infty} \leq \|u(x, t_1)\|_{L^\infty} + \|e^1\|_{l^\infty} \leq \|u(x, t_1)\|_{L^\infty} + \|e^1\|_{l^2} + \|\delta_x^+ e^1\|_{l^2} \leq M_0 + 1,
$$

which immediately implies (2.6.9) for $n = 1$.

Now assuming that (2.6.9) is valid for all $0 \leq n \leq m-1 \leq \frac{T_0/\varepsilon^\beta}{\tau} - 1$, it needs to prove that it is still valid when $n = m$. Under the assumption (B), the error of the nonlinear term η^n for $1 \leq n \leq m-1$ can be controlled as

$$
\|\eta^n\|_{l^2} \leq C_2\varepsilon^2\|e^n\|_{l^2}, \quad 1 \leq n \leq m-1. \tag{2.6.22}
$$

Define the "energy" for the error vector $e^n \in X_M (n \geq 0)$ as

$$
S^n = \|\delta_t^+ e^n\|_{l^2}^2 + \frac{1}{2}\left(\|\delta_x^+ e^n\|_*^2 + \|\delta_x^+ e^{n+1}\|_*^2\right) + \frac{1}{2}\left(\|e^n\|_{l^2}^2 + \|e^{n+1}\|_{l^2}^2\right), \quad n \geq 0.
$$

By Lemma 2.6.4, it is easy to see that

$$S^0 = \|\delta_t^+ e^0\|_{l^2}^2 + \frac{1}{2}\|\delta_x^+ e^1\|_*^2 + \frac{1}{2}\|e^1\|_{l^2}^2 \lesssim \tau^4.$$

Multiplying both sides of (2.6.21) by $h\left(e_j^{n+1} - e_j^{n-1}\right)$, summing up for j and using the Young's inequality, the inequality (2.6.22), the Lemma 2.6.2, 2.6.3 and 2.6.5, we derive

$$\begin{aligned} S^n - S^{n-1} &= h\sum_{j=0}^{M-1}\left(\xi_j^n - \eta_j^n\right)\left(e_j^{n+1} - e_j^{n-1}\right) \\ &\le \tau\varepsilon^{-\beta}\left(\|\xi^n\|_{l^2}^2 + \|\eta^n\|_{l^2}^2\right) + \tau\varepsilon^{\beta}\left(\|\delta_t^+ e^n\|_{l^2}^2 + \|\delta_t^+ e^{n-1}\|_{l^2}^2\right) \\ &\lesssim \tau\varepsilon^{\beta}\left(S^n + S^{n-1}\right) + \tau\varepsilon^{-\beta}\left(h^4+\tau^2\right)^2, \quad 1 \le n \le m-1. \end{aligned} \tag{2.6.23}$$

Summing the above inequalities from 1 to $m-1$, there exists a constant $C_3 > 0$ such that

$$S^{m-1} \le S^0 + C_3\tau\varepsilon^{\beta}\sum_{n=0}^{m-1} S^n + C_3 T_0 \varepsilon^{-2p}\left(h^4+\tau^2\right)^2. \tag{2.6.24}$$

Then the discrete Gronwall's inequality suggests that there exists a constant $\tau_2 > 0$ sufficiently small such that when $0 < \tau \le \tau_2$, the following holds

$$S^{m-1} \le \left(S^0 + C_3 T_0\varepsilon^{-2\beta}\left(h^4+\tau^2\right)^2\right)e^{2C_3 m\varepsilon^p\tau} \lesssim \varepsilon^{-2\beta}\left(h^4+\tau^2\right)^2. \tag{2.6.25}$$

From the definition of S^{m-1} and Lemma 2.6.4, we can obtain that $\|e^m\|_{l^2}^2 + \|\delta_x^+ e^m\|_{l^2}^2 \le C_4 S^{m-1}$ when $0 < \varepsilon \le 1$, which immediately implies

$$\|e^m\|_{l^2} + \|\delta_x^+ e^m\|_{l^2} \lesssim \frac{h^4}{\varepsilon^\beta} + \frac{\tau^2}{\varepsilon^\beta}. \tag{2.6.26}$$

The first inequality in (2.6.9) is valid for $n = m$ and it remains to estimate $\|u^m\|_{l^\infty}$. In fact, the discrete Sobolev inequality implies

$$\|e^m\|_{l^\infty} \lesssim \|e^m\|_{l^2} + \|\delta_x^+ e^m\|_{l^2} \lesssim \frac{h^4}{\varepsilon^\beta} + \frac{\tau^2}{\varepsilon^\beta}. \tag{2.6.27}$$

Thus, there exist $h_0 > 0$ and $\tau_3 > 0$ sufficiently small such that when $0 < h \le h_0\varepsilon^{\beta/4}$ and $0 < \tau \le \tau_3\varepsilon^{\beta/2}$, we can obtain

$$\|u^m\|_{l^\infty} \le \|u(x,t_m)\|_{L^\infty} + \|e^m\|_{l^\infty} \le M_0 + 1, \quad 1 \le m \le \frac{T_0/\varepsilon^\beta}{\tau}. \tag{2.6.28}$$

Under the stability condition (2.6.5) and the choice of $\tau_0 = \min\{\tau_1, \tau_2, \tau_3\}$, the estimates in (2.6.9) are valid when $n = m$. Hence, the proof of Theorem 2.6.1 is completed by the method of mathematical induction.

2.6.3 Numerical results

In this section, we present the numerical results of the semi-implicit 4cFD method for the NKGE (2.1.1) up to the time at $O(\varepsilon^{-\beta})$ with $0 \le \beta \le 2$. In the numerical experiments, we take $a = 0$, $b = 2\pi$ and choose the initial data as

$$\phi(x) = \frac{3}{2+\cos(x)}, \qquad \gamma(x) = \sin(x), \qquad 0 \le x \le 2\pi. \tag{2.6.29}$$

Denote $u^n_{h,\tau}$ as the numerical solution at time $t = t_n$ obtained by the semi-implicit 4cFD method with mesh size h and time step τ. The 'exact' solution is obtained numerically by the exponential wave integrator Fourier pseudospectral method with a very fine mesh size and a very small time step, e.g. $h_e = \pi/256$ and $\tau_e = 2 \times 10^{-5}$. The errors are displayed at $t = 1/\varepsilon^{\beta}$ with $\beta = 0$ (fixed time dynamics), $\beta = 1$ (intermediate long-time dynamics) and $\beta = 2$ (long-time dynamics), respectively. For spatial error analysis, the time step is set as $\tau_e = 2 \times 10^{-5}$ such that the temporal error can be neglected; for temporal error analysis, we set the mesh size as $h_e = \pi/256$ such that the spatial error can be ignored.

Tables 2.10-2.15 present the spatial and temporal errors for different $0 < \varepsilon \le 1$ and $\beta = 0$, $\beta = 1$ and $\beta = 2$, respectively. From Tables 2.10-2.15 and additional similar numerical results not shown here for brevity, we can draw the following observations:

(i) For any fixed $\varepsilon = \varepsilon_0 > 0$ or $\beta = 0$, the 4cFD methods are fourth-order accurate in space and second-order accurate in time (cf. Tables 2.10&2.11 and the first rows in Tables 2.12-2.15).

(ii) In the intermediate long-time regime, i.e., $\beta = 1$, the fourth order convergence in space and second order convergence in time can be observed only when $0 < h \lesssim \varepsilon^{1/4}$ and $0 < \tau \lesssim \varepsilon^{1/2}$ (cf. upper triangles above the diagonals (corresponding to $h \sim \varepsilon^{1/4}$ and $\tau \sim \varepsilon^{1/2}$, and being labelled in bold letters) in Tables 2.12&2.13), which confirm our error bounds.

(iii) In the long-time regime, i.e., $\beta = 2$, the fourth order convergence in space and second order convergence in time can be observed only when $0 < h \lesssim \varepsilon^{1/2}$ and $0 < \tau \lesssim \varepsilon^{1/2}$ (cf. upper triangles above the diagonals (corresponding to $h \sim \varepsilon^{1/2}$ and $\tau \sim \varepsilon^{1/2}$, and being labelled in bold letters) in Tables 2.14&2.15), which again confirm our error estimates. In summary, our numerical results confirm our rigorous error estimates and show that they are sharp.

$e_{h,\tau_e}(t=1/\varepsilon^\beta)$	$h_0=\pi/8$	$h_0/2$	$h_0/2^2$	$h_0/2^3$	$h_0/2^4$
$\varepsilon_0=1$	1.50E-2	9.58E-4	6.02E-5	3.75E-6	2.37E-7
order	-	3.97	3.99	4.00	3.98
$\varepsilon_0/2$	1.02E-2	6.61E-4	4.14E-5	2.61E-6	1.65E-7
order	-	3.95	4.00	3.99	3.98
$\varepsilon_0/2^2$	8.89E-3	5.83E-4	3.66E-5	2.32E-6	1.45E-7
order	-	3.93	3.99	3.98	4.00
$\varepsilon_0/2^3$	8.51E-3	5.60E-4	3.52E-5	2.24E-6	1.38E-7
order	-	3.93	3.99	3.97	4.02

Table 2.10: Spatial errors of the semi-implicit 4cFD (2.6.1) for the NKGE (2.1.1) with $\beta=0$ and initial data (2.6.29).

$e_{h_e,\tau}(t=1/\varepsilon^\beta)$	$\tau_0=0.1$	$\tau_0/2$	$\tau_0/2^2$	$\tau_0/2^3$	$\tau_0/2^4$	$\tau_0/2^5$
$\varepsilon_0=1$	1.66E-2	4.32E-3	1.10E-3	2.77E-4	6.96E-5	1.74E-5
order	-	1.94	1.97	1.99	1.99	2.00
$\varepsilon_0/2^1$	9.53E-3	2.48E-3	6.30E-4	1.59E-4	3.98E-5	9.98E-6
order	-	1.94	1.98	1.99	2.00	2.00
$\varepsilon_0/2^2$	8.22E-3	2.13E-3	5.40E-4	1.36E-4	3.41E-5	8.55E-6
order	-	1.95	1.98	1.99	2.00	2.00
$\varepsilon_0/2^3$	7.86E-3	2.03E-3	5.16E-4	1.30E-4	3.26E-5	8.16E-6
order	-	1.95	1.98	1.99	2.00	2.00
$\varepsilon_0/2^4$	7.76E-3	2.01E-3	5.09E-4	1.28E-4	3.22E-5	8.06E-6
order	-	1.95	1.98	1.99	1.99	2.00

Table 2.11: Temporal errors of the semi-implicit 4cFD (2.6.1) for the NKGE (2.1.1) with $\beta=0$ and initial data (2.6.29).

$e_{h,\tau_e}(t=1/\varepsilon^\beta)$	$h_0=\pi/8$	$h_0/2$	$h_0/2^2$	$h_0/2^3$	$h_0/2^4$
$\varepsilon_0=1$	1.50E-2	**9.58E-4**	6.02E-5	3.75E-6	2.37E-7
order	-	**3.97**	3.99	4.00	3.98
$\varepsilon_0/2^4$	8.21E-2	3.09E-3	**1.41E-4**	9.29E-6	5.90E-7
order	-	4.73	**4.45**	3.92	3.98
$\varepsilon_0/2^8$	4.44E-1	8.01E-2	9.17E-3	**5.77E-4**	3.57E-5
order	-	2.47	3.13	**3.99**	4.01
$\varepsilon_0/2^12$	4.57E-1	7.96E-1	1.20E-1	7.76E-3	**5.41E-4**
order	-	-0.80	2.73	3.95	**3.84**

Table 2.12: Spatial errors of the semi-implicit 4cFD (2.6.1) for the NKGE (2.1.1) with $\beta=1$ and initial data (2.6.29).

$e_{h_e,\tau}(t=1/\varepsilon^\beta)$	$\tau_0=0.2$	$\tau_0/2$	$\tau_0/2^2$	$\tau_0/2^3$	$\tau_0/2^4$	$\tau_0/2^5$
$\varepsilon_0=1$	**6.02E-2**	1.66E-2	4.32E-3	1.10E-3	2.77E-4	6.96E-5
order	**-**	1.86	1.94	1.97	1.99	1.99
$\varepsilon_0/2^2$	9.52E-2	**2.75E-2**	7.10E-3	1.79E-3	4.49E-4	1.12E-4
order	-	**1.79**	1.95	1.99	2.00	2.00
$\varepsilon_0/2^4$	4.35E-1	1.09E-1	**2.69E-2**	6.76E-3	1.69E-3	4.24E-4
order	-	2.00	**2.02**	1.99	2.00	1.99
$\varepsilon_0/2^6$	1.54	5.55E-1	1.49E-1	**3.64E-2**	9.02E-3	2.26E-3
order	-	1.47	1.90	**2.03**	2.01	2.00
$\varepsilon_0/2^8$	3.28	9.71E-1	5.28E-1	1.30E-1	**3.24E-2**	8.04E-3
order	-	1.76	0.88	2.02	**2.00**	2.01

Table 2.13: Temporal errors of the semi-implicit 4cFD (2.6.1) for the NKGE (2.1.1) with $\beta=1$ and initial data (2.6.29).

$e_{h,\tau_e}(t=1/\varepsilon^\beta)$	$h_0=\pi/8$	$h_0/2$	$h_0/2^2$	$h_0/2^3$	$h_0/2^4$
$\varepsilon_0=1$	1.50E-2	**9.58E-4**	6.02E-5	3.75E-6	2.37E-7
order	-	**3.97**	3.99	4.00	3.98
$\varepsilon_0/2^2$	1.02E-1	7.23E-3	**5.00E-4**	3.21E-5	1.99E-6
order	-	3.82	**3.85**	3.96	4.01
$\varepsilon_0/2^4$	7.80E-1	6.89E-2	8.26E-3	**5.05E-4**	3.17E-5
order	-	3.50	3.06	**4.03**	3.99
$\varepsilon_0/2^6$	5.13E-1	5.48E-1	8.43E-2	7.49E-3	**4.83E-4**
order	-	-0.10	2.70	3.49	**3.95**

Table 2.14: Spatial errors of the semi-implicit 4cFD (2.6.1) for the NKGE (2.1.1) with $\beta=2$ and initial data (2.6.29).

$e_{h_e,\tau}(t=1/\varepsilon^\beta)$	$\tau_0=0.2$	$\tau_0/2$	$\tau_0/2^2$	$\tau_0/2^3$	$\tau_0/2^4$	$\tau_0/2^5$
$\varepsilon_0=1$	**6.02E-2**	1.66E-2	4.32E-3	1.10E-3	2.77E-4	6.96E-5
order	**-**	1.86	1.94	1.97	1.99	1.99
$\varepsilon_0/2$	2.23E-1	**5.92E-2**	1.50E-2	3.78E-3	9.46E-4	2.37E-4
order	-	**1.91**	1.98	1.99	2.00	2.00
$\varepsilon_0/2^2$	5.25E-1	1.46E-1	**3.86E-2**	9.85E-3	2.48E-3	6.20E-4
order	-	1.85	**1.92**	1.97	1.99	2.00
$\varepsilon_0/2^3$	1.40	4.82E-1	1.14E-1	**2.80E-2**	7.03E-3	1.76E-3
order	-	1.54	2.08	**2.03**	1.99	2.00
$\varepsilon_0/2^4$	3.26	1.56	4.83E-1	1.17E-1	**2.95E-2**	7.36E-3
order	-	1.06	1.69	2.05	**1.99**	2.00

Table 2.15: Temporal errors of the semi-implicit 4cFD (2.6.1) for the NKGE (2.1.1) with $\beta=2$ and initial data (2.6.29).

2.7 A semi-implicit Fourier spectral method

In this section, we carry out the full-discretization with Fourier spectral method in spatial discretization and rigorously prove the error bounds. We just show the numerical scheme and error estimate of a semi-implicit scheme, which use the semi-implicit finite difference (2.2.3) in time combined with the Fourier spectral method in space. Other three methods are similar and we omit the details here for brevity.

For an integer $m \geq 0$, $\Omega = (a, b)$, we denote by $H^m(\Omega)$ the standard Sobolev space with norm

$$\|z\|_m^2 = \sum_{l \in \mathbb{Z}} (1 + |\mu_l|^2)^m |\widehat{z}_l|^2, \quad \text{for} \quad z(x) = \sum_{l \in \mathbb{Z}} \widehat{z}_l e^{i\mu_l(x-a)}, \quad \mu_l = \frac{2\pi l}{b-a}, \tag{2.7.1}$$

where $\widehat{z}_l (l \in \mathbb{Z})$ are the Fourier transform coefficients of the function $z(x)$ [7, 8]. For $m = 0$, the space is exactly $L^2(\Omega)$ and the corresponding norm is denoted as $\|\cdot\|$. Furthermore, we denote by $H_{\mathrm{p}}^m(\Omega)$ the space of $H^m(\Omega)$ which consists of functions with derivatives of order up to $m-1$ being $(b-a)$-periodic. We see that the space $H^m(\Omega)$ with fractional m is also well-defined which consists of functions such that $\|\cdot\|_m$ is finite [133].

2.7.1 The method and its stability

Let M be an even positive integer and define the spatial mesh size $h := \Delta x = (b-a)/M$, then the grid points are chosen as

$$x_j := a + jh, \quad j \in \mathcal{T}_M^0 = \{j \mid j = 0, 1, \ldots, M\}. \tag{2.7.2}$$

Define $C_{\mathrm{p}}(\Omega) = \{u \in C(\Omega) \mid u(a) = u(b)\}$ and

$$\begin{aligned} Y_M &:= \operatorname{span}\left\{e^{i\mu_l(x-a)}, \quad x \in \overline{\Omega}, \quad l \in \mathcal{T}_M\right\}, \\ \mathcal{T}_M &= \left\{l \mid l = -\frac{M}{2}, -\frac{M}{2}+1, \ldots, \frac{M}{2}-1\right\}. \end{aligned}$$

For any $u(x) \in C_{\mathrm{p}}(\Omega)$ and a vector $u \in X_M$, let $P_M : L^2(\Omega) \to Y_M$ be the standard L^2-projection operator onto Y_M, $I_M : C_{\mathrm{p}}(\Omega) \to Y_M$ or $I_M : X_M \to Y_M$ be the trigonometric interpolation operator [133], i.e.,

$$(P_M u)(x) = \sum_{l \in \mathcal{T}_M} \widehat{u}_l e^{i\mu_l(x-a)}, \quad (I_M u)(x) = \sum_{l \in \mathcal{T}_M} \widetilde{u}_l e^{i\mu_l(x-a)}, \quad x \in \overline{\Omega}, \tag{2.7.3}$$

where

$$\widehat{u}_l = \frac{1}{b-a}\int_a^b u(x)e^{-i\mu_l(x-a)}dx, \quad \widetilde{u}_l = \frac{1}{M}\sum_{j=0}^{M-1} u_j e^{-i\mu_l(x_j-a)}, \quad l \in \mathcal{T}_M, \tag{2.7.4}$$

with u_j interpreted as $u(x_j)$ when involved.

We apply the Fourier spectral method [77, 133] for discretizing the NKGE (2.1.1) in space, i.e., find

$$u_M(x,t) = \sum_{l\in\mathcal{T}_M} \widehat{(u_M)}_l(t)e^{i\mu_l(x-a)} \in Y_M, \quad x \in \overline{\Omega}, \quad t \geq 0, \tag{2.7.5}$$

such that

$$\partial_{tt}u_M(x,t) - \partial_{xx}u_M(x,t) + u_M(x,t) + \varepsilon^2 P_M f(u_M(x,t)) = 0, \ \ x \in \overline{\Omega}, \ \ t \geq 0, \tag{2.7.6}$$

with $f(u) = u^3$. Denote $u_M^n(x)$ and $\widehat{(u_M^n)}_l$ be the approximations of $u_M(x,t_n)$ and $\widehat{(u_M)}_l(t_n)$. Plugging the (2.7.5) into (2.7.6), noticing the orthogonality of the Fourier basis functions and combining the semi-implicit finite difference (2.2.3) in temporal discretization, we have for $l \in \mathcal{T}_M$, $n \geq 1$,

$$\frac{\widehat{(u_M^{n+1})}_l - 2\widehat{(u_M^n)}_l + \widehat{(u_M^{n-1})}_l}{\tau^2} + \frac{1+\mu_l^2}{2}\left(\widehat{(u_M^{n+1})}_l + \widehat{(u_M^{n-1})}_l\right) + \varepsilon^2(\widehat{f(u_M^n)})_l = 0. \tag{2.7.7}$$

Choosing $u_M^0(x) = (P_M\phi)(x)$, the semi-implicit finite difference Fourier spectral (FDFS) discretization for the NKGE (2.1.1) is to update $u_M^{n+1}(x) \in Y_M$ as

$$u_M^{n+1}(x) = \sum_{l\in\mathcal{T}_M} \widehat{(u_M^{n+1})}_l e^{i\mu_l(x-a)}, \quad x \in \overline{\Omega}, \quad n \geq 0, \tag{2.7.8}$$

where

$$\begin{aligned} \widehat{(u_M^1)}_l &= \left[1 - \frac{\tau^2}{2}(1+\mu_l^2)\right]\widehat{\phi}_l + \tau\widehat{\gamma}_l - \frac{\varepsilon^2\tau^2}{2}\widehat{(f(\phi))}_l, \ l \in \mathcal{T}_M, \\ \widehat{(u_M^{n+1})}_l &= -\widehat{(u_M^{n-1})}_l + \frac{4}{2+\tau^2(1+\mu_l^2)}\widehat{(u_M^n)}_l - \frac{2\varepsilon^2\tau^2(\widehat{f(u_M^n)})_l}{2+\tau^2(1+\mu_l^2)}, \ l \in \mathcal{T}_M, \ n \geq 1. \end{aligned} \tag{2.7.9}$$

However, the above procedure is not suitable in practice since it is difficult to compute the Fourier coefficients in (2.7.9). An efficient implementation is achieved by choosing $u_M^0(x)$ as the interpolation of $\phi(x)$, i.e., $u_M^0 = (I_M\phi)(x)$, and approximating the integrals in (2.7.9) by a quadrature rule on the grids. Let u_j^n be the numerical approximation of $u(x_j,t_n)$ for $j\in\mathcal{T}_M^0$ and $n\ge 0$ and denote $u^n=(u_0^n,u_1^n,\cdots,u_M^n)\in\mathbb{R}^{M+1}$. Denote $u_j^0=\phi(x_j)$ for $j\in\mathcal{T}_M^0$, then the semi-implicit finite difference Fourier pseudospectral (FDFP) method for discretizing the NKGE (2.1.1) via (2.2.3) with a Fourier pseudospectral discretization in space is to find u^{n+1} ($n\ge 0$) as

$$u_j^{n+1}=\sum_{l\in\mathcal{T}_M}\widetilde{(u^{n+1})}_l e^{i\mu_l(x_j-a)},\quad j\in\mathcal{T}_M^0, \tag{2.7.10}$$

where

$$\begin{aligned}&\widetilde{(u^1)}_l=\left[1-\frac{\tau^2}{2}(1+\mu_l^2)\right]\widetilde{\phi}_l+\tau\widetilde{\gamma}_l-\frac{\varepsilon^2\tau^2}{2}\widetilde{(f(\phi))}_l,\quad l\in\mathcal{T}_M,\\&\widetilde{(u^{n+1})}_l=-\widetilde{(u^{n-1})}_l+\frac{4}{2+\tau^2(1+\mu_l^2)}\widetilde{(u^n)}_l-\frac{2\varepsilon^2\tau^2\widetilde{(f(u^n))}_l}{2+\tau^2(1+\mu_l^2)},\ l\in\mathcal{T}_M,\ n\ge 1.\end{aligned} \tag{2.7.11}$$

Similar to the von Neumann stability analysis of the FDTD methods for the NKGE (2.1.1), let $T_0>0$ be a fixed constant and $0\le\beta\le 2$, and denote

$$\sigma_{\max}:=\max_{0\le n\le T_0\varepsilon^{-\beta}/\tau}\|u^n\|_{l^\infty}^2, \tag{2.7.12}$$

then we can conclude the stability of the semi-implicit FDFP method in the following lemma.

Lemma 2.7.1. *(stability) For the semi-implicit FDFP* (2.7.10)-(2.7.11) *applied to the NKGE* (2.1.1) *up to the time $t=T_0/\varepsilon^\beta$, when $\sigma_{max}\le\varepsilon^{-2}$, the semi-implicit FDFP* (2.7.10)-(2.7.11) *is unconditionally stable for any $h>0$ and $\tau>0$; and when $\sigma_{max}>\varepsilon^{-2}$, this scheme is conditionally stable under the stability condition*

$$0<\tau<\frac{2}{\sqrt{\sigma_{\max}-1}},\quad h>0,\quad 0<\varepsilon\le 1. \tag{2.7.13}$$

Proof. We only need to replace λ_l in (2.3.17) by μ_l defined in (2.7.1) and the stability of the semi-implicit FDFP (2.7.10)-(2.7.11) follows immediately. □

2.7.2 Error estimates

In order to obtain an error estimate for the semi-implicit FDFS/FDFP method, we assume that there exists an integer $m_0\ge 1$ such that the exact solution of the NKGE

(2.1.1) up to the time $T_\varepsilon = T_0/\varepsilon^\beta$ with $\beta \in [0,2]$ and $T_0 > 0$ fixed satisfies

$$
(C) \quad \begin{aligned}
&u(x,t) \in C\left([0,T_\varepsilon]; H_p^{m_0+1}\right) \cap C^2\left([0,T_\varepsilon]; H^2\right) \cap C^3\left([0,T_\varepsilon]; H^1\right) \cap C^4\left([0,T_\varepsilon]; L^2\right),\\
&\|u(x,t)\|_{L^\infty\left([0,T_\varepsilon]; H_p^{m_0+1}\right)} \lesssim 1, \quad \|\partial_{tt}u(x,t)\|_{L^\infty([0,T_\varepsilon];H^2)} \lesssim 1,\\
&\|\partial_{ttt}u(x,t)\|_{L^\infty([0,T_\varepsilon];H^1)} \lesssim 1, \quad \|\partial_{tttt}u(x,t)\|_{L^\infty([0,T_\varepsilon];L^2)} \lesssim 1.
\end{aligned}
$$

Under the above assumption (C), let

$$
M_1 := \max_{\varepsilon\in(0,1]}\{\|u(x,t)\|_{L^\infty([0,T_\varepsilon];L^\infty)}\} \lesssim 1,
$$

then we can establish the following error bounds for the semi-implicit FDFS (2.7.8)-(2.7.9).

Theorem 2.7.1. *Let $u_M^n(x)$ be the approximation obtained from the FDFS* (2.7.8)-(2.7.9). *Under the assumption (C), there exist constants $h_0 > 0$ and $\tau_0 > 0$ sufficiently small and independent of ε such that for any $0 < \varepsilon \le 1$, when $0 < h \le h_0$ and $0 < \tau \le \varepsilon^{\beta/2}\tau_0$ and under the stability condition* (2.7.13), *we have the following error estimates*

$$
\begin{aligned}
&\|u(x,t_n) - u_M^n(x)\|_s \lesssim h^{1+m_0-s} + \frac{\tau^2}{\varepsilon^\beta}, \quad s = 0,1,\\
&\|u_M^n(x)\|_{L^\infty} \le 1 + M_1, \quad 0 \le n \le \frac{T_0/\varepsilon^\beta}{\tau}.
\end{aligned}
\tag{2.7.14}
$$

Remark 2.7.1. *The FDFS* (2.7.8)-(2.7.9) *is a semi-discretization to the NKGE* (2.1.1), *while the* (2.7.10)-(2.7.11) *is a full-discretization. The same error estimate in Theorem 2.7.1 holds for the FDFP* (2.7.10)-(2.7.11) *and the proof is quite similar to that of Theorem 2.7.1.*

Proof. For the semi-implicit FDFS method, we will prove (2.7.14) by the method of mathematical induction and the stability condition (2.7.13) is assumed in the proof. From the discretization of the initial data, i.e., $u_M^0 = P_M\phi$, we have

$$
\begin{aligned}
&\|u(x,t=0) - u_M^0\|_s = \|\phi - P_M\phi\|_s \lesssim h^{1+m_0-s},\\
&\|u_M^0(x)\|_{L^\infty} \le \|P_M\phi - \phi\|_{L^\infty} + \|\phi\|_{L^\infty} \le Ch^{m_0} + M_1.
\end{aligned}
\tag{2.7.15}
$$

Thus, there exists a constant $h_1 > 0$ sufficiently small and independent of ε such that, when $0 < h \leq h_1$, the error bounds in (2.7.14) are valid for $n = 0$.

For $0 \leq n \leq T_0\varepsilon^{-\beta}/\tau$, denote the "error" function

$$e^n(x) := P_M u(x,t_n) - u_M^n(x) = \sum_{l \in \mathcal{T}_M} \widehat{e}_l^n e^{i\mu_l(x-a)}, \quad x \in \overline{\Omega}, \tag{2.7.16}$$

then we have

$$\widehat{e}_l^n = \widehat{u}_l(t_n) - \widehat{(u_M^n)}_l, \quad l \in \mathcal{T}_M, \quad n \geq 0, \tag{2.7.17}$$

with $\widehat{u}_l(t_n)(l \in \mathcal{T}_M)$ are the Fourier transform coefficients of $u(x,t_n)$. Using the triangle inequality and Parseval's equality, we get

$$\begin{aligned} \|u(x,t_n) - u_M^n(x)\|_s &\leq \|u(x,t_n) - P_M u(x,t_n)\|_s + \|e^n(x)\|_s \\ &\lesssim h^{1+m_0-s} + \|e^n(x)\|_s, \quad s = 0,1, \quad 0 \leq n \leq \frac{T_0/\varepsilon^\beta}{\tau}. \end{aligned}$$

Thus, we only need to estimate $\|e^n(x)\|_s$ for $0 \leq n \leq T_0\varepsilon^{-\beta}/\tau$.

We begin with the local truncation errors $\xi^n(x) \in Y_M$ of the scheme (2.7.8)-(2.7.9) given as

$$\xi^n(x) = \sum_{l \in \mathcal{T}_M} \widehat{\xi}_l^n e^{i\mu_l(x-a)}, \tag{2.7.18}$$

with

$$\begin{aligned} \widehat{\xi}_l^0 &= \delta_t^+ \widehat{u}_l(0) - \widehat{\gamma}_l + \frac{\tau}{2}\left[(1+\mu_l^2)\widehat{\phi}_l + \varepsilon^2 \widehat{(f(\phi))}_l\right], \ l \in \mathcal{T}_M, \\ \widehat{\xi}_l^n &= \delta_t^2 \widehat{u}_l(t_n) + \frac{1+\mu_l^2}{2}\left[\widehat{u}_l(t_{n+1}) + \widehat{u}_l(t_{n-1})\right] + \varepsilon^2 \widehat{(f(u))}_l(t_n), \ l \in \mathcal{T}_M, \ n \geq 1. \end{aligned} \tag{2.7.19}$$

Under the assumption (C), by applying the Taylor expansion to (2.7.19), it leads to

$$\begin{aligned} \|\xi^0\| &\lesssim \sqrt{\sum_{l \in \mathcal{T}_M} |\widehat{\xi}_l^0|^2} \lesssim \tau^2 \|\partial_{ttt} u\|_{L^\infty([0,T_\varepsilon];L^2)} \lesssim \tau^2, \\ \|\xi^n\| &\lesssim \sqrt{\sum_{l \in \mathcal{T}_M} |\widehat{\xi}_l^n|^2} \lesssim \tau^2 \left(\|\partial_{tttt} u\|_{L^\infty([0,T_\varepsilon];L^2)} + \|\partial_{tt} u\|_{L^\infty([0,T_\varepsilon];H^2)}\right) \lesssim \tau^2. \end{aligned} \tag{2.7.20}$$

Similarly, we can also obtain $\|\xi^0\|_1 \lesssim \tau^2 \|\partial_{ttt} u\|_{L^\infty([0,T_\varepsilon];H^1)}$.

Next, we denote the error of the nonlinear term

$$\eta^n(x) = \sum_{l \in \mathcal{T}_M} \widehat{\eta}_l^n e^{i\mu_l(x-a)}, \tag{2.7.21}$$

with

$$\widehat{\eta}_l^n = \varepsilon^2 \left(\widehat{(f(u))}_l(t_n) - (\widehat{f(u_M^n)})_l \right), \; l \in \mathcal{T}_M, \; n \geq 1. \tag{2.7.22}$$

For each $l \in \mathcal{T}_M$, subtracting (2.7.7) from (2.7.19), we obtain the equation for the "error" function $\widehat{e}_l^n$ as

$$\begin{aligned} &\delta_t^2 \widehat{e}_l^n + \frac{1+\mu_l^2}{2} \left(\widehat{e}_l^{n+1} + \widehat{e}_l^{n-1} \right) = \widehat{\xi}_l^n - \widehat{\eta}_l^n, \quad 1 \leq n \leq \frac{T_0/\varepsilon^\beta}{\tau} - 1, \\ &\widehat{e}_l^0 = 0, \quad \widehat{e}_l^1 = \tau \widehat{\xi}_l^0, \quad l \in \mathcal{T}_M. \end{aligned} \tag{2.7.23}$$

For $n = 1$, the error equation (2.7.23) and the estimate (2.7.20) imply

$$\|e^1(x)\|_s = \tau \|\xi^0\|_s \lesssim \tau^3. \tag{2.7.24}$$

Thus, we immediately obtain

$$\|u(x,t_1) - u_M^1(x)\|_s \leq \|u(x,t_1) - P_M u(x,t_1)\|_s + \|e^1(x)\|_s \lesssim h^{1+m_0-s} + \tau^2. \tag{2.7.25}$$

In view of the triangle inequality, discrete Sobolev inequality and the assumption (C), there exist constants $h_2 > 0$ and $\tau_1 > 0$ sufficiently small and independent of ε such that when $0 < h \leq h_2$ and $0 < \tau \leq \tau_1$, we have

$$\|u_M^1(x)\|_{L^\infty} \leq 1 + M_1. \tag{2.7.26}$$

Therefore, the estimates in (2.7.14) are valid when $n = 1$.

Now we assume that (2.7.14) is valid for all $1 \leq n \leq m-1 \leq T_0\varepsilon^{-\beta}/\tau - 1$, then we need to show that it is still valid when $n = m$. Under the assumption (C), we have

$$\begin{aligned} \|\eta^n\| = \sqrt{\sum_{l \in \mathcal{T}_M} |\widehat{\eta}_l^n|^2} &\leq \varepsilon^2 \|u^3(x,t_n) - (u_M^n(x))^3\| \\ &\leq 3\varepsilon^2 (1+M_1)^2 \|u(x,t_n) - u_M^n(x)\| \\ &\lesssim \varepsilon^2 \left(h^{1+m_0} + \|e^n(x)\| \right), \quad 1 \leq n \leq m-1. \end{aligned} \tag{2.7.27}$$

Define the "energy" for the error $e^n(x) \in Y_M (n \geq 0)$ as

$$S^n = \|\delta_t^+ e^n\|^2 + \frac{1}{2} \left(\|e^n\|_1^2 + \|e^{n+1}\|_1^2 \right), \quad n \geq 0. \tag{2.7.28}$$

It is easy to see that

$$S^0 = \|\delta_t^+ e^0\|^2 + \frac{1}{2}\|e^1\|_1^2 \lesssim \tau^4.$$

Noticing $0 \leq \beta \leq 2$, multiplying both sides of (2.7.23) by $\left(\overline{\widehat{e}_l^{n+1}} - \overline{\widehat{e}_l^{n-1}}\right)$, summing up for $l \in \mathcal{T}_M$, taking the real part and using the Young's inequality, the inequality (2.7.27), we have

$$\begin{aligned} S^n - S^{n-1} &= \mathrm{Re} \sum_{l\in\mathcal{T}_M} \left(\widehat{\xi}_l^n - \widehat{\eta}_l^n\right)\left(\overline{\widehat{e}_l^{n+1}} - \overline{\widehat{e}_l^{n-1}}\right) \\ &\leq \tau\varepsilon^{-\beta}\left(\|\xi^n\|^2 + \|\eta^n\|^2\right) + \tau\varepsilon^{\beta}\left(\|\delta_t^+ e^n\|^2 + \|\delta_t^+ e^{n-1}\|^2\right) \\ &\lesssim \tau\varepsilon^{\beta}\left(S^n + S^{n-1}\right) + \tau\varepsilon^{-\beta}\left(\varepsilon^2 h^{1+m_0} + \tau^2\right)^2, \quad 1 \leq n \leq m-1. \end{aligned} \tag{2.7.29}$$

Summing the above inequalities from 1 to $m-1$, there exists a constant $C > 0$ such that

$$S^{m-1} \leq S^0 + C\tau\varepsilon^{\beta}\sum_{n=0}^{m-1} S^n + CT_0\varepsilon^{-2\beta}\left(\varepsilon^2 h^{1+m_0} + \tau^2\right)^2. \tag{2.7.30}$$

By the discrete Gronwall's inequality, there exists a constant $\tau_2 > 0$ sufficiently small such that when $0 < \tau \leq \tau_2$, we have

$$S^{m-1} \leq \left(S^0 + CT_0\varepsilon^{-2\beta}\left(\varepsilon^2 h^{1+m_0} + \tau^2\right)^2\right)e^{2Cm\varepsilon^{\beta}\tau} \lesssim \left(h^{1+m_0} + \frac{\tau^2}{\varepsilon^{\beta}}\right)^2. \tag{2.7.31}$$

From the definition of S^{m-1}, we can obtain $\|e^m\|_1^2 \lesssim S^{m-1} \lesssim \left(h^{1+m_0} + \tau^2/\varepsilon^{\beta}\right)^2$, which implies

$$\|u(x,t_m) - u_M^m(x)\|_s \leq \|u(x,t_m) - P_M u(x,t_m)\|_s + \|e^m(x)\|_s \lesssim h^{1+m_0-s} + \frac{\tau^2}{\varepsilon^{\beta}}. \tag{2.7.32}$$

The inverse inequality and triangle inequality will imply that there exist constants $h_3 > 0$ and $\tau_3 > 0$ sufficiently small such that when $0 < h \leq h_3$ and $0 < \tau \leq \varepsilon^{\beta/2}\tau_3$, we have

$$\|u_M^m(x)\|_{L^\infty} \leq \|u(x,t_m) - u_M^m(x)\|_{L^\infty} + \|u(x,t_m)\|_{L^\infty} \leq 1 + M_1. \tag{2.7.33}$$

Thus, choosing $h_0 = \min\{h_1, h_2, h_3\}$ and $\tau_0 = \min\{\tau_1, \tau_2, \tau_3\}$, the error bounds in (2.7.14) are still valid when $n = m$. Hence, the proof of Theorem 2.7.1 is completed by the method of mathematical induction. □

From this theorem, the spatial/temporal resolution capacity of the FDFP method for the NKGE (2.1.1) up to the time $t = T_0/\varepsilon^{\beta}$ with $0 \leq \beta \leq 2$ is: $h = O(1)$ and

$\tau = O(\varepsilon^{\beta/2})$. In fact, given an accuracy bound $\delta_0 > 0$, the ε-scalability of the FDFP method is:

$$h = O(\sqrt{\delta_0}) = O(1), \quad \tau = O(\varepsilon^{\beta/2}\sqrt{\delta_0}) = O(\varepsilon^{\beta/2}), \quad 0 < \varepsilon \leq 1.$$

2.7.3 Numerical results

In this subsection, the numerical results are exhibited to validate the error bounds of the FDFP (2.7.10)-(2.7.11) for the NKGE (2.1.1) up to the time $t = T_0/\varepsilon^\beta$ with $0 \leq \beta \leq 2$. In our numerical experiments, we choose the initial data as

$$\phi(x) = \frac{1}{2+\cos(x)}, \qquad \gamma(x) = \frac{1}{2}\cos(x), \qquad 0 \leq x \leq 2\pi. \tag{2.7.34}$$

Denote $u^n_{h,\tau}$ as the numerical solution at time $t = t_n$ obtained by the semi-implicit FDFP (2.7.10)-(2.7.11) with mesh size h and time step τ. The 'exact' solution $u(x,t)$ is obtained numerically by the time-splitting Fourier pseudospectral method with a very fine mesh size and a very small time step, e.g. $h_e = \pi/64$ and $\tau_e = 10^{-5}$. The errors are denoted as $e(x,t_n) = u(x,t_n) - I_N(u^n_{h,\tau})(x)$. In order to quantify the numerical errors, we measure the H^1 norm of $e(x,t_n)$.

The errors are displayed at $t = 1/\varepsilon^\beta$ with $\beta = 0$, $\beta = 1$ and $\beta = 2$, respectively. For spatial error analysis, the time step is set as $\tau = 10^{-4}$ such that the temporal error can be neglected; for temporal error analysis, we set the mesh size as $h = \pi/64$ such that the spatial error can be ignored. Table 2.16 shows the spatial errors under different mesh size and Tables 2.17 - 2.19 display the temporal errors for $\beta = 0$, $\beta = 1$ and $\beta = 2$, respectively.

From Tables 2.16 - 2.19, we can draw the following observations of the FDFP method for the long-time dynamics of the NKGE (2.1.1):

(i) In space, the FDFP (2.7.10)-(2.7.11) is uniformly and spectrally accurate for any $0 < \varepsilon \leq 1$ and $0 \leq \beta \leq 2$ (cf. each row in Table 2.16) and the spatial errors are almost independent of ε (cf. each column in Table 2.16).

(ii) In time, for any fixed $\varepsilon = \varepsilon_0 > 0$ and $\beta = 0$, the FDFP (2.7.10)-(2.7.11) is second-order accurate (cf. Table 2.17 and the first rows in Tables 2.18&2.19). For $\beta = 1$, the second order convergence in time can be observed only when $0 < \tau \lesssim \varepsilon^{1/2}$

(cf. upper triangles above the diagonals (corresponding to $\tau \sim \varepsilon^{1/2}$, and being labelled in bold letters) in Table 2.18), which confirm our error bounds. For $\beta = 2$, the second order convergence in time can be observed only when $0 < \tau \lesssim \varepsilon$ (cf. upper triangles above the diagonals (corresponding to $\tau \sim \varepsilon$, and being labelled in bold letters) in Table 2.19), which again confirm our error estimates. In summary, our numerical results confirm our rigorous error estimates and show that they are sharp.

	$\|e(\cdot, 1/\varepsilon^\beta)\|_1$	$h_0 = \pi/2$	$h_0/2$	$h_0/2^2$	$h_0/2^3$
$\beta = 0$	$\varepsilon_0 = 1$	4.87E-2	1.58E-2	1.30E-4	6.17E-8
	$\varepsilon_0/2$	8.41E-2	1.34E-2	1.28E-4	6.13E-8
	$\varepsilon_0/2^2$	9.44E-2	1.27E-2	1.27E-4	6.19E-8
	$\varepsilon_0/2^3$	9.71E-2	1.25E-2	1.27E-4	6.10E-8
$\beta = 1$	$\varepsilon_0 = 1$	4.87E-2	1.58E-2	1.30E-4	6.17E-8
	$\varepsilon_0/2$	1.94E-1	1.93E-2	8.38E-5	1.61E-7
	$\varepsilon_0/2^2$	1.36E-2	1.29E-2	1.22E-4	2.60E-7
	$\varepsilon_0/2^3$	4.78E-2	1.92E-2	1.76E-4	5.35E-7
$\beta = 2$	$\varepsilon_0 = 1$	4.87E-2	1.58E-2	1.30E-4	6.17E-8
	$\varepsilon_0/2$	3.43E-2	1.31E-2	1.32E-4	3.03E-7
	$\varepsilon_0/2^2$	1.28E-1	3.85E-3	1.28E-5	7.19E-7
	$\varepsilon_0/2^3$	8.30E-2	9.65E-3	6.83E-5	5.26E-6

Table 2.16: Spatial errors of the semi-implicit FDFP (2.7.10)-(2.7.11) for the NKGE (2.1.1) with (2.7.34) for different β and ε.

2.8 Comparisons of different spatial discretizations

We adapt the finite difference discretization in time and compare different spatial discretizations for the NKGE (2.1.1) in the long-time regime with the same initial data

$$\phi(x) = \frac{2}{2+\cos(x)}, \qquad \gamma(x) = \frac{1}{1+\sin^2(x)}, \qquad 0 \le x \le 2\pi. \tag{2.8.1}$$

$\|e(\cdot,1/\varepsilon^\beta)\|_1$	$\tau_0 = 0.1$	$\tau_0/2$	$\tau_0/2^2$	$\tau_0/2^3$	$\tau_0/2^4$	$\tau_0/2^5$
$\varepsilon_0 = 1$	1.86E-1	4.73E-2	1.19E-2	2.98E-3	7.47E-4	1.87E-4
order	-	1.98	1.99	2.00	2.00	2.00
$\varepsilon_0/2^1$	1.83E-1	4.67E-2	1.18E-2	2.95E-3	7.39E-4	1.85E-4
order	-	1.97	1.98	2.00	2.00	2.00
$\varepsilon_0/2^2$	1.82E-1	4.64E-2	1.17E-2	2.93E-3	7.34E-4	1.84E-4
order	-	1.97	1.99	2.00	2.00	2.00
$\varepsilon_0/2^3$	1.82E-1	4.63E-2	1.17E-2	2.93E-3	7.33E-4	1.83E-4
order	-	1.97	1.98	2.00	2.00	2.00
$\varepsilon_0/2^4$	1.82E-1	4.63E-2	1.17E-2	2.92E-3	7.32E-4	1.83E-4
order	-	1.97	1.98	2.00	2.00	2.00

Table 2.17: Temporal errors of the semi-implicit FDFP (2.7.10)-(2.7.11) for the NKGE (2.1.1) with $\beta = 0$ and initial data (2.7.34).

$\|e(\cdot,1/\varepsilon^\beta)\|_1$	$\tau_0 = 0.1$	$\tau_0/2$	$\tau_0/2^2$	$\tau_0/2^3$	$\tau_0/2^4$	$\tau_0/2^5$
$\varepsilon_0 = 1$	**1.86E-1**	4.73E-2	1.19E-2	2.98E-3	7.47E-4	1.87E-4
order	**-**	1.98	1.99	2.00	2.00	2.00
$\varepsilon_0/2^2$	6.13E-1	**1.62E-1**	4.11E-2	1.03E-2	2.58E-3	6.46E-4
order	-	**1.92**	1.98	2.00	2.00	2.00
$\varepsilon_0/2^4$	2.12	5.45E-1	**1.39E-1**	3.52E-2	8.83E-3	2.21E-3
order	-	1.96	**1.97**	1.98	2.00	2.00
$\varepsilon_0/2^6$	7.88	3.33	8.65E-1	**2.15E-1**	5.38E-2	1.34E-2
order	-	1.24	1.94	**2.01**	2.00	2.01
$\varepsilon_0/2^8$	2.04E+1	7.71	3.50	9.49E-1	**2.42E-1**	6.02E-2
order	-	1.40	1.14	1.88	**1.97**	1.99

Table 2.18: Temporal errors of the semi-implicit FDFP (2.7.10)-(2.7.11) for the NKGE (2.1.1) with $\beta = 1$ and initial data (2.7.34).

$\|e(\cdot, 1/\varepsilon^{\beta})\|_1$	$\tau_0 = 0.1$	$\tau_0/2$	$\tau_0/2^2$	$\tau_0/2^3$	$\tau_0/2^4$	$\tau_0/2^5$
$\varepsilon_0 = 1$	**1.86E-1**	4.73E-2	1.19E-2	2.98E-3	7.47E-4	1.87E-4
order	**-**	1.98	1.99	2.00	2.00	2.00
$\varepsilon_0/2$	7.36E-1	**1.96E-1**	4.97E-2	1.25E-2	3.12E-3	7.82E-4
order	-	**1.91**	1.98	1.99	2.00	2.00
$\varepsilon_0/2^2$	1.88	5.16E-1	**1.35E-1**	3.45E-2	8.67E-3	2.17E-3
order	-	1.87	**1.93**	1.97	1.99	2.00
$\varepsilon_0/2^3$	9.68	3.61	9.20E-1	**2.29E-1**	5.71E-2	1.43E-2
order	-	1.42	1.97	**2.01**	2.00	2.00
$\varepsilon_0/2^4$	2.40E+1	8.71	3.70	9.85E-1	**2.50E-1**	6.27E-2
order	-	1.46	1.24	1.91	**1.98**	2.00

Table 2.19: Temporal errors of the semi-implicit FDFP (2.7.10)-(2.7.11) for the NKGE (2.1.1) with $\beta = 2$ and initial data (2.7.34).

Figure 2.2 depicts the spatial errors of the finite difference methods with different spatial discretizations when $\varepsilon = 1$ for different mesh size h. Figure 2.3 shows the spatial errors of the finite difference methods with different ε at time $t = 1/\varepsilon^2$. Based on the above comparisons, in view of the spatial accuracy and ε-scalability, we conclude that the FDFP method performs much better than the FDTD and 4cFD methods for the discretization of the NKGE (2.1.1). In particular, in the long-time regime, the FDFP method is uniformly spectral accuracy, while the spatial errors of the FDTD and 4cFD methods depend explicitly on the small parameter ε.

The accuracy and ε-scalability in space could be improved by using higher order finite difference discretizations, but the spatial errors still depend on the small parameter ε in the long-time regime. Similarly, the spatial error bounds of the finite element and finite volume discretizations in space also depend on the parameter ε in the long-time regime. Uniform error bounds in space for the long-time dynamics can be achieved by the spectral method. For the spectral method, the computation of the Laplacian operator is carried out in the Fourier space. In contrast to the finite difference, finite

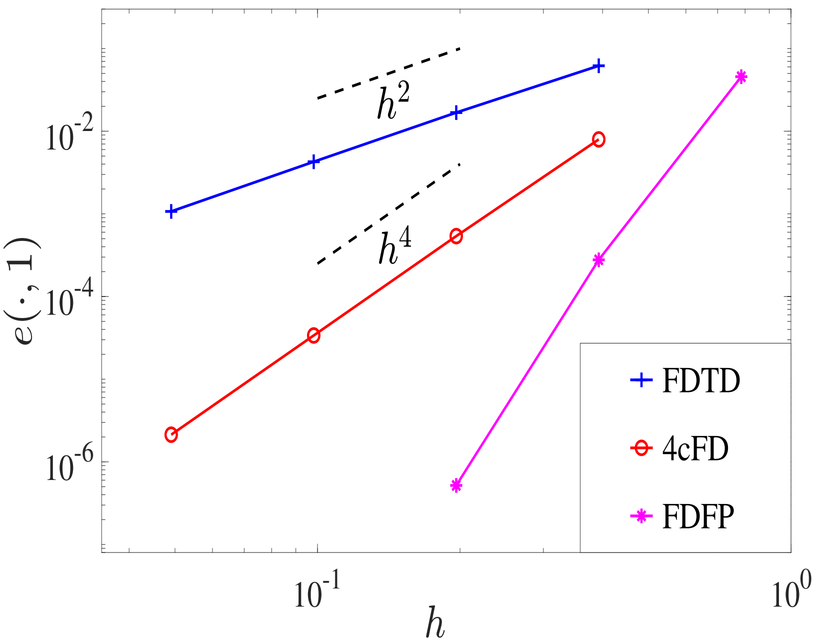

Figure 2.2: Comparison of spatial errors of different methods for the NKGE (2.1.1) with $\varepsilon = 1$.

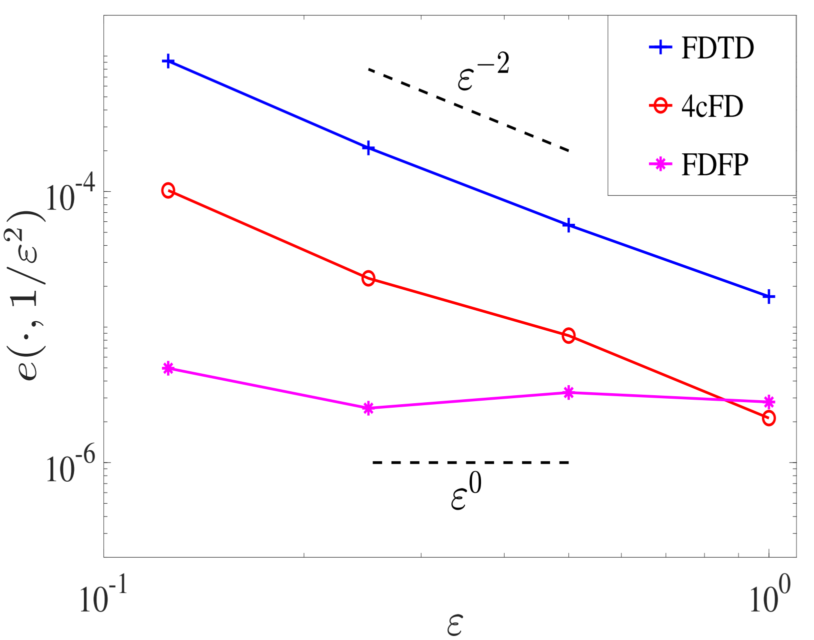

Figure 2.3: Spatial errors of different methods for the NKGE (2.1.1) at time $t = 1/\varepsilon^2$ with different ε.

element and finite volume methods, the spectral approximations of the differential operator, i.e., the Laplacian operator, are exact for all the Fourier modes [143]. From the proofs of the error bounds for the FDTD and 4cFD methods, we can observe that the errors of the approximations for the Laplacian operator accumulate in the long-time regime, which result in the spatial errors depending on the small parameter ε. By using the spectral discretization in space, the spatial errors are just from the projection and the nonlinear term. In the long-time regime, the accumulation of the spatial errors from the nonlinearity is independent of the small parameter ε since the strength of the nonlinearity is at $O(\varepsilon^2)$.

In summary, the spectral method performs much better than other spatial discretizations for the long-time dynamics of the NKGE with weak nonlinearity. In order to get uniform spatial error bounds in the long-time numerical simulations, the spectral discretization in space is a good choice.

Chapter 3

Error Estimates of an Exponential Wave Integrator

In this chapter, in order to improve the temporal resolution capacity of the finite difference methods in the long-time regime, an exponential wave integrator (EWI) is adapted to solve the NKGE (1.4.1) with rigorous stability and convergence analysis established up to the time $t = T_0/\varepsilon^\beta$ with $\beta \in [0, 2]$ [57]. Again, for simplicity of notations, the numerical schemes and their analysis are only presented in 1D, i.e., the NKGE (2.1.1). Generalizations to higher dimensions are straightforward and the error estimates remain valid with minor modifications.

3.1 Semi-discretization in time by an exponential wave integrator

In this section, we discretize the NKGE (2.1.1) in time by the exponential wave integrator (EWI) [9, 36, 38, 59, 73, 78, 79]. Define the operator

$$\langle \nabla \rangle = \sqrt{1 - \Delta}, \tag{3.1.1}$$

through its action in the Fourier space by [56, 141]:

$$\langle \nabla \rangle z(x) = \sum_{l \in \mathbb{Z}} \sqrt{1 + |\mu_l|^2}\, \widehat{z}_l e^{i\mu_l (x-a)}, \quad \text{for} \quad z(x) = \sum_{l \in \mathbb{Z}} \widehat{z}_l e^{i\mu_l (x-a)}, \quad x \in [a, b].$$

In addition, we introduce the operator $\langle \nabla \rangle^{-1}$ as

$$\langle \nabla \rangle^{-1} z(x) = \sum_{l \in \mathbb{Z}} \frac{\widehat{z}_l}{\sqrt{1 + |\mu_l|^2}} e^{i\mu_l (x-a)}, \quad x \in [a, b].$$

It is obvious that

$$\|\langle\nabla\rangle^{-1}z\|_s = \|z\|_{s-1} \le \|z\|_s.$$

We can rewrite the NKGE (2.1.1) as

$$\partial_{tt}u(x,t) + \langle\nabla\rangle^2 u(x,t) + \varepsilon^2 u^3(x,t) = 0, \quad x \in \Omega = (a,b), \quad t > 0. \tag{3.1.2}$$

By using the variation-of-constant formula and noting $v = \partial_t u$, we get the solution of NKGE (3.1.2) near $t = t_n$:

$$\begin{aligned} u(t_n+s) = &\cos(\langle\nabla\rangle s)u(t_n) + \langle\nabla\rangle^{-1}\sin(\langle\nabla\rangle s)v(t_n) \\ &- \varepsilon^2\int_0^s \langle\nabla\rangle^{-1}\sin(\langle\nabla\rangle(s-\theta))f^n(\theta)d\theta, \end{aligned} \tag{3.1.3}$$

where $f^n(\theta) := u^3(t_n+\theta)$. Taking $s = \pm\tau$ in (3.1.3) and then summing them up, we have

$$u(t_{n+1}) + u(t_{n-1}) = 2\cos(\langle\nabla\rangle\tau)u(t_n) - \varepsilon^2\int_0^\tau \langle\nabla\rangle^{-1}\sin(\langle\nabla\rangle(\tau-\theta))\left[f^n(\theta) + f^n(-\theta)\right]d\theta. \tag{3.1.4}$$

Then, we need to use proper quadratures to approximate the integral in (3.1.4). If the Gautschi-type quadrature [6, 9, 61, 64, 65, 67, 73] is applied, we have the following Gautschi-type EWI method

$$u^{n+1} = \begin{cases} \cos(\langle\nabla\rangle\tau)\phi + \langle\nabla\rangle^{-1}\sin(\langle\nabla\rangle\tau)\gamma - G^0, & n = 0, \\ -u^{n-1} + 2\cos(\langle\nabla\rangle\tau)u^n - 2G^n, & n \ge 1, \end{cases} \tag{3.1.5}$$

where

$$G^n = \varepsilon^2\langle\nabla\rangle^{-2}\left[1 - \cos(\langle\nabla\rangle\tau)\right](u^n)^3, \quad n \ge 0. \tag{3.1.6}$$

Another way to approximate the integral in (3.1.4) is using the standard trapezoidal rule, i.e., the EWI with Deuflhard-type quadrature [46, 47, 71, 165]

$$u^{n+1} = \begin{cases} \cos(\langle\nabla\rangle\tau)\phi + \langle\nabla\rangle^{-1}\sin(\langle\nabla\rangle\tau)\gamma - D^0, & n = 0, \\ -u^{n-1} + 2\cos(\langle\nabla\rangle\tau)u^n - 2D^n, & n \ge 1, \end{cases} \tag{3.1.7}$$

where

$$D^n = \frac{\varepsilon^2}{2}\tau\langle\nabla\rangle^{-1}\sin(\langle\nabla\rangle\tau)(u^n)^3, \quad n \ge 0.$$

3.2 The EWI-FP method and its stability

In this section, we show the numerical scheme and its analysis of the EWI with Gautschi-type quadrature Fourier pseudospectral (EWI-FP) method. For the EWI with Deulfhard-type quadrature Fourier pseudospectral method, the full-discretization is similar and we omit the details here for brevity. We use the same notations for the semi-implicit FDFP method in Chapter 2.

We want to find

$$u_M(x,t) = \sum_{l\in\mathcal{T}_M} \widehat{(u_M)}_l(t) e^{i\mu_l(x-a)} \in Y_M, \quad x\in\overline{\Omega}, \quad t\geq 0, \tag{3.2.1}$$

such that

$$\partial_{tt}u_M(x,t) - \partial_{xx}u_M(x,t) + u_M(x,t) + \varepsilon^2 P_M f(u_M(x,t)) = 0, \quad x\in\overline{\Omega}, \quad t\geq 0, \tag{3.2.2}$$

with $f(v)=v^3$.

Denote $\widehat{(u_M^n)}_l$ and $u_M^n(x)$ be the approximations of $\widehat{(u_M)}_l(t_n)$ and $u_M(x,t_n)$, respectively. Choosing $u_M^0(x) = (P_M\phi)(x)$, a Gautschi-type exponential integrator Fourier spectral (EWI-FS) method for discretizing the NKGE (2.1.1) via (3.1.5) is to update the numerical approximation $u_M^{n+1}(x)\in Y_M (n\geq 0)$ as

$$u_M^{n+1}(x) = \sum_{l\in\mathcal{T}_M} \widehat{(u_M^{n+1})}_l e^{i\mu_l(x-a)}, \quad x\in\overline{\Omega}, \quad n\geq 0, \tag{3.2.3}$$

where

$$\begin{aligned} &\widehat{(u_M^1)}_l = p_l\widehat{\phi}_l + q_l\widehat{\gamma}_l + r_l\widehat{(f(\phi))}_l, \quad l\in\mathcal{T}_M, \\ &\widehat{(u_M^{n+1})}_l = -\widehat{(u_M^{n-1})}_l + 2p_l\widehat{(u_M^n)}_l + 2r_l\widehat{(f(u_M^n))}_l, \quad l\in\mathcal{T}_M, \quad n\geq 1, \end{aligned} \tag{3.2.4}$$

with

$$\zeta_l = \sqrt{1+\mu_l^2}, \tag{3.2.5}$$

and the coefficients defined as

$$p_l = \cos(\tau\zeta_l), \quad q_l = \frac{\sin(\tau\zeta_l)}{\zeta_l}, \quad r_l = \frac{\varepsilon^2(\cos(\tau\zeta_l)-1)}{\zeta_l^2}. \tag{3.2.6}$$

Similar to the FDFS method, due to the difficulty of computing the integrals in (3.2.4), we need to choose $u_M^0(x)$ as the interpolation of $\phi(x)$, i.e., $u_M^0(x) = (I_M\phi)(x)$, and approximate the integrals in (3.2.4) by a quadrature rule on the grids. Let u_j^n be the approximation of $u(x_j, t_n)$ and denote $u_j^0 = \phi(x_j)(j = 0, 1, \cdots, M)$. For $n = 0, 1, \cdots$, a Gautschi-type exponential integrator Fourier pseudospectral (EWI-FP) discretization for the NKGE (2.1.1) is

$$u_j^{n+1} = \sum_{l \in \mathcal{T}_M} \widetilde{u}_l^{n+1} e^{i\mu_l(x_j - a)}, \quad j = 0, 1, \cdots, M, \tag{3.2.7}$$

where

$$\begin{aligned} &\widetilde{u}_l^1 = p_l \widetilde{\phi}_l + q_l \widetilde{\gamma}_l + r_l \big(\widetilde{f(\phi)}\big)_l, \quad l \in \mathcal{T}_M, \\ &\widetilde{u}_l^{n+1} = -\widetilde{u}_l^{n-1} + 2p_l \widetilde{u}_l^n + 2r_l \big(\widetilde{f(u^n)}\big)_l, \quad l \in \mathcal{T}_M, \quad n \geq 1, \end{aligned} \tag{3.2.8}$$

with the coefficients p_l, q_l and r_l are given in (3.2.6).

The EWI-FP (3.2.7)-(3.2.8) is explicit, time symmetric and easy to extend to 2D and 3D. The memory cost is $O(M)$ and the computational cost per time step is $O(M \ln M)$.

Let $T_0 > 0$ be a fixed constant and $0 \leq \beta \leq 2$, and denote

$$\sigma_{\max} := \max_{0 \leq n \leq T_0 \varepsilon^{-\beta}/\tau} \|u^n\|_{l^\infty}^2, \tag{3.2.9}$$

where $\|u\|_{l^\infty} = \max_{0 \leq j \leq M-1} |u_j|$ for $u \in X_M$. According to the standard von Neumann stability analysis, we can conclude the stability results of the EWI-FP (3.2.7)-(3.2.8) for the NKGE (2.1.1) in the following lemma.

Lemma 3.2.1. *(stability) For any $0 < \varepsilon \leq 1$, the EWI-FP (3.2.7)-(3.2.8) is conditionally stable under the stability condition*

$$0 < \tau \leq \frac{2h}{\sqrt{\pi^2 + h^2(1 + \sigma_{\max})}}, \quad h > 0. \tag{3.2.10}$$

Proof. Replacing the nonlinear term by $f(u) = \varepsilon^2 \sigma_{\max} u$ and plugging

$$u_j^{n-1} = \sum_{l \in \mathcal{T}_M} \widehat{U}_l e^{2ijl\pi/M}, \; u_j^n = \sum_{l \in \mathcal{T}_M} \xi_l \widehat{U}_l e^{2ijl\pi/M}, \; u_j^{n+1} = \sum_{l \in \mathcal{T}_M} \xi_l^2 \widehat{U}_l e^{2ijl\pi/M},$$

into (3.2.8) with ξ_l the amplification factor of the lth mode in phase space, we obtain the following characteristic equation

$$\xi_l^2 - 2\theta_l \xi_l + 1 = 0, \quad l \in \mathcal{T}_M, \tag{3.2.11}$$

with

$$\theta_l = \cos(\tau\zeta_l) + \frac{\varepsilon^2\sigma_{\max}(\cos(\tau\zeta_l)-1)}{\zeta_l^2} = 1 - \left(\frac{2\varepsilon^2\sigma_{\max}}{\zeta_l^2}+2\right)\sin^2\left(\frac{\tau\zeta_l}{2}\right),\ l \in \mathcal{T}_M.$$

Since the characteristic equation (3.2.11) implies $\xi_l = \theta_l \pm \sqrt{\theta_l^2 - 1}$, it indicates that the stability of the EWI-FP (3.2.7)-(3.2.8) amounts to

$$|\xi_l| \le 1 \iff |\theta_l| \le 1, \quad l \in \mathcal{T}_M. \tag{3.2.12}$$

Noticing $\sin(x) \le x$ for $x \ge 0$, under the condition (3.2.10), we have

$$0 < \left(\frac{2\varepsilon^2\sigma_{\max}}{\zeta_l^2}+2\right)\sin^2\left(\frac{\tau\zeta_l}{2}\right) \le \left(\frac{2\varepsilon^2\sigma_{\max}}{\zeta_l^2}+2\right)\cdot\left(\frac{\tau\zeta_l}{2}\right)^2 \le 2, \tag{3.2.13}$$

which immediately leads to the conclusion. $\square$

Remark 3.2.1. *The stability of the EWI-FP* (3.2.7)-(3.2.8) *is related to* $\sigma_{\max}$*, dependent on the boundedness of the* l^∞ *norm of the numerical solution* u^n *at the previous time step. The error estimates up to the previous time step could ensure such a bound in the* l^∞ *norm, by making use of the discrete Sobolev inequality, and such an error estimate could be recovered at the next time step, as given by the Theorem 3.3.1 presented in Section 3.3.*

3.3 Error estimates for EWI-FP

In this section, we will rigorously establish the uniform error bounds of the EWI-FS (3.2.3)-(3.2.4)/EWI-FP (3.2.7)-(3.2.8) for the NKGE (2.1.1) up to the time $t = T_0/\varepsilon^\beta$ with $0 \le \beta \le 2$. Motivated by the results in [43, 88, 89, 118] and references therein, we assume that there exists an integer $m_0 \ge 1$ such that the exact solution $u(x,t)$ of the NKGE (2.1.1) up to the time $T_\varepsilon = T_0/\varepsilon^\beta$ with $\beta \in [0,2]$ and $T_0 > 0$ fixed satisfies

$$\text{(D)} \qquad \begin{aligned} & u(x,t) \in L^\infty\left([0,T_\varepsilon]; L^\infty \cap H_p^{m_0+1}\right),\ \partial_t u(x,t) \in L^\infty\left([0,T_\varepsilon]; W^{1,4}\right), \\ & \partial_{tt} u(x,t) \in L^\infty\left([0,T_\varepsilon]; H^1\right), \\ & \|u(x,t)\|_{L^\infty\left([0,T_\varepsilon]; L^\infty\cap H_p^{m_0+1}\right)} \lesssim 1, \quad \|\partial_t u(x,t)\|_{L^\infty([0,T_\varepsilon];W^{1,4})} \lesssim 1, \\ & \|\partial_{tt} u(x,t)\|_{L^\infty([0,T_\varepsilon];H^1)} \lesssim 1. \end{aligned}$$

Under the assumption (D), we let

$$M_1 := \max_{\varepsilon\in(0,1]} \{\|u(x,t)\|_{L^\infty([0,T_\varepsilon];L^\infty)} + \|\partial_t u(x,t)\|_{L^\infty([0,T_\varepsilon];L^\infty)}\} \lesssim 1,$$

$$M_2 := \sup_{v\neq 0, |v|\leq 1+M_1} |v|^2 \lesssim 1.$$

Assuming

$$\tau \leq \min\left\{\frac{1}{8}, \frac{\pi h}{3\sqrt{\pi^2 + h^2(1+M_2)}}\right\}, \tag{3.3.1}$$

we can establish the following error bounds of the EWI-FS (3.2.3)-(3.2.4).

Theorem 3.3.1. *Let $u_M^n(x)$ be the approximation obtained from the EWI-FS* (3.2.3) -(3.2.4)*, under the stability condition* (3.2.10)*, the assumptions (D) and* (3.3.1)*, there exist constants $h_0 > 0$ and $\tau_0 > 0$ sufficiently small and independent of ε, such that for any $0 < \varepsilon \leq 1$ and $0 \leq \beta \leq 2$, when $0 < h \leq h_0$, $0 < \tau \leq \tau_0$, we have*

$$\begin{aligned} &\|u(x,t_n) - u_M^n(x)\|_s \lesssim h^{1+m_0-s} + \varepsilon^{2-\beta}\tau^2, \quad s = 0,1, \\ &\|u_M^n(x)\|_{L^\infty} \leq 1 + M_1, \quad 0 \leq n \leq \frac{T_0/\varepsilon^\beta}{\tau}. \end{aligned} \tag{3.3.2}$$

Remark 3.3.1. *(1). The EWI-FS* (3.2.3)-(3.2.4) *is a semi-discretization to the NKGE* (2.1.1)*, while the EWI-FP* (3.2.7)-(3.2.8) *is a full-discretization. The error estimates for the EWI-FP* (3.2.7)-(3.2.8) *are quite similar as those in Theorem 3.3.1 and we omit the details here for brevity.*

(2). In 2D/3D case, Theorem 3.3.1 is still valid under the technical condition $\tau \lesssim \sqrt{C_d(h)}$, where $C_d(h) = 1/|\ln h|$ for $d = 2$; and resp., $C_d(h) = h^{1/2}$ for $d = 3$.

These results are very useful in practical computations on how to select mesh size and time step such that the numerical results are trustable. The error bounds indicate that the ε-scalability of the EWI-FS(3.2.3)-(3.2.4)/EWI-FP (3.2.7)-(3.2.8) up to the time at $O(\varepsilon^{-\beta})$ is uniform in terms of ε and should be taken as:

$$h = O(1), \quad \tau = O(1), \quad \text{for any} \quad 0 < \varepsilon \leq 1 \quad \text{and} \quad 0 \leq \beta \leq 2.$$

Proof of Theorem 3.3.1. The key points of the proof are to deal with the nonlinearity and overcome the main difficulty for obtaining the uniform bound of the solution $u_M^n(x)$, i.e., $\|u_M^n(x)\|_{L^\infty} \lesssim 1$. Since the EWI-FS (3.2.3)-(3.2.4) is explicit and the nonlinear term only depends on the previous steps, we adapt the energy method with suitable "energy" combined with the method of mathematical induction, which is widely used in the literature [4, 9, 10, 11]. The nonlinear part is controlled by the L^∞ norm of the error functions from previous steps by means of the discrete Sobolev inequality and inverse inequality.

The exact solution of the NKGE (2.1.1) can be written as

$$u(x,t) = \sum_{l\in\mathbb{Z}} \widehat{u}_l(t) e^{i\mu_l(x-a)}, \quad x \in \overline{\Omega}, \quad t \geq 0, \tag{3.3.3}$$

where $\widehat{u}_l(t)(l \in \mathbb{Z})$ are the Fourier transform coefficients of $u(x,t)$. Similar to the derivation of (3.1.3)-(3.1.4), for $l \in \mathbb{Z}$, we have

$$\widehat{u}_l(\tau) = \widehat{\phi}_l \cos(\tau\zeta_l) + \widehat{\gamma}_l \frac{\sin(\tau\zeta_l)}{\zeta_l} - \frac{\varepsilon^2}{\zeta_l}\int_0^\tau \widehat{F}_l^0(\omega)\sin(\zeta_l(\tau-\omega))d\omega, \tag{3.3.4}$$

and for $n \geq 1$,

$$\widehat{u}_l(t_{n+1}) = -\widehat{u}_l(t_{n-1}) + 2\cos(\tau\zeta_l)\widehat{u}_l(t_n) - \frac{\varepsilon^2}{\zeta_l}\int_0^\tau \widehat{(F_+^n)}_l(\omega)\sin(\zeta_l(\tau-\omega))d\omega, \tag{3.3.5}$$

where

$$\widehat{(F_+^n)}_l(\omega) = \widehat{F}_l^n(-\omega) + \widehat{F}_l^n(\omega), \quad \widehat{F}_l^n(\omega) = \widehat{(f(u))}_l(t_n+\omega). \tag{3.3.6}$$

For $0 \leq n \leq T_0\varepsilon^{-\beta}/\tau$, denote the "error" function

$$\eta^n(x) := P_M u(x,t_n) - u_M^n(x) = \sum_{l\in\mathcal{T}_M} \widehat{\eta}_l^n e^{i\mu_l(x-a)}, \ x \in \overline{\Omega}, \tag{3.3.7}$$

with $\widehat{\eta}_l^n = \widehat{u}_l(t_n) - \widehat{(u_M^n)}_l$, $l \in \mathcal{T}_M$. By the assumption (D) and triangle inequality, we have

$$\|u(x,t_n) - u_M^n(x)\|_s \leq \|u(x,t_n) - P_M u(x,t_n)\|_s + \|\eta^n(x)\|_s \lesssim h^{1+m_0-s} + \|\eta^n(x)\|_s.$$

Thus, we only need to estimate $\|\eta^n(x)\|_s$ for $0 \leq n \leq T_0\varepsilon^{-\beta}/\tau$.

Now, we proceed to prove the error bounds in (3.3.2) by employing the energy method combined with the method of mathematical induction in the following three main steps.

Step 1. The growth of the "error" function. Define the local truncation errors $\xi^{n+1}(x)$ for $0 \le n \le T_0\varepsilon^{-\beta}/\tau - 1$ as

$$\xi^{n+1}(x) = \sum_{l \in \mathcal{T}_M} \widehat{\xi}_l^{n+1} e^{i\mu_l(x-a)}, \tag{3.3.8}$$

with

$$\begin{aligned}
\widehat{\xi}_l^1 &:= \widehat{u}_l(\tau) - p_l\widehat{\phi}_l - q_l\widehat{\gamma}_l - r_l\widehat{(f(\phi))}_l = -\frac{\varepsilon^2}{\zeta_l}\int_0^\tau \widehat{W}_l^1(\omega)\sin(\zeta_l(\tau-\omega))d\omega, \\
\widehat{\xi}_l^{n+1} &:= \widehat{u}_l(t_{n+1}) + \widehat{u}_l(t_{n-1}) - 2p_l\widehat{u}_l(t_n) - 2r_l\widehat{(f(u))}_l(t_n), \\
&= -\frac{\varepsilon^2}{\zeta_l}\int_0^\tau \widehat{W}_l^{n+1}(\omega)\sin(\zeta_l(\tau-\omega))d\omega, \quad 1 \le n \le T_0\varepsilon^{-\beta}/\tau - 1,
\end{aligned}$$

where

$$\widehat{W}_l^{n+1}(\omega) = \begin{cases} \widehat{F}_l^0(\omega) - \widehat{(f(\phi))}_l, & l \in \mathcal{T}_M, \quad n = 0, \\ \widehat{(F_+^n)}_l(\omega) - 2\widehat{F}_l^n(0), & l \in \mathcal{T}_M, \quad 1 \le n \le T_0\varepsilon^{-\beta}/\tau - 1, \end{cases} \tag{3.3.9}$$

and the coefficients p_l, q_l and r_l are given in (3.2.6).

For each $l \in \mathcal{T}_M$, subtracting (3.2.4) from (3.3.4)-(3.3.5), we obtain the equation for the "error" function $\widehat{\eta}_l^{n+1}$ as

$$\begin{aligned}
&\widehat{\eta}_l^{n+1} = -\widehat{\eta}_l^{n-1} + 2\cos(\tau\zeta_l)\widehat{\eta}_l^n + \widehat{\xi}_l^{n+1} + \widehat{\chi}_l^{n+1}, \quad 1 \le n \le T_0\varepsilon^{-\beta}/\tau - 1, \\
&\widehat{\eta}_l^0 = 0, \quad \widehat{\eta}_l^1 = \widehat{\xi}_l^1,
\end{aligned} \tag{3.3.10}$$

and the nonlinear term errors $\chi^{n+1}(x) \in Y_M$ with

$$\widehat{\chi}_l^{n+1} := \frac{2\varepsilon^2(1-\cos(\tau\zeta_l))}{\zeta_l^2}\widehat{V}_l^{n+1}, \quad \widehat{V}_l^{n+1} = (\widehat{f(u_M^n)})_l - \widehat{F}_l^n(0). \tag{3.3.11}$$

Step 2. Estimates for the cases $n = 0$ and $n = 1$. From the discretization of the initial data, i.e., $u_M^0(x) = P_M\phi(x)$, we have

$$\|u(x, t=0) - u_M^0(x)\|_s = \|\phi - P_M\phi\|_s \lesssim h^{1+m_0-s}, \quad \|u_M^0(x)\|_{L^\infty} \le Ch^{m_0} + M_1.$$

Therefore, there exists a constant $h_1 > 0$ sufficiently small and independent of ε such that, when $0 < h \le h_1$, the error estimates in (3.3.2) are valid for $n = 0$.

Since the calculation for the first step ($n = 1$) is different from others, we investigate the first step separately. Under the assumption (D), we get

$$
\begin{aligned}
\|\phi^3 - u^3(\cdot,\omega)\|^2 &= \int_a^b |u^3(x,0) - u^3(x,\omega)|^2 dx \\
&\le 9M_2^2 \int_a^b |u(x,0) - u(x,\omega)|^2 dx \\
&= 9M_2^2 \int_a^b \left| \int_0^\omega \partial_s u(x,s) ds \right|^2 dx \\
&\le 9M_2^2 \int_a^b \omega \int_0^\omega |\partial_s u(x,s)|^2 ds dx \\
&\le 9M_2^2 \omega^2 \|\partial_t u(\cdot,t)\|^2_{L^\infty([0,T_\varepsilon];L^2)} \\
&\lesssim \omega^2, \quad 0 \le \omega \le \tau.
\end{aligned}
\tag{3.3.12}
$$

Similarly, we have $\|\phi^3 - u^3(\cdot,\omega)\|_1^2 \lesssim \omega^2,\ 0 \le \omega \le \tau$.

Under the condition (3.3.1), we get

$$
0 < \tau\zeta_l \le \frac{\pi}{3}, \quad \frac{1}{2} \le \cos(\zeta_l\tau) < 1, \quad 0 \le \sin(\zeta_l(\tau-\omega)) \le \sin(\zeta_l\tau) < 1, \quad 0 \le \omega \le \tau.
$$

Noticing $\widehat{\eta}_l^1 = \widehat{\xi}_l^1$ and the definition of $\widehat{\xi}_l^1$, by the Hölder inequality, we obtain

$$
\begin{aligned}
\left|\widehat{\eta}_l^1\right|^2 &= \left| \frac{\varepsilon^2}{\zeta_l} \int_0^\tau \widehat{W}_l^1(\omega) \sin(\zeta_l(\tau-\omega)) d\omega \right|^2 \\
&\le \varepsilon^4 \int_0^\tau \sin(\zeta_l(\tau-\omega)) d\omega \cdot \int_0^\tau \left|\widehat{W}_l^1(\omega)\right|^2 \sin(\zeta_l(\tau-\omega)) d\omega \\
&\le \tau\varepsilon^4 \Big[1 - \cos(\zeta_l\tau)\Big] \frac{\sin(\zeta_l\tau)}{\zeta_l\tau} \int_0^\tau \left|\widehat{W}_l^1(\omega)\right|^2 d\omega. \\
&\le \frac{1}{2}\tau\varepsilon^4 \int_0^\tau \left|\widehat{W}_l^1(\omega)\right|^2 d\omega.
\end{aligned}
\tag{3.3.13}
$$

Multiplying both sides of the above equalities by $(1+\mu_l^2)^s$ and then summing up for $l \in \mathcal{T}_M$, the Parseval's identity equality, triangle inequality, (3.3.9) and (3.3.12) lead to

$$
\begin{aligned}
\|\eta^1(x)\|_s^2 &\le \frac{1}{2}\tau\varepsilon^4 \sum_{l\in\mathcal{T}_M} \left(1+\mu_l^2\right)^s \int_0^\tau \left|\widehat{W}_l^1(\omega)\right|^2 d\omega \\
&= \frac{1}{2}\tau\varepsilon^4 \sum_{l\in\mathcal{T}_M} \left(1+\mu_l^2\right)^s \int_0^\tau \left| \widehat{(f(u))}_l(\omega) - \widehat{(f(\phi))}_l \right|^2 d\omega \\
&\lesssim \tau\varepsilon^4 \int_0^\tau \|u^3(\cdot,\omega) - \phi^3\|_s^2 d\omega \\
&\lesssim \tau^4\varepsilon^4, \quad s = 0, 1.
\end{aligned}
$$

Thus, we immediately can obtain

$$\|u(x,t_1) - u_M^1(x)\|_s \le \|u(x,t_1) - P_M u(x,t_1)\|_s + \|\eta^1(x)\|_s \lesssim h^{1+m_0-s} + \varepsilon^2\tau^2.$$

By the triangle inequality and inverse inequality, there exist $h_2 > 0$ and $\tau_1 > 0$ sufficiently small such that when $0 < h \le h_2$ and $0 < \tau \le \tau_1$, we have

$$\|u_M^1(x)\|_{L^\infty} \le 1 + M_1. \tag{3.3.14}$$

Therefore, the estimates in (3.3.2) are valid when $n = 1$.

Step 3. Estimates for the cases $2 \le n \le T_0\varepsilon^{-\beta}/\tau$. Assume that the estimates in (3.3.2) are valid for all $1 \le n \le m \le T_0\varepsilon^{-\beta}/\tau - 1$, then we need to prove that they are still valid when $n = m+1$.

On the one hand, under the assumption (D), by the Hölder inequality, we have

$$\begin{aligned}
&\|2u^3(\cdot,t_n) - u^3(\cdot,t_n-\omega) - u^3(\cdot,t_n+\omega)\|^2 \\
\le& \int_a^b \left|\int_0^\omega \int_{-s}^s \partial_{\theta\theta} u^3(x,t_n+\theta)d\theta ds\right|^2 dx \\
\le& \int_a^b \omega \int_0^\omega 2s \int_{-s}^s \left|\partial_{\theta\theta} u^3(x,t_n+\theta)\right|^2 d\theta ds dx \\
\le& \int_0^\omega 2\omega s \int_{-s}^s \left(9M_2^2\|\partial_{\theta\theta}u(\cdot,t_n+\theta)\|^2 + 36M_2\|\partial_\theta u(\cdot,t_n+\theta)\|_{L^4}^4\right) d\theta ds \\
\lesssim& \, \omega^4\left[\|\partial_t u(\cdot,t)\|^4_{L^\infty([0,T_\varepsilon];L^4)} + \|\partial_{tt}u(\cdot,t)\|^2_{L^\infty([0,T_\varepsilon];L^2)}\right] \\
\lesssim& \, \tau^4, \quad 0 \le \omega \le \tau.
\end{aligned} \tag{3.3.15}$$

Similarly, we have $\|u^3(\cdot,t_n-\omega) + u^3(\cdot,t_n+\omega) - 2u^3(\cdot,t_n)\|_1^2 \lesssim \tau^4,\ 0 \le \omega \le \tau$.

On the other hand, noticing the definitions of $\widehat{\xi}_l^{n+1}$ and $\widehat{\chi}_l^{n+1}$, similar to (3.3.13), we have

$$\begin{aligned}
\left|\widehat{\xi}_l^{n+1}\right|^2 &= \left|\frac{\varepsilon^2}{\zeta_l}\int_0^\tau \widehat{W}_l^{n+1}(\omega)\sin(\zeta_l(\tau-\omega))d\omega\right|^2 \\
&\lesssim \tau\varepsilon^4\Big[1-\cos(\tau\zeta_l)\Big]\int_0^\tau \left|\widehat{W}_l^{n+1}(\omega)\right|^2 d\omega, \quad l \in \mathcal{T}_M, \quad 1 \le n \le m,
\end{aligned} \tag{3.3.16}$$

$$\begin{aligned}
|\widehat{\chi}_l^{n+1}|^2 &= \left|\frac{2\varepsilon^2(1-\cos(\tau\zeta_l))}{\zeta_l^2}\widehat{V}_l^{n+1}\right|^2 \\
&= \left|\frac{2\varepsilon^2}{\zeta_l}\widehat{V}_l^{n+1}\int_0^\tau \sin(\zeta_l(\tau-\omega))d\omega\right|^2 \\
&\lesssim \tau^2\varepsilon^4\Big[1-\cos(\tau\zeta_l)\Big]\left|\widehat{V}_l^{n+1}\right|^2, \quad l \in \mathcal{T}_M, \quad 1 \le n \le m.
\end{aligned} \tag{3.3.17}$$

Multiplying the above inequalities with $(1+\mu_l^2)^s(s=0,1)$, dividing them by $1-\cos(\tau\zeta_l)$ and then summing up $l\in\mathcal{T}_M$, for $1\le n\le m$, the Parseval's identity equality, triangle inequality,(3.3.9), (3.3.11) and (3.3.15) lead to

$$\begin{aligned}
&\sum_{l\in\mathcal{T}_M}\frac{(1+\mu_l^2)^s}{1-\cos(\tau\zeta_l)}\left|\widehat{\xi}_l^{n+1}\right|^2\\
&\lesssim \tau\varepsilon^4\sum_{l\in\mathcal{T}_M}\left(1+\mu_l^2\right)^s\int_0^\tau\left|\widehat{W}_l^{n+1}(\omega)\right|^2d\omega\\
&\lesssim \tau\varepsilon^4\int_0^\tau\|u^3(\cdot,t_n-\omega)+u^3(\cdot,t_n+\omega)-2u^3(\cdot,t_n)\|_s^2d\omega\\
&\lesssim \tau^6\varepsilon^4,
\end{aligned}\tag{3.3.18}$$

$$\begin{aligned}
\sum_{l\in\mathcal{T}_M}\frac{(1+\mu_l^2)^s}{1-\cos(\tau\zeta_l)}\left|\widehat{\chi}_l^{n+1}\right|^2 &\lesssim \tau^2\varepsilon^4\sum_{l\in\mathcal{T}_M}(1+\mu_l^2)^s\left|\widehat{V}_l^{n+1}\right|^2\\
&\lesssim \tau^2\varepsilon^4\|u^3(\cdot,t_n)-(u_M^n)^3\|_s^2\\
&\lesssim \tau^2\varepsilon^4M_2^2\|u(\cdot,t_n)-u_M^n\|_s^2\\
&\lesssim \tau^2\varepsilon^4\left(h^{1+m_0-s}+\varepsilon^{2-\beta}\tau^2\right)^2.
\end{aligned}\tag{3.3.19}$$

Define the "energy" function as

$$\mathcal{E}^n=\sum_{l\in\mathcal{T}_M}\widehat{\mathcal{E}}_l^n,\ \widehat{\mathcal{E}}_l^n=(1+\mu_l^2)^s\left[|\widehat{\eta}_l^n|^2+\left|\widehat{\eta}_l^{n+1}\right|^2+\frac{\cos(\tau\zeta_l)}{1-\cos(\tau\zeta_l)}\left|\widehat{\eta}_l^{n+1}-\widehat{\eta}_l^n\right|^2\right].\tag{3.3.20}$$

For $n=0$, we have

$$\mathcal{E}^0=\sum_{l\in\mathcal{T}_M}\frac{(1+\mu_l^2)^s}{1-\cos(\tau\zeta_l)}\left|\widehat{\eta}_l^1\right|^2\le\tau\varepsilon^4\sum_{l\in\mathcal{T}_M}\left(1+\mu_l^2\right)^s\int_0^\tau\left|\widehat{W}_l^1(\omega)\right|^2d\omega\lesssim\tau^4\varepsilon^4.$$

Noticing $0\le\beta\le2$, multiplying both sides of (3.3.10) by $(1+\mu_l^2)^s\left(\widehat{\eta}_l^{n+1}-\ \widehat{\eta}_l^{n-1}\right)$, dividing it by $1-\cos(\tau\zeta_l)$ and summing up for $l\in\mathcal{T}_M$, the Young's inequality and (3.3.16)-(3.3.19) result in

$$\begin{aligned}
\mathcal{E}^n-\mathcal{E}^{n-1}&\le\sum_{l\in\mathcal{T}_M}\frac{(1+\mu_l^2)^s}{1-\cos(\tau\zeta_l)}\left|\widehat{\xi}_l^{n+1}+\widehat{\chi}_l^{n+1}\right|\cdot\left|\widehat{\eta}_l^{n+1}-\widehat{\eta}_l^{n-1}\right|\\
&\le\sum_{l\in\mathcal{T}_M}\frac{(1+\mu_l^2)^s}{1-\cos(\tau\zeta_l)}\left(2\varepsilon^\beta\tau\left|\widehat{\eta}_l^{n+1}-\widehat{\eta}_l^n\right|^2+2\varepsilon^\beta\tau\left|\widehat{\eta}_l^n-\widehat{\eta}_l^{n-1}\right|^2\right.\\
&\qquad\left.+\frac{1}{\varepsilon^\beta\tau}\left|\widehat{\xi}_l^{n+1}+\widehat{\chi}_l^{n+1}\right|^2\right)
\end{aligned}$$

$$
\begin{aligned}
&\leq \sum_{l\in\mathcal{T}_M} \frac{4\varepsilon^\beta\tau\cos(\tau\zeta_l)}{1-\cos(\tau\zeta_l)}(1+\mu_l^2)^s\left(\left|\widehat{\eta}_l^{n+1}-\widehat{\eta}_l^{n}\right|^2+\left|\widehat{\eta}_l^{n}-\widehat{\eta}_l^{n-1}\right|^2\right)\\
&\quad+\sum_{l\in\mathcal{T}_M}\frac{2(1+\mu_l^2)^s}{\varepsilon^\beta\tau(1-\cos(\tau\zeta_l))}\left(\left|\widehat{\xi}_l^{n+1}\right|^2+\left|\widehat{\chi}_l^{n+1}\right|^2\right)\\
&\leq 4\varepsilon^\beta\tau\left(\mathcal{E}^n+\mathcal{E}^{n-1}\right)+C\varepsilon^{4-\beta}\tau\left(h^{1+m_0-s}+\tau^2\right)^2,\quad 1\leq n\leq m,
\end{aligned}
$$

where the constant C is independent of h, τ and ε. Summing the above inequality for $n=1,2,\cdots,m$, and noticing the condition $\tau\leq 1/8$, we get

$$
\mathcal{E}^m \lesssim \mathcal{E}^0+\varepsilon^\beta\tau\sum_{n=0}^{m-1}\mathcal{E}^n+T_0\varepsilon^{4-2\beta}\left(h^{1+m_0-s}+\tau^2\right)^2,\quad 1\leq m\leq T_0\varepsilon^{-\beta}/\tau-1. \tag{3.3.21}
$$

Hence, the Gronwall's inequality suggests that there exists a constant $\tau_2>0$ sufficiently small, such that when $0\leq\tau\leq\tau_2$, the following holds for $1\leq m\leq T_0\varepsilon^{-\beta}/\tau-1$,

$$
\mathcal{E}^m\lesssim\mathcal{E}^0+\varepsilon^{4-2\beta}\left(h^{1+m_0-s}+\tau^2\right)^2\lesssim\varepsilon^{4-2\beta}\left(h^{1+m_0-s}+\tau^2\right)^2. \tag{3.3.22}
$$

Recalling the definition of $\mathcal{E}^m$ in (3.3.20), for $1\leq m\leq T_0\varepsilon^{-\beta}/\tau-1$, we can obtain the error estimate

$$
\|\eta^{m+1}\|_s^2=\sum_{l\in\mathcal{T}_M}(1+\mu_l^2)^s\left|\widehat{\eta}_l^{m+1}\right|^2\leq\mathcal{E}^m\lesssim\varepsilon^{4-2\beta}\left(h^{1+m_0-s}+\tau^2\right)^2,
$$

by combining (3.3.20) with the Parseval's identity equality and (3.3.22), which immediately concludes that the first inequality in (3.3.2) is valid for $n=m+1$.

Lastly, we have to prove the error estimate of $\|u_M^{m+1}(x)\|_{L^\infty}$ for $1\leq m\leq T_0\varepsilon^{-\beta}/\tau-1$. In fact, the inverse inequality and triangle inequality will imply that there exist $h_3>0$ and $\tau_3>0$ sufficiently small such that when $0<h\leq h_3$ and $0<\tau\leq\tau_3$, we have

$$
\|u_M^{m+1}(x)\|_{L^\infty}\leq\|u(x,t_{m+1})-u_M^{m+1}(x)\|_{L^\infty}+\|u(x,t_{m+1})\|_{L^\infty}\leq 1+M_1.
$$

Overall, under the choice of $h_0=\min\{h_1,h_2,h_3\}$ and $\tau_0=\min\{\tau_1,\tau_2,\tau_3\}$, the proof of Theorem 3.3.1 is completed by the method of mathematical induction. □

3.4 Extensions to other spatial discretizations

For comparisons, we also introduce the exponential wave integrator finite difference (EWI-FD)/exponential wave integrator fourth-order compact finite difference (EWI-4cFD) method which is based on applying finite difference/fourth-order compact finite difference to spatial discretization followed by the Gautschi-type exponential wave integrator in temporal discretization [9, 57].

Let $u_j(t)$ be the approximation of $u(x_j, t)$ for $j = 0, 1, \cdots, M$. Applying the finite difference to discretize the NKGE (2.1.1) in space, we get

$$\frac{\mathrm{d}^2}{\mathrm{d}t^2} u_j(t) - \delta_x^2 u_j(t) + u_j(t) + \varepsilon^2 f(u_j(t)) = 0, \quad j = 0, 1, \cdots, M-1, \tag{3.4.1}$$

with $u_0(t) = u_M(t)$ and $u_{-1}(t) = u_{M-1}(t)$. Let $U(t) = (u_0(t), u_1(t), \cdots, u_{M-1}(t))^T$ and $F(U(t)) = (f(u_0(t)), f(u_1(t)), \cdots, f(u_{M-1}(t)))^T$, then the above ODEs (3.4.1) can be rewritten as

$$U''(t) + BU(t) + \varepsilon^2 F(U(t)) = 0, \quad t \geq 0, \tag{3.4.2}$$

where B is an $M \times M$ matrix independent of t. Since the matrix B is normal, there exists an orthogonal matrix P and a diagonal matrix Λ such that

$$B = P^{-1} \Lambda P.$$

Let $V(t) = PU(t)$ and multiply P to both sides of (3.4.2), we obtain

$$V''(t) + \Lambda V(t) + \varepsilon^2 PF(U(t)) = 0, \quad t \geq 0. \tag{3.4.3}$$

We can also use the Gautschi-type exponential wave integrator to discretize the above second-order ODEs. We omit the details here for brevity and the scheme of the EWI-FD is the same as just replacing μ_l in (3.2.5) by λ_l defined in (2.3.15).

For the EWI-4cFD method, the idea is the same as that of the EWI-FD method and replace the matrix B in (3.4.2) by the normal matrix A^{-1} defined in (2.6.11). By the definition of the fourth-order compact operator, the scheme of the EWI-4cFD can be obtained straightforwardly by replacing μ_l in (3.2.5) by

$$\nu_l = \frac{\lambda_l}{\sqrt{1 - h^2 \lambda_l^2 / 12}}. \tag{3.4.4}$$

Similar to the stability analysis of the EWI-FP method, we have the following stability results for the EWI-FD and EWI-4cFD methods.

Lemma 3.4.1. *(stability) For any $0 < \varepsilon \leq 1$, the EWI-FD is conditionally stable under the stability condition*

$$0 < \tau \leq \frac{2h}{\sqrt{4 + h^2(1 + \sigma_{\max})}}, \quad h > 0, \tag{3.4.5}$$

and the EWI-4cFD method is conditionally stable under the stability condition

$$0 < \tau \leq \frac{2h}{\sqrt{6 + h^2(1 + \sigma_{\max})}}, \quad h > 0. \tag{3.4.6}$$

Proof. We only need to replace μ_l in (3.2.5) by λ_l defined in (2.3.15) for the EWI-FD method and ν_l defined in (3.4.4) for the EWI-4cFD and the stability claim follows immediately. $\square$

Assume that the exact solution of the NKGE (2.1.1) up to the time $T_\varepsilon = T_0/\varepsilon^2$ satisfies

$$(E) \qquad \begin{aligned} &u(x,t) \in C^2\left([0,T_\varepsilon]; L^\infty\right) \cap C^1\left([0,T_\varepsilon]; L^\infty\right) \cap C\left([0,T_\varepsilon]; W_p^{6,\infty}\right), \\ &\|u(x,t)\|_{L^\infty([0,T_\varepsilon];L^\infty)} + \|\partial_{xxxxxx} u(x,t)\|_{L^\infty([0,T_\varepsilon];L^\infty)} \lesssim 1, \\ &\|\partial_t u(x,t)\|_{L^\infty([0,T_\varepsilon];L^\infty)} \lesssim 1, \quad \|\partial_{tt} u(x,t)\|_{L^\infty([0,T_\varepsilon];L^\infty)} \lesssim 1, \end{aligned}$$

then we have the following error estimates for the EWI-FD and EWI-4cFD methods:

Theorem 3.4.1. *Let u_j^n be the approximation obtained from the EWI-FD, under the stability condition* (3.4.5)*, the assumptions (E) and* (3.3.1)*, there exist constants $h_0 > 0$ and $\tau_0 > 0$ sufficiently small and independent of ε, such that for any $0 < \varepsilon \leq 1$ and $0 \leq \beta \leq 2$, when $0 < h \leq h_0$, $0 < \tau \leq \tau_0$, we have*

$$\|e^n\|_{l^2} \lesssim \frac{h^2}{\varepsilon^\beta} + \varepsilon^{2-\beta}\tau^2, \quad \|u^n\|_{l^\infty} \leq 1 + M_1, \quad 0 \leq n \leq \frac{T_0/\varepsilon^\beta}{\tau}, \tag{3.4.7}$$

where

$$e^n = (e_0^n, e_1^n, \cdots, e_M^n)^T, \quad \textit{with} \quad e_j^n = u(x_j, t_n) - u_j^n, \quad 0 \leq j \leq M, \quad n \geq 0.$$

Theorem 3.4.2. *Let u_j^n be the approximation obtained from the EWI-4cFD, under the stability condition* (3.4.6)*, the assumptions (E) and* (3.3.1)*, there exist constants $h_0 > 0$ and $\tau_0 > 0$ sufficiently small and independent of ε, such that for any $0 < \varepsilon \leq 1$ and $0 \leq \beta \leq 2$, when $0 < h \leq h_0$, $0 < \tau \leq \tau_0$, we have*

$$\|e^n\|_{l^2} \lesssim \frac{h^4}{\varepsilon^\beta} + \varepsilon^{2-\beta}\tau^2, \quad \|u^n\|_{l^\infty} \leq 1 + M_1, \quad 0 \leq n \leq \frac{T_0/\varepsilon^\beta}{\tau}. \tag{3.4.8}$$

Proof. Follow the analogous proof to Theorem 3.3.1 and we omit the details here for brevity. □

3.5 Numerical results and comparisons

In this section, we present the numerical results of the above EWI methods for the NKGE (2.1.1) to support our error estimates and compare the results of different spatial discretizaitons. We begin with the numerical test for the EWI-FP (3.2.7)-(3.2.8). In our numerical experiments for the EWI-FP method, we choose the initial data as

$$\phi(x) = \frac{1}{2 + \cos^2(x)} \quad \text{and} \quad \gamma(x) = \sin(x), \quad x \in (0, 2\pi). \tag{3.5.1}$$

The 'exact' solution $u(x,t)$ is computed by the time-splitting Fourier pseudospectral method with a very fine mesh size $h_e = \pi/32$ and a very small time step $\tau_e = 5 \times 10^{-4}$. Denote $u_{h,\tau}^n$ as the numerical solution at $t = t_n$ by the EWI-FP (3.2.7)-(3.2.8) with mesh size h and time step τ. The errors are denoted as $e(x,t_n) \in Y_M$ with $e(x,t_n) = u(x,t_n) - I_M(u_{h,\tau}^n)(x)$. In order to quantify the numerical results, we measure the H^1 norm of $e(\cdot, t_n)$.

The numerical computation is carried out on a time interval $[0, T_0/\varepsilon^\beta]$ with $0 \leq \beta \leq 2$ and $T_0 > 0$ fixed. Here, we also study the following three cases with respect to different β:

Case I. Fixed time dynamics up to the time at $O(1)$, i.e., $\beta = 0$;

Case II. Intermediate long-time dynamics up to the time at $O(\varepsilon^{-1})$, i.e., $\beta = 1$;

Case III. Long-time dynamics up to the time at $O(\varepsilon^{-2})$, i.e., $\beta = 2$.

	$\|e(\cdot, 1/\varepsilon^{\beta})\|_1$	$h_0 = \pi/2$	$h_0/2$	$h_0/2^2$	$h_0/2^3$
$\beta = 0$	$\varepsilon_0 = 1$	4.05E-2	8.80E-3	1.53E-4	7.19E-8
	$\varepsilon_0/2$	4.78E-2	8.48E-3	1.58E-4	2.37E-8
	$\varepsilon_0/2^2$	5.17E-2	8.36E-3	1.59E-4	1.15E-8
	$\varepsilon_0/2^3$	5.28E-2	8.33E-3	1.59E-4	1.00E-8
	$\varepsilon_0/2^4$	5.31E-2	8.32E-3	1.59E-4	9.89E-9
$\beta = 1$	$\varepsilon_0 = 1$	4.05E-2	8.80E-3	1.53E-4	7.19E-8
	$\varepsilon_0/2$	3.98E-2	6.27E-3	5.61E-5	4.19E-8
	$\varepsilon_0/2^2$	1.57E-2	8.14E-3	1.33E-4	4.03E-8
	$\varepsilon_0/2^3$	1.02E-2	3.17E-3	2.82E-5	1.08E-8
	$\varepsilon_0/2^4$	6.08E-3	3.44E-3	1.41E-5	1.98E-8
$\beta = 2$	$\varepsilon_0 = 1$	4.05E-2	8.80E-3	1.53E-4	7.19E-8
	$\varepsilon_0/2$	4.04E-2	8.46E-3	1.40E-4	9.30E-8
	$\varepsilon_0/2^2$	6.12E-2	4.18E-3	1.57E-5	6.90E-8
	$\varepsilon_0/2^3$	1.01E-1	3.25E-3	1.45E-4	1.35E-7
	$\varepsilon_0/2^4$	6.05E-2	1.31E-3	1.34E-4	4.16E-7

Table 3.1: Spatial errors of the EWI-FP (3.2.7)-(3.2.8) for the NKGE (2.1.1) with initial data (3.5.1) and different β or ε.

The errors are displayed at $t = 1/\varepsilon^{\beta}$ with different ε and β. In order to test the spatial errors, we fix the time step as $\tau = 5 \times 10^{-4}$ such that the temporal error can be ignored and solve the NKGE (2.1.1) under different mesh size h. Table 3.1 depicts the spatial errors for $\beta = 0$, $\beta = 1$ and $\beta = 2$. Then, we check the temporal errors for different $0 \le \varepsilon \le 1$ and $0 \le \beta \le 2$ with different time step τ and a very fine mesh size $h = \pi/32$ such that the spatial errors can be neglected. Tables 3.2-3.4 show the temporal errors for $\beta = 0$, $\beta = 1$ and $\beta = 2$, respectively.

From Tables 3.1-3.4 and additional similar numerical results not shown here for brevity, we can draw the following observations on the EWI-FP (3.2.7)-(3.2.8) for the

$\|e(\cdot,1/\varepsilon^\beta)\|_1$	$\tau_0=0.2$	$\tau_0/2$	$\tau_0/2^2$	$\tau_0/2^3$	$\tau_0/2^4$	$\tau_0/2^5$
$\varepsilon_0=1$	4.59E-2	1.13E-2	2.82E-3	7.04E-4	1.76E-4	4.37E-5
order	-	2.02	2.00	2.00	2.00	2.01
$\varepsilon_0/2$	1.48E-2	3.66E-3	9.11E-4	2.27E-4	5.68E-5	1.41E-5
order	-	2.02	2.01	2.00	2.00	2.01
$\varepsilon_0/2^2$	4.05E-3	1.00E-3	2.49E-4	6.23E-5	1.55E-5	3.86E-6
order	-	2.02	2.01	2.00	2.01	2.01
$\varepsilon_0/2^3$	1.04E-3	2.56E-4	6.39E-5	1.59E-5	3.98E-6	9.89E-7
order	-	2.02	2.00	2.01	2.00	2.01
$\varepsilon_0/2^4$	2.61E-4	6.44E-5	1.61E-5	4.01E-6	1.00E-6	2.49E-7
order	-	2.02	2.00	2.01	2.00	2.01
$\varepsilon_0/2^5$	6.53E-5	1.61E-5	4.02E-6	1.00E-6	2.51E-7	6.23E-8
order	-	2.02	2.00	2.01	1.99	2.01

Table 3.2: Temporal errors of the EWI-FP (3.2.7)-(3.2.8) for the NKGE (2.1.1) with $\beta=0$ and initial data (3.5.1).

NKGE (2.1.1) up to the time of the order of $O(\varepsilon^{-\beta})$ with $0\le\beta\le 2$:

(i) In space, the EWI-FP (3.2.7)-(3.2.8) is uniformly and spectrally accurate for any $0<\varepsilon\le 1$ and $0\le\beta\le 2$ (cf. each row in Table 3.1) and the spatial errors are almost independent of ε (cf. each column in Table 3.1).

(ii) In time, for any fixed $\varepsilon=\varepsilon_0>0$, the EWI-FP (3.2.7)-(3.2.8) is uniformly second-order accurate (cf. the first rows in Tables 3.2-3.4), which agree with those results in the literature. In addition, Tables 3.2-3.4 illustrate that the error bounds of temporal discretization for the EWI-FP (3.2.7)-(3.2.8) uniformly behave like $O(\varepsilon^2\tau^2)$ for the fixed time dynamics up to the time at $O(1)$, i.e., $\beta=0$ (cf. each row and column in Table 3.2), and $O(\varepsilon\tau^2)$ for the intermediate long-time dynamics up to the time of the order of $O(\varepsilon^{-1})$, i.e., $\beta=1$ (cf. each row and column in Table 3.3), and resp. $O(\tau^2)$ for the long-time dynamics up to the time of the order of $O(\varepsilon^{-2})$, i.e., $\beta=2$ (cf. each row and column in Table 3.4). In summary, our numerical results confirm the error

$\lVert e(\cdot,1/\varepsilon^\beta)\rVert_1$	$\tau_0=0.2$	$\tau_0/2$	$\tau_0/2^2$	$\tau_0/2^3$	$\tau_0/2^4$	$\tau_0/2^5$
$\varepsilon_0=1$	4.59E-2	1.13E-2	2.82E-3	7.04E-4	1.76E-4	4.37E-5
order	-	2.02	2.00	2.00	2.00	2.01
$\varepsilon_0/2$	1.30E-2	3.22E-3	8.04E-4	2.01E-4	5.02E-5	1.25E-5
order	-	2.01	2.00	2.00	2.00	2.01
$\varepsilon_0/2^2$	5.76E-3	1.43E-3	3.56E-4	8.90E-5	2.23E-5	5.57E-6
order	-	2.01	2.01	2.00	2.00	2.00
$\varepsilon_0/2^3$	2.30E-3	5.72E-4	1.43E-4	3.57E-5	8.92E-6	2.23E-6
order	-	2.01	2.00	2.00	2.00	2.00
$\varepsilon_0/2^4$	1.66E-3	4.11E-4	1.03E-4	2.56E-5	6.41E-6	1.60E-6
order	-	2.01	2.00	2.01	2.00	2.00
$\varepsilon_0/2^5$	4.18E-4	1.04E-4	2.59E-5	6.48E-6	1.62E-6	4.05E-7
order	-	2.01	2.01	2.00	2.00	2.00

Table 3.3: Temporal errors of the EWI-FP (3.2.7)-(3.2.8) for the NKGE (2.1.1) with $\beta=1$ and initial data (3.5.1).

bounds in Theorem 3.3.1 and demonstrate that they are sharp.

For the EWI-FD and EWI-4cFD methods, we show the numerical results at $t=1/\varepsilon^2$ with the initial data

$$\phi(x)=\frac{3}{2+\sin^2(x)},\quad \gamma(x)=\frac{3}{1+\cos^2(x)},\quad x\in(0,2\pi). \tag{3.5.2}$$

The 'exact' solution is computed by the time-splitting Fourier pseudospectral method with a very fine mesh size $h_e=\pi/2^{13}$ and a very small time step $\tau_e=10^{-4}$. Denote $u^n_{h,\tau}$ as the numerical solution at t_n obtained by the EWI-FD/EWI-4cFD method with mesh size h and time step τ. In order to test the numerical results, we define the error function as follows:

$$e_{h,\tau}(t_n)=\lVert u(\cdot,t_n)-u^n_{h,\tau}\rVert_{l^2}.$$

From Tables 3.5-3.8 for the EWI-FD and EWI-4cFD methods and additional similar numerical results not shown here for brevity, we can draw the following observations:

$\|e(\cdot,1/\varepsilon^\beta)\|_1$	$\tau_0=0.2$	$\tau_0/2$	$\tau_0/2^2$	$\tau_0/2^3$	$\tau_0/2^4$	$\tau_0/2^5$
$\varepsilon_0=1$	4.59E-2	1.13E-2	2.82E-3	7.04E-4	1.76E-4	4.37E-5
order	-	2.02	2.00	2.00	2.00	2.01
$\varepsilon_0/2$	3.17E-2	7.83E-3	1.95E-3	4.88E-4	1.22E-4	3.04E-5
order	-	2.02	2.01	2.00	2.00	2.00
$\varepsilon_0/2^2$	2.51E-2	6.23E-3	1.55E-3	3.88E-4	9.70E-5	2.42E-5
order	-	2.01	2.01	2.00	2.00	2.00
$\varepsilon_0/2^3$	3.28E-2	8.14E-3	2.03E-3	5.08E-4	1.27E-4	3.17E-5
order	-	2.01	2.00	2.00	2.00	2.00
$\varepsilon_0/2^4$	2.50E-2	6.23E-3	1.56E-3	3.89E-4	9.72E-5	2.43E-5
order	-	2.00	2.00	2.00	2.00	2.00
$\varepsilon_0/2^5$	2.88E-2	7.17E-3	1.79E-3	4.47E-4	1.12E-4	2.79E-5
order	-	2.01	2.00	2.00	2.00	2.01

Table 3.4: Temporal errors of the EWI-FP (3.2.7)-(3.2.8) for the NKGE (2.1.1) with $\beta=2$ and initial data (3.5.1).

(i) In time, for any fixed $\varepsilon=\varepsilon_0>0$ or in the long-time regime ($\beta=2$), the EWI-FD and EWI-4cFD methods are both uniformly second-order accurate (cf. each row in Tables 3.6&3.8) and the temporal errors are almost independent of ε (cf. each column in Tables 3.6&3.8).

(ii) In space, for the long-time regime, i.e. $\beta=2$, the second order convergence of the EWI-FD method can be observed only when $0<h\lesssim\varepsilon$ (cf. upper triangles above the diagonals (corresponding to $h\sim\varepsilon$, and being labelled in bold letters) in Table 3.5). For the EWI-4cFD method, the second order convergence can be observed only when $0<h\lesssim\varepsilon^{1/2}$ (cf. upper triangles above the diagonals (corresponding to $h\sim\varepsilon^{1/2}$, and being labelled in bold letters) in Table 3.7)

The above numerical results confirm our error estimates for the EWI-FD and EWI-4cFD methods.

Comparing the EWI-FP, EWI-FD and EWI-4cFD methods, the temporal errors are

$e_{h,\tau_e}(t=1/\varepsilon^2)$	$h_0=\pi/32$	$h_0/2$	$h_0/2^2$	$h_0/2^3$	$h_0/2^4$	$h_0/2^5$
$\varepsilon_0=1$	**1.84E-3**	4.63E-4	1.16E-4	2.90E-5	7.24E-6	1.81E-6
order	**-**	1.99	2.00	2.00	2.00	2.00
$\varepsilon_0/2$	7.86E-3	**2.01E-3**	5.04E-4	1.26E-4	3.16E-5	7.89E-6
order	-	**1.97**	2.00	2.00	2.00	2.00
$\varepsilon_0/2^2$	2.28E-2	6.01E-3	**1.51E-3**	3.79E-4	9.47E-5	2.37E-5
order	-	1.92	**1.99**	1.99	2.00	2.00
$\varepsilon_0/2^3$	1.40E-1	3.28E-2	8.44E-3	**2.12E-3**	5.32E-4	1.33E-4
order	-	2.09	1.96	**1.99**	1.99	2.00
$\varepsilon_0/2^4$	4.31E-2	7.57E-2	1.37E-2	3.84E-3	**1.00E-3**	2.53E-4
order	-	-0.81	2.47	1.83	**1.94**	1.98

Table 3.5: Spatial errors of the EWI-FD for the NKGE (2.1.1) with $\beta = 2$ and initial data (3.5.2).

uniformly second-order accurate in the long-time regime, which agree with the claim that the temporal resolution capacity of the Gautschi-type exponential wave integrator for wave-type equation is independent of the spatial discretization in the literature [9, 66]. For the spatial discretization, the errors of the finite difference methods depend on the small parameter $\varepsilon \in (0, 1]$. The spatial resolution capacity of the EWI-4cFD method is better than that of the EWI-FD method, which means that the EWI-4cFD method needs less mesh grids in space than that of the EWI-FD to get the same errors. While the error of the spectral method is uniform which performs best among these three methods, especially when $0 < \varepsilon \ll 1$.

$e_{h,\tau_e}(t=1/\varepsilon^2)$	$\tau_0=0.2$	$\tau_0/2$	$\tau_0/2^2$	$\tau_0/2^3$	$\tau_0/2^4$	$\tau_0/2^5$
$\varepsilon_0=1$	2.13E-2	4.84E-3	1.19E-3	2.95E-4	7.35E-5	1.84E-5
order	-	2.14	2.02	2.01	2.00	2.00
$\varepsilon_0/2$	9.05E-3	2.03E-3	5.04E-4	1.26E-4	3.13E-5	7.75E-6
order	-	2.16	2.01	2.00	2.01	2.01
$\varepsilon_0/2^2$	1.46E-2	3.74E-3	9.35E-4	2.34E-4	5.84E-5	1.46E-5
order	-	1.96	2.00	2.00	2.00	2.00
$\varepsilon_0/2^3$	2.24E-2	5.59E-3	1.40E-3	3.49E-4	8.70E-5	2.17E-5
order	-	2.00	2.00	2.00	2.00	2.00
$\varepsilon_0/2^4$	1.27E-2	3.16E-3	7.91E-4	1.98E-4	4.94E-5	1.27E-5
order	-	2.01	2.00	2.00	2.00	1.96

Table 3.6: Temporal errors of the EWI-FD for the NKGE (2.1.1) with $\beta=2$ and initial data (3.5.2).

$e_{h,\tau_e}(t=1/\varepsilon^2)$	$h_0=\pi/8$	$h_0/2$	$h_0/2^2$	$h_0/2^3$	$h_0/2^4$
$\varepsilon_0=1$	4.44E-3	**2.82E-4**	1.71E-5	1.06E-6	6.65E-8
order	-	**3.98**	4.04	4.01	3.99
$\varepsilon_0/2^2$	2.34E-2	3.46E-3	**2.03E-4**	1.25E-5	7.97E-7
order	-	2.76	**4.09**	4.02	3.97
$\varepsilon_0/2^4$	7.51E-2	1.54E-2	1.97E-3	**1.35E-4**	8.40E-6
order	-	2.29	2.97	**3.87**	4.01
$\varepsilon_0/2^6$	2.25E-1	1.93E-1	5.06E-2	2.97E-3	**2.17E-4**
order	-	0.22	1.93	4.09	**3.77**

Table 3.7: Spatial errors of the EWI-4cFD for the NKGE (2.1.1) with $\beta=2$ and initial data (3.5.2).

$e_{h,\tau_e}(t=1/\varepsilon^2)$	$\tau_0 = 0.2$	$\tau_0/2$	$\tau_0/2^2$	$\tau_0/2^3$	$\tau_0/2^4$	$\tau_0/2^5$
$\varepsilon_0 = 1$	2.13E-2	4.84E-3	1.19E-3	2.95E-4	7.35E-5	1.84E-5
order	-	2.14	2.02	2.01	2.00	2.00
$\varepsilon_0/2$	9.05E-3	2.03E-3	5.04E-4	1.26E-4	3.14E-5	7.85E-6
order	-	2.16	2.01	2.00	2.00	2.00
$\varepsilon_0/2^2$	1.46E-2	3.74E-3	9.35E-4	2.34E-4	5.85E-5	1.46E-5
order	-	1.96	2.00	2.00	2.00	2.00
$\varepsilon_0/2^3$	2.24E-2	5.59E-3	1.40E-3	3.49E-4	8.72E-5	2.18E-5
order	-	2.00	2.00	2.00	2.00	2.00
$\varepsilon_0/2^4$	1.27E-2	3.16E-3	7.91E-4	1.98E-4	4.95E-5	1.24E-5
order	-	2.01	2.00	2.00	2.00	2.00

Table 3.8: Temporal errors of the EWI-4cFD for the NKGE (2.1.1) with $\beta = 2$ and initial data (3.5.2).

Chapter 4

Error Estimates of Time-Splitting Methods

In this chapter, we are going to study another popular numerical integrator: the time-splitting method for temporal discretization [17, 47, 81, 102, 159]. We first reformulate the NKGE (2.1.1) into a relativistic nonlinear Schrödinger equation (NLSE) and then adapt the time-splitting methods to discretize it [12]. The key idea of the method is splitting the relativistic NLSE in a proper way such that the linear part can be solved exactly in phase space and the nonlinear part can be integrated exactly in physical space [14, 15].

We begin with recalling the construction of a time-splitting integrator for a general equation in the form [47, 109, 136]:

$$\partial_t y = \Phi(y) = \mathcal{A}y + \mathcal{B}y, \tag{4.0.1}$$

where Φ is usually a nonlinear operator and the operator-splitting $\Phi(y) = \mathcal{A}y + \mathcal{B}y$ can be quite arbitrary; in particular, $\mathcal{A}$ and $\mathcal{B}$ can be two non-commutative operators. We aim to get the approximations y^n of the solution at $t_n = n\tau (n = 0, 1, 2, \cdots)$, where $\tau > 0$ is the time step. By the Strang-splitting formula [55, 136], the second-order time-splitting integrator for (4.0.1), $y^{n+1} = [\Phi_2(\tau)](y^n)$, can be constructed as

$$y^{(1)} = \exp(\frac{1}{2}\tau\mathcal{A})y^n, \quad y^{(2)} = \exp(\tau\mathcal{B})y^{(1)}, \quad y^{n+1} = \exp(\frac{1}{2}\tau\mathcal{A})y^{(2)}, \tag{4.0.2}$$

which is explicit and symmetric, i.e., $\Phi_2(\tau)\Phi_2(-\tau) = 1$. It is easy to check that the approximation error of Strang-splitting is of second order $O(\tau^2)$ by the Taylor expansion and it is possible to construct the time-splitting method with higher order [16, 162].

In general, the operators $\mathcal{A}$ and $\mathcal{B}$ can be interchanged without affecting the accuracy order of the splitting method.

4.1 A relativistic NLSE

Denote $\dot{u}(x,t) = \partial_t u(x,t)$ and set

$$\psi(x,t) = u(x,t) - i\langle\nabla\rangle^{-1}\dot{u}(x,t), \quad x \in= [a,b], \quad t \geq 0. \tag{4.1.1}$$

By a short calculation, we can reformulate the NKGE (2.1.1) into a relativistic NLSE in $\psi := \psi(x,t)$ as

$$\begin{cases} i\partial_t\psi(x,t) + \langle\nabla\rangle\psi(x,t) + \varepsilon^2\langle\nabla\rangle^{-1} f\left(\frac{1}{2}\left(\psi + \overline{\psi}\right)\right)(x,t) = 0, \quad x \in \Omega, \quad t > 0, \\ \psi(a,t) = \psi(b,t), \qquad \partial_x\psi(a,t) = \partial_x\psi(b,t), \quad t \geq 0, \\ \psi(x,0) = \psi_0(x) := \phi(x) - i\langle\nabla\rangle^{-1}\gamma(x), \quad x \in [a,b], \end{cases} \tag{4.1.2}$$

where $f(v) = v^3$ and $\overline{\psi}$ denotes the complex conjugate of ψ. After solving the relativistic NLSE (4.1.2) and noticing (4.1.1), we can recover the solution of the NKGE (2.1.1) by

$$u(x,t) = \frac{1}{2}\left(\psi(x,t) + \overline{\psi}(x,t)\right), \qquad \partial_t u(x,t) = \frac{i}{2}\left(\langle\nabla\rangle\psi(x,t) - \langle\nabla\rangle\overline{\psi}(x,t)\right). \tag{4.1.3}$$

We remark here that the NKGE (2.1.1) can also be reformulated as the following first-order (in time) PDEs:

$$\begin{cases} \partial_t u(x,t) - \dot{u}(x,t) = 0, \quad x \in (a,b), \quad t > 0, \\ \partial_t\dot{u}(x,t) - \partial_{xx}u(x,t) + u(x,t) + \varepsilon^2 u^3(x,t) = 0, \quad x \in (a,b), \quad t > 0, \\ u(a,t) = u(b,t), \qquad \partial_x u(a,t) = \partial_x u(b,t), \qquad t \geq 0, \\ u(x,0) = \phi(x), \quad \dot{u}(x,0) = \gamma(x), \qquad x \in [a,b]. \end{cases} \tag{4.1.4}$$

4.2 Semi-discretization in time by time-splitting method

In order to discretize the NKGE (2.1.1) in time by a time-splitting method, we can first discretize the relativistic NLSE (4.1.2) by a time-splitting method and then recover the solution of the NKGE (2.1.1) via (4.1.3). In fact, the relativistic NLSE (4.1.2) can be decomposed into the following two subproblems via the time-splitting technique [31, 84, 86, 102, 141, 145]

$$\begin{cases} i\partial_t\psi(x,t) + \langle\nabla\rangle\psi(x,t) = 0, \quad x \in (a,b), \quad t > 0, \\ \psi(a,t) = \psi(b,t), \qquad \partial_x\psi(a,t) = \partial_x\psi(b,t), \quad t \geq 0, \\ \psi(x,0) = \psi_0(x), \qquad x \in [a,b], \end{cases} \tag{4.2.1}$$

and

$$\begin{cases} i\partial_t\psi(x,t) + \varepsilon^2\langle\nabla\rangle^{-1} f\Big(\frac{1}{2}(\psi + \overline{\psi})\Big)(x,t) = 0, \quad x \in [a,b], \quad t > 0, \\ \psi(x,0) = \psi_0(x), \qquad x \in [a,b]. \end{cases} \tag{4.2.2}$$

The linear equation (4.2.1) can be solved exactly in phase space and the associated evolution operator is given by

$$\psi(\cdot,t) = \varphi_T^t(\psi_0) := e^{it\langle\nabla\rangle}\psi_0, \quad t \geq 0, \tag{4.2.3}$$

which satisfies the isometry relation

$$\|\varphi_T^t(v_0)\|_s = \|v_0\|_s, \quad s \geq 0, \quad t \in \mathbb{R}.$$

Recalling that the nonlinear part of (4.2.2) is real, this implies that $\partial_t\left(\psi + \overline{\psi}\right)(x,t) = 0$ for any fixed $x \in [a,b]$. Thus $\psi + \overline{\psi}$ is invariant in time, i.e.,

$$\left(\psi + \overline{\psi}\right)(x,t) \equiv \left(\psi + \overline{\psi}\right)(x,0) = \psi_0(x) + \overline{\psi_0}(x), \quad x \in [a,b], \quad t \geq 0. \tag{4.2.4}$$

Plugging (4.2.4) into (4.2.2), we get

$$\begin{cases} i\partial_t\psi(x,t) + \varepsilon^2\langle\nabla\rangle^{-1} f\Big(\frac{1}{2}(\psi_0 + \overline{\psi_0})\Big)(x) = 0, \quad x \in [a,b], \quad t > 0, \\ \psi(x,0) = \psi_0(x), \qquad x \in [a,b]. \end{cases} \tag{4.2.5}$$

Thus (4.2.5) (and (4.2.2)) can be integrated exactly in time as:

$$\psi(x,t) = \varphi_V^t(\psi_0) := \psi_0(x) + \varepsilon^2 t\, F(\psi_0(x)), \quad t \geq 0, \tag{4.2.6}$$

where the operator F is defined by

$$F(\phi) = i\langle\nabla\rangle^{-1}G(\phi), \qquad G(\phi) = f\Big(\frac{1}{2}(\phi + \overline{\phi})\Big). \tag{4.2.7}$$

Let $\tau > 0$ be the time step and define $t_n = n\tau$ for $n = 0, 1, \ldots$. Denote $\psi^{[n]} := \psi^{[n]}(x)$ be the approximation of $\psi(x, t_n)$ for $n \geq 0$, then a second-order semi-discretization of the relativistic NLSE (4.1.2) via the Strang-splitting can be given as:

$$\psi^{[n+1]} = \mathcal{S}_\tau(\psi^{[n]}) = \varphi_T^{\tau/2} \circ \varphi_V^\tau \circ \varphi_T^{\tau/2}(\psi^{[n]}), \qquad n = 0, 1, 2, \ldots, \tag{4.2.8}$$

with $\psi^{[0]} = \psi_0 = u_0 - i\langle\nabla\rangle^{-1}u_1$. Noticing (4.1.3) and (4.2.8), we can get a second-order semi-discretization of the NKGE (2.1.1):

$$u^{[n]} = \frac{1}{2}\left(\psi^{[n]} + \overline{\psi^{[n]}}\right), \quad \dot{u}^{[n]} = \frac{i}{2}\left(\langle\nabla\rangle\psi^{[n]} - \langle\nabla\rangle\overline{\psi^{[n]}}\right), \quad n = 0, 1, \ldots, \tag{4.2.9}$$

where $u^{[n]} := u^{[n]}(x)$ and $\dot{u}^{[n]} := \dot{u}^{[n]}(x)$ are the approximations of $u(x, t_n)$ and $\partial_t u(x, t_n)$ $(n = 0, 1, 2, \ldots)$, respectively.

We remark here that another way to discretize the NKGE (2.1.1) in time by a time-splitting method, which is exactly the same discretization as the one presented above, is to discretize the NKGE (4.1.4) by a time-splitting method. In fact, the NKGE (4.1.4) can be decomposed into the following two subproblems via the time-splitting technique [47]

$$\begin{cases} \partial_t u(x,t) - \dot{u}(x,t) = 0, \\ \partial_t \dot{u}(x,t) - \partial_{xx} u(x,t) + u(x,t) = 0, \quad x \in (a,b), \quad t > 0, \\ u(a,t) = u(b,t), \qquad \partial_x u(a,t) = \partial_x u(b,t), \qquad t \geq 0, \\ u(x,0) = \phi(x), \quad \dot{u}(x,0) = \gamma(x), \qquad x \in [a,b], \end{cases} \tag{4.2.10}$$

and

$$\begin{cases} \partial_t u(x,t) = 0, \\ \partial_t \dot{u}(x,t) + \varepsilon^2 u^3(x,t) = 0, \quad x \in [a,b], \quad t > 0, \\ u(x,0) = \phi(x), \quad \dot{u}(x,0) = \gamma(x), \qquad x \in [a,b]. \end{cases} \tag{4.2.11}$$

Similarly, the linear problem (4.2.10) can be solved exactly in phase space and the associated evolution operator is given by

$$\begin{pmatrix} u(\cdot,t) \\ \dot{u}(\cdot,t) \end{pmatrix} = \chi_T^t \begin{pmatrix} \phi \\ \gamma \end{pmatrix} := \begin{pmatrix} \cos(t\langle\nabla\rangle)\phi + \langle\nabla\rangle^{-1}\sin(t\langle\nabla\rangle)\gamma \\ -\langle\nabla\rangle\sin(t\langle\nabla\rangle)\phi + \cos(t\langle\nabla\rangle)\gamma \end{pmatrix}, \quad t \geq 0. \tag{4.2.12}$$

From (4.2.11), we obtain immediately that $u(x,t)$ is invariant in time for any fixed $x \in [a,b]$, i.e.,

$$u(x,t) \equiv u(x,0) = \phi(x), \qquad x \in [a,b]. \tag{4.2.13}$$

Plugging (4.2.13) into (4.2.11), we get

$$\begin{cases} \partial_t u(x,t) = 0, \\ \partial_t \dot{u}(x,t) + \varepsilon^2 u^3(x,0) = 0, \quad x \in [a,b], \quad t > 0, \\ u(x,0) = \phi(x), \quad \dot{u}(x,0) = \gamma(x), \quad x \in [a,b], \quad t \geq 0. \end{cases} \tag{4.2.14}$$

Thus (4.2.14) (and (4.2.11)) can be integrated exactly in time as:

$$\begin{pmatrix} u(\cdot,t) \\ \dot{u}(\cdot,t) \end{pmatrix} = \chi_V^t \begin{pmatrix} \phi \\ \gamma \end{pmatrix} := \begin{pmatrix} \phi \\ \gamma - \varepsilon^2 t \phi^3 \end{pmatrix}, \quad t \geq 0. \tag{4.2.15}$$

Let $u^{[n]} := u^{[n]}(x)$ and $\dot{u}^{[n]} := \dot{u}^{[n]}(x)$ be the approximations of $u(x,t_n)$ and $\dot{u}(x,t) = \partial_t u(x,t_n)$ ($n = 0,1,2,\ldots$), respectively, which are the solutions of the NKGE (4.1.4) (and (2.1.1)). Then a second-order semi-discretization of the NKGE (4.1.4) (and (2.1.1)) via the second-order Strang-splitting [47] can be given as:

$$\begin{pmatrix} u^{[n+1]} \\ \dot{u}^{[n+1]} \end{pmatrix} = \mathcal{S}_\tau \begin{pmatrix} u^{[n]} \\ \dot{u}^{[n]} \end{pmatrix} = \chi_T^{\tau/2} \circ \chi_V^{\tau} \circ \chi_T^{\tau/2} \begin{pmatrix} u^{[n]} \\ \dot{u}^{[n]} \end{pmatrix}, \quad n = 0,1,\ldots, \tag{4.2.16}$$

with $u^{[0]} = u_0$ and $\dot{u}^{[0]} = u_1$. In fact, it is easy to verify that (4.2.1), (4.2.2), (4.2.3) and (4.2.6) are equivalent to (4.2.10), (4.2.11), (4.2.12) and (4.2.15), respectively. Thus it is straightforward to get that (4.2.8) is equivalent to (4.2.16), and (4.2.9) is the same as (4.2.16).

Remark 4.2.1. *Another second-order semi-discretization of the relativistic NLSE* (4.1.2) *can be given as*

$$\psi^{[n+1]} = \varphi_V^{\tau/2} \circ \varphi_T^{\tau} \circ \varphi_V^{\tau/2}(\psi^{[n]}), \qquad n = 0,1,2,\ldots\ , \tag{4.2.17}$$

which can immediately generate a semi-discretization of the NKGE (2.1.1) *via* (4.2.9). *Again, it is easy to check that this discretization is the same as the discretization of the*

NKGE (4.1.4) *(and* (2.1.1)*) by a similar second-order Strang-splitting as*

$$\begin{pmatrix} u^{[n+1]} \\ \dot{u}^{[n+1]} \end{pmatrix} = \chi_V^{\tau/2} \circ \chi_T^{\tau} \circ \chi_V^{\tau/2} \begin{pmatrix} u^{[n]} \\ \dot{u}^{[n]} \end{pmatrix}, \qquad n = 0, 1, 2, \ldots. \tag{4.2.18}$$

Furthermore, the above second-order time-splitting discretization of the NKGE (2.1.1) *is equivalent to an exponential wave integrator (EWI) via the trapezoidal quadrature (or Deuflhard-type exponential integrator) for discretizing the NKGE* (2.1.1) *directly (cf. [47, 165]).*

Remark 4.2.2. *It is straightforward to design higher order semi-discretization of the NKGE* (2.1.1) *via the relativistic NLSE* (4.1.2) *by adopting a higher order time-spitting method, e.g., the fourth-order partition Runge-Kutta time-splitting method [16, 144, 145, 146].*

4.3 The TSFP method

Let M be an even positive integer and define the spatial mesh size $h = (b-a)/M$, then the grid points are chosen as

$$x_j := a + jh, \quad j \in \mathcal{T}_M^0 = \{j \mid j = 0, 1, \ldots, M\}. \tag{4.3.1}$$

Let ψ_j^n be the numerical approximation of $\psi(x_j, t_n)$ for $j \in \mathcal{T}_M^0$ and $n \geq 0$ and denote $\psi^n = (\psi_0^n, \psi_1^n, \ldots, \psi_M^n)^T \in \mathbb{C}^{M+1}$ for $n = 0, 1, \ldots$. Then a time-splitting Fourier pseudospectral (TSFP) method for discretizing the relativistic NLSE (4.1.2) via (4.2.8) with a Fourier pseudospectral discretization in space can be given as

$$\begin{aligned}
\psi_j^{(n,1)} &= \sum_{l \in \mathcal{T}_M} e^{i\frac{\tau\zeta_l}{2}}\, \widetilde{(\psi^n)}_l\, e^{i\mu_l(x_j-a)}, \\
\psi_j^{(n,2)} &= \psi_j^{(n,1)} + \varepsilon^2 \tau\, F_j^n, \qquad F_j^n = i \sum_{l \in \mathcal{T}_M} \frac{1}{\zeta_l} (\widetilde{G(\psi^{(n,1)})})_l\, e^{i\mu_l(x_j-a)}, \\
\psi_j^{n+1} &= \sum_{l \in \mathcal{T}_M} e^{i\frac{\tau\zeta_l}{2}}\, (\widetilde{\psi^{(n,2)}})_l\, e^{i\mu_l(x_j-a)}, \quad j \in \mathcal{T}_M^0, \quad n = 0, 1, \ldots,
\end{aligned} \tag{4.3.2}$$

where $\zeta_l = \sqrt{1+\mu_l^2}$ for $l \in \mathcal{T}_M$, $\psi^{(n,k)} = (\psi_0^{(n,k)}, \psi_1^{(n,k)}, \ldots, \psi_M^{(n,k)})^T \in \mathbb{C}^{M+1}$ for $k = 1, 2$, $G(\psi^{(n,1)}) := (G(\psi_0^{(n,1)}), G(\psi_2^{(n,1)}), \ldots, G(\psi_M^{(n,1)}))^T \in \mathbb{R}^{M+1}$ and

$$\psi_j^0 = \phi(x_j) - i \sum_{l\in\mathcal{T}_M} \frac{\widetilde{\gamma}_l}{\sqrt{1+|\mu_l|^2}} e^{i\mu_l(x_j-a)}, \qquad j \in \mathcal{T}_M^0.$$

Let u_j^n and $\dot{u}_j^n$ be the approximations of $u(x_j,t_n)$ and $\dot{u}(x_j,t_n)$, respectively, for $j \in \mathcal{T}_M^0$ and $n \geq 0$, and denote $u^n = (u_0^n, u_1^n, \ldots, u_M^n)^T \in \mathbb{R}^{M+1}$ and $\dot{u}^n = (\dot{u}_0^n, \dot{u}_1^n, \ldots, \dot{u}_M^n)^T \in \mathbb{R}^{M+1}$ for $n = 0, 1, \ldots$. Combining (4.3.2) and (4.2.9), we can obtain a full-discretization of the NKGE (2.1.1) by the TSFP method as

$$\begin{aligned} u_j^{n+1} &= \frac{1}{2}\left(\psi_j^{n+1} + \overline{\psi_j^{n+1}}\right), \\ \dot{u}_j^{n+1} &= \frac{i}{2}\sum_{l\in\mathcal{T}_M} \zeta_l \left[\widetilde{(\psi^{n+1})}_l - \widetilde{(\overline{\psi^{n+1}})}_l\right] e^{i\mu_l(x_j-a)}, \end{aligned} \qquad j \in \mathcal{T}_M^0, \quad n \geq 0, \tag{4.3.3}$$

with

$$u_j^0 = \phi(x_j), \qquad \dot{u}_j^0 = \gamma(x_j), \qquad j \in \mathcal{T}_M^0.$$

Specifically, plugging (4.3.2) into (4.3.3) or discretizing (4.2.16) directly in space by the Fourier pseudospectral method, we get a full-discretization of the NKGE (2.1.1) by the TSFP method (in explicit formulation in the original variable u) as

$$\begin{aligned} u_j^{(n,1)} &= \mathcal{L}_u\left(\frac{\tau}{2}, u^n, \dot{u}^n\right)_j, & \dot{u}_j^{(n,1)} &= \mathcal{L}_{\dot{u}}\left(\frac{\tau}{2}, u^n, \dot{u}^n\right)_j, \\ u_j^{(n,2)} &= u_j^{(n,1)}, & \dot{u}_j^{(n,2)} &= \dot{u}_j^{(n,1)} - \tau\varepsilon^2\left(u_j^{(n,1)}\right)^3, \\ u_j^{n+1} &= \mathcal{L}_u\left(\frac{\tau}{2}, u^{(n,2)}, \dot{u}^{(n,2)}\right)_j, & \dot{u}_j^{n+1} &= \mathcal{L}_{\dot{u}}\left(\frac{\tau}{2}, u^{(n,2)}, \dot{u}^{(n,2)}\right)_j, \end{aligned} \tag{4.3.4}$$

where

$$\begin{aligned} \mathcal{L}_u(\tau, u, \dot{u})_j &= \sum_{l\in\mathcal{T}_M}\left[\cos(\tau\zeta_l)\widetilde{u}_l + \zeta_l^{-1}\sin(\tau\zeta_l)\widetilde{\dot{u}}_l\right] e^{i\mu_l(x_j-a)}, \\ \mathcal{L}_{\dot{u}}(\tau, u, \dot{u})_j &= \sum_{l\in\mathcal{T}_M}\left[-\zeta_l\sin(\tau\zeta_l)\widetilde{u}_l + \cos(\tau\zeta_l)\widetilde{\dot{u}}_l\right] e^{i\mu_l(x_j-a)}, \end{aligned} \qquad j \in \mathcal{T}_M^0. \tag{4.3.5}$$

The TSFP method (4.3.4) (or (4.3.3) with (4.3.2)) for the NKGE (2.1.1) is explicit, time symmetric and easy to be extended to higher dimensions. The memory cost of the TSFP is $O(M)$ and the computational cost per time step is $O(M\ln M)$. In addition, the total cost for the long-time dynamics up to the time $T_\varepsilon = T_0/\varepsilon^\beta$ $(0 \leq \beta \leq 2)$ with $T_0 > 0$ fixed is $O\left(\frac{M T_\varepsilon \ln M}{\tau}\right) = O\left(\frac{MT_0 \ln M}{\tau\varepsilon^\beta}\right)$.

4.4 Error estimates for TSFP

In this section, we establish error bounds of the TSFP method (4.3.3) via (4.3.2) (or equivalently (4.3.4)) for the NKGE (2.1.1) up to the time at $O(\varepsilon^{-2})$, which are uniformly valid for $0 < \varepsilon \leq 1$.

4.4.1 Main results

Motivated by the discussions in [43, 51, 118] and references therein, we make the following assumptions on the exact solution $u := u(x,t)$ of the NKGE (2.1.1) up to the time at $T_\varepsilon = T_0/\varepsilon^\beta$ with $\beta \in [0,2]$ and $T_0 > 0$ fixed:

$$(F) \qquad \begin{aligned} &u \in L^\infty\Big([0,T_\varepsilon]; H_{\rm p}^{m+1}\Big), && \partial_t u \in L^\infty\Big([0,T_\varepsilon]; H_{\rm p}^{m}\Big), \\ &\|u\|_{L^\infty\left([0,T_\varepsilon]; H_{\rm p}^{m+1}\right)} \lesssim 1, && \|\partial_t u\|_{L^\infty\left([0,T_\varepsilon]; H_{\rm p}^{m}\right)} \lesssim 1, \end{aligned}$$

with $m \geq 1$. Then we can establish the following error bounds of the TSFP method.

Theorem 4.4.1. *Let u^n be the numerical approximation obtained from the TSFP* (4.3.2)-(4.3.3) *(or equivalently* (4.3.4)*). Under the assumption (F), there exist $h_0 > 0$ and $\tau_0 > 0$ sufficiently small and independent of ε such that, for any $0 < \varepsilon \leq 1$, when $0 < h \leq h_0$ and $0 < \tau \leq \tau_0$, we have the error estimates for $s \in (1/2, m]$*

$$\|u(\cdot,t_n) - I_M(u^n)\|_s + \|\partial_t u(\cdot,t_n) - I_M(\dot{u}^n)\|_{s-1} \lesssim h^{1+m-s} + \varepsilon^{2-\beta}\tau^2, \quad 0 \leq n \leq \frac{T_0/\varepsilon^\beta}{\tau}. \tag{4.4.1}$$

Furthermore, there exists a constant $\overline{M} > 0$ which depends on T_0, $\|\psi_0\|_{m+1}$ and $\|\psi\|_{L^\infty([0,T_\varepsilon];H_p^m)}$ such that when $0 < h \leq h_0$ and $0 < \tau \leq \tau_0$, the numerical solution satisfies

$$\|I_M(u^n)\|_{m+1} + \|I_M(\dot{u}^n)\|_m \leq \overline{M}, \quad 0 \leq n \leq \frac{T_0/\varepsilon^\beta}{\tau}. \tag{4.4.2}$$

4.4.2 Preliminary estimates

In this subsection, we prepare some results for proving the main theorem. Denote

$$F_t : \ \phi \mapsto e^{-it\langle\nabla\rangle} F\Big(e^{it\langle\nabla\rangle}\phi\Big), \quad t \in \mathbb{R},$$

where F is defined by (4.2.7), then we have the following proposition on the properties of F_t.

Proposition 4.4.1. *(i) Let $s > 1/2$, then for any $t \in \mathbb{R}$, the function $F_t : H^s(\Omega) \to H^{s+1}(\Omega)$ is C^∞ and satisfies*

$$\begin{aligned} &\|F_t(\phi)\|_{s+1} \le C\|\phi\|_s^3, \quad \|F_t'(\phi)(\eta)\|_{s+1} \le C\|\phi\|_s^2\,\|\eta\|_s, \\ &\|F_t''(\phi)(\eta,\zeta)\|_{s+1} \le C\|\phi\|_s\,\|\eta\|_s\,\|\zeta\|_s. \end{aligned} \tag{4.4.3}$$

(ii) If $s \ge 1$, then the derivatives with respect to t satisfy

$$\|\partial_t F_t(\phi)\|_s \le C\|\phi\|_s^3, \quad \left\|\partial_t^2 F_t(\phi)\right\|_s \le C\|\phi\|_{s+1}^3, \quad \|\partial_t F_t'(\phi)(\eta)\|_s \le C\|\phi\|_s^2\|\eta\|_s. \tag{4.4.4}$$

(iii) Assume $s > 1/2$, $\phi, \eta \in B_R^s := \{v \in H^s(\Omega), \|v\|_s \le R\}$, then there exists a constant $L > 0$ depending on R such that for all $t \in \mathbb{R}$ and $\sigma \in [0, s]$, the Lipschitz estimate is valid:

$$\|G(\phi) - G(\eta)\|_\sigma \le L\|\phi - \eta\|_\sigma, \quad \|F_t(\phi) - F_t(\eta)\|_{\sigma+1} \le L\|\phi - \eta\|_\sigma. \tag{4.4.5}$$

Proof. Firstly, we recall the inequality which was established in [34]:

$$\|vw\|_\sigma \le C\|v\|_\sigma\,\|w\|_s, \quad v \in H^\sigma(\Omega), \quad w \in H^s(\Omega), \tag{4.4.6}$$

for $s > 1/2$ and $\sigma \in [0, s]$. Hence for $\phi \in H^s(\Omega)$, one has

$$\begin{aligned} \|F_t(\phi)\|_{s+1} &= \left\|F\left(e^{it\langle\nabla\rangle}\phi\right)\right\|_{s+1} = \left\|f\left(\frac{1}{2}\left(e^{it\langle\nabla\rangle}\phi + e^{-it\langle\nabla\rangle}\overline{\phi}\right)\right)\right\|_s \\ &\le C\left\|e^{it\langle\nabla\rangle}\phi + e^{-it\langle\nabla\rangle}\overline{\phi}\right\|_s^3 \le C\|\phi\|_s^3. \end{aligned}$$

Noticing that $f(v) = v^3$, a direct calculation gives

$$F'(\phi)(\eta) = \frac{3i}{8}\langle\nabla\rangle^{-1}(\phi + \overline{\phi})^2(\eta + \overline{\eta}), \tag{4.4.7}$$

which implies that

$$\|F'(\phi)(\eta)\|_{s+1} = \frac{3}{8}\left\|(\phi + \overline{\phi})^2(\eta + \overline{\eta})\right\|_s \le C\|\phi\|_s^2\|\eta\|_s. \tag{4.4.8}$$

Note that

$$F_t'(\phi)(\eta) = e^{-it\langle\nabla\rangle}F'\left(e^{it\langle\nabla\rangle}\phi\right)\left(e^{it\langle\nabla\rangle}\eta\right),$$

which immediately yields the second inequality in (4.4.3). The second derivative of F takes the form

$$F''(\phi)(\eta,\zeta) = \frac{3i}{4}\langle\nabla\rangle^{-1}(\phi+\overline{\phi})(\eta+\overline{\eta})(\zeta+\overline{\zeta}),$$

which leads to that

$$\|F''(\phi)(\eta,\zeta)\|_{s+1} = \frac{3}{4}\left\|(\phi+\overline{\phi})(\eta+\overline{\eta})(\zeta+\overline{\zeta})\right\|_s \le C\|\phi\|_s\|\eta\|_s\|\zeta\|_s.$$

Thus the last inequality in (4.4.3) can be obtained by recalling

$$F_t''(\phi)(\eta,\zeta) = e^{-it\langle\nabla\rangle}F''\left(e^{it\langle\nabla\rangle}\phi\right)\left(e^{it\langle\nabla\rangle}\eta, e^{it\langle\nabla\rangle}\zeta\right).$$

The first derivative of F_t with respect to t reads as

$$\partial_t F_t(\phi) = -i\langle\nabla\rangle F_t(\phi) + e^{-it\langle\nabla\rangle}F'(\mu)(i\langle\nabla\rangle\mu), \quad \mu = e^{it\langle\nabla\rangle}\phi.$$

Applying (4.4.3), (4.4.6) and (4.4.7), we obtain

$$\begin{aligned}
\|\partial_t F_t(\phi)\|_s &\le \|F_t(\phi)\|_{s+1} + \|F'(\mu)(i\langle\nabla\rangle\mu)\|_s \\
&\le C\|\phi\|_s^3 + C\|(\mu+\overline{\mu})^2(\langle\nabla\rangle\mu - \langle\nabla\rangle\overline{\mu})\|_{s-1} \\
&\le C\|\phi\|_s^3 + C\|(\mu+\overline{\mu})^2\|_s\|\langle\nabla\rangle(\mu-\overline{\mu})\|_{s-1} \\
&\le C\|\phi\|_s^3 + C\|\mu+\overline{\mu}\|_s^2\|\mu-\overline{\mu}\|_s \\
&\le C\|\phi\|_s^3.
\end{aligned}$$

Further computations give that

$$\begin{aligned}
\partial_t^2 F_t(\phi) = &-\langle\nabla\rangle^2 F_t(\phi) - 2i\langle\nabla\rangle e^{-it\langle\nabla\rangle}F'(\mu)(i\langle\nabla\rangle\mu) + e^{-it\langle\nabla\rangle}F'(\mu)(-\langle\nabla\rangle^2\mu) \\
&+ e^{-it\langle\nabla\rangle}F''(\mu)(i\langle\nabla\rangle\mu, i\langle\nabla\rangle\mu),
\end{aligned}$$

which leads to that

$$\begin{aligned}
\|\partial_t^2 F_t(\phi)\|_s \le\ &\|F_t(\phi)\|_{s+2} + 2\|F'(\mu)(i\langle\nabla\rangle\mu)\|_{s+1} + \|F'(\mu)(-\langle\nabla\rangle^2\mu)\|_s \\
&+ \|F''(\mu)(i\langle\nabla\rangle\mu, i\langle\nabla\rangle\mu)\|_s \\
\le\ & C\|\phi\|_{s+1}^3 + C\|(\mu+\overline{\mu})^2\langle\nabla\rangle^2(\mu+\overline{\mu})\|_{s-1} + C\|(\mu+\overline{\mu})(\langle\nabla\rangle(\mu-\overline{\mu}))^2\|_{s-1} \\
\le\ & C\|\phi\|_{s+1}^3 + C\|\mu+\overline{\mu}\|_s^2\|\mu+\overline{\mu}\|_{s+1} + C\|\mu+\overline{\mu}\|_s\|\mu-\overline{\mu}\|_{s+1}^2
\end{aligned}$$

$$\leq C\|\phi\|_{s+1}^3.$$

For the last inequality of (4.4.4), note that

$$\partial_t F_t'(\phi)(\eta) = -i\langle\nabla\rangle F_t'(\phi)(\eta) + e^{-it\langle\nabla\rangle}F''(\mu)(\nu, i\langle\nabla\rangle\mu) + e^{-it\langle\nabla\rangle}F'(\mu)(i\langle\nabla\rangle\nu),$$

where $\nu = e^{it\langle\nabla\rangle}\eta$. Thus

$$\begin{aligned}
\|\partial_t F_t'(\phi)(\eta)\|_s &\leq \|F_t'(\phi)(\eta)\|_{s+1} + \|F''(\mu)(\nu, i\langle\nabla\rangle\mu)\|_s + \|F'(\mu)(i\langle\nabla\rangle\nu)\|_s \\
&\leq C\|\phi\|_s^2\|\eta\|_s + C\|(\mu+\overline{\mu})(\nu+\overline{\nu})\langle\nabla\rangle(\mu-\overline{\mu})\|_{s-1} + C\|\mu+\overline{\mu}\|_s^2\|\nu-\overline{\nu}\|_s \\
&\leq C\|\phi\|_s^2\|\eta\|_s + C\|\mu+\overline{\mu}\|_s\|\nu+\overline{\nu}\|_s\|\langle\nabla\rangle\mu - \langle\nabla\rangle\overline{\mu}\|_{s-1} \\
&\leq C\|\phi\|_s^2\|\eta\|_s,
\end{aligned}$$

which completes the proof for (4.4.4).

For the Lipschitz estimate (4.4.5), a straightforward calculation shows that

$$\begin{aligned}
\|G(\phi) - G(\eta)\|_\sigma &= \left\| f\Big(\frac{1}{2}(\phi+\overline{\phi})\Big) - f\Big(\frac{1}{2}(\eta+\overline{\eta})\Big)\right\|_\sigma \\
&= \frac{1}{8}\left\|\left[(\phi+\overline{\phi})^2 + (\phi+\overline{\phi})(\eta+\overline{\eta}) + (\eta+\overline{\eta})^2\right](\phi-\eta+\overline{\phi}-\overline{\eta})\right\|_\sigma \\
&\leq C\left\|(\phi+\overline{\phi})^2 + (\phi+\overline{\phi})(\eta+\overline{\eta}) + (\eta+\overline{\eta})^2\right\|_s\left\|\phi-\eta+\overline{\phi}-\overline{\eta}\right\|_\sigma \\
&\leq C\left(\left\|\phi+\overline{\phi}\right\|_s^2 + \|\eta+\overline{\eta}\|_s^2\right)\|\phi-\eta\|_\sigma \\
&\leq CR^2\|\phi-\eta\|_\sigma.
\end{aligned}$$

Noticing that

$$\begin{aligned}
\|F_t(\phi) - F_t(\eta)\|_{\sigma+1} &= \left\|F(e^{it\langle\nabla\rangle}\phi) - F(e^{it\langle\nabla\rangle}\eta)\right\|_{\sigma+1} = \left\|G(e^{it\langle\nabla\rangle}\phi) - G(e^{it\langle\nabla\rangle}\eta)\right\|_\sigma \\
&\leq CR^2\|\phi-\eta\|_\sigma,
\end{aligned}$$

the proof is completed. □

Concerning on the flow $\mathcal{S}_\tau$ in (4.2.8), we have the stability estimate as follows.

Lemma 4.4.1. *Assume $\phi_0, \eta_0 \in B_R^s$ with $s > 1/2$, then for any $\tau > 0$, we have*

$$\|\mathcal{S}_\tau(\phi_0) - \mathcal{S}_\tau(\eta_0)\|_s \leq (1 + L\varepsilon^2\tau)\|\phi_0 - \eta_0\|_s,$$

where L depends on R.

Proof. Since the operator $e^{i\tau\langle\nabla\rangle}$ is an isometry, we only need to consider the operator associated with the nonlinear subproblem. By the definition and the Lipschitz estimate (4.4.5), we have

$$\begin{aligned}\|\varphi_V^\tau(\phi_0)-\varphi_V^\tau(\eta_0)\|_s &\le \|\phi_0-\eta_0\|_s+\varepsilon^2\tau\|F(\phi_0)-F(\eta_0)\|_s\\ &\le \|\phi_0-\eta_0\|_s+L\varepsilon^2\tau\|\phi_0-\eta_0\|_s\\ &\le (1+L\varepsilon^2\tau)\|\phi_0-\eta_0\|_s,\end{aligned}$$

which completes the proof. □

Lemma 4.4.2. *Denote the exact solution of* (4.1.2) *with initial data* ψ_0 *as* $\psi(t)=\mathcal{S}_{e,t}(\psi_0)$. *Assume* $\psi(t)\in H^{s+1}(s\ge 1)$, *then for* $0<\varepsilon\le 1$ *and* $0<\tau\le 1$, *the local error of the Strang splitting* (4.2.8) *is bounded by*

$$\|\mathcal{S}_\tau(\psi(t_n))-\mathcal{S}_{e,\tau}(\psi(t_n))\|_s\le M_0\varepsilon^2\tau^3,$$

where M_0 *depends on* $\|\psi\|_{L^\infty([0,T_\varepsilon];H^{s+1})}$.

Proof. For simplicity of notation, we denote $\psi_n=\psi(t_n)$. An application of the Duhamel's principle leads to the following representation of the exact solution

$$\psi(t_n+t)=e^{it\langle\nabla\rangle}\psi_n+\varepsilon^2 e^{it\langle\nabla\rangle}\int_0^t e^{-i\theta\langle\nabla\rangle}F\left(\psi(t_n+\theta)\right)d\theta. \tag{4.4.9}$$

Introducing $\eta_n(t):=e^{-i(t_n+t)\langle\nabla\rangle}\psi(t_n+t)$, we have

$$\eta_n(t)=\eta_n(0)+\varepsilon^2\int_0^t F_{t_n+\theta}(\eta_n(\theta))d\theta. \tag{4.4.10}$$

Applying the Taylor expansion

$$F_t(v_1+v_2)=F_t(v_1)+F_t'(v_1)(v_2)+\int_0^1(1-\theta)F_t''(v_1+\theta v_2)(v_2^2)d\theta,$$

we yield

$$\begin{aligned}\eta_n(\tau)&=\eta_n(0)+\varepsilon^2\int_0^\tau F_{t_n+\theta}\Big(\eta_n(0)+\varepsilon^2\int_0^\theta F_{t_n+\theta_1}\left(\eta_n(\theta_1)\right)d\theta_1\Big)d\theta\\ &=\eta_n(0)+\varepsilon^2\int_0^\tau F_{t_n+\theta}(\eta_n(0))d\theta+\varepsilon^4\int_0^\tau\int_0^\theta F_{t_n+\theta}'(\eta_n(0))F_{t_n+\theta_1}(\eta_n(\theta_1))d\theta_1 d\theta\end{aligned}$$

$$
\begin{aligned}
&+\varepsilon^6\int_0^\tau\int_0^1(1-\zeta)F''_{t_n+\theta}\left((1-\zeta)\eta_n(0)+\zeta\eta_n(\theta)\right)\left(\int_0^\theta F_{t_n+\theta_1}(\eta_n(\theta_1))d\theta_1\right)^2 d\zeta d\theta\\
&=\eta_n(0)+\varepsilon^2\int_0^\tau F_{t_n+\theta}(\eta_n(0))d\theta+\varepsilon^4\int_0^\tau\int_0^\theta F'_{t_n+\theta}(\eta_n(0))F_{t_n+\theta_1}(\eta_n(0))d\theta_1 d\theta\\
&+\varepsilon^6\int_0^\tau\int_0^1(1-\zeta)F''_{t_n+\theta}\left((1-\zeta)\eta_n(0)+\zeta\eta_n(\theta)\right)\left(\int_0^\theta F_{t_n+\theta_1}\left(\eta_n(\theta_1)\right)d\theta_1\right)^2 d\zeta d\theta\\
&+\varepsilon^6\int_0^\tau\int_0^\theta\int_0^1 F'_{t_n+\theta}(\eta_n(0))F'_{t_n+\theta_1}\left((1-\zeta)\eta_n(0)+\zeta\eta_n(\theta_1)\right)\\
&\qquad\qquad\left(\int_0^{\theta_1} F_{t_n+\theta_2}\left(\eta_n(\theta_2)\right)d\theta_2\right)d\zeta d\theta_1 d\theta.
\end{aligned}
$$

Twisting the variable back, we obtain

$$
\begin{aligned}
\mathcal{S}_{e,\tau}(\psi_n)&=e^{i(t_n+\tau)\langle\nabla\rangle}\eta_n(\tau)\\
&=e^{i\tau\langle\nabla\rangle}\psi_n+\varepsilon^2 e^{i\tau\langle\nabla\rangle}\int_0^\tau F_\theta\left(\psi_n\right)d\theta+\varepsilon^6 e^{i\tau\langle\nabla\rangle}E_3\\
&\quad+\varepsilon^4 e^{i\tau\langle\nabla\rangle}\int_0^\tau\int_0^\theta F'_\theta\left(\psi_n\right)F_{\theta_1}\left(\psi_n\right)d\theta_1 d\theta,
\end{aligned}
\tag{4.4.11}
$$

where $E_3=E_{3,1}+E_{3,2}$ with

$$
\begin{aligned}
E_{3,1}&=\int_0^\tau\int_0^1(1-\zeta)F''_\theta\Big((1-\zeta)\psi_n+\zeta e^{-i\theta\langle\nabla\rangle}\psi(t_n+\theta)\Big)\\
&\qquad\left(\int_0^\theta F_{\theta_1}\Big(e^{-i\theta_1\langle\nabla\rangle}\psi(t_n+\theta_1)\Big)d\theta_1\right)^2 d\zeta d\theta,\\
E_{3,2}&=\int_0^\tau\int_0^\theta\int_0^1 F'_\theta(\psi_n)F'_{\theta_1}\Big((1-\zeta)\psi_n+\zeta e^{-i\theta_1\langle\nabla\rangle}\psi(t_n+\theta_1)\Big)\\
&\qquad\left(\int_0^{\theta_1} F_{\theta_2}\Big(e^{-i\theta_2\langle\nabla\rangle}\psi(t_n+\theta_2)\Big)d\theta_2\right)d\zeta d\theta_1 d\theta.
\end{aligned}
$$

On the other hand, noticing (4.2.6), for the Strang splitting we get

$$
\mathcal{S}_\tau(\psi_n)=e^{i\tau\langle\nabla\rangle/2}\left[e^{i\tau\langle\nabla\rangle/2}\psi_n+\varepsilon^2\tau F\Big(e^{i\tau\langle\nabla\rangle/2}\psi_n\Big)\right]=e^{i\tau\langle\nabla\rangle}\left(\psi_n+\varepsilon^2\tau F_{\tau/2}(\psi_n)\right).
$$

Then the local truncation error can be written as

$$
\mathcal{S}_\tau(\psi_n)-\mathcal{S}_{e,\tau}(\psi_n)=\varepsilon^2 e^{i\tau\langle\nabla\rangle}r_1-\varepsilon^4 e^{i\tau\langle\nabla\rangle}r_2-\varepsilon^6 e^{i\tau\langle\nabla\rangle}E_3. \tag{4.4.12}
$$

where

$$
r_1=\tau F_{\tau/2}(\psi_n)-\int_0^\tau F_\theta(\psi_n)d\theta,\quad r_2=\int_0^\tau\int_0^\theta F'_\theta\left(\psi_n\right)F_{\theta_1}\left(\psi_n\right)d\theta_1 d\theta.
$$

Next we estimate each term individually. Express the quadrature error in the second-order Peano form,

$$r_1 = -\tau^3 \int_0^1 \kappa_2(\theta) \partial_\omega^2 F_\omega(\psi_n)|_{\omega=\theta\tau} d\theta, \quad \kappa_2(\theta) = \frac{1}{2} \min\{\theta^2, (1-\theta)^2\}.$$

Applying (4.4.4), we obtain

$$\|r_1\|_s \leq C\tau^3 \|\psi_n\|_{s+1}^3 \int_0^1 \kappa_2(\theta) d\theta \lesssim \tau^3. \tag{4.4.13}$$

Inserting the identities

$$F_{\theta_1}(\psi_n) = F_{\tau/2}(\psi_n) + \int_{\tau/2}^{\theta_1} \partial_\omega F_\omega(\psi_n) d\omega, \quad F'_\theta(\psi_n) = F'_{\tau/2}(\psi_n) + \int_{\tau/2}^{\theta} \partial_\omega F'_\omega(\psi_n) d\omega$$

into the double integral term, we get

$$\begin{aligned} r_2 = &\frac{1}{2}\tau^2 F'_{\tau/2}(\psi_n) F_{\tau/2}(\psi_n) + \int_0^\tau \int_0^\theta F'_{\tau/2}(\psi_n) \int_{\tau/2}^{\theta_1} \partial_\omega F_\omega(\psi_n) d\omega d\theta_1 d\theta \\ &+ \int_0^\tau \theta \int_{\tau/2}^{\theta} \partial_\omega F'_\omega(\psi_n) F_{\tau/2}(\psi_n) d\omega d\theta \\ &+ \int_0^\tau \int_0^\theta \int_{\tau/2}^{\theta} \int_{\tau/2}^{\theta_1} \partial_\omega F'_\omega(\psi_n) \partial_{\omega_1} F_{\omega_1}(\psi_n) d\omega_1 d\omega d\theta_1 d\theta. \end{aligned}$$

By definition, we have

$$F'_{\tau/2}(\psi_n) F_{\tau/2}(\psi_n) = e^{-i\frac{\tau}{2}\langle\nabla\rangle} F'(e^{i\frac{\tau}{2}\langle\nabla\rangle}\psi_n)\Big(F(e^{i\frac{\tau}{2}\langle\nabla\rangle}\psi_n)\Big) = 0,$$

by recalling (4.4.7) and the fact that $F(\cdot)$ is purely imaginary. Applying (4.4.3) and (4.4.4), we obtain

$$\begin{aligned} \|r_2\|_s \leq &\, C\tau^3 \|\psi_n\|_s^2 \sup_{0\leq\omega\leq\tau} \|\partial_\omega F_\omega(\psi_n)\|_s + C\tau^3 \|\psi_n\|_s^2 \left\|F_{\tau/2}(\psi_n)\right\|_s \\ &+ C\tau^4 \|\psi_n\|_s^2 \sup_{0\leq\omega\leq\tau} \|\partial_\omega F_\omega(\psi_n)\|_s \\ \leq &\, C\tau^3 \|\psi_n\|_s^5 \lesssim \tau^3. \end{aligned} \tag{4.4.14}$$

Using (4.4.3), we derive

$$\begin{aligned} \|E_3\|_s \leq &\, \|E_{3,1}\|_s + \|E_{3,2}\|_s \\ \leq &\, C\tau^3 \sup_{0\leq\theta\leq\tau} \|\psi(t_n+\theta)\|_s \sup_{0\leq\theta\leq\tau} \left\|F_\theta\Big(e^{-i\theta\langle\nabla\rangle}\psi(t_n+\theta)\Big)\right\|_s^2 \\ &+ C\tau^3 \|\psi_n\|_s^2 \sup_{0\leq\theta\leq\tau} \|\psi(t_n+\theta)\|_s^2 \sup_{0\leq\theta\leq\tau} \left\|F_\theta\Big(e^{-i\theta\langle\nabla\rangle}\psi(t_n+\theta)\Big)\right\|_s \\ \leq &\, C\tau^3 \sup_{0\leq\theta\leq\tau} \|\psi(t_n+\theta)\|_s^7 \lesssim \tau^3. \end{aligned} \tag{4.4.15}$$

Combining (4.4.12)-(4.4.15), we arrive at the conclusion and the proof is complete. □

4.4.3 Proof for TSFP

Proof. Similar to the proof of the TSFP method for the Dirac equation [7], the proof will be divided into two parts: (I) to prove the convergence of the semi-discretization, and (II) to complete the error analysis by comparing the semi-discretization (4.2.8) and the full discretization (4.3.2).

Part I (Convergence of the semi-discretization) Firstly, we observe that the assumption (F) is equivalent to the regularity of $\psi(x,t)$ as

$$\psi \in L^\infty\left([0,T_\varepsilon]; H_{\mathrm{p}}^{m+1}\right), \quad \|\psi\|_{L^\infty\left([0,T_\varepsilon];H_{\mathrm{p}}^{m+1}\right)} \lesssim 1.$$

Now, we give a global error on the Strang splitting (4.2.8): there exists $\tau_0 > 0$ independent of ε such that when $\tau \le \tau_0$, the error of the Strang splitting satisfies

$$\|\psi^{[n]} - \psi(\cdot,t_n)\|_m \le M_1\tau^2\varepsilon^{2-\beta}, \quad \|\psi^{[n]}\|_m \le R+1, \quad 0 \le n \le \frac{T_0/\varepsilon^\beta}{\tau}, \tag{4.4.16}$$

where $R := \|\psi\|_{L^\infty([0,T_\varepsilon];H_{\mathrm{p}}^m)}$ and M_1 depends on T_0, R and $\|\psi\|_{L^\infty([0,T_\varepsilon];H_{\mathrm{p}}^{m+1})}$. Furthermore, for the regularity of $\psi^{[n]}$, we have $\psi^{[n]} \in H_{\mathrm{p}}^{m+1}$ when $\tau \le \tau_0$ with

$$\|\psi^{[n]}\|_{m+1} \le M_2, \quad 0 \le n \le \frac{T_0/\varepsilon^\beta}{\tau}, \tag{4.4.17}$$

where M_2 depends on T_0, R and $\|\psi_0\|_{m+1}$.

We apply a standard induction argument for proving (4.4.16). Firstly, it is obvious for $n=0$ since $\psi^{[0]} = \psi_0 \in B_R^m$. Assume $\psi^{[k]} \in B_{R+1}^m$ for $0 \le k \le n < \frac{T_0/\varepsilon^\beta}{\tau}$. Denote $e^{[k]} = \psi^{[k]} - \psi(\cdot,t_k)$. By definition,

$$e^{[k+1]} = \mathcal{S}_\tau(\psi^{[k]}) - \mathcal{S}_\tau(\psi(t_k)) + \mathcal{S}_\tau(\psi(t_k)) - \mathcal{S}_{e,\tau}(\psi(t_k)).$$

Using Lemmas 4.4.1 and 4.4.2, we get when $\tau \le 1$,

$$\left\|e^{[k+1]}\right\|_m - \|e^{[k]}\|_m \le L\varepsilon^2\tau\left\|e^{[k]}\right\|_m + M_0\varepsilon^2\tau^3,$$

where L and M_0 depend on R and $\left\|\psi\right\|_{L^\infty([0,T_\varepsilon];H_{\mathrm{p}}^{m+1})}$, respectively, as claimed in Lemmas 4.4.1 and 4.4.2. Summing the above inequality for $k = 0,\dots,n$, one gets

$$\left\|e^{[n+1]}\right\|_m \le \left\|e^{[0]}\right\|_m + L\varepsilon^2\tau\sum_{k=0}^{n}\left\|e^{[k]}\right\|_m + M_0\varepsilon^2\tau^3(n+1)$$

$$\leq M_0 T_0 \varepsilon^{2-\beta}\tau^2 + L\varepsilon^2\tau \sum_{k=0}^{n} \left\| e^{[k]} \right\|_m.$$

Applying the Gronwall's inequality, we derive

$$\left\| e^{[n+1]} \right\|_m \leq M_0 T_0 e^{LT_0} \varepsilon^{2-\beta}\tau^2, \quad 0 \leq n < \frac{T_0/\varepsilon^\beta}{\tau}.$$

Then the triangle inequality yields that

$$\left\| \psi^{[n+1]} \right\|_m \leq \left\| \psi(\cdot, t_{n+1}) \right\|_m + 1, \quad 0 \leq n < \frac{T_0/\varepsilon^\beta}{\tau},$$

when $0 < \tau \leq \tau_0$ with $\tau_0 := \min\{1, (M_0T_0)^{-1/2} e^{-LT_0/2} \varepsilon^{\beta/2-1}\}$ and the induction for (4.4.16) is completed. For the last inequality (4.4.17), recalling (4.2.6) and (4.4.3), we have

$$\begin{aligned}
\left\| \psi^{[n+1]} \right\|_{m+1} &= \left\| \varphi_V^\tau (e^{i\tau/2\langle\nabla\rangle} \psi^{[n]}) \right\|_{m+1} \\
&\leq \left\| e^{i\tau/2\langle\nabla\rangle} \psi^{[n]} \right\|_{m+1} + \varepsilon^2\tau \left\| F\left(e^{i\tau/2\langle\nabla\rangle} \psi^{[n]}\right) \right\|_{m+1} \\
&\leq \left\| \psi^{[n]} \right\|_{m+1} + C\varepsilon^2\tau \left\| \psi^{[n]} \right\|_m^3 \\
&\leq \left\| \psi^{[n]} \right\|_{m+1} + C\varepsilon^2\tau (R+1)^3 \\
&\leq \left\| \psi^{[0]} \right\|_{m+1} + C(n+1)\varepsilon^2\tau (R+1)^3 \\
&\leq \left\| \psi_0 \right\|_{m+1} + CT_0 (R+1)^3,
\end{aligned}$$

and (4.4.17) is established.

Part II (Convergence of the full discretization) For $0 \leq n \leq \frac{T_0/\varepsilon^\beta}{\tau}$, we rewrite the error as

$$\psi(\cdot, t_n) - I_M(\psi^n) = \psi(\cdot, t_n) - \psi^{[n]} + \psi^{[n]} - P_M(\psi^{[n]}) + P_M(\psi^{[n]}) - I_M(\psi^n). \quad (4.4.18)$$

For $0 \leq s \leq m$, the regularity result (4.4.17) implies that

$$\|\psi^{[n]} - P_M(\psi^{[n]})\|_s \leq CM_2 h^{1+m-s}, \quad (4.4.19)$$

and by (4.4.16),

$$\|\psi(\cdot, t_n) - \psi^{[n]}\|_s \leq \|\psi(\cdot, t_n) - \psi^{[n]}\|_m \leq M_1 \tau^2 \varepsilon^{2-\beta}. \quad (4.4.20)$$

Thus, it remains to establish the error bound for the error

$$e^n := P_M(\psi^{[n]}) - I_M(\psi^n), \quad 0 \le n \le \frac{T_0/\varepsilon^\beta}{\tau}.$$

Now, we'll use an induction to show that when h is sufficiently small, we have

$$\|e^n\|_l \le M_3 h^{1+m-l}, \quad l \in (1/2, m+1]; \quad \|I_M(\psi^n)\|_m \le C(1+R)+1, \tag{4.4.21}$$

where M_3 depends on T_0, R and $\|\psi_0\|_{m+1}$.

For $n = 0$, (4.4.21) is obvious by using the projection and interpolation errors [133]:

$$\begin{aligned}
&\|e^0\|_l = \|P_M(\psi_0) - I_M(\psi_0)\|_l \le C h^{1+m-l}\|\psi_0\|_{m+1},\\
&\|I_M(\psi^0)\|_m \le \|\psi_0\|_m + \|I_M(\psi_0) - \psi_0\|_m \le R + Ch\|\psi_0\|_{m+1} \le 1+R,
\end{aligned}$$

when h is small enough. For $n \ge 1$, assume (4.4.21) holds for $0 \le k \le n < \frac{T_0/\varepsilon^\beta}{\tau}$. We rewrite (4.3.2) as

$$\begin{aligned}
&\psi^{(n,1)} = e^{i\tau\langle\nabla\rangle/2} I_M(\psi^n), \quad \psi^{(n,2)} = \psi^{(n,1)} + i\varepsilon^2\tau\langle\nabla\rangle^{-1} I_M(G(\psi^{(n,1)})),\\
&I_M(\psi^{n+1}) = e^{i\tau\langle\nabla\rangle/2} I_M(\psi^{(n,2)}).
\end{aligned}$$

Hence we get $\psi^{(n,1)}, \psi^{(n,2)} \in Y_M$. Similarly, (4.2.8) can be expressed as

$$\psi^{\langle n,1\rangle} = e^{i\tau\langle\nabla\rangle/2}\psi^{[n]}, \;\; \psi^{\langle n,2\rangle} = \psi^{\langle n,1\rangle} + i\varepsilon^2\tau\langle\nabla\rangle^{-1}G(\psi^{\langle n,1\rangle}), \;\; \psi^{[n+1]} = e^{i\tau\langle\nabla\rangle/2}\psi^{\langle n,2\rangle},$$

which implies that

$$\begin{aligned}
&P_M(\psi^{\langle n,1\rangle}) = e^{i\tau\langle\nabla\rangle/2} P_M(\psi^{[n]}),\\
&P_M(\psi^{\langle n,2\rangle}) = P_M(\psi^{\langle n,1\rangle}) + i\varepsilon^2\tau\langle\nabla\rangle^{-1} P_M(G(\psi^{\langle n,1\rangle})),\\
&P_M(\psi^{[n+1]}) = e^{i\tau\langle\nabla\rangle/2} P_M(\psi^{\langle n,2\rangle}).
\end{aligned}$$

Thus by definition, we get

$$\begin{aligned}
\|e^{n+1}\|_l &= \left\|P_M(\psi^{[n+1]}) - I_M(\psi^{n+1})\right\|_l = \left\|P_M(\psi^{\langle n,2\rangle}) - I_M(\psi^{(n,2)})\right\|_l\\
&\le \left\|P_M(\psi^{\langle n,1\rangle}) - I_M(\psi^{(n,1)})\right\|_l + \varepsilon^2\tau\left\|P_M(G(\psi^{\langle n,1\rangle})) - I_M(G(\psi^{(n,1)}))\right\|_{l-1}\\
&\le \|e^n\|_l + \varepsilon^2\tau\left\|P_M(G(\psi^{\langle n,1\rangle})) - I_M(G(\psi^{\langle n,1\rangle}))\right\|_l
\end{aligned}$$

$$
\begin{aligned}
&+ \varepsilon^2\tau\Big\|I_M(G(\psi^{\langle n,1\rangle})) - I_M(G(\psi^{(n,1)}))\Big\|_{\min\{l,m\}} \\
&\le \|e^n\|_l + C\varepsilon^2\tau h^{1+m-l}\Big\|G(\psi^{\langle n,1\rangle})\Big\|_{m+1} + C\varepsilon^2\tau\Big\|G(\psi^{\langle n,1\rangle}) - G(\psi^{(n,1)})\Big\|_{\min\{l,m\}} \\
&\le \|e^n\|_l + C\varepsilon^2\tau h^{1+m-l}\|\psi^{\langle n,1\rangle}\|_{m+1}^3 + CL\varepsilon^2\tau\|\psi^{\langle n,1\rangle} - \psi^{(n,1)}\|_l \\
&\le (1+CL\varepsilon^2\tau)\|e^n\|_l + CM_2^3\varepsilon^2\tau h^{1+m-l} + CL\varepsilon^2\tau\Big\|P_M(\psi^{[n]}) - \psi^{[n]}\Big\|_l \\
&\le (1+CL\varepsilon^2\tau)\|e^n\|_l + CM_2(L+M_2^2)\varepsilon^2\tau h^{1+m-l},
\end{aligned}
$$

where we have used the fact that $\psi^{[n]}, \psi^{\langle n,1\rangle}, G(\psi^{\langle n,1\rangle}) \in H^{m+1}$, (4.4.5) and L depends on $\|\psi^{\langle n,1\rangle}\|_m$ and $\|\psi^{(n,1)}\|_m$, or equivalently depends on R due to (4.4.16) and (4.4.21) by induction. Hence

$$
\begin{aligned}
\|e^{n+1}\|_l &\le e^{CL\varepsilon^2\tau}\|e^n\|_l + CM_2(L+M_2^2)\varepsilon^2\tau h^{1+m-l} \\
&\le e^{CL\varepsilon^2(n+1)\tau}\|e^0\|_l + CM_2(L+M_2^2)\varepsilon^2\tau h^{1+m-l}\sum_{k=0}^{n} e^{kCL\varepsilon^2\tau} \\
&\le Ce^{CLT_0}h^{1+m-l}\|\psi_0\|_{m+1} + \frac{LM_2+M_2^3}{L}e^{CLT_0}h^{1+m-l} \\
&\le M_3 h^{1+m-l},
\end{aligned}
$$

where M_3 depends on T_0, R and $\|\psi_0\|_{m+1}$. The second inequality in (4.4.21) can be derived by using the triangle inequality and (4.4.16):

$$
\|I_M(\psi^n)\|_m \le \|P_M(\psi^{[n]})\|_m + \|e^n\|_m \le C\|\psi^{[n]}\|_m + M_3 h \le C(1+R)+1,
$$

when $h \le h_0 := 1/M_3$. Furthermore, it follows from (4.4.21) that for any $0 \le n \le \frac{T_0/\varepsilon^\beta}{\tau}$,

$$
\|I_M(\psi^n)\|_{m+1} \le \|P_M(\psi^{[n]})\|_{m+1} + \|e^n\|_{m+1} \le C\|\psi^{[n]}\|_{m+1} + M_3 \le CM_2 + M_3,
$$

which immediately gives (4.4.2) by recalling (4.3.3).

Combining (4.4.18)-(4.4.21), we derive for $s \in (1/2, m]$,

$$
\|\psi(\cdot,t_n) - I_M(\psi^n)\|_s \le M_1\tau^2\varepsilon^{2-\beta} + M_4 h^{1+m-s},
$$

where M_1 depends on T_0, R and $\|\psi\|_{L^\infty([0,T_\varepsilon];H_{\mathrm{p}}^{m+1})}$, and M_4 depends on T_0, R and $\|\psi_0\|_{m+1}$. Recalling (4.3.3), we obtain error bounds for u^n and $\dot{u}^n$ as

$$
\|u(\cdot,t_n) - I_M(u^n)\|_s = \frac{1}{2}\left\|\psi(\cdot,t_n) + \overline{\psi(\cdot,t_n)} - I_M(\psi^n) - I_M(\overline{\psi^n})\right\|_s
$$

$$
\begin{aligned}
&\leq \|\psi(\cdot,t_n)-I_M(\psi^n)\|_s \leq M_1\tau^2\varepsilon^{2-\beta}+M_4h^{1+m-s},\\
\|\dot{u}(\cdot,t_n)-I_M(\dot{u}^n)\|_{s-1} &= \frac{1}{2}\|\langle\nabla\rangle(\psi(\cdot,t_n)-\overline{\psi(\cdot,t_n)})-\langle\nabla\rangle(I_M(\psi^n)-I_M(\overline{\psi^n}))\|_{s-1}\\
&\leq \|\psi(\cdot,t_n)-I_M(\psi^n)\|_s \leq M_1\tau^2\varepsilon^{2-\beta}+M_4h^{1+m-s},
\end{aligned}
$$

which shows (4.4.1) and the proof for Theorem 4.4.1 is completed. □

Remark 4.4.1. *We remark here that the same error bounds can be established under the same assumption for the other Strang splitting*

$$
\psi^{[n+1]}=\mathcal{S}_\tau(\psi^{[n]})=\varphi_V^{\tau/2}\circ\varphi_T^{\tau}\circ\varphi_V^{\tau/2}(\psi^{[n]}),
$$

and the corresponding full discretization. Note that

$$
\begin{aligned}
\mathcal{S}_\tau(\psi_n) &= \varphi_V^{\tau/2}\Big[e^{i\tau\langle\nabla\rangle}\psi_n+\frac{1}{2}\varepsilon^2\tau e^{i\tau\langle\nabla\rangle}F(\psi_n)\Big]\\
&= e^{i\tau\langle\nabla\rangle}\psi_n+\frac{1}{2}\varepsilon^2\tau e^{i\tau\langle\nabla\rangle}F(\psi_n)+\frac{1}{2}\varepsilon^2\tau F\Big(e^{i\tau\langle\nabla\rangle}\psi_n+\frac{1}{2}\varepsilon^2\tau e^{i\tau\langle\nabla\rangle}F(\psi_n)\Big)\\
&= e^{i\tau\langle\nabla\rangle}\psi_n+\frac{1}{2}\varepsilon^2\tau e^{i\tau\langle\nabla\rangle}F(\psi_n)+\frac{1}{2}\varepsilon^2\tau F\Big(e^{i\tau\langle\nabla\rangle}\psi_n\Big)+E_2,
\end{aligned}
$$

where

$$
E_2=\frac{1}{4}\varepsilon^4\tau^2\int_0^1 F'\Big(e^{i\tau\langle\nabla\rangle}\psi_n+\frac{\theta}{2}\varepsilon^2\tau e^{i\tau\langle\nabla\rangle}F(\psi_n)\Big)\Big(e^{i\tau\langle\nabla\rangle}F(\psi_n)\Big)d\theta.
$$

Thus by (4.4.11)*, we get*

$$
\mathcal{S}_\tau(\psi_n)-\mathcal{S}_{e,\tau}(\psi_n)=\varepsilon^2e^{i\tau\langle\nabla\rangle}r_3+E_2-\varepsilon^4e^{i\tau\langle\nabla\rangle}r_2-\varepsilon^6e^{i\tau\langle\nabla\rangle}E_3, \tag{4.4.22}
$$

where

$$
r_3=\frac{\tau}{2}\left(F_0(\psi_n)+F_\tau(\psi_n)\right)-\int_0^\tau F_\theta(\psi_n)d\theta=\frac{\tau^3}{2}\int_0^1\theta(1-\theta)\partial_\omega^2F_\omega(\psi_n)|_{\omega=\theta\tau}d\theta\lesssim\tau^3.
$$

It remains to estimate E_2. By (4.4.7)*, we have*

$$
\begin{aligned}
&F'\Big(e^{i\tau\langle\nabla\rangle}\psi_n+\frac{\theta}{2}\varepsilon^2\tau e^{i\tau\langle\nabla\rangle}F(\psi_n)\Big)\Big(e^{i\tau\langle\nabla\rangle}F(\psi_n)\Big)\\
&\quad=\frac{3i}{8}\langle\nabla\rangle^{-1}\Big[e^{i\tau\langle\nabla\rangle}\Big(\psi_n+\frac{\theta}{2}\varepsilon^2\tau F(\psi_n)\Big)+e^{-i\tau\langle\nabla\rangle}\Big(\overline{\psi_n}-\frac{\theta}{2}\varepsilon^2\tau F(\psi_n)\Big)\Big]^2\\
&\qquad\qquad\Big(e^{i\tau\langle\nabla\rangle}F(\psi_n)-e^{-i\tau\langle\nabla\rangle}F(\psi_n)\Big)\\
&\quad=-3\langle\nabla\rangle^{-1}\Big[\mathrm{Re}\Big(e^{i\tau\langle\nabla\rangle}\Big(\psi_n+\frac{\theta}{2}\varepsilon^2\tau F(\psi_n)\Big)\Big)\Big]^2\sin(\tau\langle\nabla\rangle)F(\psi_n),
\end{aligned}
$$

which implies that

$$\begin{aligned}
&\left\|F'\Big(e^{i\tau\langle\nabla\rangle}\psi_n+\frac{\theta}{2}\varepsilon^2\tau e^{i\tau\langle\nabla\rangle}F(\psi_n)\Big)\Big(e^{i\tau\langle\nabla\rangle}F(\psi_n)\Big)\right\|_s\\
&\quad\leq C\left\|\psi_n+\frac{\theta}{2}\varepsilon^2\tau F(\psi_n)\right\|_s^2\ \left\|\sin(\tau\langle\nabla\rangle)F(\psi_n)\right\|_s\\
&\quad\leq C\tau\left(\|\psi_n\|_s+\varepsilon^2\tau\|F(\psi_n)\|_s\right)^2\|F(\psi_n)\|_{s+1}\\
&\quad\leq C\tau\left(\|\psi_n\|_s+C\varepsilon^2\tau\|\psi_n\|_s^3\right)^2\|\psi_n\|_s^3\lesssim\tau.
\end{aligned}$$

This suggests that $E_2\lesssim\varepsilon^4\tau^3$, which directly yields that

$$\mathcal{S}_\tau(\psi_n)-\mathcal{S}_{e,\tau}(\psi_n)\lesssim\varepsilon^2\tau^3.$$

Then the error estimates can be derived by similar and standard arguments.

4.5 Extensions to other spatial discretizaitons

In this section, we introduce the time-splitting finite difference (TS-FD)/time-splitting fourth-order compact finite difference (TS-4cFD) method which applies the finite difference/fourth-order compact finite difference discretization in space combined with the time-splitting integrator.

Similar to the exponential wave integrator, we just need to replace ζ_l in (4.3.2) by λ_l defined in (2.7.1) for the TS-FD method and ν_l defined in (3.4.4) for the TS-4cFD method.

Assume that the exact solution of the NKGE (2.1.1) up to the time $T_\varepsilon=T_0/\varepsilon^\beta$ satisfies

$$(G)\qquad \begin{aligned}
&u(x,t)\in L^\infty\left([0,T_\varepsilon];W_p^{6,\infty}\right),\quad \partial_t u(x,t)\in L^\infty\left([0,T_\varepsilon];L^\infty\right)\\
&\|u(x,t)\|_{L^\infty([0,T_\varepsilon];W^{6,\infty})}\lesssim 1,\quad \|\partial_t u(x,t)\|_{L^\infty([0,T_\varepsilon];L^\infty)}\lesssim 1,
\end{aligned}$$

then we have the following error estimates for the TS-FD and TS-4cFD methods:

Theorem 4.5.1. *Let u_j^n be the approximation obtained from the TS-FD, under the assumption (G), there exist constants $h_0>0$ and $\tau_0>0$ sufficiently small and independent of ε, such that for any $0<\varepsilon\leq 1$ and $0\leq\beta\leq 2$, when $0<h\leq h_0$, $0<\tau\leq\tau_0$,* *we have*

$$\|e^n\|_{l^2} \lesssim \frac{h^2}{\varepsilon^\beta} + \varepsilon^{2-\beta}\tau^2, \quad \|u^n\|_{l^\infty} \le 1 + M_1, \quad 0 \le n \le \frac{T_0/\varepsilon^{-\beta}}{\tau}, \tag{4.5.1}$$

where

$$e^n = (e_0^n, e_1^n, \cdots, e_M^n)^T, \quad \textit{with} \quad e_j^n = u(x_j, t_n) - u_j^n, \quad 0 \le j \le M, \quad n \ge 0.$$

Theorem 4.5.2. *Let u_j^n be the approximation obtained from the TS-4cFD, under the assumption (G), there exist constants $h_0 > 0$ and $\tau_0 > 0$ sufficiently small and independent of ε, such that for any $0 < \varepsilon \le 1$ and $0 \le \beta \le 2$, when $0 < h \le h_0$, $0 < \tau \le \tau_0$, we have*

$$\|e^n\|_{l^2} \lesssim \frac{h^4}{\varepsilon^\beta} + \varepsilon^{2-\beta}\tau^2, \quad \|u^n\|_{l^\infty} \le 1 + M_1, \quad 0 \le n \le \frac{T_0/\varepsilon^{\beta}}{\tau}. \tag{4.5.2}$$

Proof. Follow the analogous proof to Theorem 4.4.1 and we omit the details here for brevity. □

4.6 Comparisons of different spatial discretizations

In this section, we present the numerical results concerning spatial and temporal accuracy of the TSFP, TS-FD and TS-4cFD methods for the NKGE (2.1.1). In our numerical experiments, we choose the initial data

$$\phi(x) = \frac{3}{2}\sin(2x) \quad \text{and} \quad \gamma(x) = \frac{5}{1+\cos^2(x)}, \quad x \in (0, 2\pi). \tag{4.6.1}$$

The computation is carried out on an interval $[0, T_0/\varepsilon^\beta]$ with $0 \le \beta \le 2$. Here, we study the following three cases with respect to different β:

(i). Fixed time dynamics up to the time at $O(1)$, i.e., $\beta = 0$;

(ii). Intermediate long-time dynamics up to the time at $O(\varepsilon^{-1})$, i.e., $\beta = 1$;

(ii). Long-time dynamics up to the time at $O(\varepsilon^{-2})$, i.e., $\beta = 2$.

The 'exact' solution $u(x,t)$ is obtained numerically by using the TSFP (4.3.2)-(4.3.3) with a fine mesh size $h_e = \pi/64$ and a very small time step $\tau_e = 10^{-5}$. Denote $u^n_{h,\tau}$ as the numerical solution obtained by the TSFP (4.3.2)-(4.3.3) with mesh size h and time step τ at the time $t = t_n$. The errors are denoted as $e(x,t_n) = u(x,t_n) - I_M(u^n_{h,\tau})(x)$. In order to quantify the numerical errors, we measure the H^1 norm of $e(\cdot, t_n)$.

The errors are displayed at $T_0 = 1$ with different ε and β. For spatial error analysis, we fix the time step as $\tau = 10^{-5}$ such that the temporal errors can be neglected; for temporal error analysis, a very fine mesh size $h = \pi/64$ is chosen such that the spatial error can be ignored. Table 4.1 shows the spatial errors under different mesh size and Figures 4.1−4.3 depict the temporal errors for $\beta = 0$, $\beta = 1$ and $\beta = 2$, respectively.

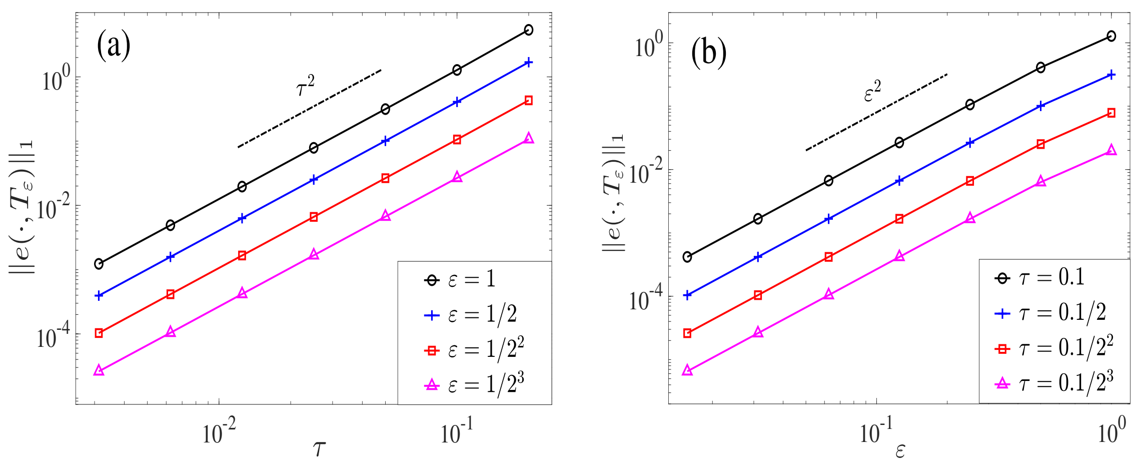

Figure 4.1: Temporal errors of the TSFP (4.3.2)-(4.3.3) for the NKGE (2.1.1) with $\beta = 0$.

From Table 4.1 and Figures 4.1-4.3, we can draw the following observations:

(i) The TSFP scheme converges uniformly for $0 < \varepsilon \le 1$ in space with exponential convergence rate.

(ii) For any fixed $\varepsilon = \varepsilon_0 > 0$, the TSFP method (4.3.2)-(4.3.3) is second-order accurate in time (cf. each line in Figures 4.1(a)−4.3(a)). When $\beta = 0$, the temporal error behaves like $O(\varepsilon^2\tau^2)$ (cf. Figure 4.1(b)), which agrees with the theoretical result in Theorem 4.4.1. Figure 4.2(b) and Figure 4.3(b) show that the temporal error is at $O(\varepsilon\tau^2)$ and $O(\tau^2)$ for $\beta = 1$ and $\beta = 2$, respectively, which is uniformly for $0 < \varepsilon \le 1$. Furthermore, Figures 4.2(b) − 4.3(b) also display a temporal error bound like $O(\varepsilon^2\tau^2)$

	$\|e(\cdot, T_\varepsilon)\|_1$	$h_0 = \pi/4$	$h_0/2$	$h_0/2^2$	$h_0/2^3$
$\beta = 0$	$\varepsilon_0 = 1$	1.12E-1	1.22E-3	5.03E-6	1.54E-12
	$\varepsilon_0/2$	8.99E-2	6.32E-4	2.05E-6	1.25E-12
	$\varepsilon_0/2^2$	9.04E-2	4.67E-4	1.95E-6	1.19E-12
	$\varepsilon_0/2^3$	8.85E-2	4.47E-4	1.93E-6	1.18E-12
	$\varepsilon_0/2^4$	8.82E-2	4.47E-4	1.93E-6	1.19E-12
	$\varepsilon_0/2^5$	8.81E-2	4.48E-4	1.93E-6	1.18E-12
$\beta = 1$	$\varepsilon_0 = 1$	1.12E-1	1.22E-3	5.03E-6	1.54E-12
	$\varepsilon_0/2$	2.14E-1	2.10E-3	1.58E-6	5.72E-13
	$\varepsilon_0/2^2$	1.08E-1	2.36E-3	7.09E-7	1.24E-12
	$\varepsilon_0/2^3$	4.47E-2	9.27E-4	7.72E-7	1.52E-13
	$\varepsilon_0/2^4$	1.14E-1	8.11E-4	7.13E-7	7.97E-13
	$\varepsilon_0/2^5$	7.29E-2	1.24E-3	9.83E-7	1.26E-12
$\beta = 2$	$\varepsilon_0 = 1$	1.12E-1	1.22E-3	5.03E-6	1.54E-12
	$\varepsilon_0/2$	5.22E-1	6.58E-3	5.81E-7	1.16E-12
	$\varepsilon_0/2^2$	5.79E-1	1.52E-3	1.82E-6	1.20E-12
	$\varepsilon_0/2^3$	5.82E-1	1.03E-3	6.05E-7	9.90E-13
	$\varepsilon_0/2^4$	9.17E-1	1.68E-3	6.69E-7	4.78E-12
	$\varepsilon_0/2^5$	7.67E-1	1.79E-3	3.52E-7	1.22E-11

Table 4.1: Spatial errors of the TSFP (4.3.2)-(4.3.3) for the NKGE (2.1.1) with initial data (4.6.1) for different β and ε.

when ε is small enough, which suggests that there may be a possibility for an improved error estimate for $\beta \in (0, 2]$.

Tables 4.2-4.3 and Figures 4.4-4.5 show the numerical results for the TS-FD and TS-4cFD methods and we can draw the following observations:

(i) In time, for any fixed $\varepsilon = \varepsilon_0 > 0$ or in the long-time regime ($\beta = 2$), the TS-FD and TS-4cFD methods are both uniformly second-order accurate (cf. Figures 4.4&4.5).

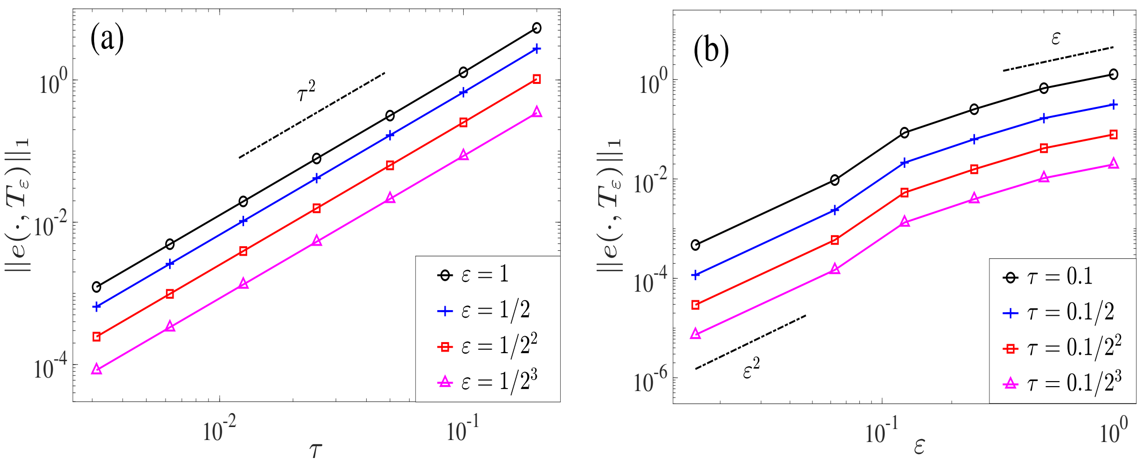

Figure 4.2: Temporal errors of the TSFP (4.3.2)-(4.3.3) for the NKGE (2.1.1) with $\beta = 1$.

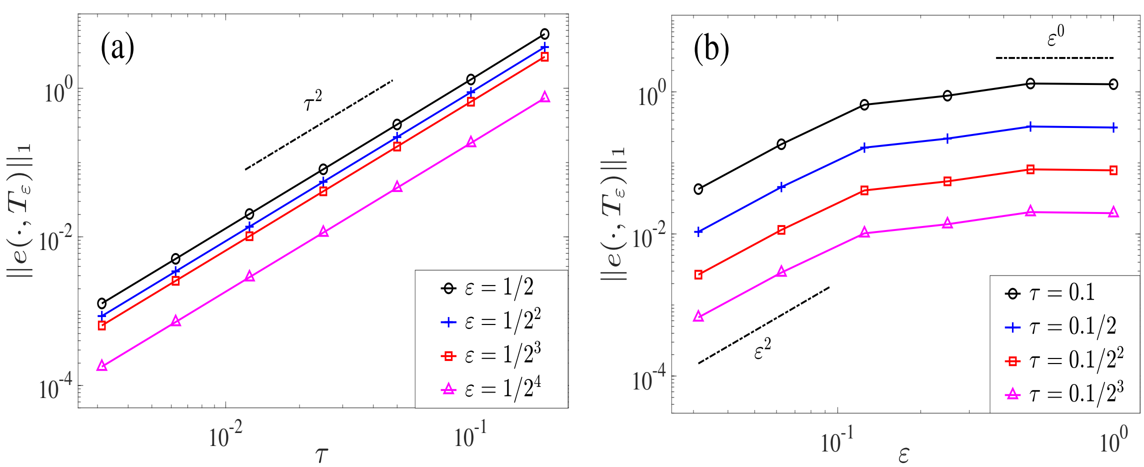

Figure 4.3: Temporal errors of the TSFP (4.3.2)-(4.3.3) for the NKGE (2.1.1) with $\beta = 2$.

In addition, Figures 4.4(b)&4.5(b) show the temporal error bound like $O(\varepsilon^2\tau^2)$ when ε is small enough, which means that the error estimates for the TS-FD and TS-4cFD methods may also be improved.

(ii) In space, for the long-time regime, i.e. $\beta = 2$, the second order convergence of the TS-FD method can be observed only when $0 < h \lesssim \varepsilon$ (cf. upper triangles above the diagonals (corresponding to $h \sim \varepsilon$, and being labelled in bold letters) in Table 4.2). For the TS-4cFD method, the second order convergence can be observed only when $0 < h \lesssim \varepsilon^{1/2}$ (cf. upper triangles above the diagonals (corresponding to $h \sim \varepsilon^{1/2}$, and

$e_{h,\tau_e}(t=1/\varepsilon^2)$	$h_0=\pi/8$	$h_0/2$	$h_0/2^2$	$h_0/2^3$	$h_0/2^4$	$h_0/2^5$
$\varepsilon_0=1$	**4.73E-2**	1.21E-2	3.01E-3	7.50E-4	1.87E-4	4.68E-5
order	**-**	1.97	2.01	2.00	2.00	2.00
$\varepsilon_0/2$	3.81E-1	**1.05E-1**	2.73E-2	6.89E-3	1.73E-3	4.32E-4
order	-	**1.86**	1.94	1.99	1.99	2.00
$\varepsilon_0/2^2$	1.16E+0	3.81E-1	**9.65E-2**	2.43E-2	6.07E-3	1.52E-3
order	-	1.61	**1.98**	1.99	2.00	2.00
$\varepsilon_0/2^3$	4.83E+0	1.55E+0	3.21E-1	**7.92E-2**	1.98E-2	4.95E-3
order	-	1.64	2.27	**2.02**	2.00	2.00
$\varepsilon_0/2^4$	1.91E+0	2.72E+0	1.89E+0	4.75E-1	**1.20E-1**	3.00E-2
order	-	-0.51	0.53	1.99	**1.98**	2.00

Table 4.2: Spatial errors of the TS-FD for the NKGE (2.1.1) with $\beta=2$ and initial data (4.6.1).

$e_{h,\tau_e}(t=1/\varepsilon^2)$	$h_0=\pi/8$	$h_0/2$	$h_0/2^2$	$h_0/2^3$	$h_0/2^4$	$h_0/2^5$
$\varepsilon_0=1$	1.61E-2	**9.12E-4**	5.44E-5	3.36E-6	2.10E-7	1.13E-8
order	-	**4.14**	4.07	4.02	4.00	4.00
$\varepsilon_0/2^2$	6.63E-2	5.57E-3	**2.98E-4**	1.83E-5	1.14E-6	7.14E-8
order	-	3.57	**4.22**	4.03	4.00	4.00
$\varepsilon_0/2^4$	9.67E-1	6.47E-2	6.43E-3	**3.80E-4**	2.36E-5	1.47E-6
order	-	3.90	3.33	**4.08**	4.01	4.00
$\varepsilon_0/2^6$	4.77E-1	7.18E-1	4.81E-2	4.32E-3	**2.78E-4**	1.73E-5
order	-	-0.59	3.90	3.48	**3.96**	4.01

Table 4.3: Spatial errors of the TS-4cFD for the NKGE (2.1.1) with $\beta=2$ and initial data (4.6.1).

being labelled in bold letters) in Table 4.3).

Comparing the TSFP, TS-FD and TS-4cFD methods, the temporal errors are uniformly second-order accurate in the long-time regime, and the error bounds may

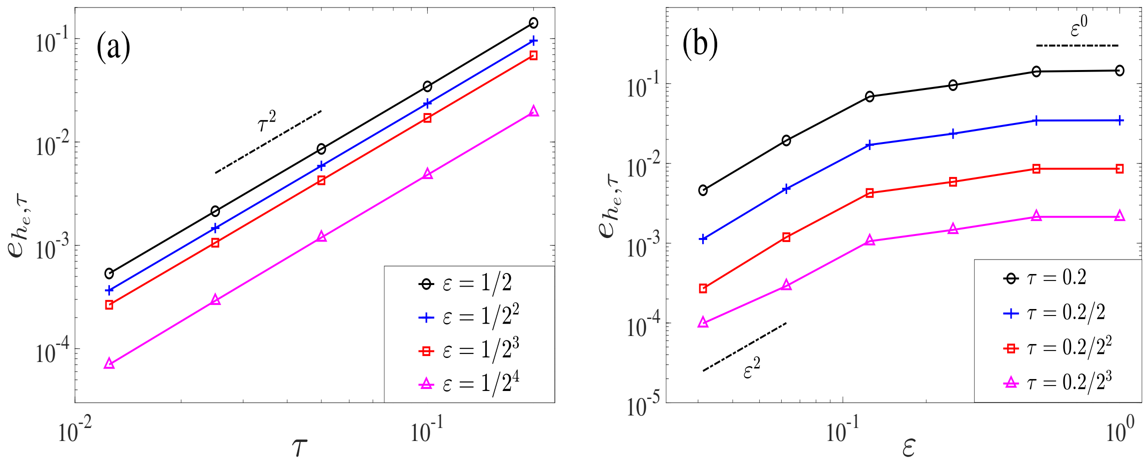

Figure 4.4: Temporal errors of the TSFD method for the NKGE (2.1.1) with $\beta = 2$.

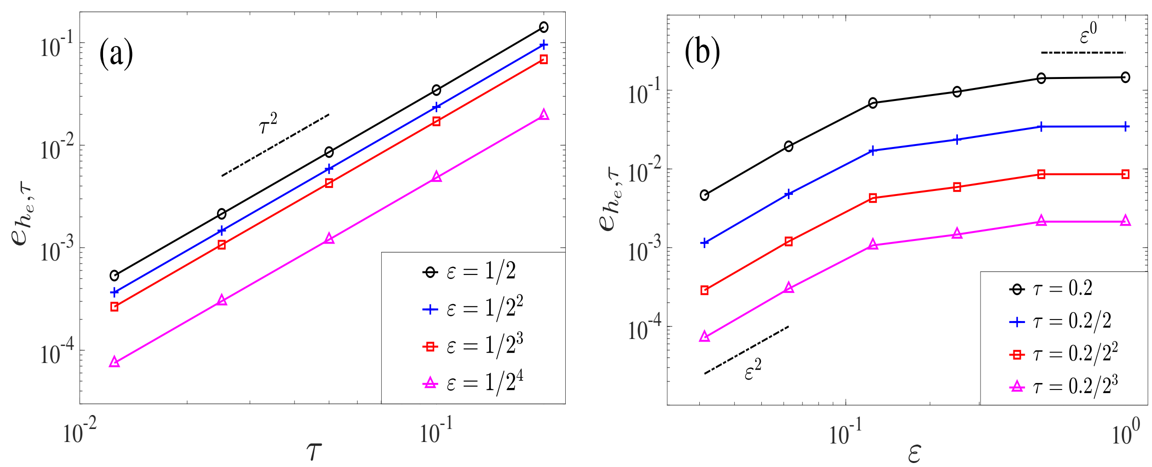

Figure 4.5: Temporal errors of the TS-4cFD method for the NKGE (2.1.1) with $\beta = 2$.

be improved to $O(\varepsilon^2\tau^2)$ when ε is small enough. For the spatial discretization, the errors of the finite difference methods depend on the small parameter $\varepsilon \in (0, 1]$. Tables 4.2-4.3 display that the spatial error of the fourth-order compact discretization is much smaller than that of the second order discretization in space under the same mesh size. The error of the spectral method is uniform which performs best among these three methods, especially when $0 < \varepsilon \ll 1$.

4.7 Comparisons with other time integrators

In this section, we use the spectral discretization in space and compare the temporal error bounds of different time integrators for solving the NKGE (2.1.1). In the numerical simulations, we choose the same initial data

$$\phi(x) = \frac{3}{2}\sin(x) \quad \text{and} \quad \gamma(x) = \frac{3}{1+\sin^2(x)}, \quad x \in (0, 2\pi). \tag{4.7.1}$$

	Methods	$\tau_0 = 0.04$	$\tau_0/2$	$\tau_0/2^2$	$\tau_0/2^3$	$\tau_0/2^4$	$\tau_0/2^5$
$\varepsilon = \frac{1}{4}$	FDFP	1.61E-1	4.04E-2	1.01E-2	2.54E-3	6.36E-4	1.59E-4
	order	-	1.99	2.00	1.99	2.00	2.00
	EWI-FP	7.34E-3	1.84E-3	4.59E-4	1.15E-4	2.87E-5	7.19E-6
	order	-	2.00	2.00	2.00	2.00	2.00
	TSFP	4.48E-3	1.12E-3	2.80E-4	7.00E-5	1.75E-5	4.35E-6
	order	-	2.00	2.00	2.00	2.00	2.01
	Methods	$\varepsilon_0 = 1$	$\varepsilon_0/2$	$\varepsilon_0/2^2$	$\varepsilon_0/2^3$	$\varepsilon_0/2^4$	$\varepsilon_0/2^5$
$\tau = 0.01$	FDFP	7.93E-3	1.01E-2	1.01E-2	1.01E-2	1.00E-2	1.00E-2
	EWI-FP	4.12E-3	1.46E-3	4.59E-4	1.24E-4	3.17E-5	7.97E-6
	TSFP	4.25E-3	1.14E-3	2.80E-4	6.93E-5	1.73E-5	4.31E-6

Table 4.4: Temporal errors of the numerical methods for the NKGE (2.1.1) with $\beta = 0$ and initial data (4.7.1).

Based on the above comparisons (cf. Tables 4.4-4.6), we conclude that the time-splitting (TS) method performs much better than the finite difference (FD) method and exponential wave integrator (EWI), especially in the long-time regime. For the fixed ε, the three time integrators are all second order in time, while the errors of the time-splitting method are much smaller than the other two methods. For $\beta = 0$, the finite difference method is uniform in terms of the small parameter ε and the EWI and TS methods behaves like $O(\varepsilon^2\tau^2)$. For $\beta > 0$, the FD method behaves like $O(\tau^2/\varepsilon^\beta)$, which indicates that the errors become much larger when $\varepsilon \to 0$. The temporal error

	Methods	$\tau_0 = 0.04$	$\tau_0/2$	$\tau_0/2^2$	$\tau_0/2^3$	$\tau_0/2^4$	$\tau_0/2^5$
$\varepsilon = \frac{1}{4}$	FDFP	3.68E-1	9.16E-2	2.29E-2	5.72E-3	1.43E-3	3.58E-4
	order	-	2.01	2.00	2.00	2.00	2.00
	EWI-FP	2.01E-2	5.03E-2	1.26E-3	3.14E-4	7.86E-5	1.97E-5
	order	-	2.00	2.00	2.00	2.00	2.00
	TSFP	7.94E-3	1.98E-3	4.96E-4	1.24E-4	3.09E-5	7.70E-6
	order	-	2.00	2.00	2.00	2.00	2.00
	Methods	$\varepsilon_0 = 1$	$\varepsilon_0/2$	$\varepsilon_0/2^2$	$\varepsilon_0/2^3$	$\varepsilon_0/2^4$	$\varepsilon_0/2^5$
$\tau = 0.01$	FDFP	7.93E-3	1.01E-2	2.29E-2	4.88E-2	1.06E-1	2.46E-1
	EWI-FP	4.12E-3	2.41E-3	1.26E-3	5.37E-4	3.28E-4	1.72E-4
	TSFP	4.25E-3	2.21E-3	4.96E-4	1.46E-4	1.45E-5	1.83E-6

Table 4.5: Temporal errors of the numerical methods for the NKGE (2.1.1) with $\beta = 1$ and initial data (4.7.1).

bounds of the EWI and TS methods are uniform in terms of ε in the long-time regime. In addition, the numerical results indicate that the TS method is very stable and allows large steps in practical computations, while the EWI method suffer from a stability constraint [165]. Comparisons between these two methods show that the temporal error of the TS method is smaller than that of the EWI method under the same time step, which suggests that it is better than the EWI method. Overall, the time-splitting method is the best choice among these time integrators to solve the NGKE (2.1.1) in the long-time regime. For the convenience, we summarize the error bounds of different numerical methods for solving the NKGE (2.1.1) in Table 4.7.

4.8 Applications

By the comparisons of various spatial discretizaions and time integrators, the TSFP method is the most accurate and effective among these methods to solve the NKGE in the long-time regime. In this section, we solve the NKGE (1.4.1) with the TSFP

	Methods	$\tau_0 = 0.04$	$\tau_0/2$	$\tau_0/2^2$	$\tau_0/2^3$	$\tau_0/2^4$	$\tau_0/2^5$
$\varepsilon = \frac{1}{4}$	FDFP	1.63E+0	4.06E-1	1.01E-1	2.53E-2	6.31E-3	1.58E-3
	order	-	2.01	2.01	2.00	2.00	2.00
	EWI-FP	6.31E-2	1.58E-2	3.94E-3	9.85E-4	2.46E-4	6.15E-5
	order	-	2.00	2.00	2.00	2.00	2.00
	TSFP	3.13E-2	7.83E-3	1.96E-3	4.89E-4	1.22E-4	3.04E-5
	order	-	2.00	2.00	2.00	2.00	2.00
	Methods	$\varepsilon_0 = 1$	$\varepsilon_0/2$	$\varepsilon_0/2^2$	$\varepsilon_0/2^3$	$\varepsilon_0/2^4$	$\varepsilon_0/2^5$
$\tau = 0.01$	FDFP	7.93E-3	1.64E-2	1.01E-2	4.96E-1	1.33E+0	5.03E+0
	EWI-FP	4.12E-3	5.71E-3	3.94E-3	5.98E-3	3.38E-3	3.73E-3
	TSFP	4.25E-3	4.43E-3	1.96E-3	1.10E-3	1.94E-4	6.86E-5

Table 4.6: Temporal errors of the numerical methods for the NKGE (2.1.1) with $\beta = 2$ and initial data (4.7.1).

Temporal \ Spatial	FD	4cFD	spectral
FD	$O(\frac{h^2}{\varepsilon^\beta} + \frac{\tau^2}{\varepsilon^\beta})$	$O(\frac{h^4}{\varepsilon^\beta} + \frac{\tau^2}{\varepsilon^\beta})$	$O(h^{m_0} + \frac{\tau^2}{\varepsilon^\beta})$
EWI	$O(\frac{h^2}{\varepsilon^\beta} + \varepsilon^{2-\beta}\tau^2)$	$O(\frac{h^4}{\varepsilon^\beta} + \varepsilon^{2-\beta}\tau^2)$	$O(h^{m_0} + \varepsilon^{2-\beta}\tau^2)$
TS	$O(\frac{h^2}{\varepsilon^\beta} + \varepsilon^{2-\beta}\tau^2)$	$O(\frac{h^4}{\varepsilon^\beta} + \varepsilon^{2-\beta}\tau^2)$	$O(h^{m_0} + \varepsilon^{2-\beta}\tau^2)$

Table 4.7: Error bounds of different numerical methods for solving the NKGE (2.1.1) with the mesh size h and time step τ up to the time at $O(\varepsilon^{-\beta})$.

method effectively in 2D and 3D cases. In 2D case, we choose the computational domain

$\Omega = (-\pi, \pi) \times (-\pi, \pi)$ and the initial data

$$\begin{aligned} \phi(x, y) &= 3e^{-x^2-y^2} \sin(x + y), \\ \gamma(x, y) &= e^{-x^2-y^2} \sin(x + y). \end{aligned} \tag{4.8.1}$$

Figures 4.6 and 4.7 show the contour plots of the solutions of the NKGE (1.4.1) in 2D under different ε.

In 3D case, we choose the computational domain $\Omega = (-\pi, \pi) \times (-\pi, \pi) \times (-\pi, \pi)$ and the initial data

$$\begin{aligned} \phi(x, y, z) &= 3e^{-x^2-y^2-z^2} \sin(x + y + z), \\ \gamma(x, y) &= e^{-x^2-y^2-z^2} \sin(x + y + z). \end{aligned} \tag{4.8.2}$$

Figures 4.8 and 4.9 depict the isosurface plots of the solutions of the NKGE (1.4.1) in 3D under different ε.

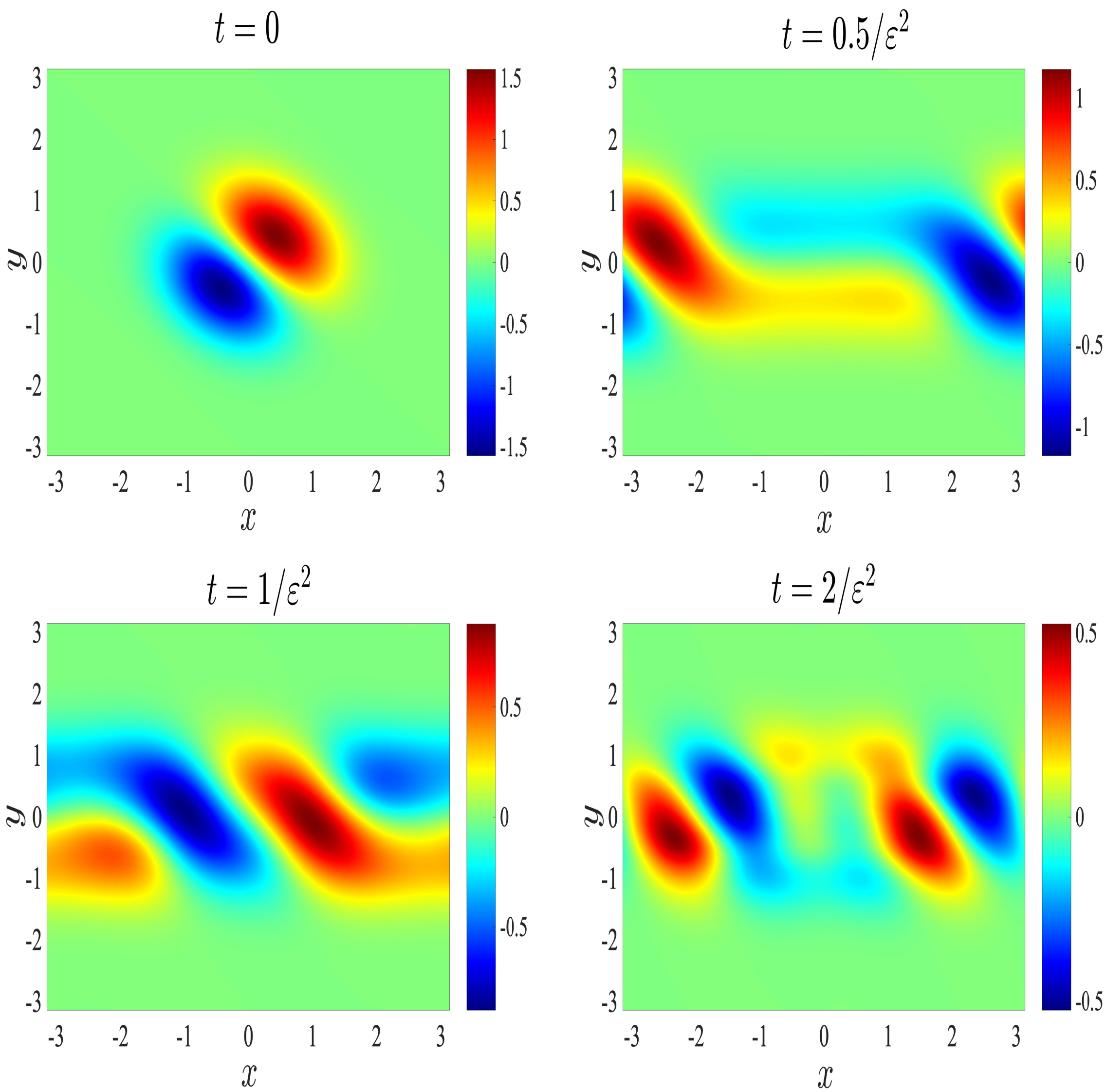

Figure 4.6: Contour plots of the solutions of 2D NKGE with (4.8.1) at different time t under $\varepsilon = 0.5$.

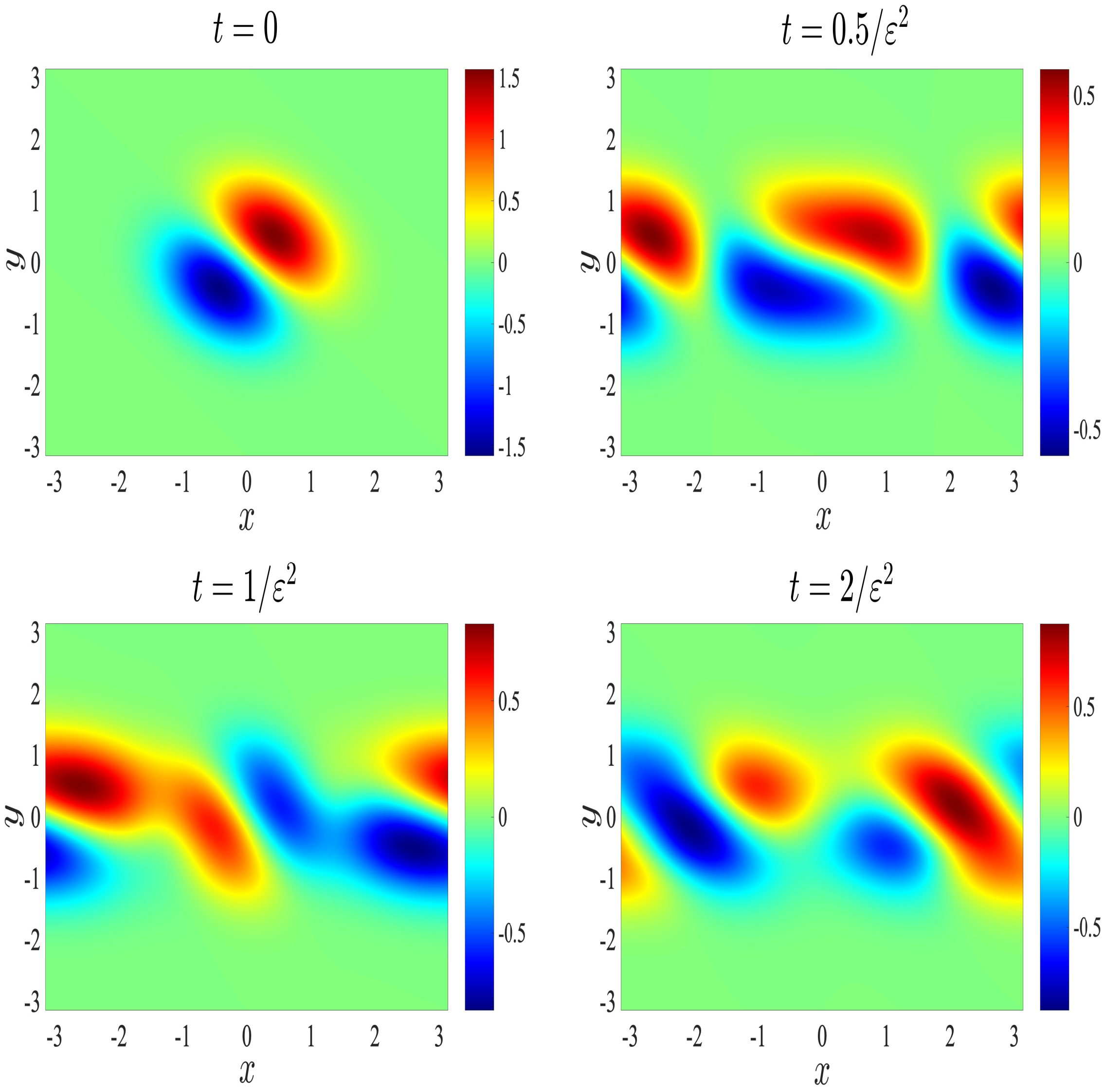

Figure 4.7: Contour plots of the solutions of 2D NKGE with (4.8.1) at different time t under $\varepsilon = 0.1$.

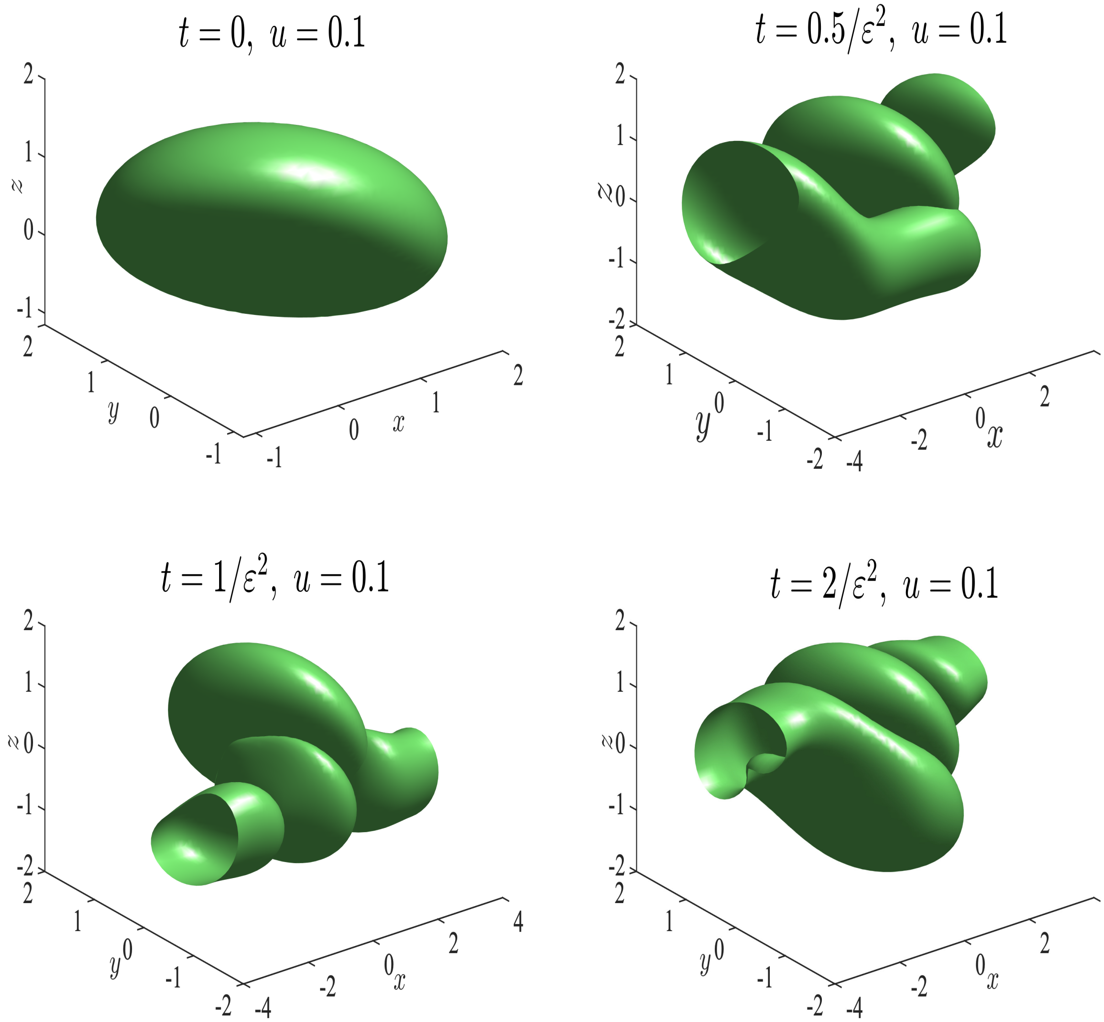

Figure 4.8: Isosurface plots of the solutions of 2D NKGE with (4.8.2) at different time t under $\varepsilon = 0.1$.

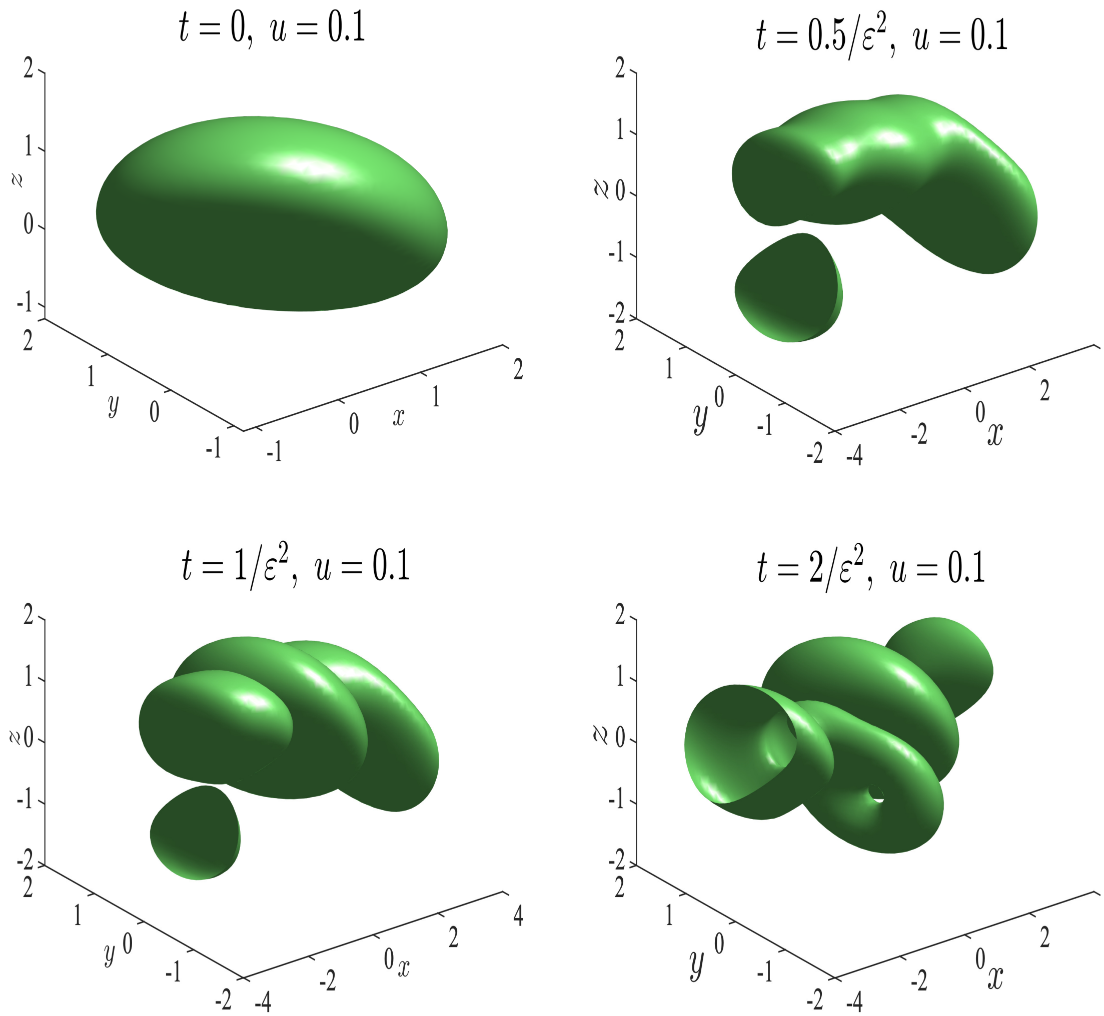

Figure 4.9: Isosurface plots of the solutions of 2D NKGE with (4.8.2) at different time t under $\varepsilon = 0.1$.

Chapter 5

Extension to an Oscillatory NKGE

In this chapter, we extend the NKGE (1.4.1) on the time interval $[0, T_0/\varepsilon^\beta]$ with $0 \leq \beta \leq 2$ to an oscillatory NKGE on a fixed time interval $[0, T_0]$. We use different numerical methods to solve the oscillatory NKGE and rigorously carry out the error bounds.

Introducing a rescaling in time by $s = \varepsilon^\beta t$ with $0 \leq \beta \leq 2$ and denoting $v(\mathbf{x}, s) := u(\mathbf{x}, s/\varepsilon^\beta) = u(\mathbf{x}, t)$, we can reformulate the NKGE (1.4.1) into the following oscillatory NKGE

$$\begin{cases} \partial_{ss} v(\mathbf{x},s) + \dfrac{1}{\varepsilon^{2\beta}}\left(-\Delta + 1\right) v(\mathbf{x}, s) + \dfrac{v^3(\mathbf{x}, s)}{\varepsilon^{2\beta-2}} = 0, \quad \mathbf{x} \in \mathbb{T}^d, \quad s > 0, \\ v(\mathbf{x}, 0) = \phi(\mathbf{x}), \quad \partial_s v(\mathbf{x}, 0) = \varepsilon^{-\beta}\gamma(\mathbf{x}), \quad \mathbf{x} \in \mathbb{T}^d. \end{cases} \tag{5.0.1}$$

Formally, the amplitude of the solution $v(\mathbf{x}, s)$ of the oscillatory NKGE (5.0.1) is at $O(1)$. Again, the oscillatory NKGE (5.0.1) is time symmetric or time reversible and conserves the energy, i.e.,

$$\begin{aligned} E_3(s) := E_3(v(\cdot, s)) &= \int_{\mathbb{T}^d} \left[|\partial_s v|^2 + \frac{1}{\varepsilon^{2\beta}}(|\nabla v|^2 + |v(\mathbf{x}, t)|^2) + \frac{1}{2\varepsilon^{2\beta-2}}|v|^4 \right] d\mathbf{x} \\ &\equiv \frac{1}{\varepsilon^{2\beta}} \int_{\mathbb{T}^d} \left[|\gamma(\mathbf{x})|^2 + |\nabla\phi(\mathbf{x})|^2 + |\phi(\mathbf{x})|^2 + \frac{\varepsilon^2}{2}|\phi(\mathbf{x})|^4) \right] d\mathbf{x} \\ &= E_3(0) = \frac{1}{\varepsilon^{2\beta}} E_1(0) = O(\varepsilon^{-2\beta}), \quad s \geq 0. \end{aligned}$$

In fact, the long-time dynamics of the NKGE (1.4.1) up to the time at $t = O(\varepsilon^{-\beta})$ is equivalent to the dynamics of the oscillatory NKGE (5.0.1) up to the fixed time at $s = O(1)$. Of course, the solution of the NKGE (1.4.1) propagates waves with wavelength at $O(1)$ in both space and time, and wave speed in space at $O(1)$ too. On the contrary, the solution of the oscillatory NKGE (5.0.1) propagates waves with

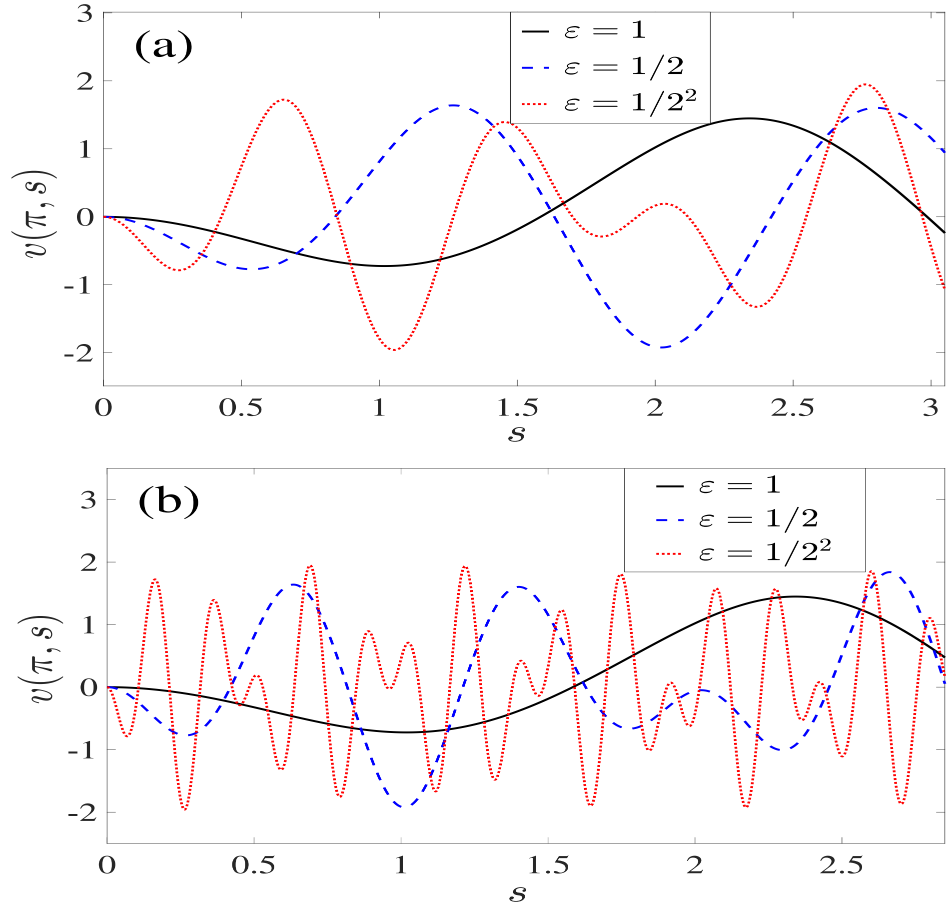

Figure 5.1: The solution $v(\pi, s)$ of the oscillatory NKGE (5.0.1) with $d = 1$ and initial data (2.5.1) for different ε and β: (a) $\beta = 1$, (b) $\beta = 2$.

wavelength at $O(1)$ in space and $O(\varepsilon^{\beta})$ in time, and wave speed in space at $O(\varepsilon^{-\beta})$. To illustrate this, Figures 5.1&5.2 show the solutions $v(\pi, s)$ and $v(x, 1)$, respectively, of the oscillatory NKGE (5.0.1) with $d = 1$, $\mathbb{T} = (0, 2\pi)$ and initial data $\phi(x) = \cos(x) + \cos(2x)$ and $\gamma(x) = \sin(x)$ for different $0 < \varepsilon \leq 1$ and β. We remark here that the oscillatory nature of the oscillatory NKGE (5.0.1) is quite different from that of the NKGE in the nonrelativistic limit regime. In fact, in the nonrelativistic limit regime of the NKGE [7, 8, 9, 11], the solution propagates waves with wavelength at $O(1)$ in space and $O(\varepsilon^2)$ in time, and wave speed in space at $O(1)$.

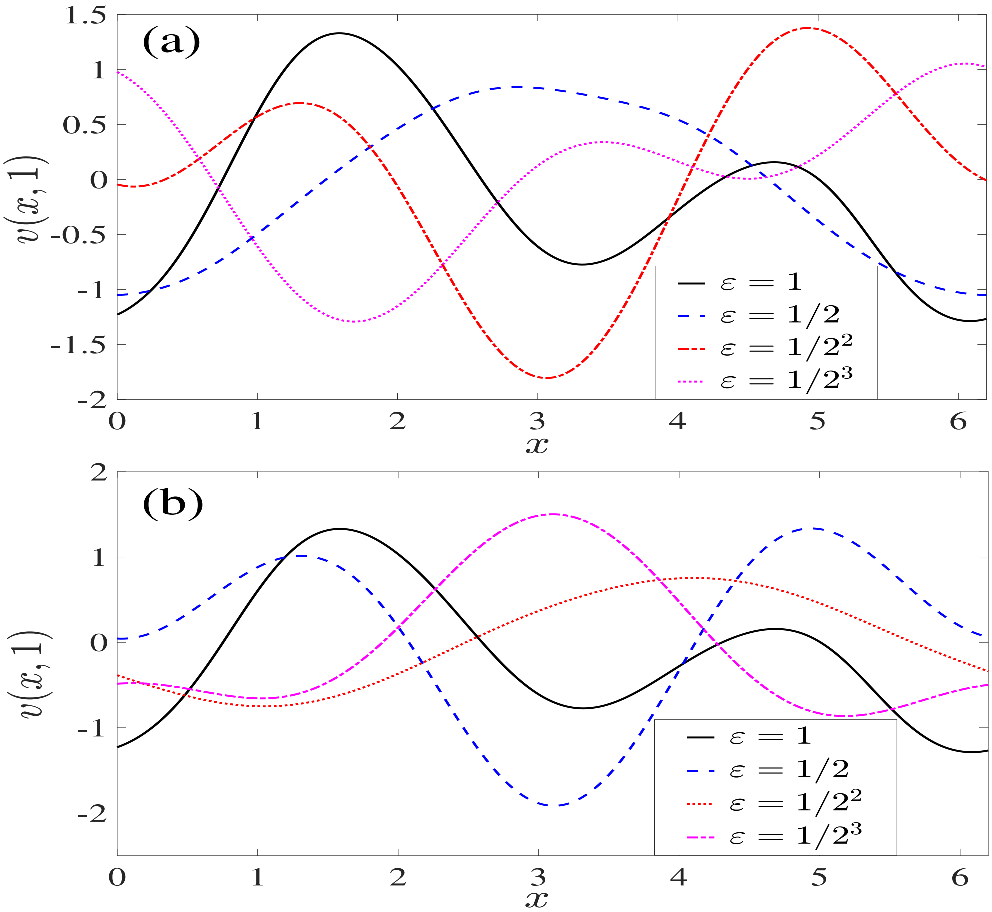

Figure 5.2: The solution $v(x, 1)$ of the oscillatory NKGE (5.0.1) with $d = 1$ and initial data $\phi(x) = \cos(x) + \cos(2x)$ and $\gamma(x) = \sin(x)$ for different ε and β: (a) $\beta = 1$, (b) $\beta = 2$.

5.1 An oscillatory NKGE in 1D

Again, for simplicity of notations, the numerical methods and their error bounds are only presented in 1D, and the results can be easily generalized to higher dimensions with minor modifications. In addition, the proofs for the error bounds are quite similar to those in the previous chapters, and thus they are omitted for brevity. We adopt similar notations as those used in Chapters 2-4 except stated otherwise. In 1D, consider the following oscillatory NKGE

$$\begin{cases} \partial_{ss}v(x,s) - \dfrac{1}{\varepsilon^{2\beta}}\partial_{xx}v(x,s) + \dfrac{1}{\varepsilon^{2\beta}}v(x,s) + \dfrac{v^3(x,s)}{\varepsilon^{2\beta-2}} = 0, \ x \in \Omega, \ s > 0, \\ v(x,0) = \phi(x), \quad \partial_s v(x,0) = \varepsilon^{-\beta}\gamma(x), \quad x \in \overline{\Omega} = [a,b], \end{cases} \tag{5.1.1}$$

with periodic boundary conditions.

5.2 FDTD methods and their error estimates

Choose the temporal step size $k := \Delta s > 0$ and denote time steps as $s_n := nk$ for $n \geq 0$. Let v_j^n be the numerical approximation of $v(x_j, s_n)$ for $j = 0, 1, \ldots, M$ and $n \geq 0$, and denote the numerical solution at time $s = s_n$ as v^n. Introduce the temporal finite difference operators as

$$\delta_s^+ v_j^n = \frac{v_j^{n+1} - v_j^n}{k}, \quad \delta_s^- v_j^n = \frac{v_j^n - v_j^{n-1}}{k}, \quad \delta_s^2 v_j^n = \frac{v_j^{n+1} - 2v_j^n + v_j^{n-1}}{k^2}.$$

We consider the following four FDTD methods:

I. The Crank-Nicolson finite difference (CNFD) method

$$\delta_s^2 v_j^n - \frac{1}{2\varepsilon^{2\beta}}\delta_x^2\left(v_j^{n+1} + v_j^{n-1}\right) + \frac{1}{2\varepsilon^{2\beta}}\left(v_j^{n+1} + v_j^{n-1}\right) + \frac{G\left(v_j^{n+1}, v_j^{n-1}\right)}{\varepsilon^{2\beta-2}} = 0, \ n \geq 1; \tag{5.2.1}$$

II. A semi-implicit energy conservative finite difference (SIFD1) method

$$\delta_s^2 v_j^n - \frac{1}{\varepsilon^{2\beta}}\delta_x^2 v_j^n + \frac{1}{2\varepsilon^{2\beta}}\left(v_j^{n+1} + v_j^{n-1}\right) + \frac{G\left(v_j^{n+1}, v_j^{n-1}\right)}{\varepsilon^{2\beta-2}} = 0, \ n \geq 1; \tag{5.2.2}$$

III. Another semi-implicit finite difference (SIFD2) method

$$\delta_s^2 v_j^n - \frac{1}{2\varepsilon^{2\beta}}\delta_x^2\left(v_j^{n+1} + v_j^{n-1}\right) + \frac{1}{2\varepsilon^{2\beta}}\left(v_j^{n+1} + v_j^{n-1}\right) + \frac{(v_j^n)^3}{\varepsilon^{2\beta-2}} = 0, \ n \geq 1; \tag{5.2.3}$$

IV. The Leap-frog finite difference (LFFD) method

$$\delta_s^2 v_j^n - \frac{1}{\varepsilon^{2\beta}}\delta_x^2 v_j^n + \frac{1}{\varepsilon^{2\beta}}v_j^n + \frac{(v_j^n)^3}{\varepsilon^{2\beta-2}} = 0, \ n \geq 1. \tag{5.2.4}$$

The initial and boundary conditions are discretized as

$$v_0^{n+1} = v_M^{n+1}, \quad v_{-1}^{n+1} = v_{M-1}^{n+1}, \quad n \geq 0; \quad v_j^0 = \phi(x_j), \quad j = 0, 1, \ldots, M. \tag{5.2.5}$$

Using the Taylor expansion and noticing (5.1.1), the first step $v^1 \in X_M$ can be computed as

$$v_j^1 = \phi(x_j) + \frac{k}{\varepsilon^\beta}\gamma(x_j) + \frac{k^2}{2\varepsilon^{2\beta}}\left[\delta_x^2\phi(x_j) - \phi(x_j) - \varepsilon^2\phi^3(x_j)\right], \quad 0 \le j \le M-1. \quad (5.2.6)$$

In fact, if we take $k = \tau\varepsilon^\beta$ in the FDTD methods in this section, then they are consistent with those FDTD methods presented in Section 2.3.1. Thus, they have the same solutions.

We remark here that, in practical computations, in order to uniformly bound the first step value $v^1 \in X_M$ for $\varepsilon \in (0, 1]$, in the above approximation (5.2.6), $k\varepsilon^{-\beta}$ and $k^2\varepsilon^{-2\beta}$ are replaced by $\sin(k\varepsilon^{-\beta})$ and $k\sin(k\varepsilon^{-2\beta})$, respectively [9, 17].

5.2.1 Stability and energy conservation

Denote

$$\tilde{\sigma}_{\max} := \max_{0\le n\le T_0/k} \|v^n\|_{l^\infty}^2. \quad (5.2.7)$$

Similar to Section 2.3.2, following the von Neumann stability analysis, we can conclude the stability of the above FDTD methods for the oscillatory NKGE (5.1.1) up to the fixed time $s = T_0$ in the following lemma.

Lemma 5.2.1. *For the above FDTD methods applied to the oscillatory NKGE* (5.1.1) *up to the fixed time $s = T_0$, we have:*

(i) The CNFD (5.2.1) is unconditionally stable for any $h > 0, k > 0$ and $0 < \varepsilon \le 1$.

(ii) When $h \ge 2$, the SIFD1 (5.2.2) is unconditionally stable for any $h > 0$ and $k > 0$; and when $0 < h < 2$, this scheme is conditionally stable under the stability condition

$$0 < k < \frac{2\varepsilon^\beta h}{\sqrt{4-h^2}}, \quad h > 0, \quad 0 < \varepsilon \le 1. \quad (5.2.8)$$

(iii) When $\tilde{\sigma}_{\max} \le \varepsilon^{-2}$, the SIFD2 (5.2.3) is unconditionally stable for any $h > 0$ and $k > 0$; and when $\tilde{\sigma}_{\max} > \varepsilon^{-2}$, this scheme is conditionally stable under the stability condition

$$0 < k < \frac{2\varepsilon^\beta}{\sqrt{\varepsilon^2\tilde{\sigma}_{\max} - 1}}, \quad h > 0, \quad 0 < \varepsilon \le 1. \quad (5.2.9)$$

(iv) The LFFD (5.2.4) is conditionally stable under the stability condition

$$0 < k < \frac{2\varepsilon^\beta h}{\sqrt{4 + h^2(1+\varepsilon^2\tilde{\sigma}_{\max})}}, \quad h > 0, \quad 0 < \varepsilon \le 1. \tag{5.2.10}$$

For the CNFD (5.2.1) and SIFD1 (5.2.2), we have the following energy conservation properties:

Lemma 5.2.2. *The CNFD (5.2.1) conserves the discrete energy as*

$$\begin{aligned}\mathcal{E}^n =& \varepsilon^{2\beta}\|\delta_s^+ v^n\|_{l^2}^2 + \frac{1}{2}\left(\|\delta_x^+ v^n\|_{l^2}^2 + \|\delta_x^+ v^{n+1}\|_{l^2}^2\right) + \frac{1}{2}\left(\|v^n\|_{l^2}^2 + \|v^{n+1}\|_{l^2}^2\right)\\ &+ \frac{h}{4}\varepsilon^2 \sum_{j=0}^{M-1}\left[|v_j^n|^4 + |v_j^{n+1}|^4\right] \equiv \mathcal{E}^0, \quad n = 0, 1, 2, \ldots.\end{aligned}$$

Similarly, the SIFD1 (5.2.2) conserves the discrete energy as

$$\begin{aligned}\tilde{\mathcal{E}}^n =& \varepsilon^{2\beta}\|\delta_s^+ v^n\|_{l^2}^2 + h\sum_{j=0}^{M-1}\left(\delta_x^+ v_j^n\right)\left(\delta_x^+ v_j^{n+1}\right) + \frac{1}{2}\left(\|v^n\|_{l^2}^2 + \|v^{n+1}\|_{l^2}^2\right)\\ &+ \frac{h}{4}\varepsilon^2 \sum_{j=0}^{M-1}\left[|v_j^n|^4 + |v_j^{n+1}|^4\right] \equiv \tilde{\mathcal{E}}^0, \quad n = 0, 1, 2, \ldots.\end{aligned}$$

5.2.2 Main results

Again, motivated by the analytical results and the assumptions on the NKGE (2.1.1), we assume that the exact solution v of the oscillatory NKGE (5.1.1) satisfies

$$(\tilde{\mathrm{A}}) \qquad \begin{aligned} v \in & C([0,T_0]; W_p^{4,\infty}) \cap C^2([0,T_0]; W^{2,\infty}) \cap C^3([0,T_0]; W^{1,\infty}) \cap C^4([0,T_0]; L^\infty),\\ &\left\|\frac{\partial^{r+q}}{\partial s^r \partial x^q} v(x,s)\right\|_{L^\infty([0,T_0];L^\infty)} \lesssim \frac{1}{\varepsilon^{\beta r}}, \quad 0 \le r \le 4, \quad 0 \le r+q \le 4.\end{aligned}$$

Define the grid 'error' function $\tilde{e}^n \in X_M (n \ge 0)$ as

$$\tilde{e}_j^n = v(x_j, s_n) - v_j^n, \quad j = 0, 1, \ldots, M, \quad n = 0, 1, 2, \ldots, \tag{5.2.11}$$

where $v^n \in X_M$ is the numerical approximation of the oscillatory NKGE (5.1.1) obtained by one of the FDTD methods.

By taking $k = \tau\varepsilon^\beta$ in the above FDTD methods and noting the error bounds in Section 2.4, we can immediately obtain error bounds of the above FDTD methods for the oscillatory NKGE (5.1.1).

Theorem 5.2.1. *Under the assumption* $(\widetilde{A})$, *there exist constants* $h_0 > 0$ *and* $k_0 > 0$ *sufficiently small and independent of* ε, *such that for any* $0 < \varepsilon \leq 1$, *when* $0 < h \leq h_0\varepsilon^{\beta/2}$ *and* $0 < k \leq k_0\varepsilon^{3\beta/2}$, *we have the following error estimates for the CNFD (5.2.1) with (5.2.5) and (5.2.6)*

$$\|\tilde{e}^n\|_{l^2} + \|\delta_x^+\tilde{e}^n\|_{l^2} \lesssim \frac{h^2}{\varepsilon^\beta} + \frac{k^2}{\varepsilon^{3\beta}}, \quad \|v^n\|_{l^\infty} \leq 1 + M_0, \quad 0 \leq n \leq \frac{T_0}{k}. \tag{5.2.12}$$

Theorem 5.2.2. *Assume* $k \lesssim h\varepsilon^\beta$ *and under the assumption* $(\widetilde{A})$, *there exist constants* $h_0 > 0$ *and* $k_0 > 0$ *sufficiently small and independent of* ε, *such that for any* $0 < \varepsilon \leq 1$, *when* $0 < h \leq h_0\varepsilon^{\beta/2}$, $0 < k \leq k_0\varepsilon^{3\beta/2}$ *and under the stability condition (5.2.8), we have the following error estimates for the SIFD1 (5.2.2) with (5.2.5) and (5.2.6)*

$$\|\tilde{e}^n\|_{l^2} + \|\delta_x^+\tilde{e}^n\|_{l^2} \lesssim \frac{h^2}{\varepsilon^\beta} + \frac{k^2}{\varepsilon^{3\beta}}, \quad \|v^n\|_{l^\infty} \leq 1 + M_0, \quad 0 \leq n \leq \frac{T_0}{k}. \tag{5.2.13}$$

Theorem 5.2.3. *Under the assumption* $(\widetilde{A})$, *there exist constants* $h_0 > 0$ *and* $k_0 > 0$ *sufficiently small and independent of* ε, *such that for any* $0 < \varepsilon \leq 1$, *when* $0 < h \leq h_0\varepsilon^{\beta/2}$, $0 < k \leq k_0\varepsilon^{3\beta/2}$ *and under the stability condition (5.2.9), we have the following error estimates for the SIFD2 (5.2.3) with (5.2.5) and (5.2.6)*

$$\|\tilde{e}^n\|_{l^2} + \|\delta_x^+\tilde{e}^n\|_{l^2} \lesssim \frac{h^2}{\varepsilon^\beta} + \frac{k^2}{\varepsilon^{3\beta}}, \quad \|v^n\|_{l^\infty} \leq 1 + M_0, \quad 0 \leq n \leq \frac{T_0}{k}. \tag{5.2.14}$$

Theorem 5.2.4. *Assume* $k \lesssim h\varepsilon^\beta$ *and under the assumption* $(\widetilde{A})$, *there exist constants* $h_0 > 0$ *and* $k_0 > 0$ *sufficiently small and independent of* ε, *such that for any* $0 < \varepsilon \leq 1$, *when* $0 < h \leq h_0\varepsilon^{\beta/2}$, $0 < k \leq k_0\varepsilon^{3\beta/2}$ *and under the stability condition (5.2.10), we have the following error estimates for the LFFD (5.2.4) with (5.2.5) and (5.2.6)*

$$\|\tilde{e}^n\|_{l^2} + \|\delta_x^+\tilde{e}^n\|_{l^2} \lesssim \frac{h^2}{\varepsilon^\beta} + \frac{k^2}{\varepsilon^{3\beta}}, \quad \|v^n\|_{l^\infty} \leq 1 + M_0, \quad 0 \leq n \leq \frac{T_0}{k}. \tag{5.2.15}$$

The above four FDTD methods share the same spatial/temporal resolution capacity for the oscillatory NKGE (5.1.1) up to the fixed time at $O(1)$. In fact, given an accuracy bound $\delta_0 > 0$, the ε-scalability of the FDTD methods for the oscillatory NKGE (5.1.1) should be taken as

$$h = O(\varepsilon^{\beta/2}\sqrt{\delta_0}) = O(\varepsilon^{\beta/2}), \quad k = O(\varepsilon^{3\beta/2}\sqrt{\delta_0}) = O(\varepsilon^{3\beta/2}), \quad 0 < \varepsilon \leq 1.$$

Again, these results are very useful for practical computations on how to select mesh size and time step such that the numerical results are trustable.

5.3 EWI-FP method and its error estimate

Let $k = \Delta s > 0$ be the temporal step size and denote time steps as $s_n := nk$ for $n \geq 0$. The Fourier spectral method for the oscillatory NKGE (5.1.1) is to find $v_M(x,s) \in X_M$, i.e.,

$$v_M(x,s) = \sum_{l \in \mathcal{T}_M} \widehat{(v_M)}_l(s) e^{i\mu_l(x-a)}, \quad x \in \overline{\Omega}, \quad s \geq 0, \tag{5.3.1}$$

such that

$$\varepsilon^{2\beta}\partial_{ss}v_M(x,s) - \partial_{xx}v_M(x,s) + v_M(x,s) + \varepsilon^2 P_M f(v_M(x,s)) = 0, \ x \in \overline{\Omega}, \ s \geq 0, \tag{5.3.2}$$

with $f(v) = v^3$. The derivations of the EWI-FS/EWI-FP discretization for the oscillatory NKGE (5.1.1) proceed in the analogous lines as those in Section 3.2 and we omit the details here for brevity. Denote $\widehat{(v_M^n)}_l$ and $v_M^n(x)$ be the approximations of $\widehat{(v_M)}_l(s_n)$ and $v_M(x,s_n)$, respectively. Choosing $v_M^0(x) = (P_M\phi)(x)$, the Gautschi-type exponential wave integrator Fourier spectral (EWI-FS) discretization for the oscillatory NKGE (5.1.1) is

$$v_M^{n+1}(x) = \sum_{l \in \mathcal{T}_M} \widehat{(v_M^{n+1})}_l e^{i\mu_l(x-a)}, \quad x \in \overline{\Omega}, \quad n \geq 0, \tag{5.3.3}$$

where

$$\begin{aligned} &\widehat{(v_M^1)}_l = \bar{p}_l\widehat{\phi}_l + \bar{q}_l\widehat{\gamma}_l + \bar{r}_l\widehat{(f(\phi))}_l, \quad l \in \mathcal{T}_M, \\ &\widehat{(v_M^{n+1})}_l = -\widehat{(v_M^{n-1})}_l + 2\bar{p}_l\widehat{(v_M^n)}_l + 2\bar{r}_l\widehat{(f(v_M^n))}_l, \quad l \in \mathcal{T}_M, \quad n \geq 1, \end{aligned} \tag{5.3.4}$$

with $\bar{\zeta}_l = \varepsilon^{-\beta}\sqrt{1+\mu_l^2} = O(\varepsilon^{-\beta})$ and the coefficients given as

$$\bar{p}_l = \cos(k\bar{\zeta}_l), \quad \bar{q}_l = \frac{\sin(k\bar{\zeta}_l)}{\varepsilon^\beta\bar{\zeta}_l}, \quad \bar{r}_l = \frac{\varepsilon^2(\cos(k\bar{\zeta}_l)-1)}{(\varepsilon^\beta\bar{\zeta}_l)^2}. \tag{5.3.5}$$

Similarly, let v_j^n be the approximation of $v(x_j, s_n)$ and denote $v_j^0 = \phi(x_j)$ ($j = 0, 1, \cdots, M$), then we can obtain the following Gautschi-type exponential wave integrator Fourier pseudospectral (EWI-FP) discretization for the oscillatory NKGE (5.1.1) as

$$v_j^{n+1} = \sum_{l\in\mathcal{T}_M} \widetilde{v}_l^{n+1} e^{i\mu_l(x_j-a)}, \quad j = 0, 1, \cdots, M, \quad n \geq 0, \tag{5.3.6}$$

where

$$\begin{aligned} &\widetilde{v}_l^1 = \bar{p}_l\widetilde{\phi}_l + \bar{q}_l\widetilde{\gamma}_l + \bar{r}_l\big(\widetilde{f(\phi)}\big)_l, \quad l \in \mathcal{T}_M, \\ &\widetilde{v}_l^{n+1} = -\widetilde{v}_l^{n-1} + 2\bar{p}_l\widetilde{v}_l^n + 2\bar{r}_l\big(\widetilde{f(v^n)}\big)_l, \quad l \in \mathcal{T}_M, \quad n \geq 1, \end{aligned} \tag{5.3.7}$$

with the coefficients $\bar{p}_l$, $\bar{q}_l$ and $\bar{r}_l$ are given in (5.3.5).

The EWI-FP (5.3.6)-(5.3.7) is also explicit, time symmetric and easy to extend to 2D and 3D. The memory cost is $O(M)$ and the computational cost per time step is $O(M \ln M)$. Similar to Lemma 3.2.1, we have the following stability result for the EWI-FP (5.3.6)-(5.3.7) with the proof omitted here for brevity.

Lemma 5.3.1. *(stability) Let $T_0 > 0$ be a fixed constant and denote*

$$\bar{\sigma}_{\max} := \max_{0\leq n\leq T_0/k} \|v^n\|_{l^\infty}^2. \tag{5.3.8}$$

The EWI-FP (5.3.6)-(5.3.7) *is conditionally stable under the stability condition*

$$0 < k \leq \frac{2\varepsilon^\beta h}{\sqrt{\pi^2 + h^2(1+\varepsilon^2\bar{\sigma}_{\max})}}, \quad h > 0, \quad 0 < \varepsilon \leq 1. \tag{5.3.9}$$

We are going to establish the error bounds of the EWI-FS/EWI-FP method for the oscillatory NKGE (5.1.1). Let $0 < T_0 < T^*$ with T^* the maximum existence time of the solution. Again, motivated by the analytical results of the oscillatory NKGE (5.1.1) and the assumption (D), we make some assumptions on the exact solution $v(x, s)$ of the oscillatory NKGE (5.1.1):

$$
(\widetilde{\mathrm{B}}) \qquad
\begin{aligned}
& v(x,s) \in L^\infty\left([0,T_0]; L^\infty \cap H_p^{m_0+1}\right), \ \partial_s v(x,s) \in L^\infty\left([0,T_0]; W^{1,4}\right), \\
& \partial_{ss} v(x,s) \in L^\infty\left([0,T_0]; H^1\right), \\
& \|v(x,s)\|_{L^\infty([0,T_0];L^\infty\cap H_p^{m_0+1})} \lesssim 1, \ \|\partial_s v(x,s)\|_{L^\infty([0,T_0];W^{1,4})} \lesssim \frac{1}{\varepsilon^\beta}, \\
& \|\partial_{ss} v(x,s)\|_{L^\infty([0,T_0];H^1)} \lesssim \frac{1}{\varepsilon^{2\beta}}, \quad m_0 \geq 1.
\end{aligned}
$$

Under the assumption $(\widetilde{B})$, let

$$
\begin{aligned}
\overline{M_1} &:= \max_{\varepsilon\in(0,1]} \left\{ \|v(x,s)\|_{L^\infty([0,T_0];L^\infty)} + \varepsilon^\beta \|\partial_s v(x,s)\|_{L^\infty([0,T_0];L^\infty)} \right\} \lesssim 1, \\
\overline{M_2} &:= \sup_{v\neq 0, |v|\leq 1+\overline{M_1}} |v|^2 \lesssim 1.
\end{aligned}
$$

Assuming

$$
k \leq \min\left\{ \frac{1}{8}\varepsilon^\beta, \frac{\varepsilon^\beta \pi h}{3\sqrt{\pi^2 + h^2(1+\varepsilon^2\overline{M_2})}} \right\}, \quad 0 < \varepsilon \leq 1, \quad 0 \leq \beta \leq 2, \tag{5.3.10}
$$

taking $\tau = k\varepsilon^{-\beta}$ and noticing the error bounds in Theorem 3.3.1, we can immediately obtain the error bounds of the EWI-FS (5.3.3)-(5.3.4) (The results for the EWI-FP (5.3.6)-(5.3.7) are quite similar and the details are skipped here for brevity):

Theorem 5.3.1. *Let $v_M^n(x)$ be the approximation obtained from the EWI-FS* (5.3.3)-(5.3.4)*, under the stability condition* (5.3.9) *and the assumptions $(\widetilde{B})$ and (5.3.10), there exist constants $h_0 > 0$ and $k_0 > 0$ sufficiently small and independent of ε, such that for any $0 < \varepsilon \leq 1$ and $0 \leq \beta \leq 2$, when $0 < h \leq h_0$, $0 < k \leq \varepsilon^\beta k_0$, we have*

$$
\begin{aligned}
& \|v(x,s_n) - v_M^n(x)\|_\lambda \lesssim h^{1+m_0-\lambda} + \varepsilon^{2-3\beta} k^2, \quad \lambda = 0, 1, \\
& \|v_M^n(x)\|_{L^\infty} \leq 1 + \overline{M_1}, \quad 0 \leq n \leq \frac{T_0}{k}.
\end{aligned} \tag{5.3.11}
$$

Based on Theorem 5.3.1, for a given accuracy bound $\delta_0 > 0$, the ε-scalability of the EWI-FS/EWI-FP method for the oscillatory NKGE (5.1.1) is:

$$
h = O(1), \quad k = O(\varepsilon^\beta \sqrt{\delta_0}) = O(\varepsilon^\beta), \quad 0 \leq \beta \leq 2.
$$

This indicates that, in order to obtain "correct" numerical solution in the fixed time interval, one has to take the meshing strategy: $h = O(1)$ and $k = O(\varepsilon^\beta)$. These results are useful for choosing mesh size and time step in practical computations such that the numerical results are trustable.

5.4 TSFP method and its error estimate

In this section, we extend the TSFP method to solve the following oscillatory complex NKGE in the whole space $\mathbb{R}^d (d = 1, 2, 3)$

$$\begin{cases} \partial_{ss} v(\mathbf{x}, s) + \dfrac{1}{\varepsilon^{2\beta}}(-\Delta + 1)v(\mathbf{x}, s) + \dfrac{|v(\mathbf{x}, s)|^2}{\varepsilon^{2\beta-2}} v(\mathbf{x}, s) = 0, \quad \mathbf{x} \in \mathbb{R}^d, \quad s > 0, \\ v(\mathbf{x}, 0) = \phi(\mathbf{x}), \quad \partial_s v(\mathbf{x}, 0) = \varepsilon^{-\beta}\gamma(\mathbf{x}), \quad \mathbf{x} \in \mathbb{R}^d. \end{cases} \tag{5.4.1}$$

For simplicity of notations, we only present the method and results in 1D. Similar to those in the literature, we truncate the oscillatory complex NKGE (5.4.1) in 1D onto a bounded interval $\Omega = (a, b)$ with periodic boundary conditions as

$$\begin{cases} \partial_{ss} v(x, s) + \dfrac{1}{\varepsilon^{2\beta}}(-\partial_{xx} + 1)v(x, s) + \varepsilon^{2-2\beta}|v(x, s)|^2 v(x, s) = 0, \quad s > 0, \\ v(a, t) = v(b, t), \quad \partial_x v(a, t) = \partial_x v(b, t), \qquad t \geq 0, \\ v(x, 0) = \phi(x), \quad \partial_s v(x, 0) = \varepsilon^{-\beta}\gamma(x), \quad x \in \overline{\Omega} = [a, b]. \end{cases} \tag{5.4.2}$$

Choose the spatial mesh size $h = (b - a)/M$ with M being an even positive integer and a temporal step size k, the grid points and time steps are denoted as

$$x_j := a + jh, \quad j \in \mathcal{T}_M^0, \quad s_n := nk, \quad n = 0, 1, 2, \ldots. \tag{5.4.3}$$

Similarly, introducing $\dot{v}(x, s) = \partial_s v(x, s)$ and

$$\begin{aligned} \eta_+(x, s) &= v(x, s) - i\varepsilon^\beta \langle\nabla\rangle^{-1}\dot{v}(x, s), \\ \eta_-(x, s) &= \overline{v}(x, s) - i\varepsilon^\beta \langle\nabla\rangle^{-1}\overline{\dot{v}}(x, s), \end{aligned} \qquad a \leq x \leq b, \quad s \geq 0, \tag{5.4.4}$$

and denoting

$$\begin{aligned} &\Phi(x, s) = \begin{pmatrix} \eta_+(x, s) \\ \eta_-(x, s) \end{pmatrix}, \quad G(\Phi) = \begin{pmatrix} f\left(\frac{1}{2}(\eta_+ + \overline{\eta_-})\right) \\ f\left(\frac{1}{2}(\overline{\eta_+} + \eta_-)\right) \end{pmatrix}, \\ &\Phi_0(x) = \begin{pmatrix} \phi(x) - i\varepsilon^{-\beta}\langle\nabla\rangle^{-1}\gamma(x) \\ \overline{\phi}(x) - i\varepsilon^{-\beta}\langle\nabla\rangle^{-1}\overline{\gamma}(x) \end{pmatrix}, \end{aligned} \tag{5.4.5}$$

with $f(\varphi) = |\varphi|^2\varphi$, then the oscillatory complex NKGE (5.4.2) can be reformulated into the following oscillatory relativistic NLSE:

$$\begin{cases} i\partial_s\Phi + \varepsilon^{-\beta}\langle\nabla\rangle\Phi + \varepsilon^{2-\beta}\langle\nabla\rangle^{-1}G(\Phi) = 0, \\ \Phi(x,0) = \Phi_0(x). \end{cases} \tag{5.4.6}$$

The above problem can be decoupled into the following two subproblems via a time-splitting technique [136]:

$$\begin{cases} i\partial_s\Phi(x,s) + \varepsilon^{-\beta}\langle\nabla\rangle\Phi(x,s) = 0, \\ \Phi(x,0) = \Phi_0(x), \end{cases} \tag{5.4.7}$$

and

$$\begin{cases} i\partial_s\Phi(x,s) + \varepsilon^{2-\beta}\langle\nabla\rangle^{-1}G(\Phi) = 0, \\ \Phi(x,0) = \Phi_0(x), \end{cases} \tag{5.4.8}$$

which can be solved exactly as

$$\Phi(\cdot,s) = e^{is\varepsilon^{-\beta}\langle\nabla\rangle}\Phi_0, \quad \Phi(x,s) = \Phi_0(x) + is\,\varepsilon^{2-\beta}\langle\nabla\rangle^{-1}G(\Phi_0(x)), \quad s \geq 0,$$

respectively.

Let Φ_j^n be the approximation of $\Phi(x_j, s_n)$ for $j \in \mathcal{T}_M^0$ and $n \geq 0$, and denote $\Phi^n = (\Phi_0^n, \Phi_1^n, \ldots, \Phi_M^n)^T$ be the solution at $s_n = nk$. Then a second-order time-splitting Fourier pseudospectral (TSFP) discretization for the oscillatory relativistic NLSE (5.4.6) is given by

$$\begin{aligned} \Phi_j^{(n,1)} &= \sum_{l\in\mathcal{T}_M} e^{\frac{ik\zeta_l}{2\varepsilon^\beta}}\ (\widetilde{\Phi^n})_l\ e^{i\mu_l(x_j-a)}, \\ \Phi_j^{(n,2)} &= \Phi_j^{(n,1)} + k\varepsilon^{2-\beta}F_j^n, \qquad\qquad j \in \mathcal{T}_M^0, \quad n \geq 0, \\ \Phi_j^{n+1} &= \sum_{l\in\mathcal{T}_M} e^{\frac{ik\zeta_l}{2\varepsilon^\beta}}\ (\widetilde{\Phi^{(n,2)}})_l\ e^{i\mu_l(x_j-a)}, \end{aligned} \tag{5.4.9}$$

with

$$\Phi_j^0 = \Phi_0(x_j), \qquad F_j^n = i\sum_{l\in\mathcal{T}_M} \frac{1}{\zeta_l}\ (\widetilde{G(\Phi^{(n,1)})})_l\ e^{i\mu_l(x_j-a)}, \qquad j \in \mathcal{T}_M^0, \quad n \geq 0.$$

Then v_j^n and $\dot{v}_j^n$ which are approximations of $v(x_j, s_n)$ and $\dot{v}(x_j, s_n)$, respectively, can be recovered by

$$\begin{aligned} v_j^{n+1} &= \frac{1}{2}\left((\eta_+)_j^{n+1} + \overline{(\eta_-)_j^{n+1}}\right), \\ \dot{v}_j^{n+1} &= \frac{i}{2\varepsilon^\beta}\sum_{l\in\mathcal{T}_M}\zeta_l\Big((\widetilde{(\eta_+)^{n+1}})_l - (\widetilde{\overline{(\eta_-)^{n+1}}})_l\Big)e^{i\mu_l(x_j-a)}, \end{aligned} \qquad j\in\mathcal{T}_M^0, \quad n\geq 0, \tag{5.4.10}$$

with $v_j^0 = \phi(x_j)$ and $\dot{v}_j^0 = \varepsilon^{-\beta}\gamma(x_j)$ for $j \in \mathcal{T}_M^0$.

We remark here that, by taking $k = \varepsilon^\beta\tau$ and assuming ϕ and γ to be real-valued in (5.4.2), the TSFP discretization (5.4.10) via (5.4.9) is the same as the TSFP discretization (4.3.3) via (4.3.2). Thus similar to the proof in Section 4.4, under the following reasonable assumptions on the exact solution v of (5.4.2)

$$(\widetilde{\mathrm{C}}) \qquad \begin{aligned} &v \in L^\infty\left([0,T_0]; H_{\mathrm{p}}^{m+1}\right), && \partial_t v \in L^\infty\left([0,T_0]; H_{\mathrm{p}}^{m}\right), \\ &\|v\|_{L^\infty\left([0,T_0];H_{\mathrm{p}}^{m+1}\right)} \lesssim 1, && \|\partial_t v\|_{L^\infty\left([0,T_0];H_{\mathrm{p}}^{m}\right)} \lesssim \frac{1}{\varepsilon^\beta}, \end{aligned}$$

with $m \geq 1$, we can establish the following error bounds of the TSFP method (5.4.10) via (5.4.9) for the oscillatory complex NKGE (5.4.2) (the proof is omitted here for brevity).

Theorem 5.4.1. *Let v^n be the numerical approximation obtained from the TSFP* (5.4.9)-(5.4.10)*. Under the assumption $(\widetilde{\mathrm{C}})$, there exist $h_0 > 0$ and $k_0 > 0$ sufficiently small and independent of ε such that, for any $0 < \varepsilon \leq 1$, when $0 < h \leq h_0$ and $0 < k \leq k_0\varepsilon^\beta$, we have the error estimates for $\lambda \in (1/2, m]$*

$$\|v(\cdot, s_n) - I_M(v^n)\|_\lambda + \|\partial_s v(\cdot, s_n) - I_M(\dot{v}^n)\|_{\lambda-1} \lesssim h^{1+m-\lambda} + \varepsilon^{2-3\beta}k^2, \quad 0 \leq n \leq \frac{T_0}{k}.$$

5.5 Numerical results

In this section, we show the numerical results of the following NKGE in the one dimension (1D)

$$\begin{cases} \partial_{ss}v(x,s) + \dfrac{1}{\varepsilon^{2\beta}}(-\Delta + 1)v(x,s) + \dfrac{|v(x,s)|^2}{\varepsilon^{2\beta-2}}v(x,s) = 0, \quad x \in \mathbb{R}, \quad s > 0, \\ v(x,0) = \phi(x), \quad \partial_s v(x,0) = \varepsilon^{-\beta}\gamma(x), \quad x \in \mathbb{R}. \end{cases} \tag{5.5.1}$$

Similar to the oscillatory NKGE (5.0.1), the solution of the oscillatory NKGE (5.5.1) propagates waves with wavelength at $O(1)$ in space and $O(\varepsilon^\beta)$ in time, and wave speed in space at $O(\varepsilon^{-\beta})$. To illustrate the rapid wave propagation in space at $O(\varepsilon^{-\beta})$, Figure 5.3 shows the solution $v(x,1)$ of the oscillatory NKGE (5.5.1) with $d=1$ and initial data

$$\phi(x) = \mathrm{sech}(x^2) \quad \text{and} \quad \gamma(x) = 0, \qquad x \in \mathbb{R}. \tag{5.5.2}$$

Similar to those in the literature, due to the fast decay of the solution of the oscillatory NKGE (5.5.1) at the far field (see [9, 48, 138] and references therein), in practical computations, we usually truncate the original whole space problem onto a bounded domain with periodic boundary conditions, which is large enough such that the truncation error is negligible. Due to the rapid outgoing waves with wave speed $O(\varepsilon^{-\beta})$, the computational domain Ω_ε has to be chosen as ε-dependent.

For the oscillatory NKGE (5.5.1), we study the following three cases :

Case I. Classical case, i.e., $\beta = 0$;

Case II. Intermediately oscillatory case, i.e., $\beta = 1$;

Case III. Highly oscillatory case, i.e., $\beta = 2$.

5.5.1 For FDTD methods

The initial data is chosen as (5.5.2) and the bounded computational domain is taken as $\Omega_\varepsilon = [-4-\varepsilon^{-\beta}, 4+\varepsilon^{-\beta}]$. The ‘exact’ solution is obtained numerically by the EWI-FP method with a very fine mesh size and a very small time step, e.g. $h_e = 1/2^{13}$ and $k_e = 2 \times 10^{-6}$. Denote $v^n_{h,k}$ as the numerical solution at $s = s_n$ obtained by a numerical method with mesh size h and time step k. In order to quantify the numerical results, we define the error function as follows:

$$\widetilde{e}_{h,k}(s_n) = \sqrt{\|v(\cdot, s_n) - v^n_{h,k}\|^2_{l^2} + \|\delta^+_x (v(\cdot, s_n) - v^n_{h,k})\|^2_{l^2}}. \tag{5.5.3}$$

Tables 5.1-5.6 show the spatial and temporal errors of the CNFD (5.2.1) for the oscillatory NKGE (5.5.1) with different β and ε. The results for other FDTD methods are quite similar and they are omitted here for brevity.

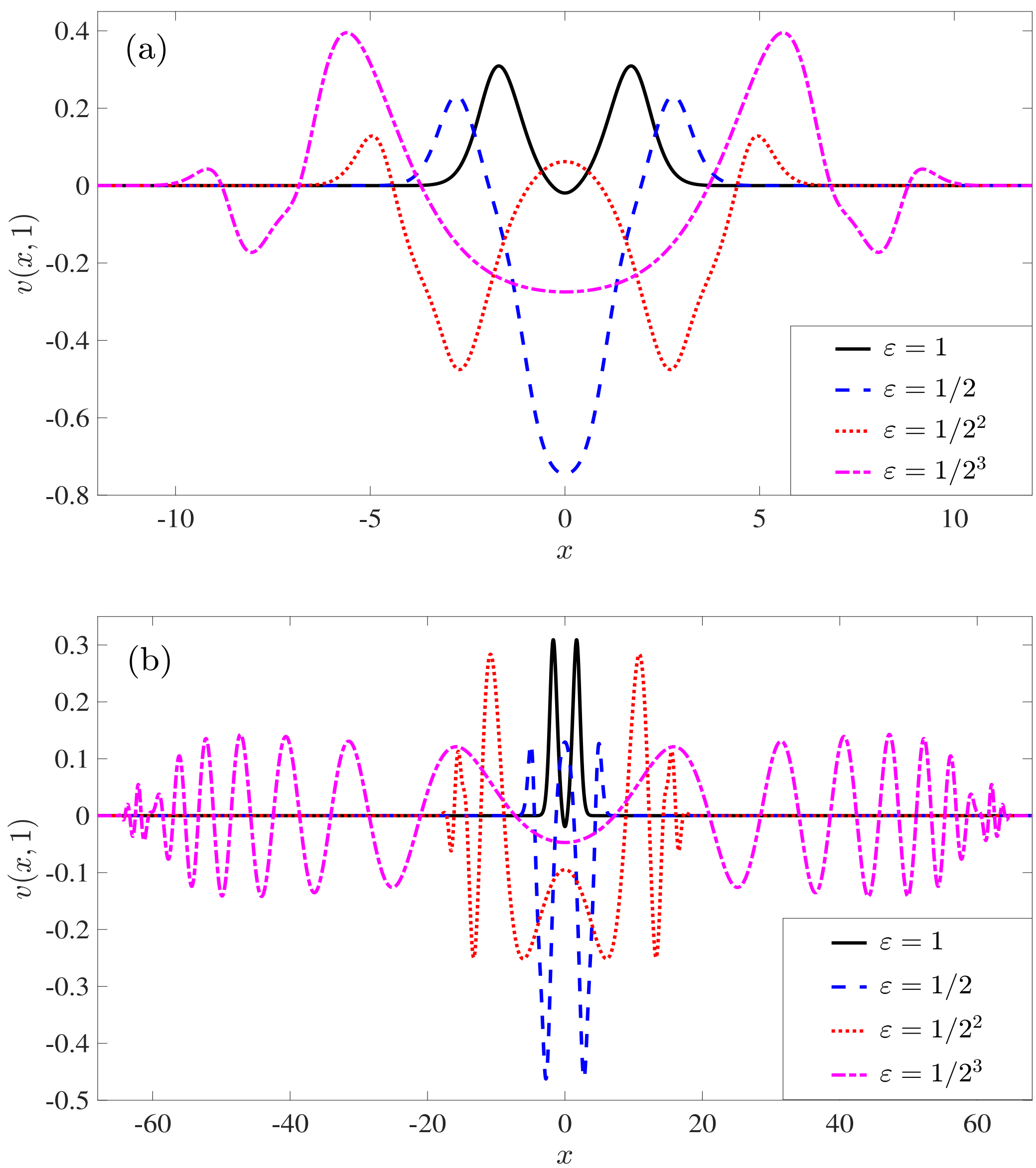

Figure 5.3: The solutions $v(x, 1)$ of the oscillatory NKGE (5.5.1) with $d = 1$ and initial data (5.5.2) for different ε and β: (a) $\beta = 1$, (b) $\beta = 2$.

From Tables 5.3-5.6 for the CNFD method and additional similar numerical results for other FDTD methods not shown here for brevity, we can draw the following observations on the FDTD methods for the oscillatory NKGE (5.5.1):

(i) For any fixed $\varepsilon = \varepsilon_0 > 0$ or $\beta = 0$, the FDTD methods are uniformly second-order

$\widetilde{e}_{h,k_e}(s=1)$	$h_0 = 1/4$	$h_0/2$	$h_0/2^2$	$h_0/2^3$	$h_0/2^4$
$\varepsilon_0 = 1$	6.17E-2	1.68E-2	4.26E-3	1.07E-3	2.68E-4
order	-	1.88	1.98	1.99	2.00
$\varepsilon_0/2$	6.20E-2	1.70E-2	4.33E-3	1.09E-3	2.73E-4
order	-	1.87	1.97	1.99	2.00
$\varepsilon_0/2^2$	6.22E-2	1.71E-2	4.36E-3	1.09E-3	2.75E-4
order	-	1.86	1.97	2.00	1.99
$\varepsilon_0/2^3$	6.22E-2	1.71E-2	4.36E-3	1.10E-3	2.75E-4
order	-	1.86	1.97	1.99	2.00
$\varepsilon_0/2^4$	6.22E-2	1.71E-2	4.37E-3	1.10E-3	2.75E-4
order	-	1.86	1.97	1.99	2.00

Table 5.1: Spatial errors of the CNFD (5.2.1) for the oscillatory NKGE (5.5.1) with $\beta = 0$ and (5.5.2).

$\widetilde{e}_{h_e,k}(s=1)$	$k_0 = 0.025$	$k_0/2$	$k_0/2^2$	$k_0/2^3$	$k_0/2^4$
$\varepsilon_0 = 1$	4.11E-3	1.05E-3	2.64E-4	6.63E-5	1.66E-5
order	-	1.97	1.99	1.99	2.00
$\varepsilon_0/2$	3.85E-3	9.82E-4	2.48E-4	6.22E-5	1.56E-5
order	-	1.97	1.99	2.00	2.00
$\varepsilon_0/2^2$	3.79E-3	9.65E-4	2.43E-4	6.11E-5	1.53E-5
order	-	1.97	1.99	1.99	2.00
$\varepsilon_0/2^3$	3.77E-3	9.61E-4	2.42E-4	6.08E-5	1.52E-5
order	-	1.97	1.99	1.99	2.00
$\varepsilon_0/2^3$	3.77E-3	9.60E-4	2.42E-4	6.07E-5	1.52E-5
order	-	1.97	1.99	2.00	2.00

Table 5.2: Temporal errors of the CNFD (5.2.1) for the oscillatory NKGE (5.5.1) with $\beta = 0$ and (5.5.2).

$\widetilde{e}_{h,k_e}(s=1)$	$h_0=1/8$	$h_0/2$	$h_0/2^2$	$h_0/2^3$	$h_0/2^4$
$\varepsilon_0=1$	**1.68E-2**	4.26E-3	1.07E-3	2.68E-4	6.72E-5
order	**-**	1.98	1.99	2.00	2.00
$\varepsilon_0/4$	5.60E-2	**1.44E-2**	3.63E-3	9.08E-4	2.27E-4
order	-	**1.96**	1.99	2.00	2.00
$\varepsilon_0/4^2$	2.00E-1	5.68E-2	**1.45E-2**	3.63E-3	9.07E-4
order	-	1.82	**1.97**	2.00	2.00
$\varepsilon_0/4^3$	4.83E-1	2.02E-1	5.70E-2	**1.45E-2**	3.63E-3
order	-	1.26	1.83	**1.97**	2.00
$\varepsilon_0/4^4$	6.21E-1	4.86E-1	2.03E-1	5.74E-2	**1.48E-2**
order	-	0.35	1.26	1.82	**1.96**

Table 5.3: Spatial errors of the CNFD (5.2.1) for the oscillatory NKGE (5.5.1) with $\beta=1$ and (5.5.2).

$\widetilde{e}_{h_e,k}(s=1)$	$k_0=0.025$	$k_0/4$	$k_0/4^2$	$k_0/4^3$	$k_0/4^4$
$\varepsilon_0=1$	**4.11E-3**	2.64E-4	1.66E-5	1.05E-6	7.82E-8
order	**-**	1.98	2.00	1.99	1.87
$\varepsilon_0/4^{2/3}$	4.88E-2	**3.24E-3**	2.04E-4	1.28E-5	8.29E-7
order	-	**1.96**	1.99	2.00	1.97
$\varepsilon_0/4^{4/3}$	4.98E-1	5.06E-2	**3.23E-3**	2.02E-4	1.28E-5
order	-	1.65	**1.98**	2.00	1.99
$\varepsilon_0/4^{6/3}$	1.75	5.18E-1	5.13E-2	**3.23E-3**	2.02E-4
order	-	0.88	1.67	**1.99**	2.00
$\varepsilon_0/4^{8/3}$	1.93	1.71	5.27E-1	5.18E-2	**3.24E-3**
order	-	0.09	0.85	1.67	**2.00**

Table 5.4: Temporal errors of the CNFD (5.2.1) for the oscillatory NKGE (5.5.1) with $\beta=1$ and (5.5.2).

$\widetilde{e}_{h,k_e}(s=1)$	$h_0 = 1/8$	$h_0/2$	$h_0/2^2$	$h_0/2^3$	$h_0/2^4$
$\varepsilon_0 = 1$	**1.68E-2**	4.26E-3	1.07E-3	2.68E-4	6.72E-5
order	**-**	1.98	1.99	2.00	2.00
$\varepsilon_0/2$	5.64E-2	**1.46E-2**	3.66E-3	9.16E-4	2.30E-4
order	-	**1.95**	2.00	2.00	2.00
$\varepsilon_0/2^2$	2.01E-1	5.71E-2	**1.46E-2**	3.65E-3	9.12E-4
order	-	1.82	**1.97**	2.00	2.00
$\varepsilon_0/2^3$	4.83E-1	2.03E-1	5.71E-2	**1.45E-2**	3.64E-3
order	-	1.25	1.83	**1.98**	1.99
$\varepsilon_0/2^4$	6.22E-1	4.86E-1	2.03E-1	5.74E-2	**1.48E-2**
order	-	0.36	1.26	1.82	**1.96**

Table 5.5: Spatial errors of the CNFD (5.2.1) for the oscillatory NKGE (5.5.1) with $\beta = 2$ and (5.5.2).

$\widetilde{e}_{h_e,k}(s=1)$	$k_0 = 0.025$	$k_0/4$	$k_0/4^2$	$k_0/4^3$	$k_0/4^4$
$\varepsilon_0 = 1$	**4.11E-3**	2.64E-4	1.66E-5	1.05E-6	7.82E-8
order	**-**	1.98	2.00	1.99	1.87
$\varepsilon_0/4^{1/3}$	4.99E-2	**3.31E-3**	2.08E-4	1.31E-5	8.48E-7
order	-	**1.96**	2.00	1.99	1.97
$\varepsilon_0/4^{2/3}$	5.03E-1	5.13E-2	**3.28E-3**	2.05E-4	1.29E-5
order	-	1.65	**1.98**	2.00	2.00
$\varepsilon_0/4^{3/3}$	1.77	5.21E-1	5.17E-2	**3.26E-3**	2.04E-4
order	-	0.88	1.67	**1.99**	2.00
$\varepsilon_0/4^{4/3}$	1.93	1.72	5.28E-1	5.19E-2	**3.25E-3**
order	-	0.08	0.85	1.67	**2.00**

Table 5.6: Temporal errors of the CNFD (5.2.1) for the oscillatory NKGE (5.5.1) with $\beta = 2$ and (5.5.2).

accurate in both spatial and temporal discretizations (cf. the first rows in Tables 5.3-5.6), which agree with those results in the literature. (ii) In the intermediate oscillatory case, i.e., $\beta = 1$, the second order convergence in space and time of the FDTD methods can be observed only when $0 < h \lesssim \varepsilon^{1/2}$ and $0 < k \lesssim \varepsilon^{3/2}$ (cf. upper triangles above the diagonals (corresponding to $h \sim \varepsilon^{1/2}$ and $k \sim \varepsilon^{3/2}$, and being labelled in bold letters) in Tables 5.3-5.4), which confirm our error bounds. (iii) In the highly oscillatory case, i.e., $\beta = 2$, the second order convergence in space and time of the FDTD methods can be observed only when $0 < h \lesssim \varepsilon$ and $0 < k \lesssim \varepsilon^3$ (cf. upper triangles above the diagonals (corresponding to $h \sim \varepsilon$ and $k \sim \varepsilon^3$, and being labelled in bold letters) in Tables 5.5-5.6), which again confirm our error bounds. In summary, our numerical results confirm our rigorous error bounds and show that they are sharp.

5.5.2 For EWI-FP method

We choose the following initial data

$$\phi(x) = 1/(e^{x^2} + e^{-x^2}) \quad \text{and} \quad \gamma(x) = 2e^{-x^2}, \qquad x \in \mathbb{R}. \tag{5.5.4}$$

The problem is solved on a bounded interval $\Omega_\varepsilon = [-4 - \varepsilon^{-\beta}, 4 + \varepsilon^{-\beta}]$, which is large enough to guarantee that the periodic boundary condition does not introduce a significant truncation error relative to the original problem. The 'exact' solution is obtained numerically by the EWI-FP method with a very fine mesh size and a very small time step, e.g. $h_e = 1/16$ and $k_e = 10^{-4}$. Denote v^n as the numerical solution at s_n by the EWI-FP (5.3.6)-(5.3.7) with mesh size h and time step k. The errors are denoted as $\tilde{e}(x, s_n) \in X_M$ with $\tilde{e}(x, s_n) = v(x, s_n) - I_M(v^n)(x)$. In order to quantify the numerical results, we measure the H^1 norm of $\tilde{e}(x, s_n)$, i.e.,

$$\|\tilde{e}(\cdot, s_n)\|_1 = \|\tilde{e}(\cdot, s_n)\| + \|\nabla\tilde{e}(\cdot, s_n)\|.$$

We first test the spatial discretization errors at $s = 1$ for different $0 < \varepsilon \leq 1$ and $0 \leq \beta \leq 2$. In order to do this, we fix the time step as $k_e = 10^{-4}$ such that the temporal error can be ignored, and solve the oscillatory NKGE (5.4.1) with different mesh size h. Table 5.7 depicts the spatial errors for $\beta = 0$, $\beta = 1$ and $\beta = 2$. Then we check the temporal errors at $s = 1$ for different $0 < \varepsilon \leq 1$ and $0 \leq \beta \leq 2$ with different time step

k and a very fine mesh size $h_e = 1/16$ such that the spatial errors can be neglected. Tables 5.8-5.10 show the temporal errors for $\beta = 0$, $\beta = 1$ and $\beta = 2$, respectively.

	$\|\tilde{e}(\cdot, 1)\|_1$	$h_0 = 1$	$h_0/2$	$h_0/2^2$	$h_0/2^3$
$\beta = 0$	$\varepsilon_0 = 1$	3.66E-2	1.15E-3	7.13E-6	9.27E-11
	$\varepsilon_0/2$	5.15E-2	5.43E-4	2.55E-6	5.08E-11
	$\varepsilon_0/2^2$	5.61E-2	6.35E-4	1.62E-6	4.58E-11
	$\varepsilon_0/2^3$	5.73E-2	6.89E-4	1.55E-6	4.41E-11
	$\varepsilon_0/2^4$	5.76E-2	7.04E-4	1.55E-6	4.40E-11
$\beta = 1$	$\varepsilon_0 = 1$	3.66E-2	1.15E-3	7.13E-6	9.27E-11
	$\varepsilon_0/2$	1.08E-1	1.23E-3	7.86E-6	1.36E-10
	$\varepsilon_0/2^2$	1.78E-1	4.00E-3	1.23E-5	3.50E-10
	$\varepsilon_0/2^3$	2.26E-1	9.90E-3	2.72E-5	8.81E-10
	$\varepsilon_0/2^4$	4.43E-2	1.81E-2	5.90E-5	2.01E-9
$\beta = 2$	$\varepsilon_0 = 1$	3.66E-2	1.15E-3	7.13E-6	9.27E-11
	$\varepsilon_0/2$	1.64E-1	3.43E-3	1.72E-5	3.35E-10
	$\varepsilon_0/2^2$	4.94E-2	1.78E-2	6.16E-5	2.03E-9
	$\varepsilon_0/2^3$	2.73E-1	1.83E-2	6.03E-5	6.92E-9
	$\varepsilon_0/2^4$	1.60E-1	1.90E-2	8.86E-5	6.95E-9

Table 5.7: Spatial errors of the EWI-FP (5.3.6)-(5.3.7) for the oscillatory NKGE (5.5.1) with initial data (5.5.4) for different β and ε.

From Tables 5.7-5.10 and additional numerical results not shown here for brevity, we can draw the following observations:

(i) In space, the EWI-FP (5.3.6)-(5.3.7) converges uniformly with exponential convergence rate for any fixed $0 < \varepsilon \leq 1$ and $0 \leq \beta \leq 2$ (cf. each row in Table 5.7).

(ii) In time, for any fixed $\varepsilon = \varepsilon_0 > 0$, the EWI-FP (5.3.6)-(5.3.7) is uniformly second-order accurate (cf. the first rows in Tables 5.8-5.10), which agree with the results in the literature. For the classical case, i.e., $\beta = 0$, Table 5.8 indicates that the temporal error

$\|\tilde{e}(\cdot,1)\|_1$	$k_0 = 0.1$	$k_0/2$	$k_0/2^2$	$k_0/2^3$	$k_0/2^4$
$\varepsilon_0 = 1$	1.08E-2	2.68E-3	6.70E-4	1.67E-4	4.18E-5
order	-	2.01	2.00	2.00	2.00
$\varepsilon_0/2$	3.99E-3	9.95E-4	2.48E-4	6.21E-5	1.55E-5
order	-	2.00	2.00	2.00	2.00
$\varepsilon_0/2^2$	1.15E-3	2.86E-4	7.15E-5	1.79E-5	4.46E-6
order	-	2.01	2.00	2.00	2.00
$\varepsilon_0/2^3$	2.98E-4	7.43E-5	1.86E-5	4.64E-6	1.16E-6
order	-	2.00	2.00	2.00	2.00
$\varepsilon_0/2^4$	7.52E-5	1.88E-5	4.68E-6	1.17E-6	2.97E-7
order	-	2.00	2.01	2.00	1.98

Table 5.8: Temporal errors of the EWI-FP (5.3.6)-(5.3.7) for the oscillatory NKGE (5.5.1) with $\beta = 0$ and initial data (5.5.4).

$\|\tilde{e}(\cdot,1)\|_1$	$k_0 = 0.1$	$k_0/2$	$k_0/2^2$	$k_0/2^3$	$k_0/2^4$
$\varepsilon_0 = 1$	**1.08E-2**	2.68E-3	6.70E-4	1.67E-4	4.18E-5
order	**-**	2.01	2.00	2.00	2.00
$\varepsilon_0/2$	2.57E-2	**6.26E-3**	1.55E-3	3.88E-4	9.69E-5
order	-	**2.04**	2.01	2.00	2.00
$\varepsilon_0/2^2$	5.01E-2	1.15E-2	**2.81E-3**	7.00E-4	1.75E-4
order	-	2.12	**2.03**	2.01	2.00
$\varepsilon_0/2^3$	2.57E-1	2.12E-2	4.78E-3	**1.17E-3**	2.91E-4
order	-	3.60	2.15	**2.03**	2.01
$\varepsilon_0/2^4$	1.70E-1	1.09E-1	7.47E-3	1.70E-3	**4.17E-4**
order	-	0.64	3.87	2.14	**2.03**

Table 5.9: Temporal errors of the EWI-FP (5.3.6)-(5.3.7) for the oscillatory NKGE (5.5.1) with $\beta = 1$ and initial data (5.5.4).

$\|\tilde{e}(\cdot,1)\|_1$	$k_0=0.1$	$k_0/4$	$k_0/4^2$	$k_0/4^3$	$k_0/4^4$
$\varepsilon_0=1$	**1.08E-2**	6.70E-4	4.18E-5	2.59E-6	1.89E-7
order	**-**	2.01	2.00	2.01	1.89
$\varepsilon_0/2$	1.98E-1	**1.10E-2**	6.85E-4	4.27E-5	2.51E-6
order	-	**2.08**	2.00	2.00	2.04
$\varepsilon_0/2^2$	3.25	1.22E-1	**6.82E-3**	4.22E-4	2.48E-5
order	-	2.37	**2.08**	2.01	2.04
$\varepsilon_0/2^3$	1.33	1.95	4.71E-2	**2.51E-3**	1.47E-4
order	-	-0.28	2.69	**2.11**	2.05
$\varepsilon_0/2^4$	4.81E-1	5.33E-1	9.88E-1	1.68E-2	**7.42E-4**
order	-	-0.07	-0.45	2.93	**2.25**

Table 5.10: Temporal errors of the EWI-FP (5.3.6)-(5.3.7) for the oscillatory NKGE (5.5.1) with $\beta=2$ and initial data (5.5.4).

of the EWI-FP (5.3.6)-(5.3.7) behaves like $O(\varepsilon^2 k^2)$ (cf. each row and column in Table 5.8); When $\beta=1$, the EWI-FP(5.3.6)-(5.3.7) converges quadratically in time when $k\lesssim\varepsilon$ (cf. each row in the upper triangle above the diagonal (corresponding to $k\sim\varepsilon$ and being labelled in bold letters) in Table 5.9). When $\beta=2$, the EWI-FP(5.3.6)-(5.3.7) converges quadratically in time when $k\lesssim\varepsilon^2$ (cf. each row in the upper triangle above the diagonal (corresponding to $k\sim\varepsilon^2$ and being labelled in bold letters) in Table 5.10). In summary, our numerical results confirm our rigorous error estimates.

5.5.3 For TSFP method

In this subsection, we report the numerical results of the TSFP method for solving the oscillatory equation (5.5.1) with the complex initial data

$$\phi(x)=(3+i)e^{-x^2/2} \quad \text{and} \quad \gamma(x)=\operatorname{sech}(x^2), \quad x\in\mathbb{R}. \tag{5.5.5}$$

The problem is solved on a bounded interval $\Omega_\varepsilon=[-8-\varepsilon^{-\beta},8+\varepsilon^{-\beta}]$, which is large enough to guarantee that the periodic boundary condition does not introduce a significant truncation error relative to the original problem. The 'exact' solution $v(x, s)$ is obtained numerically by using the TSFP (5.4.9)-(5.4.10) with a fine mesh size $h_e = 1/16$ and a very small time step $k_e = 5 \times 10^{-6}$. We also measure the H^1 norm and the errors are displayed at $T_0 = 1$ with different ε and β.

	$\|\tilde{e}(\cdot, 1)\|_1$	$h_0 = 1$	$h_0/2$	$h_0/2^2$	$h_0/2^3$
$\beta = 0$	$\varepsilon_0 = 1$	1.40E-1	1.63E-3	5.20E-6	1.09E-10
	$\varepsilon_0/2$	1.08E-1	2.30E-3	4.59E-6	9.72E-11
	$\varepsilon_0/2^2$	7.59E-2	2.01E-3	4.42E-6	9.66E-11
	$\varepsilon_0/2^3$	6.31E-2	2.01E-3	4.40E-6	9.67E-11
	$\varepsilon_0/2^4$	5.95E-2	2.01E-3	4.40E-6	9.68E-11
$\beta = 1$	$\varepsilon_0 = 1$	1.40E-1	1.63E-3	5.20E-6	1.09E-10
	$\varepsilon_0/2$	1.78E-1	3.29E-3	6.61E-6	1.60E-10
	$\varepsilon_0/2^2$	1.35E-1	3.12E-3	8.78E-6	2.40E-10
	$\varepsilon_0/2^3$	8.48E-2	3.29E-3	1.12E-5	3.34E-10
	$\varepsilon_0/2^4$	1.00E-1	1.62E-3	1.18E-5	4.10E-10
$\beta = 2$	$\varepsilon_0 = 1$	1.40E-1	1.63E-3	5.20E-6	1.09E-10
	$\varepsilon_0/2$	3.23E-1	4.59E-3	1.00E-5	2.43E-10
	$\varepsilon_0/2^2$	1.28E-1	1.53E-3	1.20E-5	4.14E-10
	$\varepsilon_0/2^3$	1.59E-1	3.61E-3	1.61E-5	1.58E-10
	$\varepsilon_0/2^4$	1.21E-1	3.81E-3	1.34E-5	2.22E-10

Table 5.11: Spatial errors of the TSFP (5.4.9)-(5.4.10) for the NKGE (5.5.1) with initial data (5.5.5) for different β and ε.

For spatial error analysis, we fix the time step as $k_e = 5 \times 10^{-6}$ such that the temporal errors can be neglected; for temporal error analysis, a very fine mesh size $h_e = 1/16$ is chosen such that the spatial error can be ignored. Table 5.11 shows the spatial errors under different mesh size for these three cases and Tables 5.12-5.14 depict the temporal errors for $\beta = 0, 1, 2$, respectively.

$\|\tilde{e}(\cdot,1)\|_1$	$k_0 = 0.1$	$k_0/2$	$k_0/2^2$	$k_0/2^3$	$k_0/2^4$	$k_0/2^5$
$\varepsilon_0 = 1$	2.91E-1	7.06E-2	1.75E-2	4.37E-3	1.09E-3	2.73E-4
order	-	2.04	2.01	2.00	2.00	2.00
$\varepsilon_0/2$	4.30E-2	1.06E-2	2.65E-3	6.63E-4	1.66E-4	4.14E-5
order	-	2.02	2.00	2.00	2.00	2.00
$\varepsilon_0/2^2$	4.84E-3	1.21E-3	3.01E-4	7.53E-5	1.88E-5	4.71E-6
order	-	2.00	2.01	2.00	2.00	2.00
$\varepsilon_0/2^3$	6.69E-4	1.67E-4	4.17E-5	1.04E-5	2.61E-6	6.52E-7
order	-	2.00	2.00	2.00	1.99	2.00
$\varepsilon_0/2^4$	1.34E-4	3.34E-5	8.35E-6	2.09E-6	5.22E-7	1.30E-7
order	-	2.00	2.00	2.00	2.00	2.01
$\varepsilon_0/2^5$	3.16E-5	7.88E-6	1.97E-6	4.92E-7	1.23E-7	3.07E-8
order	-	2.00	2.00	2.00	2.00	2.00

Table 5.12: Temporal errors of the TSFP (5.4.9)-(5.4.10) for the NKGE (5.5.1) with $\beta = 0$ and initial data (5.5.5).

From Tables 5.11-5.14 and additional results not shown here, we can draw the following observations, which verify the efficiency of the TSFP (5.4.9)-(5.4.10):

(1). The TSFP (5.4.9)-(5.4.10) is uniformly and spectrally accurate in space for any $0 < \varepsilon \leq 1$ and $0 \leq \beta \leq 2$.

(2). Tables 5.12-5.14 illustrate that for any fixed $\varepsilon = \varepsilon_0 > 0$, the TSFP method is second-order accurate in time when k is small enough. Specifically, for $\beta = 0$, Table 5.12 indicates that the temporal error bounds of the TSFP method behave like $O(\varepsilon^2 k^2)$, which confirms the estimate in Theorem 5.4.1. In the cases $\beta = 1$ and $\beta = 2$, the second order convergence in time can be observed only when the time step k is under some meshing strategy (cf. the upper triangles above the diagonals in Tables 5.13 and 5.14). When $\beta = 1$, the TSFP converges quadratically in the regime $k \lesssim \varepsilon$ (the upper triangle above the diagonal in Table 5.13). While for $\beta = 2$, the upper triangle above the diagonal in Table 5.14 shows that the temporal error is at $O(k^2/\varepsilon^2)$ when $k \lesssim \varepsilon^2$.

$\|\tilde{e}(\cdot,1)\|_1$	$k_0 = 0.1$	$k_0/2$	$k_0/2^2$	$k_0/2^3$	$k_0/2^4$	$k_0/2^5$
$\varepsilon_0 = 1$	**2.91E-1**	7.06E-2	1.75E-2	4.37E-3	1.09E-3	2.73E-4
order	**-**	2.04	2.01	2.00	2.00	2.00
$\varepsilon_0/2$	2.70E-1	**6.45E-2**	1.60E-2	3.98E-3	9.94E-4	2.48E-4
order	-	**2.07**	2.01	2.01	2.00	2.00
$\varepsilon_0/2^2$	2.96E-1	6.71E-2	**1.64E-2**	4.09E-3	1.02E-3	2.55E-4
order	-	2.14	**2.03**	2.00	2.00	2.00
$\varepsilon_0/2^3$	4.74E-1	6.90E-2	1.60E-2	**3.92E-3**	9.76E-4	2.44E-4
order	-	2.78	2.11	**2.03**	2.01	2.00
$\varepsilon_0/2^4$	4.21E-1	1.31E-1	1.81E-2	4.18E-3	**1.03E-3**	2.55E-4
order	-	1.68	2.86	2.11	**2.02**	2.01
$\varepsilon_0/2^5$	4.30E-1	1.33E-1	3.84E-2	5.10E-3	1.18E-3	**2.90E-4**
order	-	1.69	1.79	2.91	2.11	**2.02**

Table 5.13: Temporal errors of the TSFP (5.4.9)-(5.4.10) for the NKGE (5.5.1) with $\beta = 1$ and initial data (5.5.5).

The numerical result is much better than the analysis for $\beta \in (0, 2]$.

5.6 Comparisons of different methods

Based on the numerical results of the CNFD method, EWI-FP method and TSFP method in the previous sections, in view of both spatial and temporal accuracy and ε-scalability, we conclude that the TSFP and EWI-FP methods perform much better than the CNFD method (the FDTD methods) for the numerical approximations of the oscillatory NKGE (5.5.1), especially when $0 < \varepsilon \ll 1$.

The solution of the oscillatory NKGE (5.5.1) has no oscillation in space and propagates waves with wavelength $O(\varepsilon^\beta)$ in time. The ε-scalability of the FDTD methods is $h = O(\varepsilon^{\beta/2})$ and $\tau = O(\varepsilon^{3\beta/2})$, which is **under-resolution** in both space and time with respect to $\varepsilon \in (0, 1]$ in terms of the resolution capacity of the Shannon's information

$\|\tilde{e}(\cdot,1)\|_1$	$k_0 = 0.1$	$k_0/4$	$k_0/4^2$	$k_0/4^3$	$k_0/4^4$	$k_0/4^5$
$\varepsilon_0 = 1$	**2.91E-1**	1.75E-2	1.09E-3	6.83E-5	4.27E-6	2.66E-7
order	**-**	2.03	2.00	2.00	2.00	2.00
$\varepsilon_0/2$	3.42	**1.56E-1**	9.61E-3	6.00E-4	3.75E-5	2.34E-6
order	-	**2.23**	2.01	2.00	2.00	2.00
$\varepsilon_0/2^2$	1.36E+1	7.32E-1	**4.08E-2**	2.53E-3	1.58E-4	9.87E-6
order	-	2.11	**2.08**	2.01	2.00	2.00
$\varepsilon_0/2^3$	7.33	2.64	1.34E-1	**7.62E-3**	4.74E-4	2.95E-5
order	-	0.74	2.15	**2.07**	2.00	2.00
$\varepsilon_0/2^4$	2.52	2.14	6.93E-1	2.76E-2	**1.57E-3**	9.75E-5
order	-	0.12	0.81	2.33	**2.07**	2.00
$\varepsilon_0/2^5$	8.99E-1	6.94E-1	5.56E-1	1.77E-1	6.46E-3	**3.66E-4**
order	-	0.19	0.16	0.83	2.39	**2.07**

Table 5.14: Temporal errors of the TSFP (5.4.9)-(5.4.10) for the NKGE (5.5.1) with $\beta = 2$ and initial data (5.5.5).

Spatial / Temporal	FD	4cFD	spectral
FD	$O(\frac{h^2}{\varepsilon^\beta} + \frac{\tau^2}{\varepsilon^{3\beta}})$	$O(\frac{h^4}{\varepsilon^\beta} + \frac{\tau^2}{\varepsilon^{3\beta}})$	$O(h^{m_0} + \frac{\tau^2}{\varepsilon^{3\beta}})$
EWI	$O(\frac{h^2}{\varepsilon^\beta} + \varepsilon^{2-3\beta}\tau^2)$	$O(\frac{h^4}{\varepsilon^\beta} + \varepsilon^{2-3\beta}\tau^2)$	$O(h^{m_0} + \varepsilon^{2-3\beta}\tau^2)$
TS	$O(\frac{h^2}{\varepsilon^\beta} + \varepsilon^{2-3\beta}\tau^2)$	$O(\frac{h^4}{\varepsilon^\beta} + \varepsilon^{2-3\beta}\tau^2)$	$O(h^{m_0} + \varepsilon^{2-3\beta}\tau^2)$

Table 5.15: Error bounds of different numerical methods for solving the NKGE (5.5.1) with the mesh size h and time step τ.

Method	CNFD	EWI-FP	TSFP
Time symmetric	Yes	Yes	Yes
Unconditionally stable	Yes	No	Yes
Explicit scheme	No	Yes	Yes
Spatial accuracy	2nd	Spectral	Spectral
Temporal accuracy	2nd	2nd	2nd
Memory cost	$O(M)$	$O(M)$	$O(M)$
Computational cost	$\gg O(M)$	$O(M \ln M)$	$O(M \ln M)$
Resolution	$h = O(\varepsilon^{\beta/2})$	$h = O(1)$	$h = O(1)$
when $0 < \varepsilon \ll 1$	$\tau = O(\varepsilon^{3\beta/2})$	$\tau = O(\varepsilon^{\beta})$	$\tau = O(\varepsilon^{\beta})$

Table 5.16: Comparison of the properties of different numerical methods for solving the NKGE (5.5.1) with M being the number of grid points in space.

theory [91, 130, 131]- to resolve a wave one needs a few points per wavelength. The ε-scalability of the EWI-FP and TSFP methods is $h = O(1)$ and $\tau = O(\varepsilon^{\beta})$, which is **optimal resolution** in both space and time with respect to $\varepsilon \in (0, 1]$. The temporal discretization error of the EWI-FP and TSFP methods behaves like $O(\varepsilon^{2-3\beta}\tau^2)$. The TSFP method is shown as equivalent to the Deuflhard-type EWI-FP method, but it has an improved error bound regarding to the small parameter $\varepsilon \in (0, 1]$ when $0 < \varepsilon \ll 1$. Thus, the TSFP method is the best choice among these methods of different spatial and temporal discretizations to solve the oscillatory NKGE (5.5.1).

For convenience, we summarize the error bounds of different numerical methods in Table 5.15 and the properties of these numerical methods for the NKGE (5.5.1) in Table 5.16.

Chapter 6

Conclusion and Future Work

This thesis is devoted to the error estimates of numerical methods for the long-time dynamics of the nonlinear Klein-Gordon equation (NKGE). The numerical methods studied here include the finite difference methods, exponential wave integrator methods as well as the time-splitting methods and particular attentions are paid on the error bounds of different numerical methods up to the time $t = T_0/\varepsilon^\beta$ with $0 \leq \beta \leq 2$ and T_0 fixed. The main work in the thesis is summarized as follows and possible topics for future work are also discussed.

1. Error estimates of finite difference methods

Finite difference discretization in time combined with different spatial discretizations is applied to solve the NKGE with weak nonlinearity in the long-time regime. Four frequently used finite difference time domain (FDTD) methods are analyzed, and their stability conditions as well as error estimates are rigorously established up to the time $t = T_0/\varepsilon^\beta$ with $0 \leq \beta \leq 2$. It is found out that all the FDTD methods share the same spatial and temporal resolution. The CNFD is unconditionally stable, while others suffer from stability conditions. The fourth-order compact finite difference (4cFD) method is also used for studying the long-time dynamics of the NKGE, which has better spatial resolution than FDTD methods. The finite difference Fourier pseudospectral (FDFP) method is investigated as well, which discretizes the NKGE by Fourier spectral method in space and has the uniformly spectral accuracy in space in the long-time regime.

2. Study of exponential wave integrator methods

Exponential wave integrator (EWI) methods are adapted to study the long-time dynamics of the NKGE with weak nonlinearity. Uniform error bounds of the exponential wave integrator Fourier pseudospectral (EWI-FP) are rigorously established and numerical results are presented to validate the error estimates. For comparisons, the numerical schemes and corresponding error estimates for the EWI methods combined with central finite difference and fourth-order compact finite difference discretizations in space are also carried out.

3. Error estimates and comparisons of time-splitting methods

The NKGE is reformulated into a relativistic nonlinear Schrödinger equation (NLSE) and the time-splitting methods are used to discretize it numerically. An efficient and accurate time-splitting Fourier pseudospectral (TSFP) method is proposed and analyzed for the long-time dynamics of the NKGE with weak nonlinearity or small initial data. Uniform error bounds of the TSFP method are rigorously carried out up to the time at $O(\varepsilon^{-2})$. The error bounds of the time-splitting finite difference (TS-FD) method and TS-4cFD method are also established. Comparisons of different time integrators and applications in 2D and 3D cases are presented.

4. Extensions to an oscillatory nonlinear Klein-Gordon equation

The error estimates of different numerical methods for the long-time dynamics of the NKGE with weak nonlinearity up to the time at $O(\varepsilon^{-\beta})$ are extended to the dynamics of an oscillatory NKGE up to the fixed time at $O(1)$. The solution of the oscillatory NKGE propagates waves with wavelength at $O(1)$ in space and $O(\varepsilon^{\beta})$ in time, and wave speed in space at $O(\varepsilon^{-\beta})$. The FDTD methods, EWI-FP method and TSFP method are studied for the oscillatory NKGE. The error bounds as well as the spacial and temporal resolution of these numerical methods are obtained straightforwardly.

Some future work is listed below:

- Improve the error estimates of the TSFP method for the NKGE in the long-time regime when $0 < \varepsilon \ll 1$.
- Propose multiscale methods to solve the NKGE in the long-time regime efficiently. The total time steps could be fixed in the long-time regime, which means that

the total computational cost for the long-time dynamics up to the time $T_\varepsilon = T_0/\varepsilon^\beta (0 \leq \beta \leq 2)$ with T_0 fixed can be reduced.

- Extend the error estimates of numerical methods to the NKGE in different scalings. Some error estimates may be established just in short-time such as the NKGE with strong nonlinearity, while we can do some numerical simulations in the long-time regime.

- Study the long-time dynamics of other partial differential equations (PDEs) such as the Dirac/nonlinear Dirac equation, Burgers-Hilbert equation, Benjamin-Bona-Mahony (BBM) equation, etc. Based on the analytical result of the life-span of these PDEs, carry out the error bounds of different numerical methods in the long-time regime.

Bibliography

[1] D. D. Bainov and E. Minchev, “Nonexistence of global solutions of the initial-boundary value problem for the nonlinear Klein–Gordon equation”, *J. Math. Phys.*, vol. 36, pp. 756–762, 1995.

[2] D. Bambusi, “Birkhoff normal form for some nonlinear PDEs”, *Comm. Math. Phys.*, vol. 234, pp. 253–285, 2003.

[3] D. Bambusi, J.-M. Delort, and B. Grébert, “Almost global existence for hamiltonian semilinear Klein-Gordon equations with small Cauchy data on Zoll manifolds”, *Comm. Pure Appl. Math.*, vol. 60, pp. 1665–1690, 2007.

[4] W. Bao and Y. Cai, “Uniform error estimates of finite difference methods for the nonlinear Schrödinger equation with wave operator”, *SIAM J. Numer. Anal.*, vol. 50, pp. 492–521, 2012.

[5] W. Bao and Y. Cai, “Optimal error estimates of finite difference methods for the Gross-Pitaevskii equation with angular momentum rotation”, *Math. Comp.*, vol. 82, pp. 99–128, 2013.

[6] W. Bao and Y. Cai, “Uniform and optimal error estimates of an exponential wave integrator sine pseudospectral method for the nonlinear Schrödinger equation with wave operator”, *SIAM J. Numer. Anal.*, vol. 52, pp. 1103–1127, 2014.

[7] W. Bao, Y. Cai, X. Jia, and Q. Tang, “Error estimates of numerical methods for the nonlinear Dirac equation in the nonrelativistic limit regime”, *Sci. China Math.*, vol. 59, pp. 1461–1494, 2016.

[8] W. Bao, Y. Cai, and X. Zhao, “A uniformly accurate multiscale time integrator pseudospectral method for the Klein-Gordon equation in the nonrelativistic limit regime”, *SIAM J. Numer. Anal.*, vol. 52, pp. 2488–2511, 2014.

[9] W. Bao and X. Dong, "Analysis and comparison of numerical methods for the Klein-Gordon equation in the nonrelativistic limit regime", *Numer. Math.*, vol. 120, pp. 189–229, 2012.

[10] W. Bao, X. Dong, and J. Xin, "Comparisons between sine-Gordon equation and perturbed nonlinear Schrödinger equations for modeling light bullets beyond critical collapse", *Phys. D*, vol. 239, pp. 1120–1134, 2010.

[11] W. Bao, X. Dong, and X. Zhao, "Uniformly accurate multiscale time integrators for highly oscillatory second order differential equations", *J. Math. Study.*, vol. 47, pp. 111–150, 2014.

[12] W. Bao, Y. Feng, and C. Su, "Uniform error bounds of a time-splitting spectral method for the long-time dynamics of the nonlinear Klein-Gordon equation with weak nonlinearity", *arXiv: 2001.10868*, 2020.

[13] W. Bao, Y. Feng, and W. Yi, "Long time error analysis of finite difference time domain methods for the nonlinear Klein-Gordon equation with weak nonlinearity", *Commun. Comput. Phys.*, vol. 26, pp. 1307–1334, 2019.

[14] W. Bao, S. Jin, and P. A. Markowich, "On time-splitting spectral approximations for the Schrödinger equation in the semiclassical regime", *J. Comput. Phys.*, vol. 175, pp. 487–524, 2002.

[15] W. Bao, S. Jin, and P. A. Markowich, "Numerical study of time-splitting spectral discretizations of nonlinear Schrödinger equations in the semiclassical regimes", *SIAM J. Sci. Comput.*, vol. 25, pp. 27–64, 2003.

[16] W. Bao and J. Shen, "A fourth-order time-splitting Laguerre-Hermite pseudospectral method for Bose-Einstein condensates", *SIAM J. Sci. Comput.*, vol. 26, pp. 2010–2028, 2005.

[17] W. Bao and C. Su, "Uniform error bounds of a finite difference method for the Klein-Gordon-Zakharov system in the subsonic limit regime", *Math. Comp.*, vol. 87, pp. 2133–2158, 2018.

[18] W. Bao and C. Su, “Uniform error estimates of a finite difference method for the Klein-Gordon-Shrödinger system in the nonrelativistic and massless limit regimes”, *Kinet. Relat. Models*, vol. 11, pp. 1037–1062, 2018.

[19] W. Bao and X. Zhao, “A uniformly accurate multiscale time integrator spectral method for the Klein–Gordon–Zakharov system in the high-plasma-frequency limit regime”, *J. Comput. Phys.*, vol. 327, pp. 270–293, 2016.

[20] W. Bao and X. Zhao, “A uniformly accurate (UA) multiscale time integrator fourier pseudospectral method for the Klein–Gordon–Schrödinger equations in the nonrelativistic limit regime”, *Numer. Math.*, vol. 135, pp. 833–873, 2017.

[21] W. Bao and X. Zhao, “Comparison of numerical methods for the nonlinear Klein-Gordon equation in the nonrelativistic limit regime”, *J. Comput. Phys.*, vol. 398, article 108886, 2019.

[22] S. Baumstark, E. Faou, and K. Schratz, “Uniformly accurate oscillatory integrators for Klein-Gordon equations with asymptotic convergence to the classical NLS splitting”, *Math. Comp.*, vol. 87, pp. 1227–1254, 2018.

[23] P. Bellan, “Fundamentals of Plasma Physics”, Cambridge University Press, 2014.

[24] P. R. Berman, “Introductory Quantum Mechanics: A Traditional Approach Emphasizing Connections with Classical Physics”, Springer, 2018.

[25] N. N. Bogoliubov and D. V. Shirkov, “Introduction to the Theory of Quantized Fields”, Interscience Publishers, 1959.

[26] J. Bourgain, “Construction of approximative and almost periodic solutions of perturbed linear Schrödinger and wave equations”, *Geom. Funct. Anal.*, vol. 6, pp. 201–230, 1996.

[27] P. Brenner and W. von Wahl, “Global classical solutions of nonlinear wave equations”, *Math. Z.*, vol. 176, pp. 87–121, 1981.

[28] F. E. Browder, “On nonlinear wave equations”, *Math. Z.*, vol. 80, pp. 249–264, 1962.

[29] J. Campbell D. Schonfeld and C. Wingate, “Resonance structure in kink-antikink interactions in ϕ^4 theory”, *Physica D*, vol. 9, pp. 1–32, 1983.

[30] W. Cao and B. Guo, “Fourier collocation method for solving nonlinear Klein-Gordon equation”, *J. Comput. Phys.*, vol. 108, pp. 296–305, 1993.

[31] R. Carles, “On Fourier time-splitting methods for nonlinear Schrödinger equations in the semiclasscial limit”, *SIAM J. Numer. Anal.*, vol. 51, pp. 3232–3258, 2013.

[32] P. Chartier, N. Crouseilles, M. Lemou, and F. Méhats, “Uniformly accurate numerical schemes for highly oscillatory Klein-Gordon and nonlinear Schrödinger equations”, *Numer. Math.*, vol. 129, pp. 211–250, 2015.

[33] P. Chartier, M. Lemou, F. Méhats, and G. Vilmart, “A new class of uniformly accurate numerical schemes for highly oscillatory evolution equations”, *Found. Comput. Math.*, vol. 20, pp. 1–33, 2020.

[34] P. Chartier, F. Méhats, M. Thalhammer, and Y. Zhang, “Improved error estimates for splitting methods applied to highly-oscillatory nonlinear Schrödinger equations”, *Math. Comp.*, vol. 85, pp. 2863–2885, 2016.

[35] S. C. Chikwendu and C. V. Easwaran, “Multiple-scale solution of initial-boundary value problems for weakly nonlinear Klein-Gordon equations on the semi-infinite line”, *SIAM J. Appl. Math.*, vol. 52, pp. 946–958, 1992.

[36] D. Cohen, E. Hairer, and C. Lubich, “Numerical energy conservation for multi-frequency oscillatory differential equations”, *BIT*, vol. 45, pp. 287–305, 2005.

[37] D. Cohen, E. Hairer, and C. Lubich, “Conservation of energy, momentum and actions in numerical discretizations of nonlinear wave equations”, *Numer. Math.*, vol. 110, pp. 113–143, 2008.

[38] D. Cohen, T. Jahnke, K. Lorenz, and C. Lubich, “Numerical integrators for highly oscillatory Hamiltonian systems: A review”, *In: Analysis, Modeling and Simulation of Multiscale Problems*, pp. 553–576, 2006.

[39] A. S. Davydov, “Quantum Mechanics”, Pergamon Press, 1976.

[40] M. Dehghan and A. Shokri, “A numerical method for one-dimensional nonlinear sine-Gordon equation using collocation and radial basis functions”, *Numer. Methods Partial Differential Equations*, vol. 24, pp. 687–698, 2008.

[41] M. Dehghan and A. Shokri, “Numerical solution of the nonlinear Klein–Gordon equation using radial basis function”, *J. Comput. Appl. Math.*, vol. 230, pp. 400–410, 2009.

[42] J.-M. Delort, “Temps d’existence pour l’équation de Klein-Gordon semi-linéaire à données petites périodiques”, *Amer. J. Math.*, vol. 120, pp. 663–689, 1998.

[43] J.-M. Delort, “On long time existence for small solutions of semi-linear Klein-Gordon equations on the torus”, *J. Anal. Math.*, vol. 107, pp. 161–194, 2009.

[44] J.-M. Delort and J. Szeftel, “Long time existence for small data nonlinear Klein-Gordon equations on tori and spheres”, *Int. Math. Res. Not. IMRN*, vol. 37, pp. 1897–1966, 2004.

[45] J.-M. Delort and J. Szeftel, “Long-time existence for semi-linear Klein–Gordon equations with small Cauchy data on Zoll manifolds”, *Amer. J. Math.*, vol. 128, pp. 1187–1218, 2006.

[46] P. Deuflhard, “A study of extrapolation methods based on multistep schemes without parasitic solutions”, *Z. Angew. Math. Phys.*, vol. 30, pp. 177–189, 1979.

[47] X. Dong, Z. Xu, and X. Zhao, “On time-splitting pseudospectral discretization for nonlinear Klein-Gordon equation in nonrelativistic limit regime”, *Commun. Comput. Phys.*, vol. 16, pp. 440–466, 2014.

[48] D. B. Duncan, “Sympletic finite difference approximations of the nonlinear Klein-Gordon equation”, *SIAM J. Numer. Anal.*, vol. 34, pp. 1742–1760, 1997.

[49] S. A. M. F. H. Easif and D. Mekaeel, “The finite difference method for ϕ^4-nonlinear Klein-Gordon equation”, *IOSR J. Eng.*, vol. 3, pp. 01–05, 2013.

[50] D. Fang, Z. Han, and Q. Zhang, “Almost global existence for the semi-linear Klein-Gordon equation on the circle”, *J. Differential Equations*, vol. 262, pp. 4610–4634, 2017.

[51] D. Fang and Q. Zhang, “Long-time existence for semi-linear Klein-Gordon equations on tori”, *J. Differential Equations*, vol. 249, pp. 151–179, 2010.

[52] E. Faou and B. Grébert, “Hamiltonian interpolation of splitting approximations for nonlinear PDEs”, *Found. Comput. Math.*, vol. 11, pp. 381–415, 2011.

[53] E. Faou, B. Grébert, and E. Paturel, “Birkhoff normal form for splitting methods applied to semi linear hamiltonian PDEs. Part I: Finite dimensional discretization”, *Numer. Math.*, vol. 114, pp. 429–458, 2010.

[54] E. Faou, B. Grébert, and E. Paturel, “Birkhoff normal form for splitting methods applied to semi linear Hamiltonian PDEs. Part II: Abstract splitting”, *Numer. Math.*, vol. 114, pp. 459–490, 2010.

[55] E. Faou, A. Ostermann, and K. Schratz, “Analysis of exponential splitting methods for inhomogeneous parabolic equations”, *IMA J. Numer. Anal.*, vol. 35, pp. 161–178, 2015.

[56] E. Faou and K. Schratz, “Asymptotic preserving schemes for the Klein-Gordon equation in the nonrelativistic limit regime”, *Numer. Math.*, vol. 126, pp. 441–469, 2014.

[57] Y. Feng, “Long time error analysis of the fourth-order compact finite difference methods for the nonlinear Klein-Gordon equation with weak nonlinearity”, *arXiv: 2003.03951*, 2020.

[58] Y. Feng and W. Yi, “Uniform error bounds of an exponential wave integrator for the long-time dynamics of the nonlinear Klein-Gordon equation”, *arXiv: 2003.11785*, 2020.

[59] L. Gauckler, “Error analysis of trigonometric integrators for seimilinear wave equations”, *SIAM J. Numer. Anal.*, vol. 53, pp. 1082–1106, 2015.

[60] L. Gauckler and C. Lubich, “Splitting integrators for nonlinear Schrödinger equations over long times”, *Found. Comput. Math.*, vol. 10, pp. 275–302, 2010.

[61] W. Gautschi, “Numerical integration of ordinary differential equations based on trigonometric polynomials”, *Numer. Math.*, vol. 3, pp. 381–397, 1961.

[62] J. Ginibre and G. Velo, "The global Cauchy problem for the nonlinear Klein-Gordon equation", *Math. Z.*, vol. 189, pp. 487–505, 1985.

[63] R. Glassey, "On the asymptotic behavior of nonlinear wave equations", *Trans. Amer. Math. Soc.*, vol. 182, pp. 187–200, 1973.

[64] V. Grimm, "A note on the Gautschi-type method for oscillatory second-order differential equations", *Numer. Math.*, vol. 102, pp. 61–66, 2005.

[65] V. Grimm, "On error bounds for the Gautschi-type exponential integrator applied to oscillatory second-order differential equations", *Numer. Math.*, vol. 100, pp. 71–89, 2005.

[66] V. Grimm, "On the use of the Gautschi-type exponential integrator for wave equations", *In: Bermúdez de Castro, A., Gómez, D., Quintela, P., Salgado, P. (eds.) Numerical Mathematics and Advanced Applications (ENUMATH2005)*, pp. 557–563, 2006.

[67] V. Grimm and M. Hochbruck, "Error analysis of exponential integrators for oscillatory second-order differential equations", *J. Phys. A*, vol. 39, pp. 5495–5507, 2006.

[68] A. M. Grundland and E. Infeld, "A family of nonlinear Klein-Gordon equations and their solutions", *J. Math. Phys.*, vol. 33, pp. 2498–2503, 1992.

[69] B. Y. Guo, L. Xun, and L. Vazquez, "A Legendre spectral method for solving the nonlinear Klein–Gordon equation", *J. Comput. Appl. Math.*, vol. 15, pp. 19–36, 1996.

[70] M. G. Hafez, M. N. Alam, and M. A. Akbar, "Exact traveling wave solutions to the Klein-Gordon equation using the novel (G'/G)-expansion method", *Results Phys.*, vol. 4, pp. 177–184, 2014.

[71] E. Hairer and C. Lubich, "Long-time energy conservation of numerical methods for oscillatory differential equations", *SIAM J. Numer. Anal.*, vol. 38, pp. 414–441, 2000.

[72] E. Hairer and C. Lubich, "Spectral semi-discretisations of nonlinear wave equations over long times", *Found. Comput. Math.*, vol. 8, pp. 319–334, 2008.

[73] E. Hairer, C. Lubich, and G. Wanner, "Geometric Numerical Integraion: Structure-Preserving Algorithms for Ordinary Differential Equations", Springer, 2006.

[74] B. C. Hall, "Quantum Theory for Mathematicians", Springer, 2013.

[75] W. Han and Z. Jin, "Life-span of classical solutions to two dimensional fully nonlinear wave equations", *J. Funct. Anal.*, vol. 270, pp. 4087–4116, 2016.

[76] N. Hayashi and P. Naumkin, "The initial value problem for the cubic nonlinear Klein-Gordon equation", *Z. Angew. Math.*, vol. 59, pp. 1002–1028, 2008.

[77] J. S. Hesthaven, S. Gottlieb, and D. Gottlieb, "Spectral Methods for Time-Dependent Problems", Cambridge University Press, 2007.

[78] M. Hochbruck and C. Lubich, "A Gautschi-type method for oscillatory second-order differential equations", *Numer. Math.*, vol. 83, pp. 402–426, 1999.

[79] M. Hochbruck and A. Ostermann, "Exponential integrators." *Acta Numer.*, vol. 19, pp. 209–286, 2000.

[80] W. T. van Horssen, "An asymptotic theory for a class of initial-boundary value problems for weakly nonlinear wave equations with an application to a model of the galloping oscillations of overhead transmission lines", *SIAM J. Appl. Math.*, vol. 48, pp. 1227–1243, 1988.

[81] Z. Huang, S. Jin, P. A. Markowich, C. Sparber, and C. Zheng, "A time-splitting spectral scheme for the Maxwell-Dirac system", *J. Comput. Phys.*, vol. 208, pp. 761–789, 2005.

[82] S. Ibrahim, M. Majdoub, and N. Masmoudi, "Global solutions for a semilinear, two-dimensional Klein-Gordon equation with exponential-type nonlinearity", *Comm. Pure Appl. Math.*, vol. 59, pp. 1639–1658, 2006.

[83] R. Imekraz, "Long time existence for semi-linear Klein-Gordon equations on compact manifolds for a generic mass", *C. R. Math. Acad. Sci. Paris*, vol. 353, pp. 831–835, 2015.

[84] T. Jahnke and C. Lubich, "Error bounds for exponential operator splittings", *BIT*, vol. 40, pp. 735–744, 2000.

[85] S. Jiménez and L. Vazquez, "Analysis of four numerical schemes for a nonlinear Klein-Gordon equation", *Appl. Math. Comput.*, vol. 35, pp. 61–94, 1990.

[86] S. Jin, P. A. Markowich, and C. Sparber, "Mathematical and computational methods for semiclassical Schrödinger equations", *Acta Numer.*, vol. 20, pp. 121–209, 2011.

[87] F. John, "Blow-up of solutions of nonlinear wave equations in three space dimensions", *Manuscripta Math.*, vol. 28, pp. 235–265, 1979.

[88] M. Keel and T. Tao, "Small data blow-up for semilinear Klein-Gordon equations", *Amer. J. Math.*, vol. 121, pp. 629–669, 1999.

[89] S. Klainerman, "Global existence of small amplitude solutions to nonlinear Klein-Gordon equations in four space-time dimensions", *Comm. Pure Appl. Math.*, vol. 38, pp. 631–641, 1985.

[90] C. Lämmerzahl, "The pseudodifferential operator square root of the Klein-Gordon equation", *J. Math. Phys.*, vol. 34, pp. 3918–3932, 1993.

[91] H. J. Landau, "Necessary density conditions for sampling and interpolation of certain entire functions", *Acta Math.*, vol. 117, pp. 37–52, 1967.

[92] R. Landes, "On Galerkin's method in the existence theory of quasilinear elliptic equations", *J. Funct. Anal.*, vol. 39, pp. 123–148, 1980.

[93] B. Leimkuhler and S. Reich, "Simulating Hamiltonian Dynamics", Cambridge University Press, 2004.

[94] R. J. Leveque, "Finite Volume Methods for Hyperbolic Problems", Cambridge University Press, 2002.

[95] S. Li and L. Vu-Quoc, "Finite difference calculus invariant structure of a class of algorithms for the nonlinear Klein-Gordon equation", *SIAM J. Numer. Anal.*, vol. 32, pp. 1839–1875, 1995.

[96] T. T. Li and Y. Zhou, "A note on the life-span of classical solutions to nonlinear wave equations in four space dimensions", *Indian Univ. Math. J.*, vol. 44, pp. 1207–1248, 1995.

[97] T. T. Li and Y. Zhou, “Nonlinear Klein-Gordon Equations”, Springer, 2017.

[98] W. Liao, J. Zhu, and A. Q. M. Khaliq, “A fourth-order compact algorithm for nonlinear reaction–diffusion equations with Neumann boundary conditions”, *Numer. Methods Partial Differential Equations*, vol. 22, pp. 600–616, 2006.

[99] H. Lindblad, “On the lifespan of solutions of nonlinear Klein-Gordon equations with small initial data”, *Comm. Pure Appl. Math.*, vol. 43, pp. 445–472, 1990.

[100] H. Lindblad and I. Rodnianski, “The weak null condition for Einstein’s equations”, *C. R. Math. Acad. Sci. Paris*, vol. 336, pp. 901–906, 2003.

[101] H. Lindblad and A. Soffer, “A remark on asymptotic completeness for the critical nonlinear Klein–Gordon equation”, *Lett. Math. Phys.*, vol. 73, pp. 249–258, 2005.

[102] C. Lubich, “On splitting methods for Schrödinger-Possion and cubic nonlinear Schrödinger equations”, *Math. Comp.*, vol. 77, pp. 2141–2153, 2008.

[103] Y. Luo, X. Li, and C. Guo, “Fourth-order compact and energy conservative scheme for solving nonlinear Klein-Gordon equation”, *Numer. Methods Partial Differential Equations*, vol. 33, pp. 1283–1304, 2017.

[104] S. Machihara, “The nonrelativistic limit of the nonlinear Klein-Gordon equation”, *Funkcial. Ekvac.*, vol. 44, pp. 243–252, 2001.

[105] S. Machihara, N. Masmoudi, and K. Nakanishi, “Nonrelativistic limit in the energy space for nonlinear Klein-Gordon equations”, *Math. Ann.*, vol. 322, pp. 603–621, 2002.

[106] S. Machihara, K. Nakanishi, and K. Ozawa, “Nonrelativistic limit in the energy space for nonlinear Klein-Gordon equations”, *Math. Ann.*, vol. 322, pp. 603–621, 2002.

[107] A. Majda, “Introduction to PDEs and Waves for the Atmosphere and Ocean”, American Mathematical Society, 2003.

[108] N. Masmoudi and K. Nakanishi, “From nonlinear Klein-Gordon equation to a system of coupled nonlinear Schrödinger equations”, *Math. Ann.*, vol. 324, pp. 359–389, 2002.

[109] R. McLachlan and G. Quispel, “Splitting methods”, *Acta Numer.*, vol. 11, pp. 341–434, 2002.

[110] R. C. McOwen, “Partial Differential Equations: Methods and Applications”, Prentice Hall, 1996.

[111] A. Mohebbi, M. Abbaszadeh, and M. Dehghan, “A high-order and unconditionally stable scheme for the modified anomalous fractional sub-diffusion equation with a nonlinear source term”, *J. Comput. Phys.*, vol. 240, pp. 36–48, 2013.

[112] C. Morawetz, “Time decay for the nonlinear Klein-Gordon equation”, *Prol. Roy. Soc. A.*, vol. 306, pp. 291–296, 1968.

[113] C. Morawetz and W. Strauss, “Decay and scattering of solutions of a nonlinear relativistic wave equation”, *Comm. Pure Appl. Math.*, vol. 25, pp. 1–31, 1972.

[114] K. Moriyama, “Normal forms and global existence of solutions to a class of cubic nonlinear Klein–Gordon equations in one-space dimension”, *Differential Integral Equations*, vol. 10, pp. 499–520, 1997.

[115] K. Nakanishi, “Scattering theory for nonlinear Klein-Gordon equation with Sobolev critical power”, *Int. Math. Res. Not. IMRN*, vol. 31, pp. 31–60, 1999.

[116] K. Nakanishi and W. Schlag, “Global dynamics above the ground state energy for the focusing nonlinear Klein-Gordon equation”, *J. Differential Equations*, vol. 250, pp. 2299–2333, 2011.

[117] T. Ohlsson, “Relativistic Quantum Physics: From Advanced Quantum Mechanics to Introductory Quantum Field Theory”, Cambridge University Press, 2011.

[118] K. Ono, “Global existence and asymptotic behavior of small solutions for semilinear dissipative Klein-Gordon equations”, *Discrete Contin. Dyn. Syst.*, vol. 9, pp. 651–662, 2003.

[119] A. Ostermann and K. Schratz, “Low regularity exponential-type integrators for semilinear Schrödinger equations in the energy space”, *Found. Comput. Math.*, vol. 18, pp. 731–755, 2018.

[120] T. Ozawa, K. Tsutaya, and Y. Tsutsumi, "Global existence and asymptotic behavior of solutions for the Klein–Gordon equations with quadratic nonlinearity in two space dimensions", *Math. Z.*, vol. 222, pp. 341–362, 1996.

[121] P. Pascual, S. Jiménez, and L. Vázquez, "Numerical simulations of a nonlinear Klein-Gordon model. Applications", *Lecture Notes in Physics*, vol. 448, pp. 211–270, 1995.

[122] H. Pecher, "Nonlinear small data scattering for the wave and Klein-Gordon equation", *Math. Z.*, vol. 185, pp. 261–270, 1984.

[123] M. Perel and I. Fialkovsky, "Exponentially localized solutions to the Klein–Gordon equation", *J. Math. Sci.*, vol. 117, pp. 3994–4000, 2003.

[124] J. J. Sakurai, "Advanced Quantum Mechanics", Addison-Wesley, 1967.

[125] A. Sánchez and L. Vázquez, "Topological soliton dynamics in a stochastic ϕ^4 model", *Phys. Lett. A*, vol. 152, pp. 184–190, 1991.

[126] L. I. Schiff, "Nonlinear meson theory of nuclear forces, I", *Phys. Rev.*, vol. 84, pp. 1–9, 1951.

[127] E. Schrödinger, "An undulatory theory of the mechanics of atoms and molecules", *Phys. Rev.*, vol. 28, pp. 1049–1070, 1926.

[128] F. Schwabl, "Advanced Quantum Mechanics", Springer, 2008.

[129] I. Segal, "The global Cauchy problem for a relativistic scalar field with power interaction", *Bull. Soc. Math. France*, vol. 91, pp. 129–135, 1963.

[130] C. E. Shannon, "A mathematical theory of communication", *Bell Syst. Tech. J.*, vol. 27, pp. 379–423, 1948.

[131] C. E. Shannon, "A mathematical theory of communication", *Bell Syst. Tech. J.*, vol. 27, pp. 623–666, 1948.

[132] J. Shatah, "Normal forms and quadratic nonlinear Klein-Gordon equations", *Comm. Pure Appl. Math.*, vol. 38, pp. 685–696, 1985.

[133] J. Shen and T. Tang, "Spectral and High-Order Methods with Applications", Science Press, 2006.

[134] J. Simon and E. Taflin, “The Cauchy problem for nonlinear Klein-Gordon equations”, *Commun. Math. Phys.*, vol. 152, pp. 433–478, 1993.

[135] M. Srednicki, “Quantum Field Theory”, Cambridge University Press, 2007.

[136] G. Strang, “On the construction and comparison of difference schemes”, *SIAM J. Numer. Anal.*, vol. 5, pp. 506–517, 1968.

[137] W. Strauss, “Decay and asymptotics for $\Box u = f(u)$”, *J. Funct. Anal.*, vol. 2, pp. 409–457, 1968.

[138] W. Strauss and L. Vázquez, “Numerical solution of a nonlinear Klein-Gordon equation”, *J. Comput. Phys.*, vol. 28, pp. 271–278, 1978.

[139] M. Struwe, “Globally regular solutions to the u^5 Klein–Gordon equation”, *Ann. Sc. Norm. Super. Pisa Cl. Sci. (5)*, vol. 15, pp. 495–513, 1989.

[140] M. Struwe, “Semi-linear wave equations”, *Bull. Amer. Math. Soc.*, vol. 26, pp. 53–85, 1992.

[141] C. Su and X. Zhao, “On time-splitting methods for nonlinear Schrödinger equation with highly oscillatory potential”, *ESAIM Math. Model. Numer. Anal.*, 10.1051/m2an/2020006, 2020.

[142] C. Sulem and P. Sulem, “The Nonlinear Schödinger Equation”, Springer-Verlag, 1999.

[143] E. Tadmor, “A review of numerical methods for nonlinear partial differential equations”, *Bull. Amer. Math. Soc.*, vol. 49, pp. 507–554, 2012.

[144] M. Thalhammer, “High-order exponential operator splitting methods for time-dependent Schrödinger equations”, *SIAM J. Numer. Anal.*, vol. 46, pp. 2022–2038, 2008.

[145] M. Thalhammer, “Convergence analysis of high-order time-splitting pseudospectral methods for nonlinear Schrödinger equations”, *SIAM J. Numer. Anal.*, vol. 50, pp. 3231–3258, 2012.

[146] M. Thalhammer, M. Caliari, and C. Neuhauser, “High-order time-splitting Hermite and Fourier spectral methods”, *J. Comput. Phys.*, vol. 228, pp. 822–832, 2009.

[147] V. Thomée, “Galerkin Finite Element Methods for Parabolic Problems”, Springer, 1997.

[148] G. Todorova and B. Yordanov, “Critical exponent for a nonlinear Klein-Gordon equation with damping”, *J. Differential Equations*, vol. 174, pp. 464–489, 2001.

[149] Y. Tourigny, “Product approximation for nonlinear Klein-Gordon equations”, *IMA J. Numer. Anal.*, vol. 9, pp. 449–462, 1990.

[150] M. Tsutsumi, “Nonrelativistic approximation of nonlinear Klein-Gordon equations in two space dimensions”, *Nonlinear Anal.*, vol. 8, pp. 637–643, 1984.

[151] L. Vázquez, L. Streit, and V. Pérez-gárcia, “Nonlinear Klein-Gordon and Schrödinger Systems: Theory and Applications”, World Scientific, 1996.

[152] F. Verhulst, “Methods and Applications of Sngular Perturbations: Boundary Layers and Multiple Timescale Dynamics”, Springer, 2005.

[153] L. Vu - Quoc and S. Li, “Invariant-conserving finite difference algorithms for the nonlinear Klein-Gordon equation”, *Comput. Methods Appl. Mech. Engrg.*, vol. 107, pp. 341–391, 1993.

[154] W. von Wahl, “Regular solutions of initial-boundary value problems for linear and nonlinear wave-equations. II”, *Math. Z.*, vol. 142, pp. 121–130, 1975.

[155] T. Wang, B. Guo, and X. Q, “Fourth-order compact and energy conservative difference schemes for the nonlinear Schrödinger equation in two dimensions”, *J. Comput. Phys.*, vol. 243, pp. 382–399, 2013.

[156] Y. Wang and X. Zhao, “Symmetric high order Gautschi-type exponential wave integrators pseudospectral method for the nonlinear Klein-Gordon equation in the nonrelativistic limit regime”, *Int. J. Numer. Anal. Model.*, vol. 15, pp. 405–427, 2018.

[157] G. B. Whitham, “Linear and Nonlinear Waves”, Wiley, 1974.

[158] J. Xin, "Modeling light bullets with the two-dimensional sine–Gordon equation", *Phys. D*, vol. 135, pp. 345–368, 2000.

[159] W. Yi, X. Ruan, and C. Su, "Optimal resolution methods for the Klein-Gordon-Dirac system in the nonrelativistic limit regime", *J. Sci. Comput.*, vol. 79, pp. 1907–1935, 2019.

[160] F. Yin, T. Tian, J. Song, and M. Zhu, "Spectral methods using Legendre wavelets for nonlinear Klein\Sine-Gordon equations", *J. Comput. Appl. Math.*, vol. 275, pp. 321–334, 2015.

[161] F. Ynduráin, "Relativistic Quantum Mechanics and Introduction to Field Theory", Springer, 1996.

[162] H. Yoshida, "Construction of higher order symplectic integrators", *Phys. Lett. A*, vol. 150, pp. 262–268, 1990.

[163] E. Zauderer, "Partial Differential Equations of Applied Mathematics", Wiley, 1983.

[164] Q. Zhang, "New exact traveling wave solutions for the nonlinear Klein-Gordon equation", *Comm. Partial Differential Equations*, vol. 35, pp. 630–668, 2010.

[165] X. Zhao, "On error estimates of an exponential wave integrator sine pseudospectral method for the Klein-Gordon-Zakharov system", *Numer. Methods Partial Differential Equations*, vol. 32, pp. 266–291, 2016.

[166] Y. Zhou and W. Han, "Life-span of solutions to critical semilinear wave equations", *Comm. Partial Differential Equations*, vol. 39, pp. 439–451, 2014.

[167] Y. Zhou, "Life span of classical solutions to $\Box u = |u|^p$ in two space dimensions", *Chin. Ann. Math. Ser. B*, vol. 14B, pp. 225–236, 1993.

[168] Y. Zhou, "Cauchy problem for semilinear wave equations in four space dimensions with small initial data", *J. Partial Differ. Equ.*, vol. 8, pp. 135–144, 1995.

List of Publications

[1] Long time error analysis of finite difference time domain methods for the nonlinear Klein-Gordon equation with weak nonlinearity (with W. Bao and W. Yi), Commun. Comput. Phys., Vol. 26 (2019), pp. 1307-1334.

[2] Uniform error bounds of an exponential wave integrator for the long-time dynamics of the nonlinear Klein-Gordon equation (with W. Yi), arXiv: 2003.11785.

[3] Long time error analysis of the fourth-order compact finite difference methods for the nonlinear Klein-Gordon equation with weak nonlinearity, arXiv: 2003.03951.

[4] Uniform error bounds of a time-splitting spectral method for the long-time dynamics of the nonlinear Klein-Gordon equation with weak nonlinearity (with W. Bao and C. Su), arXiv:2001.10868.

[5] Spatial resolution of different discretizations over long-time for the Dirac equation with small potentials (with J. Yin), preprint.

[6] Temporal resolution of different integrators for the long-time dynamics of the Dirac equation with small potentials (with W. Bao and J. Yin), in preparation.